UNIVERSITÀ DEGLI STUDI DI PADOVA

UNIVERSITA' DEGLI STUDI DI PADOVA

Dipartimento di Ingegneria Industriale DII

Corso di Laurea Magistrale in Ingegneria Energetica

Integration of concentrated solar thermal technology with fossil fuelled power plants: the example of a coal fired plant

Relatore: Prof. Andrea Lazzaretto

Correlatore: Ing. Sergio Rech

Laureando: Ilaria Danuso

Matricola: 1104683

Anno Accademico 2016/2017

Desidero ringraziare l'Ing. Enrico Grigolon per aver contribuito con la sua esperienza alla realizzazione di questa tesi.

Contents

List of Figures

List of Tables

Abstract

The integration of concentrating solar power plants (CSP) and conventional fossil power systems offers the possibility to enhance the performance of the latter by either reducing the fuel consumption or boosting the power output. The purposes of this work are to provide a concise description of the four CSP technologies (Parabolic Trough, Linear Fresnel Reflectors, Solar Towers and Parabolic Dishes) and a review of the available studies on hybrid solar-traditional systems, which will be the base for the case study. From this summary, it is deduced that for coal fired power plants, the most promising integration options are the highest temperature preheater replacement and the generation of steam which is sent to the turbine. The starting point for the hybrid plant simulations is the model of a power plant located in Fusina (Venice), built in Engineering Equation Solver (EES). Twelve hybrid solutions are proposed and compared; among these, four are selected and further analysed. The highest hybrid cycle efficiencies are obtained when high pressure steam is generated from the drainage water of the last feedwater preheater, while the most consistent fuel reduction comes from the last preheater replacement. An example of annual performance analysis is also carried out for the preheater replacement solution.

Sommario

L'integrazione di impianti a concentrazione solare (CSP) e impianti convenzionali a combustibile fossile offre la possibilità di migliorare le prestazioni di questi ultimi riducendone il consumo di combustibile o aumentandone la potenza utile prodotta. Questo lavoro si pone gli obiettivi di fornire una breve descrizione delle quattro tecnologie CSP (Parabolic Trough, Linear Fresnel Reflectors, Solar Towers e Parabolic Dishes) e una review bibliografica degli studi disponibili sugli impianti ibridi, che saranno la base per le simulazioni numeriche. Da questo riassunto, si deduce che, per gli impianti a carbone, le opzioni di integrazione più promettenti sono la sostituzione del preriscaldatore dell'acqua di alimento a più alta temperatura e la generazione di vapore da inviare in turbina. Il punto di partenza per simulare le configurazioni ibride è il modello di un impianto termoelettrico situato a Fusina (Venezia), scritto in Engineering Equation Solver (EES). Dodici configurazioni ibride sono proposte e confrontate; tra queste, quattro sono selezionate ed ulteriormente analizzate. Le efficienze del ciclo ibrido più elevate sono ottenute quando vapore in alta pressione viene generato dall'acqua di drenaggio dell'ultimo preriscaldatore, mentre la riduzione del consumo di combustibile più consistente si ha con la sostituzione dello stesso preriscaldatore. Un esempio di analisi di prestazione annuale è inoltre realizzato per la soluzione in cui il preriscaldatore viene sostituito.

Introduction

This thesis work is focused on the integration of concentrated solar power (CSP) plants with traditional fossil fuelled systems. These plants combine the renewable energy source environmental advantages with the reliability of fossil fuels: if a CSP section is added to a conventional power plant, this one can either use the solar energy to reduce the fuel consumption or to boost its power output. When a traditional power system, such as a gas turbine, is integrated with a solar-only CSP plant it allows to increase the load factor of the system by providing power when the solar source is not available. The four CSP technologies are described in the first chapter, in order to explain the concept of the solar concentration and to learn the applicative temperature range for each of them. A bibliography review is provided for researches on hybrid plants: in the second chapter, different articles are summarised with the purpose of providing a reference for the case study. A case study is proposed for a coal fuelled power plant: various integration options are proposed and added to the base cycle model. The simulation results include different efficiency parameters (such as solar radiation- and heat-to-electric efficiency) and other indicators relative to the CSP section such as: solar radiation and heat power input, solar share, fuel reduction, solar power and solar field area. The purpose of the case study is to identify which configurations would be better when applied to the power plant model: to achieve this, the different solutions are compared to each other. The selected options are further investigated, not only in terms of performance parameters, but also to understand the way the thermodynamic cycle is altered after the solar input is included.

Chapter 1

Concentrating Solar Power

In this chapter, the main concepts of the Concentrating Solar Power technology are analyzed. Each of the four different plant configurations is discussed in detail, with explanations of the components of a solar field (mirrors, receiver, heat transfer fluid, thermal storage). Some cost considerations are reported and, in the conclusion, a summarizing table provide a comparison between the four technologies.

1.1 The Oil Crisis

Following the Arab-Israeli war in 1973, Arab members of the OPEC (Organization of Petroleum Exporting Countries) imposed an embargo on the United States for their support to Israel; the oil prices raised up to 70% of their benchmark value and remained very high even after the crisis had been solved. The embargo, as well as other factors (such as high inflation and the depletion of the spare capacity in the East Texas oil fields) made the U.S. government ponder on their energetic independence. The incorrect belief that oil reserves were running out was widespread and a recession was feared. Nonetheless, these events helped to give birth to new energy policies and research funds were increased substantially, even if not all the efforts were intentionally aimed to reduce CO_2 emissions (policymakers recognized the climate issue after 1988, when NASA climatologist James Hansen warned against the human contribution to global warming); in

this context, alternative energy sources received great attention, and the use of solar energy was no exception [2] [3]. Interest and incentives in Concentrating Solar Power (CSP) started as a consequence of the oil crisis; the success of the SEGS plant built in California brought interest in this technology in Europe and other countries. Nowadays, Spain and the U.S. are the countries with the highest number of operating CSP plants.

1.2 Concentrating Solar Power

A concentrated solar power (CSP) plant is an energy production system in which the irradiance from the Sun is focused by mirrors on a receiver; the heat generated is then transferred to a power conversion block. Concentrating the beams allows to overcome one of the biggest issues of utilizing solar energy, that is to say its dilution [4]. The collecting mirrors are spread over a generally large surface, but can focus the irradiance on a significantly smaller area: a fundamental parameter to consider is the ratio of these two surfaces, which is defined Concentration Ratio (CR). Different configurations of CSP are characterized by typical a range of CR, which according to Balzani and Armaroli ([4]) goes from 10 to 10000 (including prototypes).

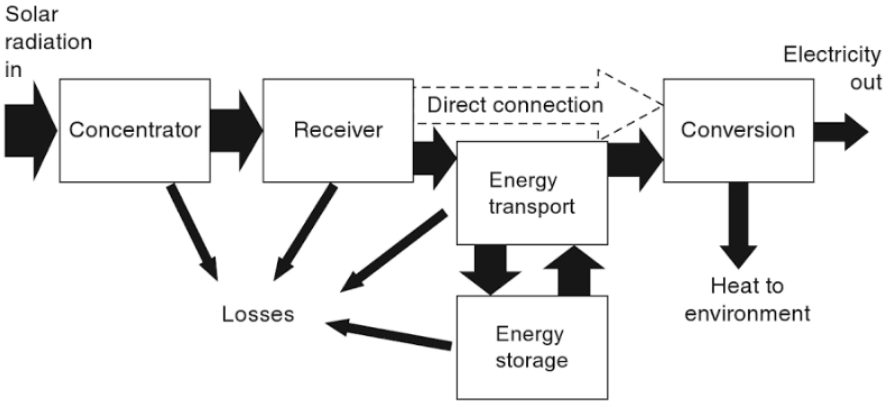

Figure 1.1: CSP scheme [5]

One of the most important advantages of concentrating the irradiance is that higher temperatures are obtained: the heat transfer fluid can reach at least 300C,

so it becomes a suitable option for power generation [4]. There are two main families of technologies based on the kind of surface the beams are concentrated on: linear focus, where the absorber surface is a tube, and point focus, where the radiation is concentrated on a focal point. The first family includes parabolic trough collectors (PTC) and linear Fresnel collectors (LFR), while the second one includes solar towers (ST) and parabolic dishes (PD). To decouple energy production and demand, thermal storages are used. Storage is a valuable asset to any renewable energy power system, as it also allows to increase the capacity factor (the amount of time a plant is active during the year). Despite introducing a consistent capital investment, the addition of a storage has been proven beneficial in lowering the cost of electricity [6]. The advantage has been widely acknowledged because, as reported in [7], all new plants built in 2015 (and planned for the next years) comprise a thermal storage. Commercial CSP plants are relatively young, even if the benefits of concentrating solar energy was already known in ancient history [4]. The fact that this is a recently commercialized technology [8] results in a low contribution in the global energy production: as found in REN 21: Renewable 2016 Global Status Report ([7]), the share of renewable energies in the power production is 23.7%, of which 1.2% comes from solar photovoltaic and 0.4% being provided by ocean, geothermal and CSP. The range of application of CSP plants goes from remote small plants of a few kW to 300 MW and more; it is reported in [8] that a 350 MW plant yield the energy equivalent of 2,3 millions of oil barrels. Like the photovoltaic (PV) technology, CSP finds its limits in the variability of the irradiance condition during day and seasons and in the non-coincidence of energy production and demand. The concentration feature adds another restriction that affects the areas where such a plant is feasible: only the direct normal irradiance (DNI) component is used. This is the amount of energy (evaluated on a direction perpendicular to the observer plane) that arrives on Earth's surface without scatterings and reflections. In this field the diffuse and reflected irradiance components are not useful for electricity generation.

As reported by [4], the geographic extension where these plants can be economically installed goes from the 35th northern and 35th southern latitudes (also called the "Sun belt"), and in [6] and [8], the DNI yearly minimum required value

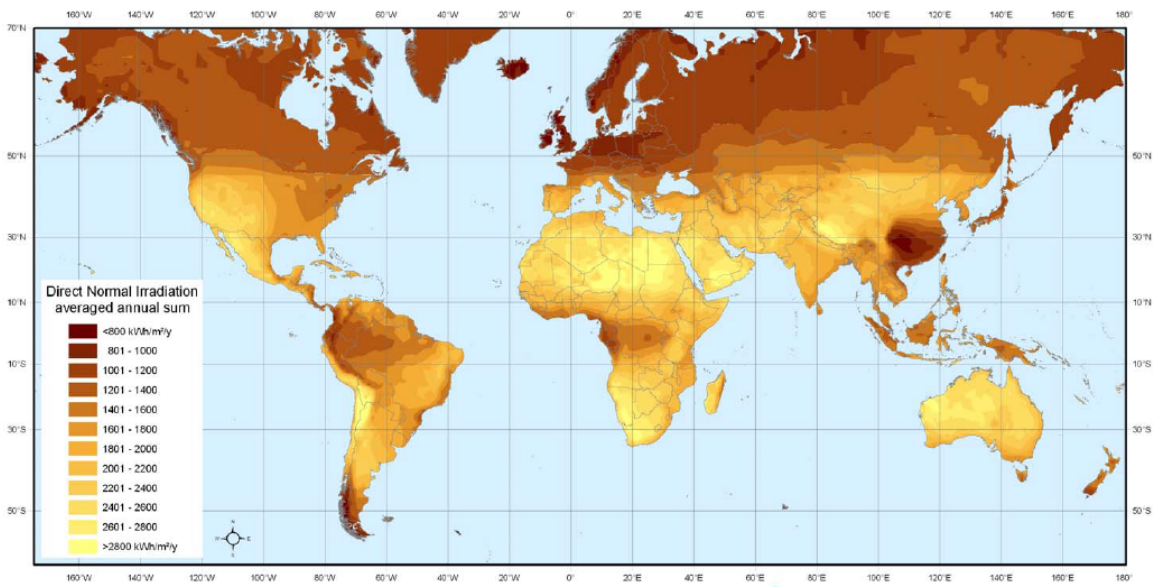

Figure 1.2: Average annual DNI [kWh/m^2/yr] (adapted from [9])

for an economically convenient plant is estimated in 1700 - 2000 kWh/mq (see figures 1.2 and 1.3). It should be noted that these limits are not so strict, as there are operating plants in countries with lower values of irradiance.

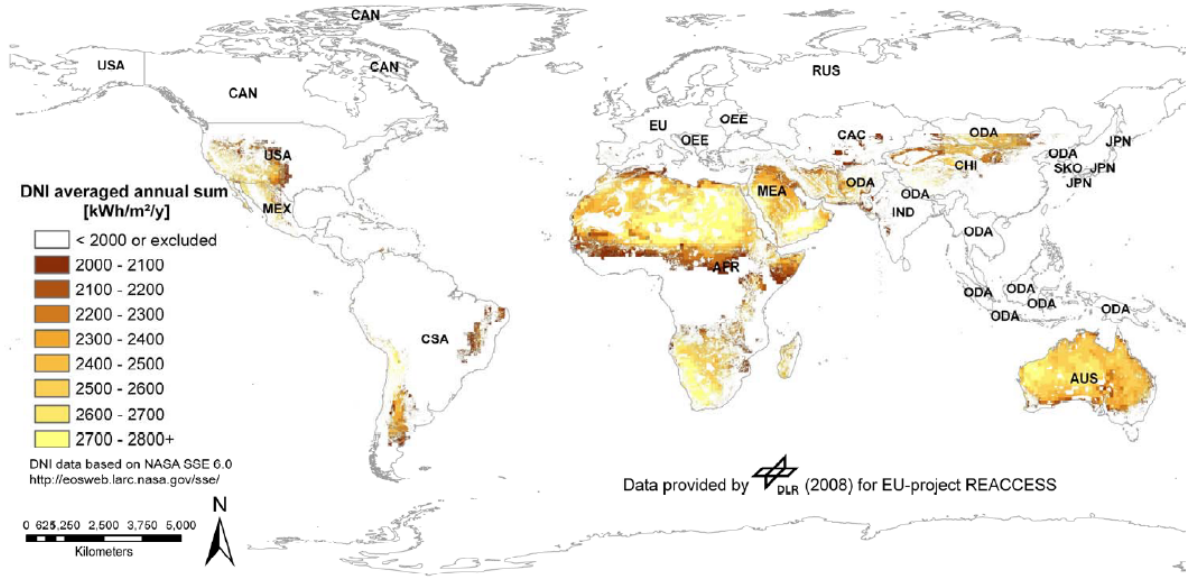

Figure 1.3: Locations with high DNI values (adapted from [9])

1.2.1 Conversion efficiency and losses

As seen in figure 1.1, a concentrating solar power plant includes different components and phases: a concentrator, a receiver, a direct or indirect means to transfer energy, a conversion cycle and a possible storage. Depending on the technology, the actual structure of each of the elements may vary: concentrators can be shaped and focused differently, the receivers may work on different principleS, the heat transfer fluid can directly link the solar field with the conversion block or two different fluids can be applied. Finally, different power cycles can be installed. All these elements are subjected to losses: therefore, the overall solar-to-electric efficiency can be written as:

$$\eta_{\text{system}} = \eta_{\text{optical}} \times \eta_{\text{receiver}} \times \eta_{\text{transport}} \times \eta_{\text{storage}} \times \eta_{\text{conversion}}$$

The efficiencies can be evaluated at a particular instant or averaged during a timescale (such as a year). The plant has a higher efficiency when the collected energy yielded by the solar field to the power conversion system increases; on the other hand, thermal losses increase with the temperature. Other than thermal losses, the concentrators are also affected by cosine losses, shading and blocking. Cosine losses are present when a mirror is not perfectly aligned with the Sun, because the apparent aperture area is reduced by a factor equal to the cosine of the incidence angle (the angle formed between the normal to a surface and the line joining the centre of the Sun with the centre of th surface). This can be interpreted as a reduction of the available collecting area, therefore the concentration ratio decreases. Shading occurs when mirrors are positioned next to each other at such a distance that prevents the sunbeams to reach the reflecting surface. Blocking is a similar effect, in which mirrors intercept part of the already reflected beams, preventing them to reach the receiver. For linear focussing systems, end losses have to be considered: these account for those sunbeams which are reflected by the mirror but are missed by the receiver. The optical efficiency includes the above-mentioned losses, as well as geometrical imperfections and tracking errors [5].

1.3 Parabolic Trough Collectors

Parabolic trough collectors (PTC) are the most mature and implemented technology so far [10]. As already mentioned, PTC concentrate the energy on a linear locus: this concentration is obtained with a row of concave mirrors, with a parabolic cross-section. Spherical mirrors are not applied, because they can't concentrate the reflected beams in a precise point, while parabolic mirrors focus them in the precise focal point of the parabola: considering all the sections that form a PTC module, the energy is concentrated in the line made by all the focal points. An assembly is defined as a row of connected collector modules, each with an independent tracking mechanism; a plant is made up of hundreds of assemblies [11]. Figure 1.4 illustrates the different elements of a PTC module. A tube (or Heat Collector Element, HCE) is placed on the focus line to absorb the energy. The fluid circulating inside raises its temperature up to approximately 400C (depending on the fluid itself) and transfers the heat in the power generation section, where it generates high pressure superheated steam at 100 bar and 370C [11]: this is the case of indirect steam generation, because two distinct fluids (one that receives the heat and the other in the Rankine cycle) are required. Direct steam generation (DSG) is in its developing stage for PTC [8].

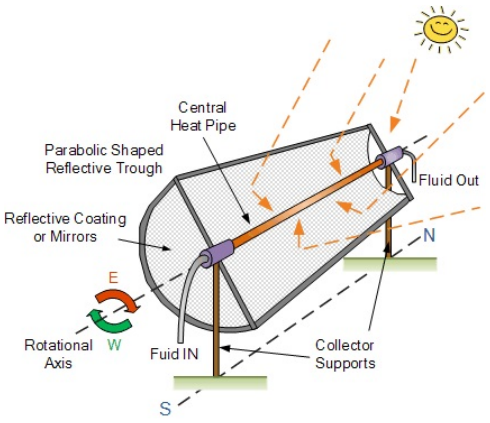

Figure 1.4: Elements of a parabolic trough collector module

In order to capture a high amount of solar energy, sun tracking is always present, and it can be achieved either with a precise mathematical algorithm or with sensors. All the commercial power plants have east-west tracking, so the rows

of mirrors are north-south aligned [8]: this configuration is adopted to maximize the captured energy over the year, and it becomes more important at higher latitude locations. The rotational axis is located at the vertex line or slightly below it. The assemblies are moved by a drive unit, which can be mechanical (motor-gearbox unit) or electro-hydraulic; the drive unit has the additional task of bringing the trough in a safety position in case of strong winds or when the plant is not active (for example, at night). If the incoming irradiance is sufficient, the plant can work at the rated power using only solar energy; a typical value for the full-load operating time in summer months is estimated in [11] as 10-12 hrs/day during summer. For less favourable periods, like during cloudy days or nights, hybrid fossil fuel/solar plants are an interesting option. Thermal storage is also advisable for increasing the load factor; it can be direct if the stored fluid is the same circulating in the HCE, or indirect if there's a secondary fluid which interfaces with the main thermal vector through heat exchangers.

1.3.1 Geometrical and performance parameters

In the following figure 1.5, presented in the document Parabolic Trough Technology [8], the fundamental geometric parameters describing the collector are illustrated: these are the length l, the focal length f, the aperture width a and the rim angle Ψ. The focal length is the distance between the vertex and the focal point of the parabola; the rim angle is the angle between the optical axis and the line between the focal point and the mirror rim.

It is sufficient to know two of the parameters (length excluded) to determine the parabolic section entirely, and they are also correlated to each other. The optical axis coincides with the symmetry axis of the parabola, and has to be directed towards the sun [8]. Commonly, the concentration ratio is given in terms of a geometrical parameter (CG) that approximates the standard definition of the energy ratios. There are two possible interpretations of CG, depending on which receiver surface is considered: the most common one is the projected rectangle of the tube absorber, the other is the lateral surface of the cylindrycal tube. Typical values for parabolic trough dimensions and performance parameters are given in [8] and [11]:

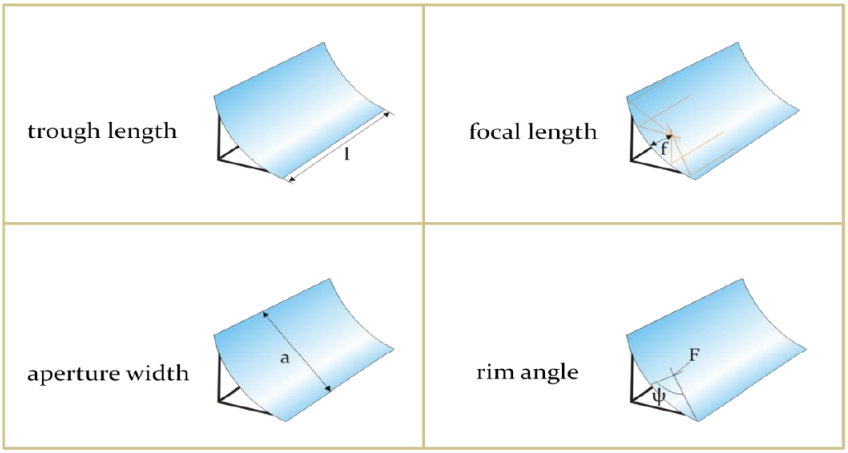

Figure 1.5: Geometrical parameters for a parabolic trough [8]

- rim angle 80
- aperture width 6m
- focal length 1.75 m
- module length 12-14 m
- lengths 100-150 m (or more)
- Cr 20 -30
- T = 300-400C

The aperture area is defined as the product of the aperture width and the collector length, and it determines the amount of energy captured by the module. Some observations on the possible range for these parameters can be found in [8]: for example, having a small rim angle implies that the mirror is narrow and will therefore concentrate a smaller amount of intercepted beams; on the other hand, if the angle is too large the concentration ratio will decrease (the reflected beams on the mirror's outer parts must cover a longer path to reach the receiver, and contribute less to the energy production). In reality, the receiver has to be positioned at a short distance from the reflector to reduce the importance of geometrical imperfections (deviations from the ideal slope of the surface, and an adequate value for the rim angle becomes more relevant.

1.3.2 Mirrors

The basic elements of a PTC plant are the mirrors used to form the parabolic reflectors. Each reflector is composed by different glass facets (for example, a 12 m long module with 5.77 m of aperture width contains 28 mirrors), which are shaped differently depending on where they are located on the parabolic surface. A high reflectivity (the fraction of the incident radiation that is reflected by the material) is the most important requirement of the facets. It is important to notice that in CSP applications, only the specular reflectivity, according to which a beam arriving to a surface is reflected symmetrically to the direction perpendicular to that surface, is considered. In other words, there is only one direction in which the rays are reflected; another type of reflection is the diffuse one, which is of no interest in this field. Since each wavelength of the solar spectrum is associated with a different energy content, it is useful to weight the reflectivity to include this effect: the average weighted reflectivity of Flabeg mirrors is 93.5% [8]. Silver-coated low-iron (less than 0.015% [8]) glass mirrors are the most frequently adopted nowadays: they have been installed since 1980s and have proven to be durable. The low-iron glass allows a high transmission of sunlight to the underlying silver layer, which has a high reflectivity on the solar spectrum range. Below the glass and silver layers, there are the protective ones, made of copper (1 layer) and epoxy varnish (3 or 4). Figure 1.6 shows a Flabeg mirror section. The overall thickness of this element is 4-5 mm; ceramic pads with special adhesive are placed below the glass element for mounting on the trough support.

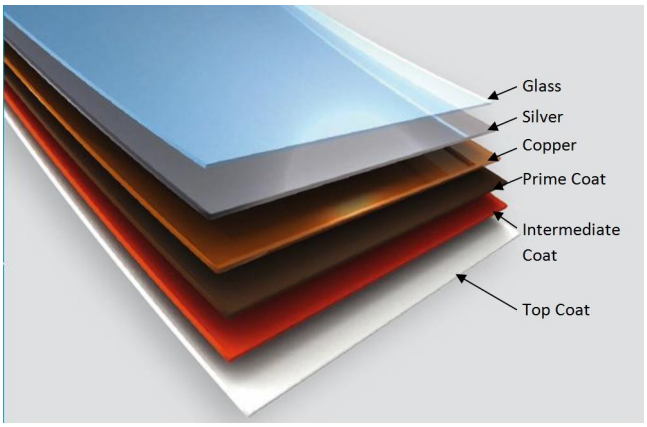

Figure 1.6: Layers composing a PTC mirror (Flabeg) [8]

Depending on the manufacturing process, slope errors for the mirror facets can be very low: it is reported in [8] that the average error can be reduced to 0.132 (Flabeg mirrors). Defining the intercept factor as the percentage of the reflected radiation that reaches the absorber, values of more than 95% can be found (increasing with the absorber diameter).

1.3.3 Absorber

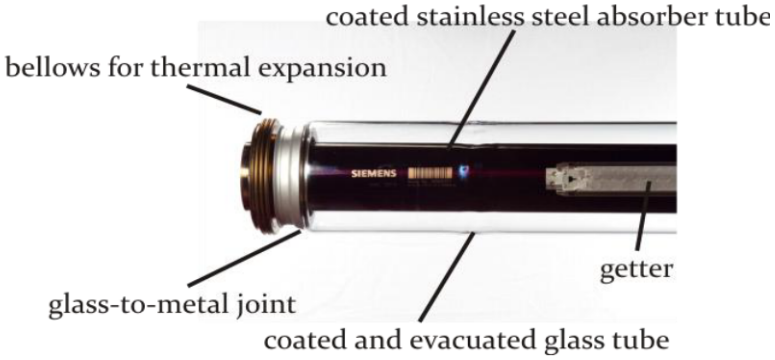

Figure 1.7: Elements of an absorber tube (Siemens) [8]

The heat collector element is a crucial part of a PTC plant design, since it has to achieve a high radiance absorption along with low heat losses, both thermal and optical. Since high temperatures differences between operative and non operative conditions and tracking movement are involved, thermal expansion of the different components and pipe flexibility must be taken into account. A HCE is composed by the absorber tube, the evacuated glass tube, the glass-to-metal joints, the bellows for thermal expansion, the gas absorbers (getters) and the fluid (cfr. figure 1.7). To improve the optical behaviour and consequently to limit the heat losses of the HCE, special coatings are applied. The absorber tube must have a high absorptance in the visible light spectrum and a low emissivity in the infrared range, so different coatings are layered: one highly reflective metallic coat (copper, aluminium or molybdenum), several layers made of cermet materials (metallic nanoparticles embedded in a ceramic matrix) with different metal content, an anti-reflection ceramic layer, adhesion layer and gas diffusion barrier. For a given wavelength, the absorption coefficient is equal to the emissivity fol-

lowing the Kirchhoff's law. Values for the absorption coefficient reach 0.95, and 0.1 for emissivity at 400C [8]. The tube diameter can't be too large nor too small: in the first case, heat losses increase, while in the second one the intercept factor remains low. Common diameters are around 70 mm. The evacuated glass helps the absorber to reduce convective losses and must have a high transmittance in the visible spectrum (the coefficient reaches 0.96) and a low reflectivity (0.04) realized with antireflective coatings. The material is borosilicate glass with an indicative 3 mm thickness; the pressure is around 0.001 mbar. A flexible connection between glass and tube is realized with bellows at the receiver ends, and there are special hydrogen absorbers called getters. Hydrogen is released with the decaying of the thermo oil, and reduces the vacuum quality.

1.3.4 Thermal fluid

The fluid has to be liquid, and should present the following properties: sufficiently high evaporation temperature (for indirect steam generation plants), low freezing temperature, thermal stability, high specific heat capacity and conductivity, low viscosity, environmentally friendly features, low flammability and explosivity, low cost and sufficient availability. Generally, the most relevant properties are the evaporation point and the stability, which determine the maximum operation temperature for the fluid. The weight of the other aspects depends on the plant characteristics. The traditional fluid for PTC is synthetic thermo oil (mixture of biphenyl/diphenyl oxide); molten salts (mixture of NaNO3 and KNO3) are being tested, although they are mainly used for storage. The main advantage of using salts is that higher temperatures can be reached, but a relevant downside is their high freezing point (120-220C) which implies a consistent investment for auxiliary heating. Direct steam generation, commonly applied to linear Fresnel plants, applies water as a thermal fluid (or organic mixtures for lower temperature applications); water evaporates in the absorber tubes when heated, allowing to reach higher temperatures and efficiencies. Even if this solution increases the costs of piping since the working fluid is high pressure steam, the main advantage comes from the missing heat exchangers section and consequently reduced heat losses.

1.3.5 Support structure

Being exposed to the wind, the support structure must be designed accurately: its purposes are to maintain the mirrors in position, to stabilize the trough and to guarantee a precise tracking. Wind isn't the only source of loads the bearing structure has to withstand, in fact the main cause of deformation is the weight of the trough itself [12]. Usually the structure is tubular and made in aluminium, which grants resistance to corrosion [8]. To keep the mirrors in place, and consequently to assure a good energy capture without additional optic losses, a high stiffness is required. A high stiffness support also allows to combine more modules for a longer assembly, and since there is one tracking unit each, the costs can be reduced; a lighter material is good to reduce both gravity related deformations and the parasitic energy required for the tracking motion. Moreover, a well designed support facilitates shipping, handling and field installation [8]. Other bearing elements are the mirrors supporting points on the frame, the absorber support, the pylons and the foundations.

1.3.6 History and experiences

Even if PTC applications were already experimented in the early 19th century, consistent research and investments started only in the 1970s after the Oil Crisis. The first plants had to overcome the initial high marketing and technical efforts, the lack of experience in the design process and a non appealing payback time [8]. The widespread use and the maturity of the parabolic trough technology recognized today mainly come from the experience of the Solar Energy Generating Systems (or SEGS), a group of nine plants installed in the Mojave Desert in California (see figure 1.8), initially under the property of the American-Israeli company Luz International Ltd. This location is ideal for solar plants because its DNI reaches 2727 $kWh/m^2/yr$ [8]. The first stage, SEGS I, started its operation in 1984, and after that other 8 plants were built until Luz declared bankruptcy in 1991 due to declining incentives and cost of energy [8]; despite this, the plants are still operating and they greatly helped to prove the commercial feasibility of this technology, as well as to reduce the costs for other similar plants. This experience

brought interest in PTC in Europe too, with the 1977 Small Solar Power System Project/Distributed Collector System (SSPS/DCS), a collaboration between the International Energy Agency (IEA) and nine countries [10]. The SEGS endeavour also laid the foundations for collectors design's evolution: Luz produced three generations of collectors, called LS-1, LS-2, LS-3, which represented the starting point for many other manufacturing companies [8]. Before bankruptcy, a fourth generation was being studied to test direct steam generation and another prototype was installed in Israel.

Figure 1.8: SEGS plants in California [10]

From LS-1 to LS-3, the aperture width and trough length has been increased; LS-1 and LS-2 use a torque box support structure (formed by rigid tubes) and a mechanical gearbox for tracking motion, while the third generation has a metal lattice support structure and hydraulic controls. Despite the progresses (especially high tracking performances [8]) introduced with the LS-3 design, the worse thermal efficiency and alignment issues balanced the incomes. The mirrors, manufactured by the German company Flabeg, have the structure described in paragraph 1.3.2. Luz collectors apply a stainless-steel tube as the HCE with a selective coating (black chrome for the first two models and cermet layer on the third), enveloped under vacuum by a glass tube. Being the LS-3 collector no longer competitive, in 1998 a joint venture of European companies and researchers aimed to design a more cost effective model [8]. The result was the Eurotrough collector, geometrically similar to the LS-3 but with a cheaper, LS-2 like torque box with less shading, good stiffness and alignment performance; the same Flabeg mirrors are employed, and the Solel Universal Vacuum Collector (UVAC) by Solel replaced

the Luz one. This brought to progressively longer modules. Another innovation introduced of hot-rolled profiles instead of the rectangular hollow profiles, which lead to further savings. The main advantages of the Eurotrough design were the reduced optical losses due to better load resistance (less deformation), the lower costs associated with a longer length (already discussed in this chapter), a more lightweight structure, and easier manufacturing, transportation and handling. A 10% cost reduction and 3% performance improvement over the LS-3 collector is estimated.

1.4 Linear Fresnel Reflectors

Even if PTC plants are the most diffused worldwide [1] , there is an alternative technology for linear focusing which substitutes the parabolic mirrors with Fresnel lenses. The major differences from the parabolic trough systems are the reflector and the receiver. The mirrors are not shaped as a parabola but they are flat or slightly bent, arranged in arrays of stripes (primary mirrors): the reflectors are the only elements which track the Sun, since the receiver tube (or tubes) is mounted on a fixed support and does not move (figure 1.9). The relative position between mirrors and receiver varies during the day causing some light aberrations.

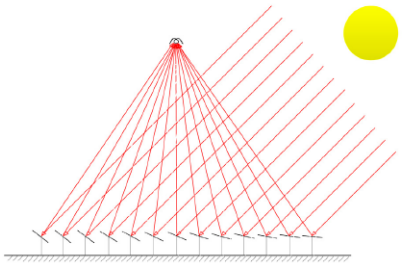

Figure 1.9: Scheme of a LFR plant [13]

A secondary reflector can be added in some cases to collect the beams that missed the absorber (the estimated fraction is 50%, according to F. and V. Orioli [7]). Some features which make Fresnel collectors appealing to investors are the low cost of manufacturing, the possibility to use them for different applications at different temperatures, the overall simplified plant structure.

1.4.1 Fresnel lenses

A Fresnel lens can be derived from a spherical lens by dividing it into concentric sections with reduced thickness, but with the same slope of the initial continuous shape (see figure 1.10) the resulting surface can be described as a chain of prisms [14]. Since the refractive power is contained only at the lens interface, it is not modified by the process, but the weight of the lens is consistently decreased [13] the most evident consequence, when applied for solar concentration, is that the wind loads do not increase when the collectors' area is increased (as would happen with parabolic troughs).

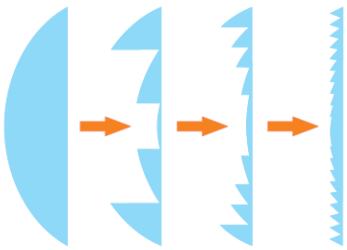

Figure 1.10: Principle of Fresnel lenses design [15]

As illustrated in figure 1.11 from Optical Design using Fresnel lenses [15], the lenses are geometrically determined by: prism pitch (or facet spacing), draft angle and slope angle.

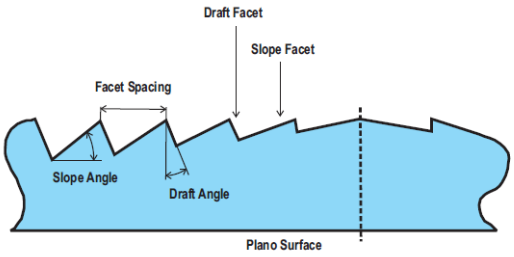

Figure 1.11: Surface of a Fresnel lens [15]

Other parameters are the focal length, which is approximated by the distance of the prism surface on the lens and the focal point, and the f-number that is the ratio of the focal length to the diameter (or diagonal) of the lens. The f-number indicates the "speed" of the lens, whose practical meaning is more easily

explained in the following figure 1.12.

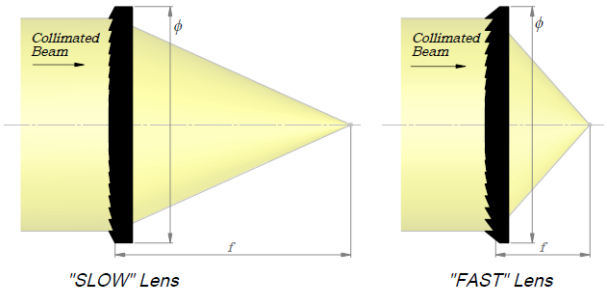

Figure 1.12: Speed of a Fresnel lens [15]

Being composed by prisms, a Fresnel lens has a higher fraction of lost light cause by the draft facets: this effect would be corrected if the facets were vertical, but this cannot be obtained in the manufacturing process. The orientation of the facets, which could be directed towards the side of the collimated beam (grooves-out design) or towards the focal point (grooves-in), has also an influence in the performance. Generally speaking, there are two categories of lenses, namely imaging and non-imaging: imaging lenses provide a precise image of the source, while non-imaging ones do not grant a good reproduction of the source. The former were adopted initially for CSP, but the latter are more convenient since only the energy transfer is important [15] [13] [16]. The efficiency of Fresnel lenses is affected by different factors such as reflective losses, f-number value (if below 1, it's not recommended for CSP use), facet corner rounding (the ideal would be a perfectly sharp corner, not feasible in reality), spectral absorption [16].

1.4.2 Geometrical and performance parameters

According to Linear Fresnel Technology [17], the geometrical parameters that define a linear Fresnel plant are: the width of the stripes, the number of mirrors that compose them, their spacing, the width of the collector, the curvature of the mirrors and the height of the absorber. Each of them affects the cost of energy, so there is an optimal value to find. In particular, if the width of the stripes is too narrow, more stripes would be required to fill up a given area (with increased costs); on the other hand, if it is too broad, the astigmatism effect

(a particular kind of aberration) has more influence on the optical performance. In general, in a broader collector all the inaccuracies (for example, geometrical inaccuracies caused by manufacturing) assume a higher weight. The same happens if the distance of the absorber tube from the mirror plane is too large (in this case, tracking errors count as well); if it is too short, problems associated with mirror shading and blocking arise. If the arrays are very distant from each other, a higher surface will be covered without any performance benefit; if they are too close it's harder to avoid shading and blocking. The possibility of choosing different values of all these parameters results in a certain freedom in the design process and in a wide range of different applications (at different temperatures). Temperatures of 300-400C can be reached with the consolidated models, but with the more recent configurations up to 500C are obtained [13]. It is stated in [18] that one of the disadvantages of this technology compared to PTC is that the angle of incidence (formed between the incoming sunbeams and the plane of the reflector) varies not only transversally to the mirrors (as it happens with the trough) but also longitudinally: the cosine effect, along with shading and blocking has a large negative impact on the energy output. These phenomena have to be considered also when the orientation of the plant has to be decided.

1.4.3 Mirrors

The reflecting elements, as already said, are silver-coated flat mirrors placed in linear arrays close to the ground, which can be up to 1 km long [18]; the overall arrangement of the stripes, even if it is not parabolic, resembles a broken up PTC. The lower weight and cost and easier manufacturing and handling allow to assemble more arrays to occupy a larger area without increasing stress loads (so the structural support requirements can be less strict than in PTC) or parasitic energy expenses [14]. Maintenance is simpler and cheaper because it is easy to access the mirrors [18]. The tracking mechanism is less advanced too because it has to det a lower weight in motion; the mirrors individually track the Sun on one axis by permanently modifying the tilt angle (which is different for different rows). A single tracking device could be installed for each row, but individual motion is preferred to increase accuracy [18].

1.4.4 Absorber

The fixed receiver can be a single tube or an assembly of tubes: in the first case, a secondary reflector is often installed, while in the second the tubes are placed in a trapezoidal cavity and allow a higher intercept factor. The actual cost-effectiveness of using an additional reflector is still under evaluation, while when multiple tubes are applied, they are non evacuated with lateral insulation (this configuration is more suitable for low temperature applications) [13]. Receivers are placed on rollers to compensate for thermal expansion (estimated in 0.6% for steel tubes at high temperatures) and are simpler than the ones used in PTC plants. The secondary receiver also acts as a thermal insulator and as a stabilizing structural element. The absorber tubes are currently non evacuated, made of stainless steel and coated with selective layers to increase the absorptance at the shorter wavelengths and to lower the emittance in the infrared [17].

1.4.5 Thermal Fluid

Commonly, these plants use water as the operating fluid in a DSG configuration, with a steam drum separating the two phases between the solar section and the power block. Higher pressures and temperatures are obtained, thus increasing the production efficiency and lowering the cost of energy [13]. It is possible to use molten salt as HTF, which could provide a baseload storage but would require an expensive heat exchanger section.

1.4.6 Compact Linear Fresnel Reflector

An alternative design allows one mirror stripe to direct the collected sunbeams to at least two receivers: this is called Compact Linear Fresnel Receiver (CLFR). The concept is described in-depth by Mills and Morrison [18], and it was developed to solve the shading and blocking issues of the mirrors, which could be limited with higher towers and larger absorber sizes but at the price of increased losses. If a wide area is occupied by the plant, there would surely be multiple towers; if these towers are sufficiently close to each other, the tracking mechanism can point the mirrors to the receiver that implies less shading (figure 1.13).

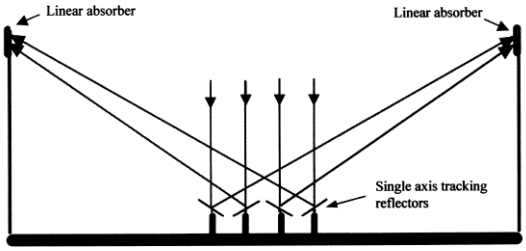

Figure 1.13: Scheme of a CLFR [18]

As a result, the land is used more effectively (the reflecting stripes are packed more densely in a given area), and shorter towers can be installed, which leads to a reduction in both costs and losses.

1.4.7 Comparison between PTC and LFR

During this paragraph advantages and disadvantages of Fresnel concentrators were presented; it is useful to compare them to PTC, since this is the benchmark technology on the market and it is conceptually similar. The aspects in the list have been discussed mostly by Gunther [17] and F. and V. Orioli [7], but have been reported by other authors as well. The advantages mainly come from the lower costs and ease of manufacturing and maintenance:

- LFR plants request a lower investment cost assuming the same aperture area;
- lower O&M costs;
- higher land efficiency and good ground coverage;
- possibility of adapting the design to the available space;
- between the rows, only the space for maintenance is required.
- suitable for applications in low DNI regions, where the costs have higher weight;
- collectors and absorbers have a simple design and can be very long;

- they allow a DSG configuration with higher efficiency in the power cycle;
- the flat mirrors allow a reduction in costs and structural strain and are easy to clean;
- the tracking is easier;
- it is easier to reach a high CR by elevating the absorber.

Many of the disadvantages derive from the performance of Fresnel lenses themselves:

- they have a lower solar-to-electric efficiency;
- shading and blocking effects become more important;
- the astigmatism phenomenon is present;
- the secondary reflector introduces a further reflecting stage, so the losses are higher;
- the absorber is far from the mirrors, so the optical ends are higher assuming the same collector length of a PTC;
- the technology is less mature than PTC.

Being a relatively recent commercialized technology, the costs analysis are mostly based on estimates or particular plants; however, cost reduction compared to PTC have been evaluated in 30% to 50% [17] [19].

1.5 Solar Towers

In the family of point focusing technologies, solar towers (ST, also known as central receiver systems) are the most common. The plant is composed by a large field of heliostats, each tracking the Sun on two axis and concentrating the solar beams on a receiver placed at the top of a tower (figure 1.14).

Being the receiver surface much smaller compared to the reflecting field, the concentration ratio is much bigger than in line focusing plants: in Global review

of solar tower technologies [20] the range proposed is between 200 and 1000. Other major differences of solar towers are: a different plant configuration, higher temperatures can be reached (up to 1000C depending on the fluid [21]), and the working fluid on the power section can be gaseous (commonly air). The high temperature allows to obtain a higher efficiency in the energy conversion process (ultra-supercritical steam cycles are feasible); the possibility to use air makes Brayton-Joules cycles suitable. Supercritical CO_2 cycles are also possible [22]. Various authors ([21], [10], [6]) state that this technology has a great cost reduction potential thanks to the different options for the heat transfer fluid and also because it is more recent than PTC.

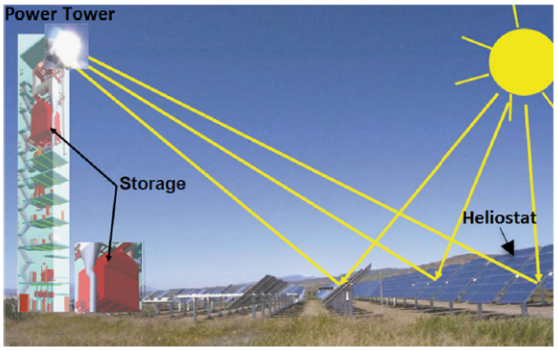

Figure 1.14: Scheme of a solar tower plant [10]

In [22], Clifford and Iverson highlighted the challenges related to the high operating temperatures: the goal of the plant design is to maintain a high heat absorption while keeping losses at an acceptable level. For example, molten salts become unstable and cannot be used at more than 600C. It is stated that above 650C, a concentration ratio higher than 900 is required to maintain a high thermal efficiencies.

1.5.1 Heliostats

A heliostat is an element comprising of flat (or slightly curved) mirrors, a tracking system, a steel frame, a structure foundation and a control system (figure 1.15). As already mentioned, the tracking system is both on the vertical and horizontal axis. Heliostats' surface can vary from 1 m^2 to 120 m^2; all reflectors in

a plant have the same aperture area. The advantages of using smaller sizes are the easier production, handling, installation and reduced wind loads, but more of them would be required to fill a given area. If the mirrors are larger, a lower number would be needed but they would have to withstand higher wind loads. Also, smaller mirrors assemblies have better optical performance but imply more complex field wiring and control systems (due to the higher number of employed elements) [23]. A 120 m^2 heliostat is composed by 28 curved facets (seven rows and four columns); the curvature of the facets helps to keep the receiver size as low as possible [20]. The optical efficiency of the reflectors is influenced by cosine losses, shading, blocking, mirror reflectivity, atmospheric attenuation and receiver spillage. An effective design of the heliostat field is crucial, since this section of the ST plant accounts for 50% of the initial cost and 40% of the total energy losses ; the cost elements are listed in [23] as drives, manufacturing facilities, mirror modules, pedestal and mirror support structure, field wiring and controls. The weight of each depends on the plant size.

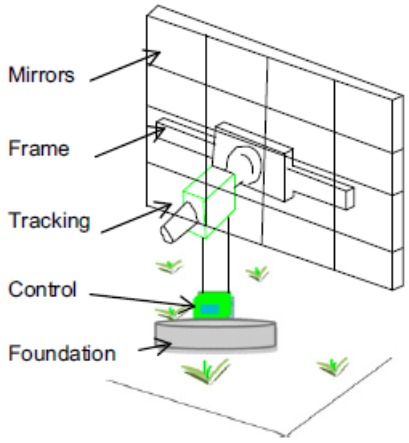

Figure 1.15: Scheme of an heliostat [21]

Heliostats are off-tracking elements, meaning that their target (the receiver) is fixed and they have to bisect the angle between the Sun's direction and the receiver's one; a higher concentration ratio is obtained if the reflected Sun's image is as small as possible. In order to achieve this, the mirrors can have a fixed (most common) or time-variable (most efficient) canting. By 2013, 30 heliostat fields had been built [24].

1.5.2 Receiver

The receiver is the other crucial element in ST plants: its technology depends on the heat collecting fluid, and the orientation of the absorbing surface is related to the geometrical arrangement of the heliostat field: if all the surface of the receiver is absorbing, it is placed on the field center with mirrors all around it (surrounding fields), as in figure 1.16; if only a side is absorbing, the heliostats occupy an angular section and the tower is placed at its vertex (north or south fields, depending on the hemisphere, figure 1.17; this is the most common layout for research plants [24]).

Figure 1.16: Tower in the centre of the heliostat field (Gemasolar plant, Spain) [20]

Figure 1.17: Tower at the vertex of the heliostat field (PS 10 and PS20 plant, Spain) [20]

Ho and Iverson in [22] classify the receivers in gas, liquid or solid depending on the phase of the heat collecting substance; another classification is found in

[20], where they are divided in two categories: tubular and volumetric. In this second approach, the tubular receivers are used with a liquid heat transfer fluid, and are further divided in external cylindrical and cavity absorbers.

In the former configuration (illustrated in figure 1.18), the stainless or alloyed steel tubes are exposed to the atmosphere and placed side by side to form a cylinder and absorb radiation coming from all directions (the heliostats are all around the tower); in the latter (figure 1.19), the tubes are inside a cavity and can receive radiation from a certain angle. External cylinder receivers suffer from higher convection losses; double cavity receivers are also used, in which case the solar field will be arranged on either side of the absorber. Volumetric receivers are applied when the HTF is air, and are made of porous wire mesh or metallic or ceramic foams; the whole component absorbs the reflected energy, which then is used to heat the air that passes through it. They are further classified in open and closed volumetric receivers: the first ones draw in ambient air, which then gets heated, the second ones use pressurized air.

Figure 1.18: External cylindrical receiver (Crescent Dunes plant) [20]

The division proposed by Ho and Iverson illustrates other different models of receivers and explains in detail how these component work; possible temperature are also reported. In the gas receivers family, other than volumetric air ones (temperature reached about 1000C), small particle air receivers and tubular gas receivers are listed. The small particle air technology (700C) uses submicron carbon particles suspended in air which absorbs the energy. Tubular gas receivers apply tubes with a particular design to enhance the radial heat distribution. The liquid receivers are divided in tubular liquid (600C) and falling film (700C): this

Figure 1.19: Cavity receiver (PS10 plant) [20]

second technology takes advantage of gravity-driven fluid motion by inclining the receiving surface. The fluid can circulate on tubes or on a wall and absorbs heat while falling; in this way the pumping energy is reduced. In the solid particle receivers design (1000C), sand-like ceramic particles are exposed to the irradiance while falling on cavity receivers. Although there is a high number of possible technologies to apply, only a few of them have actually been implemented: the most common one is the tubular receiver (with gas or liquid HTF). Other possibilities could perform better in terms of temperature (with consequently high power cycles efficiencies) but would also introduce challenges and issues with the HTF and materials.

1.5.3 Tower

The tower supports the receiver and provides other functions: it can accommodate a small storage, it serves as a target to calibrate the heliostats and insulation for the tubes. It also has to withstand the wind loads while avoiding shading. Towers are either made of steel lattice or reinforced concrete; the height can go from 30 m up to 165 m [24]. In [20] it is stated that there is no evident connection between the tower height and the plant output power.

1.5.4 Brayton-Joule cycle

Since Brayton-Joule cycles are a suitable option for the power generating section that is not available in PTC and LFR, it is useful to list the advantages associated with this configuration [23]:

- they can rapidly switch from the solar input to another fuel, thus increasing availability and load factor and becoming more attarctive to investors;
- they have high efficiency at partial loads and adapt rapidly to load variations;
- they can be used in a combined heat and power (CHP) configuration, generating useful heat other than electricity;
- they work at high temperatures (1000C), so they offer an opportunity of development for solar towers;
- they can insert electricity in different tension levels, generally imply easier permitting, they are more compact than a Rankine cycle plant and have less environmental impact;
- they can be built in a modular way, so they can be installed in grounds unsuitable for other CSP technologies.

1.5.5 History and experiences

The first experimental plants were the Solar-One and Solar-Two, built in California. The Solar One was a 10 MW plant, with water-steam as HTF, which operated from 1982 to 1988, and it proved the feasibility of the ST technology. The Solar-One was redesigned into the Solar-Two, which operated from 1996 to 1999 and employed molten salts and a storage. Research and experiment on solar towers was dropped by the U.S. Department of Energy (DOE) after the Solar-Two was decommissioned due to budget constraints, but it has recently being reintroduced again due to interest on this CSP technologies (particularly for the high temperatures reached and the performance improvements brought by the storage).

The first commercial solar tower plant was the PS-10 (figure 1.17), built in Spain. It has an output rated power of 10 MW, the HTF is water and the receiver is a cavity type, the tower is 115 m high and the occupied area is 55000 m^2. Near this plant, another one, named PS-20, started operating in 2009; it is a 20 MW plant with a 165 m tower, cavity receiver and occupies 80000 m^2. These two plants are still operative today; other working or experimental sites are located in Germany, USA, India, China, France, Israel, Australia, Turkey [20] [1].

1.6 Parabolic Dish/Engine

Parabolic dish (or parabolic engine) collectors are formed by a satellite-like reflector, composed of smaller mirrors, that focuses the collected radiation on a focal point. In this focal point, a Stirling engine is usually installed. Figure 1.20 illustrates the dish concept, and a power plant is represented in figure 1.21. The size of this technology is smaller than other CSP (from 3 to 25 KW) but it has the peculiarity of being modular [25], so it can be installed in stand-alone or decentralized configurations.

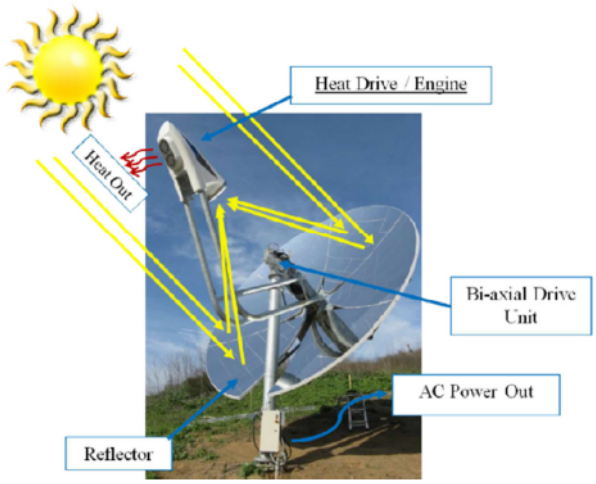

Figure 1.20: Scheme of a parabolic dish [10]

As the other CSP applications, solar dishes began to be studied after the 1970s crisis. Up to this day, it's the least implemented of the four technologies (the NREL website [1] only reports one operating plant).

Hafez et al. [26] listed the advantages of this technology:

- high power density;
- high efficiency;
- modularity;
- versatility (they can be applied in different fields, like cooking, water heating, irrigation, water distillation and desalination);
- resistance to moisture;
- possibility of hybridization;
- long lifetime;
- possibility for local manufacturers to produce some parts of the dish (and consequently to reduce the capital cost.

Figure 1.21: Parabolic dish plant (Maricopa Solar Project, USA) [10]

1.6.1 Mirrors

In the document "A Compendium of solar dish/Stirling technology" [27] the basic concepts of this CSP application are described. The ideal shape for the concentrator would be that of a paraboloid, since the area in which the beams are concentrated is very small; in reality, the paraboloid is approximated with multiple spherical mirrors or membranes stretched on a rim with vacuum between the two sides. The material is low-iron thin-glass (or plastic) coated with silver

or aluminium. Their performance is evaluated with two parameters: reflectance and specularity. Silver has the higher reflectance, while aluminium has a lower value but it is spread over a larger spectrum; specularity is defined as the ability to disperse the reflected light over a smaller angle (ideally, the beams should be reflected with an angle equal and opposite as the incidence angle). When plastic films are used, a lower cost and weight is obtained, as long as a higher flexibility; the disadvantages are the need to utilize stabilizers (plastic deteriorates with long exposures to ultraviolet) and the impossibility to apply mechanical washing.

1.6.2 Support structure

The mirrors are supported by a structure, which can belong to three categories: in a structural optical configuration, the reflective facets are combined directly with the structural elements (this causes inefficiencies and warp); in a space frame the mirrors are separated from the structure itself, which can be a tubular frame or a truss frame. The third structure is provided by stretched membranes, which use the atmospheric pressure to provide the curvature of the facets; since the shape they assume is spherical, the focal length must be adapted (specifically, it must be longer). The parabolic reflector tracks the Sun on two axis; there are two methods for the tracking system: in the azimuth elevation, the planes of rotation are one parallel to the ground and the other normal to it, while the polar tracking method uses an axis parallel to the Earth's axis of rotation.

1.6.3 Receiver

The receiver has the tasks of absorbing as much of the reflected radiation as possible and to transfer it to the engine. It is a cavity type receiver, with an area of aperture that has to be big enough to let the beams enter but small enough to limit heat losses. The absorber is placed behind this window. External receivers could theoretically be used but cavity type are favoured because of lower heat losses at high working temperatures. The cavity also re-irradiates the energy that is not immediately absorbed: another advantage related to the high value of the cavity area compared to that of the absorber is that a lower flux density is reached.

When a the flux on the cavity is too high, in fact, the materials are subjected to stress and heat transfer becomes more difficult. Cavity receivers also protect the absorber from the wind and reduce convection losses. This element operates between very high temperatures and the ambient temperature due to starts and stops and during cloudy periods: this causes thermal fatigue, which can lead to failure.

There are two ways for transmitting the heat to the engine: the first possibility is to place the tubes in which the engine's working fluid flows directly in the concentrated flux area, the second is to apply an intermediate fluid (a liquid metal) which vaporizes when it absorbs the beams and then condensates, releasing heat to the engine's tubes.

1.6.4 Stirling engine

The Stirling engine is based on the cycle of the same name, which comprises of the following phases: two isothermal (compression and expansion) and two isochores. A peculiarity of this cycle is that it presents the same efficiency of a Carnot cycle operating between the same temperatures, and it yields more power assuming the same mass. The engine has two pistons and a regenerator: in the compression phase, the first piston moves toward the other and, in doing so, heat is ceded to the outside. In the second phase, the volume is kept constant by a simultaneous motion of the pistons; subsequently, heat is absorbed at a constant temperature while the volume increases (the second piston alone is moved) . The last transformation is another isochore. The main issue is that these phases (especially the isothermals) are really hard to approximate in reality, but these engines are nonetheless applied because the heat input can come from any source: in the present case, from solar concentration. There are two possible configurations: free piston and kinematic (both are applied in parabolic dishes), and they have a required operative time of about 60000 h [27]. Combined heat and power is also a field of application, since it is easy to recover the heat output. Being a closed cycle, any operating fluid can be used [appunti lezione]. Regarding the efficiency, these engines work best at very high temperatures, which are easily obtained with CSP; in [27], it is stated that the conversion efficiency can reach 30-40%

at 600-800C; since higher temperatures can be reached, the engines are usually applied at their limit (imposed by the materials).

The working fluid is a gas, usually hydrogen or helium. Helium has less issues regarding material compatibility and it is overall safer, but hydrogen is preferred because it leads to higher efficiencies. The fluid is pressurized (5 to 20 MPa).

1.6.5 History and experiences

The first solar dish application was implemented in 1984 in the Advanco Vanguard plant: it applied a 25 kW Stirling engine and obtained a solar-to-electric efficiency of 29.4%. The dish diameter was 11 m and it used 336 mirror facets. Other experimental setups have been built; according to the nrel website, the only operating commercial plant today is located at the Tooele Army Depot, Utah: it is composed by 429 dishes, each with an aperture area of 35 m^2, a turbine power output of 1,5 MW and helium as the HTF.

1.7 Storage

Renewable energy sources can be divided into two categories: predictable and non-predictable. In the first one there are traditional hydroelectric (with a reservoir) and biomass, whose power output is known and does not depend by the ambient condition. In the second there are run-of-the-river hydroelectric, wind and solar sources: these are strongly dependent by aleatory parameters such as water flow rate, wind speed and climate in general. For this second category, introducing an energy storage in the plant design greatly helps to stabilize the power output during periods when the source is not available (for example when the wind speed is lower than the cut-in value of the turbine, during clouds passage or night for solar plants), and becomes essential in standalone plants. A more regular energy output facilitates the electric grid management and allows to achieve a better power quality. In general, storages can be either electrochemical (batteries) or thermal (tanks). In CSP applications, the thermal storage is used either to extend the operating time or to shift the timing of generation. The parameter solar multiple is defined as the ration of the CSP actual solar field's size to the

size it should have to feed the turbine at full load, referred to the local DNI; if a storage is adopted to increase the capacity factor, this value is about 3-4, while if the storage is smaller and applied to yield power when it's needed the parameter is about 1.1-1.5 [28]. There are different technologies that can be applied in the CSP field: the most common one is the two tank indirect storage (figure 1.22), frequently adopted with PTC, in which there is an intermediate heat exchanger between the HTF and the storage medium (molten salt). In the two tank technology there is also the possibility to use the same HTF that is heated in the solar field as the storage medium, thus removing the additional heat exchange (and therefore losses). It has been tested both for molten salts and thermal oil, but with the latter there is a limitation on the maximum working temperature, which must not exceed 400C for chemical stability. An environmental issue also arises when large quantities of hot oil are accumulated, due to its flammability.

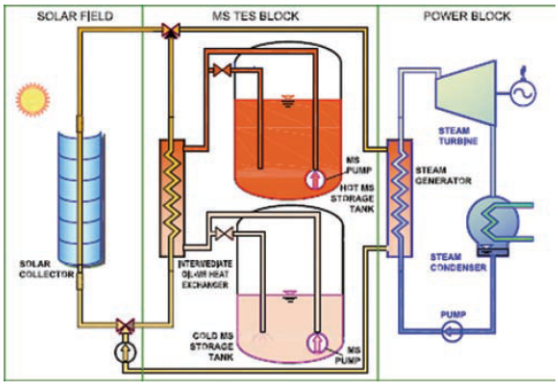

Figure 1.22: Scheme of a two tank storage system [28]

Other technologies under development are the single tank system, in which stratification is exploited in a oil reservoir (in some projects molten salts are applied), systems with solid materials for storage (concrete) or thermo-chemical processes based projects [28].

1.8 Heat Transfer Fluid

Heat transfer fluids used in CSP are mainly molten salts, water and thermal oil. For solar towers the HTF can also be a gas such as air, and for parabolic dishes

the working fluid for the Stirling engine is hydrogen or helium. Looking at the current state of operating plants (figure 1.30 [1]) , it can be seen that:

- the HTF most applied in PTC is thermal oil, followed by molten salts and a couple of water/steam plants (with a DSG method). A pilot hybrid plant in Morocco uses air;
- most solar towers apply water and molten salts, one plant uses air and another liquid sodium;
- LFR plants use mostly direct steam generation with water (DSG is also possible with a diathermic oil).

The advantages and drawbacks of using a given fluid in a particular technology have already been discussed in the previous paragraphs. The same website provides more details about the specific kind of fluid used in some of the plants: most of them apply a thermal oil called Dowtherm A, produced by the company Dow. This fluid is described as an eutectic mixture (i.e. a mixture whose fusion point is lower than the fusion points of the single components) of biphenyl and diphenyl oxide (respectively C12H10 and C12H10O). The range of possible working temperatures goes from 15 to 400C and the pressure can go from atmospheric to 10,6 bar [29]. Another thermal oil product found in CSP application is called Xceltherm, by the company Radco, which is a methylethylated aromatic mixture. According to the datasheet provided in the website [30], it can reach temperatures up to 370C at a low pressure. Among thermal oils, another possible HTF is Therminol by Solutia, which is made by hydrogenated terphenyl, and is suitable for applications from 0 to 345C [31]. Molten salts can be also used in PTC and ST: according to Archimede Solar Energy [32], this mixture of 60% NaNO3 and 40% KNO3 overcomes the temperature limit of about 300-400C imposed by the synthetic oils' thermal stability, reaching values up to 550C. It is used also as a fertilizer and thus it is cheap and easy to find. As already discussed in the PTC section (see paragraph 1.3.4) , an important disadvantages in using molten salts is that, compared with synthetic oil, they have a high freezing temperature (238 C as reported in [Archimede], versus -24C declared for Xceltherm oil).

1.9 Cost considerations

As for other electricity generating power plants, identifying the factors that influence the cost of CSP is quite complex. In a plant commission and operation, different subjects are involved and each of them has a particular function and interest in the process, such as the commissioners, the suppliers, the owner, the O&M service provider. The cost of generation is affected by the perception and division of risk between the various participants; some of the aspects that must be taken into account are the plant site's features (such as the DNI, land use, water availability etc.), the chosen CSP technology, the size, the cost of land, storage capacity and others. A very important element to consider is the local electric market and incentives situation. The result is that comparing CSP to other technologies and market trends forecasting become a difficult task, also considering that CSP is relatively less mature compared to fossil fuels and other renewables. One of the advantage of being in the early stage of deployment is that concentrated solar systems show a consisted cost reduction potential [28].

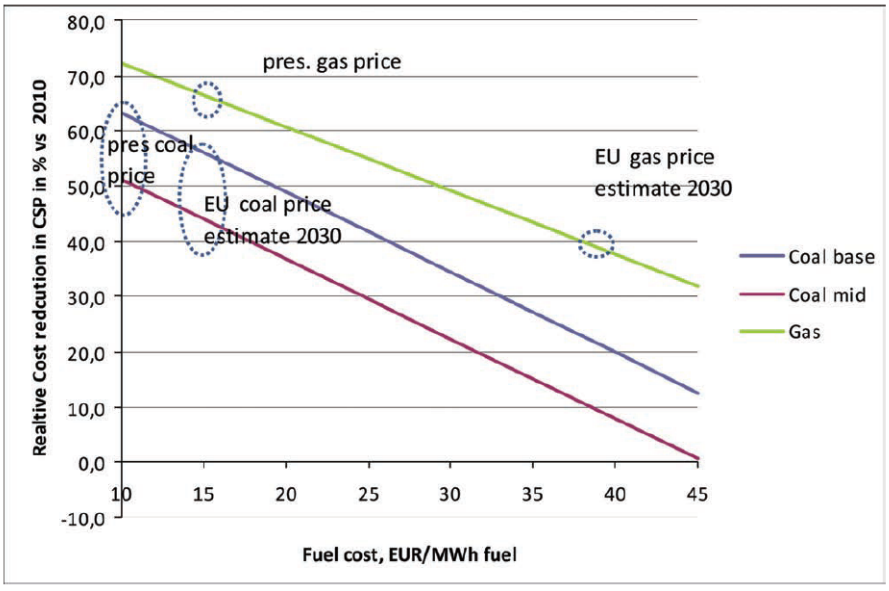

Figure 1.23: Cost reduction to reach competitiveness with fuel sources [28]

When comparing CSP with coal or gas fired plants, it is useful to define a break even cost, i.e. the cost of energy coming from the renewable source that the source itself needs to become more convenient than the reference source. In figure 1.23,

this is shown in terms of percentage reduction in CSP cost that would realize the break-even point at a given coal/gas price. To become competitive with today's prices, a reduction of 50-70% is needed. The progress could be accelerated by raising the price of CO_2 certificates. A comparison has also to be made with other renewable technologies, in particular PV. When the possibility of installing a CSP plant or a large PV has to be evaluated, different elements must be considered: as a mature and widespread solar application, PV is expected to realize grid parity in the next years, but this introduces a challenge in the electric grid management. The impact could be eased by CSP because, unlike PV, it is not a decentralized generating system and could improve the renewable share in the grid. The choice between the two solar technologies is again influenced by the market structure, the prices of electricity in different time steps and the future cost evolution. Another tool for assessing the cost-competitiveness is to predict a value for the learning rate, namely the percentage reduction in costs when the installed capacity is doubled. If a certain growth rate can be assumed, then it is possible to evaluate the period of time needed for a certain cost reduction: for example, starting from a 500 MW growth per year and assuming a 15 - 30% range of new plants built each year, a 50% cost reduction would be achieved between 2021-2031 (see figure 1.24).

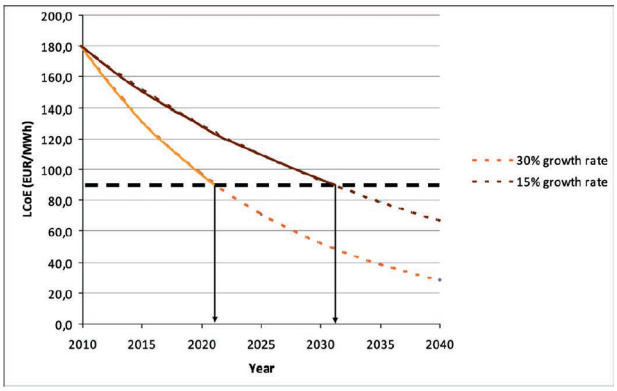

Figure 1.24: Cost reduction to reach competitiveness with fuel sources [28]

An important parameter to evaluate for an electricity generating facility is the levelised cost of electricity, or LCOE, defined as the price of electricity required for a project to balance revenue and costs, assuming a discount rate for the interest

on the invested capital. The higher the electricity selling price, the higher the return on invested capital. In [6], the values for the LCOE given for PTC and ST are 0.2-0.36 $/kWh and 0.17-0.29 $/kWh respectively (assuming a 10% discount rate). Another estimate of this parameter for CSP is given in [28] at about 15-22 ?cents/kWh; the cost of electricity from fossil fuel is 2-3 times lower. Currently, these values are considered high. Further experience in the field of concentrated solar thermal will lower these costs by improving the efficiency and reducing the capital costs. The factors that affects the LCOE of a CSP plants are:

- initial investment cost;
- plant's load factor and efficiency;
- available DNI;
- O&M and capital costs;
- presence and performance of a storage system.

For renewable energy sources, the investment cost is generally very high, while the OM cost is low. Technologies which are less mature are considered more risky by financiers, therefore their LCOE will be higher; on the other hand this effect leads to great cost reduction opportunities. Regarding the influence of DNI on the cost of electricity, it is estimated to decrease at a rate of 4.5% for every 100 kWh/m^2/yr above 2100 kWh/m^2/yr (figure 1.25).

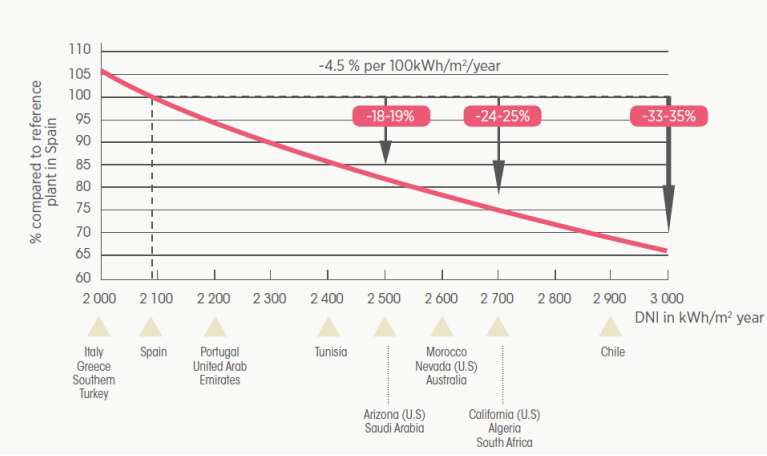

Figure 1.25: LCOE reduction with DNI [6]

1.10 Comparison of CSP technologies

On the National Renewable Energy Laboratory website [1], data and information about operating CSP plants around the world are available. In this paper, data have been re-elaborated in order to summarize the current situation of this technology. The following tables and histograms have been created to show the number of operating plants and the cumulative power output sorted by country and technology, the number of plants using a certain HTF and storage system.

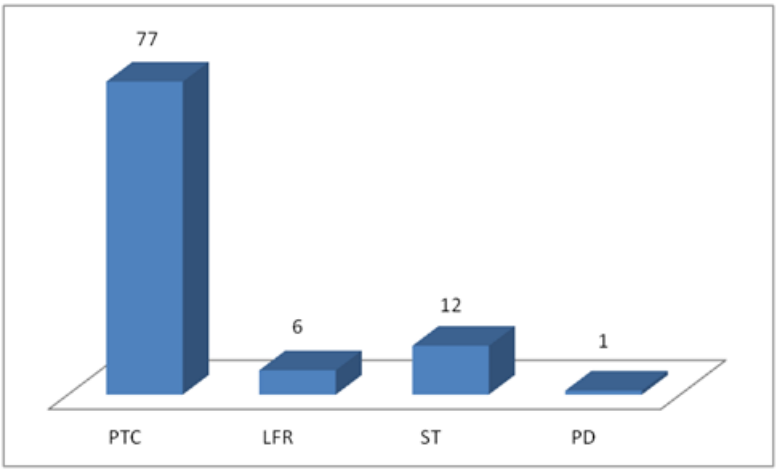

Figure 1.26: Number of operating plants by technology [adapted from [1]]

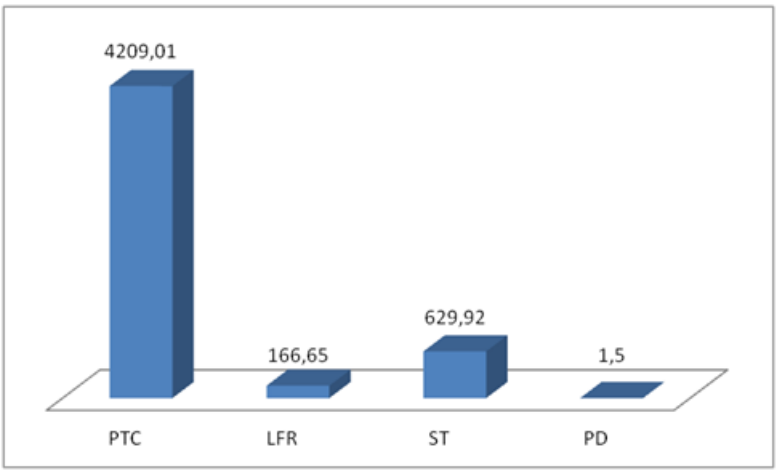

Figure 1.27: Cumulative power output by technology [adapted from [1]]

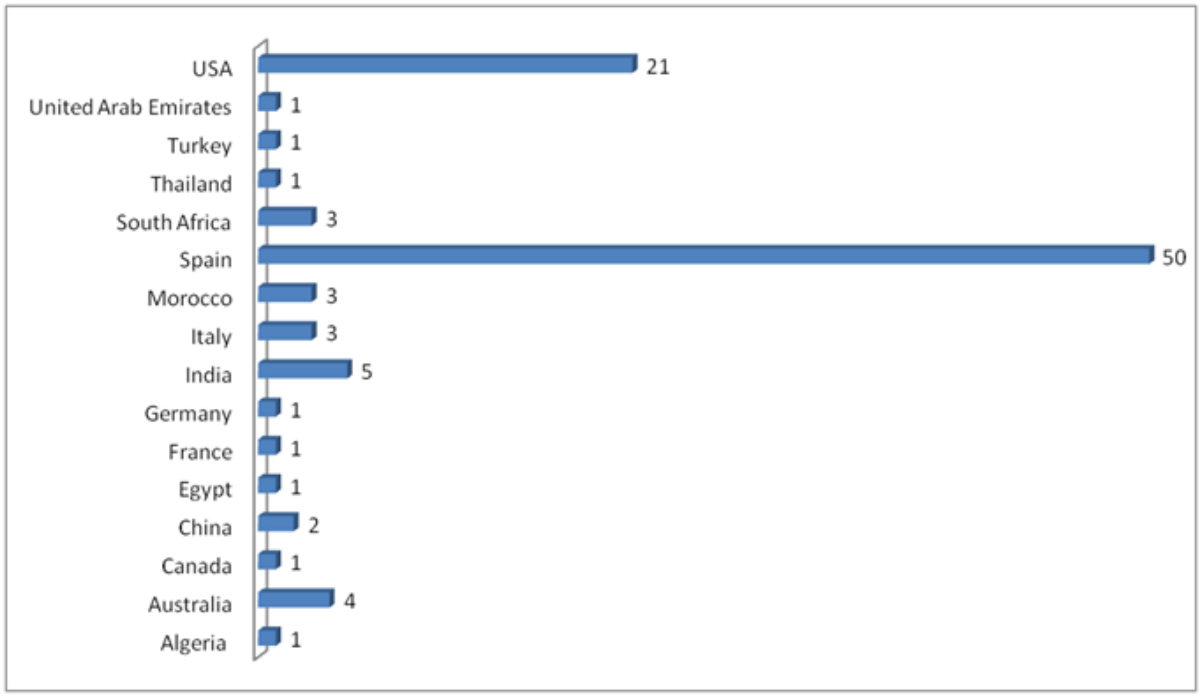

Figure 1.28: Number of operating plants by country [adapted from [1]]

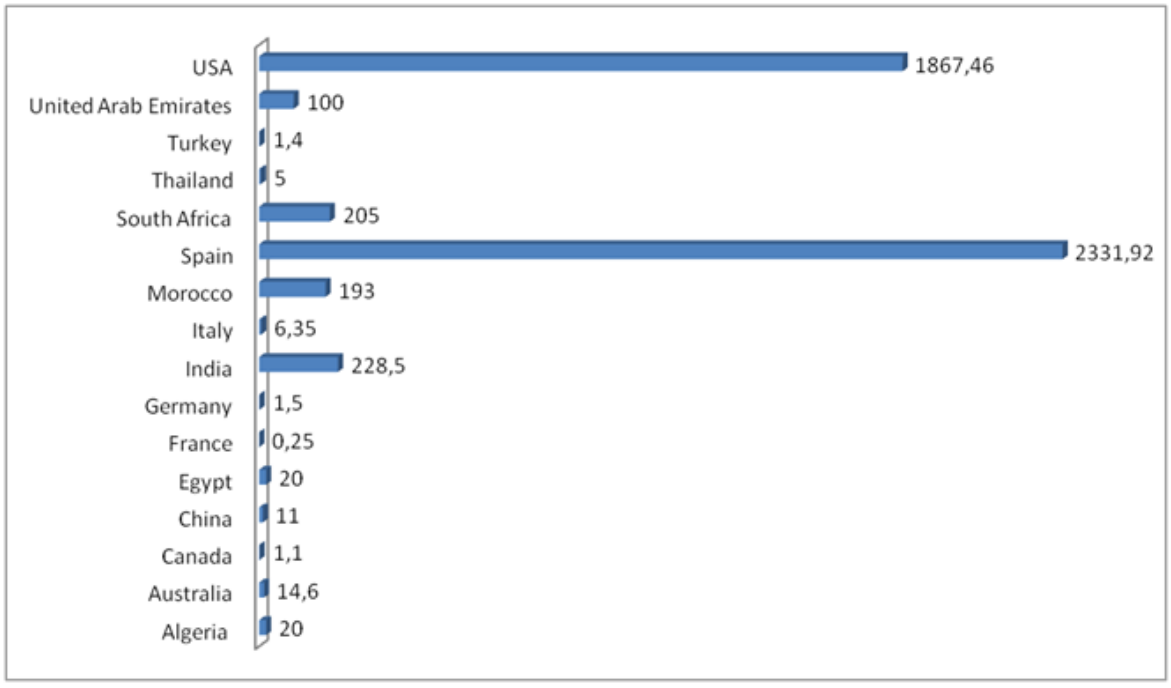

Figure 1.29: Cumulative power output for each country [adapted from [1]]

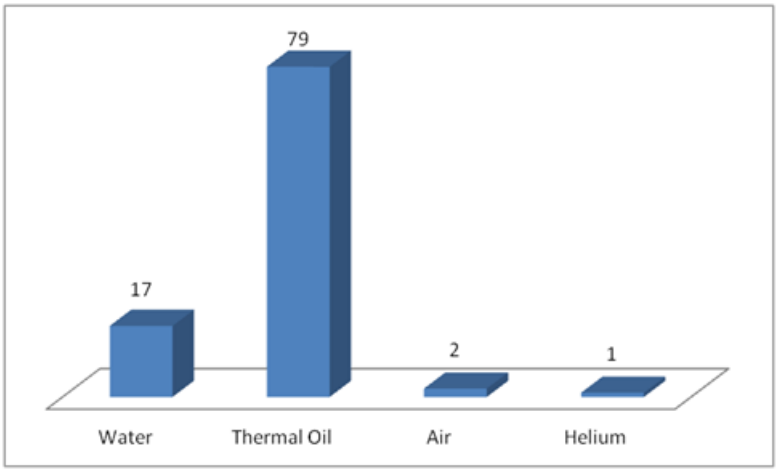

Figure 1.30: Number of operating plants in which a certain HTF is applied [adapted from [1]]

Storage technology	2-tank indirect	Other
n of plants	31	21

Table 1.1: Storage technologies [adapted from [1]]

A comparison between the four different technologies has been carried out by different authors in terms of performance parameters, consumption of natural resources and various elements of cost. The following table 1.2 reports various items as found in different articles (mainly [10],[6],[19],[33],[28]); the analyzed parameters are:

- annual solar-to-electricity efficiency;
- peak solar-to-electricity efficiency;
- annual capacity factor;
- concentration ratio;
- operating temperature;
- land use;
- water consumption for wet or dry cooling;

- cost per kWh for generating 100 MWe at two different DNI values.

Technology	**PTC**	**LFR**	**ST**	**PD**
Annual solar-to-electricity efficiency [%]	11-18	8-13	7-20	12-26
Peak solar-to-electricity efficiency [%]	14-27	18-22	20-35	20-31.25
Annual capacity factor [%]	25-43	22-70	55	25-28
Concentration ratio [-]	15-80	10-100	150-1500	100-1300
Maximum temperature [C]	300-550	250-300	250-680	120-1500
Land use [$\mathbf{m^2/MWh/yr}$]	6-8	4-6	8-12	8-12
Water for wet/dry cooling [$\mathbf{m^3/MWh}$]	3-4/0.3	3-4/0.2	3-4/0.2	0.05-0.1
Cost at 2000 kWh/m^2/yr [€/kWh]	0.187-0.265	0.230	0.200	-
Cost at 2500 kWh/m^2/yr [€/kWh]	0.163-0.210	0.200	0.200	-

Table 1.2: Comparison of different parameters of the four PTC technologies

In table 1.2 the parameter values are limited by the lowest and higher numbers found in literature; on the last two rows showing the costs of energy for PTC, the lowest value represents the cost with a storage included, while the higher is obtained without a storage. Both the costs estimated for the solar tower include storage, while no data are available for parabolic dishes.

Very similar ranges for the abovementioned parameters have been found by different researchers; since LFR and PD are not yet mature technologies, there are less information available on their performance. As seen in table 1.2, efficiency values (both annual and peak) are almost on the same range for PTC and ST; LFR are less efficient than the others and PD show the highest values: as already said, this can be explained with their peculiar design, in which the power conversion unit is closer to the solar receiver and absorber than in the other technologies. It should be also noted that PD are still in an experimental stage. The presence of a storage have a great influence on the capacity factor, which increases, and on the cost of electricity, which is reduced. According to [CSP], there is an optimum capacity for the storage that depends on many conditions, which are site-specific (plant size, technology, fluid applied) and also depend on the electricity market.

An adequate size should be found in order to counter balance the storage system's investment cost. Apart from the storage presence, the electricity cost also depends on the available DNI on an inversely proportional trend. The values of the operating temperatures and concentration ratios have already been discussed in the previous sections; the ranges of temperature are very wide in some cases because of the possible use of different thermal fluids. PTC and LFR require a smaller area than ST to produce a given energy output; Zhang et al [33] gave a qualitative comparison of the land use for the four technologies, and stated that PD have the smallest requirements. The discrepancy with the value in the table may come from the fact that, other than being in the experimental stage, PD are modular so it can be difficult to establish a single value. The water consumption refers to the condensing method of the power cycle: this is an important parameter to estimate because CSP plants are usually installed in arid areas, where water availability can be an issue. Dry cooling reduces the consumption but is also less efficient; PD do not require water for the engine, but only for mirror washing.

1.11 Conclusions

Concentrating solar power is a relatively new renewable technology, which gained interest during the Oil Crisis in the 1970s. It is a thermal solar source in which mirrors collects direct irradiance and focus it on a receiver. In the receiver, an appropriate fluid absorbs the heat and transfer the energy, directly or indirectly, into a power conversion block (which is commonly a Rankine cycle, but other systems can be installed). A storage system can be included in the plant. The irradance can be collected with two methods: with line focus systems (Parabolic Troughs or Linear Fresnel Collectors) or with point focus systems (Solar Towers and Parabolic Dishes). Concentration ratio is defined as the ratio between the reflectors' area and the receiver's area, and it presents higher values in the point focus technology. Parabolic trough are the most mature and diffused plants; Fresnel collectors systems show a lower efficiency than PTC but lower costs; solar towers allow to reach higher temperatures than the previous technologies;

parabolic dishes are still in an experimental stage. In table 1.2, different performance and cost parameters are listed for the four technologies. Since CSP is a relatively recent field, its costs are expected to decrease with increasing experience, leading to a lower investment risk and better performance. New CSP installations can raise the renewable electricity share in the market, serving as baseload powerplants.

Chapter 2

Concentrated solar power hybrid plants

CSP plants represent an opportunity to increase the share of solar generated electricity in the total production in those areas where a sufficient annual radiation is available. As seen in the previous chapter, this technology is not yet widely known and applied, but several test facilities proved its potential and feasibility and the interest in this field is increasing. In order to facilitate the diffusion of concentrated thermal solar in the energy generation systems, and thus realizing a transition from fossil fuels to renewable sources, it is possible to hybridize the solar field with a conventional or non-conventional power plant: in such a configuration, the solar section and the power generating block share a certain amount of components, depending on the desired level of hybridization. This chapter is focused on the studies on hybrid solar-conventional plants: the purpose is to provide a small review summary of the main results, in particular for coal plants hybridizations.

2.0.1 Integration approaches

Most hybrid CSP plants are PTC coupled with a gas turbine combined cycle (integrated solar combined cycles, or ISCC); other possibilities for the non-solar section are coal-fired, biomass and waste, geothermal and wind plants. The prin-

ciple on which these systems are designed is the sharing of equipment, which leads to a lower cost, since (except for wind power) these components are mostly the Rankine-cycle ones, which are mass produced and mature, and there is also the possibility of retrofitting an existing plant. The effects are a higher load factor compared with the one obtainable in CSP only, a reduced financial risk, an extension of the suitable locations for the solar plant (in terms of lower acceptable DNI) and an installation closer to the load ([34], [35]). Often, hybrid plants are described with the solar share parameters, which is the percentage of the CSP rated power with respect to the other technology's rated power.
The integration of solar energy can be realized to follow one of these two approaches: fuel saving (FS) or power boosting (PB). In the fuel saving mode, the additional input is used to reduce the fuel consumption rather than to increase the power output, which is maintained constant. In the power boosting operation, the goal is to increase the plant's output, employing the solar input along with a fixed fuel mass flow rate. Another element to consider is the state of the plant: if the model describes a new project that has yet to be installed, the assessment is called a green-field analysis, while if the plant is already existing and has to be retrofitted with a solar section, it is the case of a brown-field analysis. The main concern with existing plants is the capacity of the components: as will be discussed later, the hybridization with a CSP section implies variations in the mass flow rates, which could fall outside of the operating range of the turbines; the system of equations, in this case, should include the domain conditions related to the critical components.

2.1 Hybridization level and configurations

Peterseim et al. [34] divided integrated solar power solutions plants in light, medium and strong hybrid synergies. Nowadays, medium synergies are the most common, and are characterized by a solar share of about 10%. The solar share of the strong synergies ranges between 30 and 90%. In the same article, the possibilities of hybridization are listed; in general, the contribution of the steam generated in the CSP section can be used to heat the feedwater, to reheat steam in the steam

turbine or to provide additional steam at high levels of pressure and temperature. The best CSP technology for a combination with another plant depends on the way the hybridization is realized, and on the site's conditions [35]. CSP can be combined with coal plants, but the effectiveness of this solution depends on how old the existing plant is. When coupled with natural gas combined cycles, the CSP can provide additional saturated steam to the high pressure drum in the heat recovery steam generator (HRSG), directly to the high pressure section of the steam turbine or it can heat the feedwater. Combination with biomass plants has been tested in one plant and is best suited with solar towers, which could be installed close to agricultural or urban centres. The hybridization with a geothermal plant can bring a consistent cost reduction since both geothermal and concentrated solar are expensive renewable sources. The CSP section can raise the temperature of the geothermal steam production. The advantage of coupling a solar power plant with a wind energy plant comes from the generally higher power yielded by the wind turbine during nights: the CSP can bring benefits to the load matching.

2.2 Concentrated solar power hybrid plants in literature

In this section, some articles focusing on the topic of integrating conventional power systems with a solar field are summarized. Size of the plant, type of synergy, analysis method and results are the main highlighted features for each of the considered paper (when details are available). The reviews are listed by the kind of plant they focus on: multiple plants, integrated solar combined cycles, coal fired power plants and other systems (including solar towers or parabolic trough fields integrated with a gas turbine, organic Rankine cycles and absorption chillers).

2.2.1 General researches on different plants

Peterseim et al.

Peterseim et al. [35] conducted an assessment aimed at finding which CSP technology would be best suited to be hybridized with a certain application; different professional figures were interviewed (such as researchers, plant operators, consultants and technology providers) and selection criteria such as feasibility, risk reduction and impact reduction were assigned or the plants possibilities. Different synergy options have been taken into account, such as feedwater heating, high pressure steam generation and others. The article then reports the possible combinations of CSP technology and synergy, which have been evaluated with a score. A general conclusion is that linear focusing systems are better suited when temperatures lower than 400C are required, while for higher values point focusing technologies are preferable. Another important observation is that the maturity of a given technology has a strong influence in the choice of the solar plant.

Libby et al.

An extended analysis on DSG application has been carried out by Libby et al. ([36]), who evaluated the possibility to hybridize existent coal plants and natural gas combined cycle plants located in southern U.S. Countries. In the hybrid project, high pressure feedwater is extracted and evaporated in line or point focus solar systems, which all use water as thermal fluid. The authors also compared DSG with thermal oil and molten salts. The results show that applying the DSG strategy the solar conversion efficiency is increased; for the combined cycles, the solar thermal input is similar for all the considered technologies, while for coal plants the input is more consistent when DSG is applied. From a thermodynamic point of view, solar towers are the best CSP technology, but each retrofit project has to be designed depending on the site's characteristics.

2.2.2 Researches on Integrated Solar Combined Cycles

Giuliano et al.

Giuliano et al. [37] analysed different configurations of solar hybrid plants and provided a comparison between the different layouts and a traditional combined cycles. The authors considered five layouts: solar tower for pressurized air heating before the combustion chamber in the gas turbine or for steam generation (with a CO_2 tower case), and PTC for steam generation. All of the considered hybrid options include a burner, which allows the plant to be operated with solar-only input, fossil-only input or a mixture of both. Three storages situations were evaluated for each plant: no storage, 7.5 hours and 15 hours storage. They conducted a numerical analysis, and the simulations were carried out for baseload operation (8760 h/year) and midload operation (6205 h/yr).

The results of the simulations show a higher solar share when the solar field's size and storage increase. The maximum solar share obtained for base-load operation was found to be 74,1% for the solar tower with molten salts and bigger storage. For the mid-load case, higher values were found; in both cases, the fossil fuel contribution was essential to provide the continuous generation. When compared to the traditional combined cycle, the smaller plants with low power block efficiency and low solar share and storage showed no reduction in CO_2 emissions; a reduction up to 68% is obtained on the other hand for larger fields with storage. The emissions are inversely proportional to the solar share and the power block efficiency. The issue highlighted by the authors becomes apparent when CO_2 reduction and LCOE are considered at the same time: the layouts which enable the highest CO_2 reduction also have the highest cost of energy, and vice-versa. None of the studied options brought advantages in both emissions and costs. Since the solar fuel is currently more expensive than conventional sources, the authors assessed the possibility of carbon trading costs and provided the breakeven points already discussed in section 1.9) at the same LCOE of a combined cycle.

Manente et al.

Manente et al. [38] studied different synergies between a triple pressure 390 MW combined cycle and PTC, LFR, ST plants in order to determine the configuration with the highest solar conversion efficiency. Six layouts were analyzed, in which the steam is extracted from several points of the HRSG and is preheated, reheated and/or evaporated up to different temperatures in a specific CSP plant. The analysis also includes economic and exergetic considerations. The simulations showed an incremental solar-to-electrical efficiency from 46,6 to 50,2% depending on the layout and an incremental solar radiation-to-electrical efficiency around 30% (relative to the layout with the highest solar-to-electrical efficiency). Regarding the specific CO_2 emissions, they were found to be 8.8% lower than in a standalone combined cycle (including the emissions of the solar field life cycle). The best configuration (also based on exergy analysis) is obtained when a fraction of steam from the highest pressure economizer is evaporated in the thermal oil PTC field and then mixed with the remaining steam in the HRSG and superheated. If the goal of the simulation was to reduce the occupied land area, then the ISCC with a LFR solar plant would be preferred.

Zhu et al.

In [39], a 500 MW combined cycle with three pressure levels is integrated with a CSP plant, which provides latent heat for the feedwater, extracted before the high pressure evaporator. The authors found that with increasing solar heat input the steam cycle efficiency and the overall plant efficiency increase. The estimated solar share for 200 MW_{th} is 17%; given a certain solar input, the solar conversion efficiency is lower at higher ambient temperature. The components often work at partial load due to the irradiation variability.

Dersch et al.

Dersch et al. [40] compared an ISCC to a traditional PTC plant and to a 310 MW combined cycle; no existing plant is considered, but two different sites were taken into account (California and Spain). The solar section provides heat for

evaporation and slight superheating to the feedwater extracted from the high pressure preheater. Two modes of operation were simulated: solar dispatching (in which power is produced when the Sun resource is available and there is no backup burner) and scheduled load (power is produced to follow a specific energy demad, so a burner is included). The former mode is more sensitive to the irradiation variabilty and shows a higher solar share (up to 10% if the plant is located n California). Lower CO_2 emissions are obtained with the ISCC configuration.

Ancona et al.

The object of this research ([41]) is a 30 MW combined cycle integrated with a LFR plant whose size is determined by the simulation. The selected site is in Bologna, Italy. The solar plant supplies heat to the heat recovery steam generator in three possible configurations: the feedwater is extracted after the high pressure economizer and then evaporated, or extracted before the economizer, preheated and evaporated, steam is generated in the solar field and sent to the HRSG superheater. In the simulation, a maximum additional flow rate of 10% is assumed. It has been observed that the third synergy allows a higher power production; the trend of the net efficiency depends on its definition: if the CSP contribution is not considered, the third case yields a higher value, otherwise it shows the minimum (efficiency is inversely proportional to the extracted mass flow). From the first to the third case, the required solar field size increases.

Baghernejad et al.

The combined cycle illustrated in [42] is composed by two 125 MW gas turbine and two HRSG with two pressure levels. The hybridization is realized with a 17 MW PTC field in Iran. The solar section provides part of the high pressure evaporation phase. Exergoeconomic analysis has been carried out to evaluate the maximum exergy efficiency and minimum cost. The authors demonstrated that the highest exergy losses are associated to the condenser, followed by the high pressure evaporator; the collector field shows the highest O&M costs.

Kelly et al.

Kelly et al. ([43]) worked on a 244 MW combined cycle located in California. The considered synergy options are: feedwater extraction and evaporation, evaporation and superheating, use of the solar heat to periodically heat the exhaust gases from the gas turbine. The simulation set an operating time of 8760 hours. The conlusions report that the preferrable configuration is the one in which the solar field provides heat for the feedwater evaporation. When the solar input increases, there is a decrease in the efficiency due to the higher temperature difference in the heat exchange process. The conversion efficiency reaches values up to 40-42% with a 2% solar share and 32-35% with a 9% solar share. The authors state that an ISCC is convenient for solar shares lower than 10%.

Horn et al.

In their article, Horn et al. ([44]) compared two different ISCCs: a one pressure level combined cycle is coupled with either a 90 MW PTC plant or a 80 MW solar tower. The location is in Egypt. In the former system, the solar field generates additional stema, in the latter it heats the exhaust gases entering the HRSG. The analysis focuses on economic aspects and compares the hybrid systems to a traditional combined cycle. A solar share of 9/8.2% respectively is obtained, and a reduction of about 600 thousand ton/CO_2 is estimated for the hybrid plant (in 25 years).

Rovira et al.

The main goal of this research ([45]) is to compare the use of direct steam generation (DSG) and heat transfer fluids for ISCC systems. The analysis is based on a 110 MW combined cycles (2 pressure levels) with a PTC field, whose size is either fixed at 50 MW or variable. A total of eight layouts (four for each of the fluid options) have been considered: feedwater extracted from the high pressure economizer and evaporated in the CSP or evaporated and superheated, feedwater extracted from the degasser, preheated and evaporated or preheated, evaporated and superheated. At a fixed size of 50 MW for the PTC section, the configura-

tions with the best performance are the ones with evaporation and superheating, but they also required a higher value of the product of area and heat transfer coefficient of the exchangers. The lower collectors' aperture area is found for the DSG evaporation synergy (this configuration is preferrable when the area is fixed as well). The main sources of irreversibility are the condenser and the receiver; the worst options are the ones which include the preheating, because of a poorer thermal matching. Use of thermal oil is hindered by the required additional heat exchanger.

2.2.3 Researches on other plants

Vogel et al.

In this paper ([46]) the researchers studied the effects of hybridization on the Shams One CSP plant (solar tower technology, located in the United Arab Emirates). In this case, the exhaust gases from two gas turbines supply heat to one of the high pressure preheater before the power block; an additional burner is included. The simulation considers an on-off operation of the turbines (no partial load). The results show an increased annual power production compared to the base case but with a higher fuel consumption. The steam turbine load factor raises, the net efficiency is 3% higher but the solar fraction decreases from 84% to 59%. The LCOE is also smaller, from 216 to 170 €/MW_{el}.

Schwarzbozl et al.

This article ([47]) focuses on a general solar tower plant who is integrated with a gas turbine (three sizes are evaluated: 1.4, 4.2, 16.1 MW); considered locations are Spain and California. The hybrid configuration chosen by the authors is the compressed air preheating before the combustion chamber in the gas turbine. Modular installation of the turbines is proposed; heat provided at different temperatures in inserted in different points of the cycle. The results show a miximum solar share of 70% with a load factor of 40% and an annual solar efficiency up to 19%. A consistent reduction in capital investment is also highlighted.

Turchi et al.

The plant analysed in [48] is a 40 MW gas turbine hybridized with a 100 MW PTC field, located in California. The exhaust gases from the turbine are sent to the preheater. The simulation compares two solar only plants and two hybrids with different solar multiples. The solar share was found to be around 57-59%, with the hybrid solution being more efficient and slightly cheaper that the pure solar one.

Fahad A. Al-Sulaiman

In [49], the author proposes an analysis of an Organic Rankine Cycle to which a PTC section is added. The solar field is used to inject heat in the steam generator of the topping Rankine cycle. Two cases are considered for the condenser: low pressure and atmospheric pressure. The plant is evaluated using exergy analysis and different organic fluids are compared. The solar collectors show the highest exergy losses; condensing at a low pressure allows to obtain a higher exergy efficiency.

Olivenza-Le al.

In this document ([50]) the research is based on the SOLUGAS Project, a 5 MW solar tower plant in Spain. A 4.6 MW regenerative gas turbine uses the solar field to preheat the air before the combustion chamber. The results report that the solar share is inversely proportional to the ambient temperature and the regenerator efficiency. The overall efficiency increases when the ratio between the combustion chamber and ambient temperatures increses, while the solar share presents an opposite trend. For a fixed value of the aforementioned ratio, an increase in the collectors' working temperature leads to a lower efficiency and a higher solar share. Values up to 40% of solar share are obtained.

Ghasemi et al.

Ghasemi et al. ([51]) conducted a simulation on a binary ORC cycle hybridized with a PTC plant. The solar input is used, along with the geothermal energy, to

heat the fluid. The results show an increase in the power production, leading to an annual 5% boost and 3.4% increment in exergy efficiency.

Dmityr Popov

In his article ([52]), the author proposed to use a concentrated solar plant to supply heat to an absorption chiller (Solar Assisted Combined Cycle), in order to refrigerate the air entering the gas turbine. A comparison between SACC and ISCC is presented: an ISCC requires more consistent modifications for a given output, and its efficiency is inversely proportional to the solar input; another disadvantage is partial load operation when the Sun is not available. The SACC configuration on the other hand consumes more fuel, has a lower efficiency than a combined cycle but higher than an ISCC because the heat is used in the topping cycle. It can also be readily applied to existent turbines.

2.2.4 Researches on coal fired power plants

Peng et al.

The conventional plant discussed in [53] is a 330 MW coal fired plant located in China, coupled with a 13.5 MW PTC field. In the chosen hybrid configuration, the solar field acts as an alternative preheater for the feedwater line, working both alone or in parallel with the traditional heat exchanger (only the highest temperature preheater has been selected). The authors modeled the plant in ASPEN and carried out an exergy analysis comparing the hybrid plant with a solar only one. The reference for comparison is a CSP plant with the same solar field specifications and capacity.

The new system leads to a better thermal matching in the solar heat exchangers; due to the better components already installed in the coal plant, exergy losses are lower in the power block, but are higher in the collectors because of the lower average temperature of heat tranfer from sun to thermal oil. Exergy losses in the feedwater preheaters are also higher in a solar hybrid plant, because of the higher temperature difference between extracted steam and feedwater. The effects of varying irradiation have been investigated: compared to a solar only power plant,

the exergy and solar-to-electric efficiencies are less sensible to a drop of the available energy source. In a hybrid plant, in fact, the mass flow rate produced by the alternative source is a small fraction of the overall steam mass evolving in the cycle; in the case of a solar plant, the whole amount of steam flow rate is generated by the solar field: when the DNI decreases, the mass drops, and the components will work in off design conditions (with reduced efficiencies).
The resulting annual net solar-to-electric efficiency is 18% for the solar only and 21% for the hybrid plant; the average annual solar-to-heat efficiencies are 52.7% and 55.6% respectively. The capacity factors are 0.223% and 0.238%. The estimated LCOE reduction from solar only to solar-coal hybrid is 20-30%.

ZekiYilmazoglu et al.

The authors ([54]) assess the feasibility to retrofit an existent 44 MW coal plant (in Turkey) with a PTC section. Two synergy options are presented: extraction and superheating of the feedwater, which is then injected in the turbine, and steam generation. Full and part loads are analysed, both in fuel saving and power boosting scenarios. The steam generation strategy allows to increase the power output (+14%), and requires less solar thermal input and collectors' surface. Emissions reduction is obtained in the part load case. A simple payback method economic analysis shows that, without adequate CO_2 taxes, these repowering options would be uneconomical.

Yan et al.

Yan et al. ([55]) report the case of a hybridized coal fired plant, located in China. The synergy consists in the feedwater extraction, which is then preheated by a direct steam generation PTC field. Integration of all the feedwater preheaters is examined (both partial and complete) in a power boosting strategy. The authors concluded that the maximum power increment (+10%) is obtained by substituting completely the highest temperature bled-off steam; this case also yields the highest solar-to-electric efficiency (45.9%). When the solar input increases, more mass flow is expanded in the turbine, therefore generating more power.

Zhai et al.

In their research ([56]), the authors present an exergetic analysis of a 600 MW coal fired power plant integrated with CSP technology; the plant is located in China, and the selected synergy is the highest temperature feedwater preheater replacement. The software used for the simulation is STAR-90. The integration aims at reducing the fuel consumption. The results show a 5.32% fuel reduction compared to the fossil base plant; assuming 3000 operating hours per year, the CO_2 reduction is estimated in 16920 ton/year. The exergy efficiency is lower in the hybrid plant than in the coal plant (from 45.47% to 44.54%, while energy efficiency goes from 47.78% to 46.35%). A sensitivity analysis is carried out for different irradiation values: the solar exergy efficiency drops faster than the energy efficiency when the DNI decreases. The authors also note how the definition of energy and exergy efficiency affects the sensitivity analysis: if the solar contribution is considered free and thus not included in the formulas, the efficiencies increase with increasing radiation. When considering the solar input too, the trend is opposite (but with a smaller slope).

Suojanen et al.

In their article *Modeling and analysis of process configurations for hybrid concentrated solar power and conventional steam power plants* ([57]), the authors analyze three possible synergies for integrating a coal fired plant (located in Morocco) with LFR technology. The hybrid plant is operated in a fuel saving mode. The three possible integration options are: highest temperature feedwater heater replacement, steam injection after the high pressure turbine and before the reheater, and steam injection after the superheater. In the last two configurations, the feedwater is extracted from the deaerator outlet, but the authors state that the extraction point can be at any position in the feedwater line. The results show that in every case the mass flow rates are unbalanced; pressure and temperature at the high pressure turbine outlet increase in the first configuration (consequently less energy is required for steam reheating) and decrease in the other two. In the third case, the flow rate expanding in the high pressure stage

increases: since this stage has the highest isentropic efficiency, the overall turbine efficiency increases. The highest fuel saving is obtained in the third case. Solar shares are respectively 4.8%, 17.6%, 15.6%, and fuel mass flow rate reductions are estimated in 4.5%, 15.9%, 18.1%.

Pierce et al.

A 600 MW coal fuelled power plant is compared to a solar only plant in this article by Pierce et al. ([58]). Both plants have the same specifications and are located in South Africa, but the location selected for the solar only plant has better irradiance conditions. The assessment is carried out with the software SAM on a hybrid solar-coal plant where the solar heat input replaces the bled-off steam from the highest pressure turbine, in power boosting mode. Even though the solar only plant has better site conditions, the hybrid system achieves good performance results: it presents a higher annual solar field efficiency, and yields more power during the year. It also proves to be 1.8 times more cost effective.

Dimityr Popov

The focus of this paper ([59]) is a 130 MW power plant located in Cyprus, integrated with an 8 MW Fresnel collector field. The author states that feedwater heaters replacement is the most mature and practical option for a hybrid plant, preferrable to the partial boiler substitution. He considers the following synergies: low pressure heaters substitution, high pressure heaters substitutions, high pressure heaters and partial economizer substitution (in fuel saving mode). The plant has been modeled in THERMOFLEX. The replacement of the lower pressure feewater heaters is the worst option, as it imposes a large capacity reduction in order to avoid overloading low pressure turbine stages; the last synergy achieves the highest fuel saving and solar heat-to-electricity efficiency, but also the highest land area, with a solar share up to 25%. This solution is best implemented in new plants with a proper economizer design, while the high pressure heaters replacement are well suited for a retrofit. The solar heat-to-electricity efficiency is 17.25%, 34.03% and 39.23% for the three synergies respectively.

Yang et al.

In the article *Research on solar aided coal-fired power generation system and performance analysis* ([60]) different synergies are compared: feedwater is extracted after the deaerator or condenser and mixed with the highest pressure bled-off steam or before the reheater, steam extraction replacements, economizer replacement or combinations of these strategies. The selected base plant is a 300 MW coal fired unit, and simulation is carried out for both thermal oil and DSG parabolic trough collectors. The results show that the instantaneous solar efficiency decreases when lower temperature feedwater heaters are replaced; depending on the thermal fluid, different values are achieved. Due to the different mass balances in the hybrid configuration, the instantaneous solar efficiency reaches a maximum for a certain solar flow rate. The solar heat-to-electricity conversion efficiency appears to be higher when the solar energy is used as a high temperature source, resulting in a higher value in the economizer replacement strategy than in the heaters replacement one.

Zhai et al.

The focus of this research by Zhai et al. ([61]) is a 600 MW coal fired plant located in Tibet. They assume three possible synergies (substituting the three high pressure feedwater heaters separately) and analyze them with or without a thermal storage. Eight operative conditions are considered, depending on the available radiation and solar field's area, and the addition of a storage is also included. They assume solar field areas from 100000 to 600000 m^2, and a fuel saving mode: the simulations are ranked according to the ratio of saved fuel mass and plant investment cost. The results show that increasing the solar field (including the storage) allows to obtain more consistent fuel savings, but the trend slows after a certain area is exceeded (due to larger storage investment costs). For a given area of 100000 m^2, the best synergy is the replacement of the second feedwater heater. If the storage is not included, the fuel saving parameter reaches a maximum for a certain area value and then decreases due to excess heat wasted if larger fields are adopted.

Prosin et al.

In their work ([62]), the authors assess the feasibility of using a solar tower with a solid particle receiver to preheat the combustion air before the combustion chamber. The point-focus solution is compared to feedwater preheating with LFR receivers: in this case, the water extracted from the deaerator is heated to feed the first stage heat exchanger. Different softwares have been used: EBSILON for plant modelling, SAM for LFR performance prediction, HFLCal for the receiver's optical performance prediction. The innovative receiver technology could provide temperatures up to 900C: in order not to excess temperature limits, the preheated air temperature is assumed to be 540C. In the base case, the air reaches 280C by heat exchange with exhaust combustion gases: the hybrid solution adds another heat exchanger between the traditionl air-gas one and the combustion chamber. With the integration, the air ratio has been increased to maintain the boiler duty constant (temperatures at the convective heat exchange surfaces are maintained constant). The case with re-circulation of flue gases is also considered. In both cases, the point-focus technology allows a higher system efficiency than feedwater preheating (40.5% and 39.8% respectively, without re-circulation, 40.9% and 39.9% with re-circulation). The solar share is also higher (11.5% and 10.8% for the two point-focus cases, 5.4% for linear-focus synergy). Stack temperature is lower than the base case in every examined integration. The lowest fuel consuption rate is achieved with particle receiver and re-circulation (-11%). The levelized cost of solar electricity generated by the solar tower is only 59% of the cost found for the LFR option.

Zhao et al.

In the article *Evaluation criteria for enhanced solar-coal hybrid power plant performance* ([63]), the authors provide a method for correctly evaluating fundamental performance parameters. As they point out, integration of an alternative energy source in a pre-existing plant causes a variation from the normal operating conditions, namely different mass flow rates in the components. By considering the equivalent enthalpy drop procedure, which takes into account these modifica-

tions, efficiency formulas become more specific for this kind of integration. Steam extraction efficiency is also introduced. The presented procedure is applied to a series of coal-fired plants with size ranging from 100 to 1000 MW located in China (selected DNI of 600 W/m^2). A PTC solar field with thermal oil is chosen for hybridization (feedwater pre-heating, all heaters are considered); a 30 MW solar-only plant of the same kind is used for comparison (no storage included). Results prove that a higher steam extraction efficiency is obtained at bigger plant sizes or, given a certain size, at higher pressure/temperature. The same tendency is found for net solar incremental efficiency. The relative efficiency improvement decreases as more low-temperature pre-heaters are substituted. A sensitivity analysis is carried out for the first stage pre-heater substitution synergy and with varying radiation: the conclusion is that the hybridization is more interesting in relatively low DNI conditions (in terms of relative solar-to-electric efficiency improvement).

Yang et al.

In this research work ([64]), the authors examine the possibility of replacing bled-off steam flows with solar collectors. The case of vacuum or flat solar thermal collectors is also taken into account to substitute lower temperature feedwater pre-heaters. Regarding the CSP application, the analysed synergy is the replacement of the first stage pre-heater with thermal oil PTC (available temperature 260C). A 200 MW power plant is modeled at design point and simulated both in power boosting and fuel saving modes. The authors point out at the issue of exceeding capacity limits by running the hybrid plant in the power boosting case: for base plants of the considered size, the limit is 220 MW. They also notice how most coal plants in China have been repowered to a bigger size, so this strategy is feasible on such retrofitted plants. The evaluated parameters are: solar-to-electric effciency in power boosting, steam consumption rate (ratio of the steam flow rate in the boiler to generated electric power), heat consumpion rate (ratio of boiler thermal power and generated electric power) and coal consumption rate per kWh of generated electricity. The results show a 9.73% increment in generated power, while the consumption rates decrease by 7.18%, 8.86% and 7.18% respectively. The solar-to-electric efficiency is 36.58%. In fuel saving mode, the coal consumption is reduced

by 6.51%. The consumption rates are slightly lower than the previous case (-6.45%, -8.11% and -6.45% respectively). Solar-to-electric efficiency is not given in this case (due to the chosen definition of the parameter).

Marco Bettiol

A 1000 MW ultra-supercritical coal-fired power plant is the subject of this thesis work ([65]). The integration strategy is focused on the high temperature feedwater line; heat from a PTC solar field with thermal oil is added to the base cycle through various heat exchangers. Both series and parallel configurations are considered in order to find the best placement for the exchangers. The series configuration allows all the feedwater pre-heaters to operate at 100% load even after hybridization, it prevents overloading the turbine stages by maintaining the design bled-off stem flows, and the feedwater can exceed 300C, with the possibility of partial replacement of the economizer load. This case is better than the more common parallel integration, as it improves thermal matching and operational flexibility. Fuel saving and power boosting modes are imposed by the available solar heat: it is therefore possible to achieve a fuel consumpion reduction even when the power output is increased. Fuel saving strategy, on the other hand, results more efficient in terms of exergy analysis and thermal matching of the heat exchangers. On an annual basis, the solar-to-electric efficiency is 17.9% for the fuel saving mode and 15.9% for power boosting mode.

2.2.5 Summary

From the previous review, some general features can be deduced:

- There are two different approaches when it comes to solar hybrid plants, depending on which power block (solar thermal or conventional) is considered as the "main" plant. When the base section is the conventional power cycle, the most frequently examined hybrid configuration is combined cycle integrated with a linear focus solar subsystem. In this field of research, many authors concluded that the best synergy is the extraction of the feedwater (all or part of it) from the Heat Recovery Steam Generator (HRSG) after

the high pressure economizer, thus providing the latent heat with the CSP section. Saturated steam is then sent back in the HRSG to evolve according to the cycle. In other options, preheating and/or superheating are also included. The solar section can also generate steam to send in the HRSG turbine.

- When the integrated CSP technology is a solar tower, the most adopted design implies the preheating of the air entering the gas turbine's combustion chamber.

- When a CSP field is going to be added to a coal fired power plant, the solar heat input can replace the steam extractions from the turbine stages.

- In the cases where the focus is on the concentrating solar plant, a common way to include a conventional plant section is to add a gas turbine whose exhaust gases are injected in the existent system.

- Most of the articles highlight the importance to evaluate performance parameters before and after hybridization: one of these indicators is the solar share (or solar fraction), which is representative of how much the solar input contributes to the power output:

$$F_{solar} = \frac{Q_{CSP}}{P_{net}}$$

A different definition of solar share is used in [57], where the same parameter is calculated for thermal output and inputs (thermal solar share).

- Generally, the highest solar share values are obtained in point focus technologies (40-70%), while for hybrid plants applying PTC and LFR the range is lower: 10-20% when the pre-existing plant is conventional, 60% if the addition is made to a CSP plant. The solar-to-electric conversion efficiency is in most cases higher than the one for a solar only plant; most researches evaluated efficiencies up to 40-60%.

- An advantage over traditional fossil plants is the CO_2 emissions reduction, while a favourable aspect over pure CSP systems is the reduction in capital costs and LCOE.

2.2.6 Summary for coal-solar hybrid plants studies

Since the focus of this work is to evaluate the performance of an integrated coal-solar power plant, general results and issues about this category analysed in the previous articles are discussed more in-depth in this paragraph. The following table 2.1 shows which article analyses a certain synergy.

Synergy	Article
Last PH	[53], [56], [57], [58], [60], [62], [64]
All high temperature PHs (togheter or separately)	[54], [55], [59], [63], [61], [65]
HP introduction	[54], [57]
IP introduction	[57]
Other	[62], [59], [60], [65]

Table 2.1: CSP-coal hybrid power plants synergies found in literature.

In the majority of the reviewed articles, the integration is located in the feedwater line. In traditional Rankine cycles, feedwater pre-heating leads to better efficiency at the price of reduced mass flow expanding in the turbines: if the condenser temperature is fixed, the cycle efficiency only depends on the average mean temperature of the positive heat exchange with an external source (combustion). This temperature raises proportionally to the feedwater temperature at the boiler inlet, since the part of low temperature pre-heating would otherwise be provided by the boiler ([66]). By replacing one or more pre-heaters with the solar contribution, this synergy allows to recover the steam "lost" for pre-heating while maintaining the regenerative configuration provided by a renewable energy source. When the power plant is operated in a fuel saving mode, this positive effected can be deduced by a reduction of the fuel consumption: less input is required to produce the same power output (see table 2.2). In a brown-field scenario, it is essential to consider both off-design behaviour and restraints of the components, in order to avoid insufficient performance or exceeding capacity limits.

The coupling between concentrated solar power and high temperature feedwater pre-heaters is also favoured in terms of thermal matching: the closer the tempera-

tures of the fluids are, the higher the heat exchange efficiency becomes. Therefore, the temperature achievable with CSP technologies is particularly suited to this application. Achieving an optimal thermal matching is the main reason why many researchers exclude integration with low temperature pre-heaters.
Another examined integration consists in producing steam in the solar field, which is then added to the cycle flow before the high or intermediate pressure turbine. In this option, the boiler load is reduced, as the flow rate evolving in it is lower than its design value. As stated by Suojanen et al. ([57]), water can be extracted from any location in the feedwater line: the most common point is after the deaerator.

Parameter	**[53]**	**[54]**	**[55]**	**[56]**	**[57]**	**[59]**
Power output [MW]	330	44	200	600	120	130
Fuel use [kg/s]	n.a.	4.3	n.a.	257.4	22.5	8.24
DNI [W/m^2]	700	506.8	n.a.	925	800	860
CSP area [$*10^-3$**m^2**]	71	35-52	n.a.	11	n.a.	170-280
Solar input [MW]	13.5	11-15	35	n.a.	16-60-40	39-68
eta$_{\text{solar to electric}}$ [%]	27.3	n.a.	45	46.35	n.a.	17-39
DELTA$_{\text{fuel}}$ [%]	n.a	14	n.a.	5.32	4.5-15.9-18.1	2.11-4.67
DELTA$_{\text{power}}$ [%]	n.a.	14	10	n.a	n.a.	n.a.

Table 2.2: CSP-coal hybrid power plants literature results summary. Multiple values for a parameter indicate more than one synergy options. "n.a." means the information is not available.

Parameter	**[61]**	**[62]**	**[63]**	**[64]**
Power output [MW]	600	750	100-1000	200
Fuel use [kg/s]	42.9	58.1	n.a.	12.325
DNI [W/m^2]	n.a.	2006.3	600	n.a.
CSP area [$*10^-3$**m^2**]	variable	39	n.a.	n.a.
Solar input [MW]	n.a.	95-20	n.a.	n.a.
eta$_{\text{solar to electric}}$ [%]	n.a.	13.9-22.3	24-28	36.58
DELTA$_{\text{fuel}}$ [%]	7	4.13-11.5	n.a.	-6.45
DELTA$_{\text{power}}$ [%]	n.a.	n.a.	n.a.	+9.73

Table 2.2: (Cont.) CSP-coal hybrid power plants literature results summary. Multiple values for a parameter indicate more than one synergy options. "n.a." means the information is not available.

The issue in some of the articles included in the review is the lack of a thorough off-design performance evaluation: unless the plant is new, the addition of a solar heat exchanger causes modifications to the system. The mass and energy balances at design condition are influenced by the new component, and have to be verified in order not to exceed capacity limits. When the working point of the components is far from design condition, components' efficiency drops: if this aspect is not considered, the results of integration could be limited and incomplete. From this review, the most promising way to include the solar input in a coal power plant is acting on the feedwater preheaters. In a fuel saving operation, a reduction of fuel consumption of about 5-10% could be obtained in the case study, in accordance with the literature results. Solar-to-electric efficiency values vary in a wider range: this could be influenced by level of hybridization, plant configuration, type of analysis and also by the definition of the parameter itself. It is reasonable to expect a value of this efficiency around 15-20%, depending on the case. Steam generation is also a common hybridisation strategy.
The purpose of this paper is to provide a comprehensive analysis of these hybrid plants: the coal plant model includes off-design evaluation, and from this starting point various integration strategies will be analysed. For each of them different

compatible CSP technologies will be compared, and the amount of solar input will vary in order to evaluate the solar field's area and to highlight different effects on the power plant.

2.3 Conclusions

The solar integration is a promising solution for traditional power plants, as it allows to reduce the amount of fuel consumption or, alternatively, to boost the power generation without increasing the power input from the fossil source. It brings advantages also to solar only plants, as a section which does not depend on the available solar radiation raises the load factor of the renewable plant. For this reason, many studies are focused on this subject.
Most frequently, the traditional power systems which are integrated with CSP are combined cycles (Integrated Solar Combined Cycles, ISCC), where the possible hybridizations consist in heating part of the feedwater with the solar radiation or preheating the exhaust gases at the gas turbine outlet. Regarding coal fired power plants, which are the selected systems for the case studies presented in the next chapter, most of the authors concluded that the most effective synergy is the high temperature feedwater heaters replacement. This can increase the amount of steam expanding in the turbine, while maintaining the positive effect of regeneration. Another frequent option is steam generation, in which water is evaporated in the solar field and sent to a turbine stage (high or intermediate pressure). Some issues that can occur after the integration are related to the base system's modification, because the normal operating conditions of the components can be altered significatively when the solar input is added.

Chapter 3

Case study: application to a coal-fired power plant

After summarising the different CSP technologies and their hybridisation options with traditional power plants, a case study is carried out for a coal power plant, with the purpose of identifying the best integration strategies for this particular system.

A model is built in the software EES to simulate the plant, starting from experimental data used as references. Systems of equations are reported in section 3.3 for each single component, differentiating between dependent and independent variables. The power plant used as a reference for the case study is the Enel coal fired plant *Andrea Palladio*, located in Fusina (Venice). A model for this plant has already been presented in the thesis work *Modello di simulazione di un impianto termoelettrico da 320 MW* by Denis Sasso ([67]). For the purpose of the present study, the previous model has been simplified and adapted in order to include the solar integration, which produces modifications to the original system.

In section 3.6 the integration options considered in this work are presented and the assumptions for building their models are explained. The variables relative to the solar section and the parameters necessary to evaluate its performance are defined in section 3.6.1. The first comparison between all the solutions shows different efficiency parameters: the conversion efficiency from primary sources, the solar radiation-to-electric and solar heat-to-electric efficiencies. A selection is

made between the twelve proposed options, and more considerations are presented for the remaining four integration strategies. A simplified analysis is carried out to evaluate the performance over a year for one integration option.

3.1 Reference works

As already mentioned, the main reference for the model examined in this paper is a thesis work by Sasso (1999/2000, [67]), in which experimental data have been used to build the equation system with the software EES. Measurements for full-load and five part-load conditions are presented; some of these values have been included in *Lookup Tables*, tables used in EES which contain data that can be called in the model by means of the command *Interpolate*. In the design model, most of the variables are given as function of the mass flow rate entering the deaerator (which has been selected to represent the load): if this mass changes, the output value of the desired variable is found with a linear intepolation between the values in the *Lookup Table*. In the off-design equation system, variables are generally given as a function of the mass flow rate entering the correspondent component. The lowest assessed load is 40%.

Compared to this reference, some modifications have been introduced to adapt the system to the solar integration. As said, most of the independent variables found in the reference model are related to the deaerator inlet mass flow: this approach is adequate if the system and its components remain unchanged, which is not the case if a CSP contribution is included. The issue is that after the integration, some flows may be redirected or added to certain points, and thermodynamic states may change: the cycle is therefore different from the coal-only base plant. In order to conceptually separate each component, those variables have been related to the mass flow rate entering that component, as has been made in the off-design reference model: with this approach, each subsystem works independently from the others.

A different, more recent reference has been used for the turbine stages and expansion line of the same power plant. These data have been kindly made availabe by Eng. Enrico Grigolon, and they include all the design parameters of the turbine

stages (intensive and extensive variables) and some off design values for high and low pressure stages ([68]).

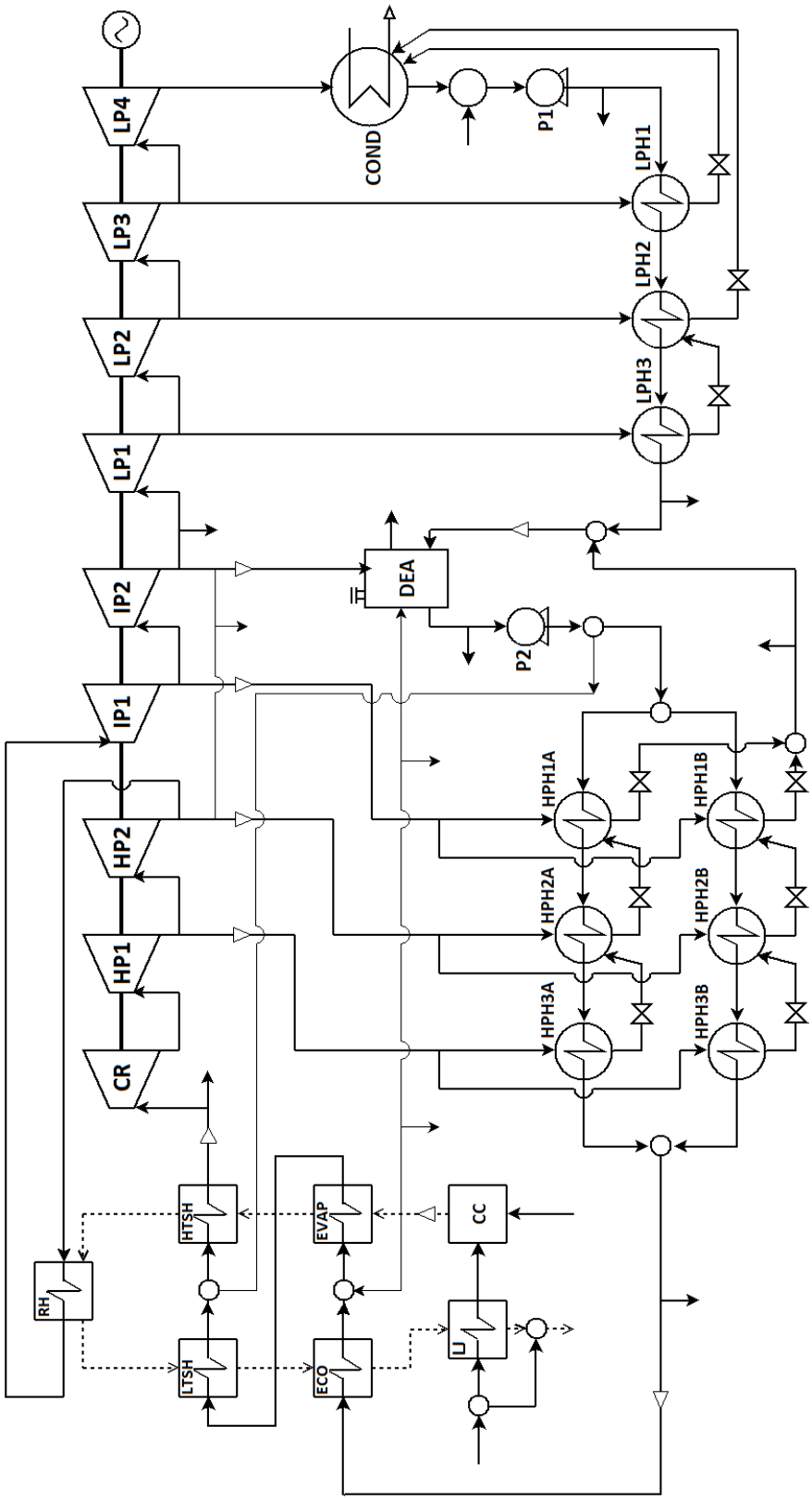

Figure 3.1: System flow chart (components)

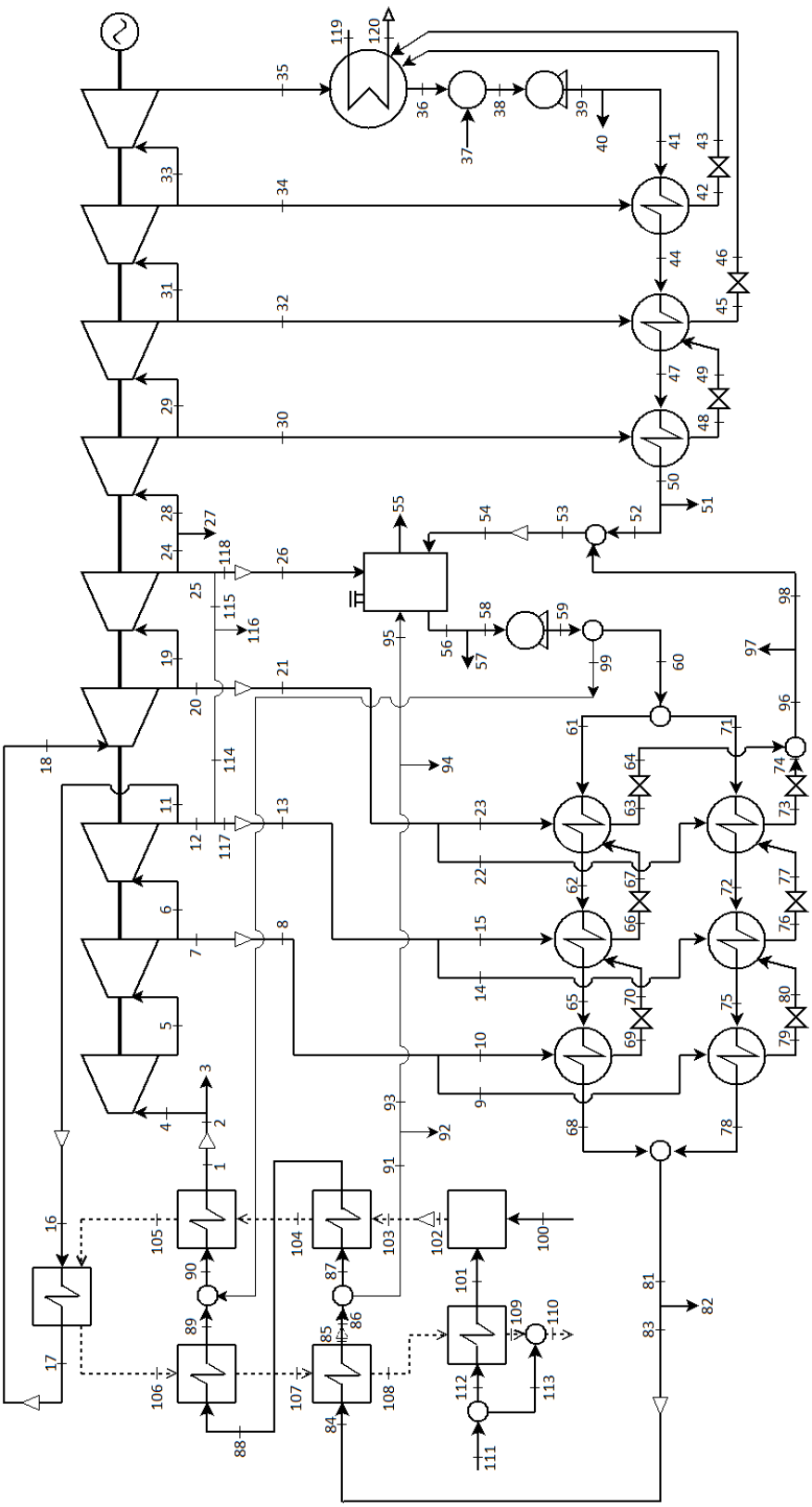

Figure 3.2: System flow chart (points)

3.2 Model building process

The system's flow chart is similar to the real power plant layout used in [67], but it has been slightly simplified (fig. 3.1 and 3.2). Especially in the high and intermediate pressure turbine stages zone, the mass flow rates in the original scheme are divided and redirected to other points. The path chosen in this case study is simpler, in order to work on a more standard flow chart and to generalize the integration results. In the reference, there are a few mass flow rates which accounts for steam or water losses throughout the plant, and are integrated back into the system after the condenser. These losses, whose entity is negligible compared to the overall mass flow rate, have not been considered here. The tempering water extracted after the feedwater pump and enterin before the high temperature superheater has ben maintained, since it is a consistent amout of water (approximately 10% of the flow rate at the turbine inlet).
Both the reference works provided data for building the system of equations: the turbine sections comprising of turbine inlet and outlet points and steam extractions follows the more recent data, while the feedwater line and boiler is based on the measurements in [67]. It is important to notice that the two references present some small differences. The methods applied for each subsystem are discussed more in detail in the following paragraph.

3.3 Power plant modelling

Each component of the power plant is described by a set of equation such as mass and energy balances, thermodynamic properties of the working fluid, and performance relations. To solve these models, some variables have to be fixed: these are called independent variables, and their number is equal to the total number of variables minus the number of equations.
Independent variables can be system variables, which are fixed parameters valid for the whole assembly of components, or local independent variables, which must be known to solve a single component, but in the overall set of equations are actually dependent variables. For example, in the turbine stage model the inlet and

outlet pressure are set as independent variables in order to find the mass flow rate expanding in the component: when the turbine is included in a complete power plant model, with the exception of the first stage inlet and last stage outlet, all the other pressures are dependent variables. The isentropic efficiency at design condition is, on the other hand, a system independent variable since it is a constant relative to that particular stage.

The components' models are presented in the following paragraphs. The numbers of equations, dependent and independent variables as well as the distinction between system and local independent variables are highlighted. The process behind the choice of independent variables and the methods applied to find the off-design performance for each subsystem is explained in the correspondent paragraph. Some variables, such as isentropic efficiencies or densities, are marked with a generic i because in the overall model they have been numbered differently from the corrisponding number of the fluid state.

In the following sections, when a thermodynamic property has to be calculated, the EES syntax has been maintained: the name of the desired property is followed by the fluid (steam in this case) and two known variables.

The complete model for the base coal-fired plant is reported in APPENDICE 1.

3.3.1 Turbine stage with extraction

The modelled power plant includes nine turbine stages (see figure 3.1: an initial action stage (CR), two high pressure (HP1, HP2), two intermediate pressure (IP1, IP2) and four low pressure (LP1, LP2, LP3, LP4) stages. The steam extraction is present in each stage except the first and last one: for these two, $\dot{m}[3]$ should be removed from the system.

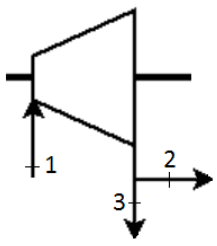

Figure 3.3: Turbine stage.

This model is composed of 16 equations and 23 variables. The 7 independent variables are:

System	Y, $\eta_{\text{is,design}}, \Delta h_{\text{is,design}}$
Local	p_1, p_2, $\dot{m}_1, T_1$

Table 3.1: System and local independent variables for a turbine stage.

The equations are:

$$h[1] = Enthalpy(Steam; p = p[1]; T = T[1])$$

$$s[1] = Entropy(Steam; p = p[1]; T = T[1])$$

$$x[1] = Quality(Steam; p = p[1]; T = T[1])$$

$$\rho[1] = Density(Steam; p = p[1]; T = T[1])$$

$$h_{\text{is}}[i] = Enthalpy(Steam; p = p[2]; s = s[1])$$

$$\Delta h_{\text{is}}[i] = h[1] - h_{\text{is}}[i]$$

$$\eta_{\text{is}}[i] = \frac{h[1] - h[2]}{h[1] - h_{\text{is}}[i]}$$

$$\eta_{\text{is}}[i] = f(\Delta h_{\text{is}}[i])$$

$$T[2] = Temperature(Steam; p = p[2]; h = h[2])$$

$$s[2] = Entropy(Steam; p = p[2]; h = h[2])$$

$$x[2] = Quality(Steam; p = p[2]; h = h[2])$$

$$p[1] = \dot{m}[1]^2 * \rho[i]^{-1} * Y[i] + \frac{\sqrt{(\dot{m}[1]^2 * \rho[i]^{-1} * Y[i])^2 + 4 * p[2]^2}}{2}$$

$$\dot{m}[1] = \dot{m}[2] + \dot{m}[3]$$

$$j[i] = f\left(\frac{\dot{m}[1]}{\dot{m}[1]_{des}}\right)$$

$$\dot{m}[3] = j[i] * \dot{m}[1]$$

$$P_{\text{m}}[i] = \dot{m}[1] * (h[1] - h[2])$$

To model a turbine stage in part-load operation, the method explained in Cooke's article *On prediction of off-design multistage turbine pressures by Stodola's*

ellipse ([68]) has been applied. The equation which relates the inlet and outlet pressures with the mass flow rate expanding in that stage is:

$$p_{in} = \dot{m}_{in}^2 * {\rho_{in}}^{-1} * Y_i + \frac{\sqrt{(\dot{m}_{in}^2 * {\rho_{in}}^{-1} * Y_i)^2 + 4 * p_{out}^2}}{2} \tag{3.1}$$

The subscript *in* and *out* stand for inlet and outlet, while i indicates the stage number. Y_i is defined as:

$$Y_i = \frac{p_{in}^2 - p_{out}^2}{p_{in}^2 * \phi_i^2} \tag{3.2}$$

Where ϕ_i is the mass flow coefficient, whose value is given in the expansion line's referance data sheet, and its definition is:

$$\phi_i = \frac{\dot{m}_{in}}{\sqrt{p_{in} * \rho_{in}}} \tag{3.3}$$

Y_i has been calculated using design data for p_{in} and p_{out} from the turbine reference. If the turbine stage is considered as a choked nozzle, as it is the case in this method, Y_i remains unchanged in off-design conditions. Consequently, it is here considered as a system independent variable. An exception to this is the first high pressure stage, whose inlet pressure is constant at all loads and the outlet changes; in this case, ϕ_i is variable. Its value has been determined with an equation interpolating the experimental data.

This method suggests to find all the pressures in the expansion lines, either by fixing the final pressure (condensing pressure) or the initial pressure (boiler outlet) and knowing the mass flow rate evolving in the stage. The approach adopted in this work is slightly different: the first and last pressure are fixed, and the mass flow rates are dependent variables.

The equation for the isentropic efficiency is given in Ray's article *Dynamic modelling of power plant turbines for controller design*:

$$\eta_{\text{is}}[i] = \eta_{\text{is,design}}[i] - 2 * \left(\sqrt{\frac{\Delta h_{\text{is,design}}[i]}{\Delta h_{\text{is}}[i]}} - 1 \right)^2 \tag{3.4}$$

This expression can be applied for fixed rotational speed, reaction turbine stages. The design value for the isentropic efficiency and Δh are independent variables found in the reference data. This equation is not adequate to describe the efficiency variation for the first high pressure stage, which is an action stage, and

the last low pressure stage. In these two cases, experimental data have been interpolated to find a more precise equation.
To evaluate the steam extraction mass flow rate, the ratio of this mass to the one at the turbine inlet has been evaluated at different loads. The results have been interpolated with a linear equation:

$$j_i = a * \left(\frac{\dot{m}[1]}{\dot{m}[1]_{des}} \right) + b \tag{3.5}$$

where a is the slope and b is the intercept. To find the equation, design values from the reference turbine data and off-design values from [67] have been used.

3.3.2 Condenser

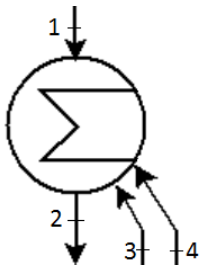

Figure 3.4: Condenser

A simplified model for the condenser is used in this work: the external water does not show up in the mass and energy balances and its inlet and outlet thermodynamic states are not evaluated. It is important to remember, however, that there are restriction on the maximum temperature at which the water exits the condenser. To the purpose of this work, the model has been implemented as follows: the steam quality at the outlet of the component is zero (saturated liquid) and the inlet and outlet temperatures are the same. The condenser also receives the drainages from the first and second low pressure preheaters.The system is made by 5 equations and 10 variables. The 5 independent variables are:

System	x[2]
Local	p_1, $\dot{m}_1, \dot{m}_3, \dot{m}_4$

Table 3.2: System and local independent variables for the condenser.

The equations are:

$$p[2] = p[1]$$

$$T[2] = Temperature(Steam; p = p[2]; x = x[2])$$

$$h[2] = Entahpy(Steam; p = p[2]; x = x[2])$$

$$s[2] = Entropy(Steam; p = p[2]; x = x[2])$$

$$\dot{m}[2] = \dot{m}[1] + \dot{m}[3] + \dot{m}[4]$$

3.3.3 Pump

Figure 3.5: Pump

In the power plant there are two pumps: on for extracting the condensed flow rate after the condenser and one after the deaerator, to raise the feedwater pressure. The model is made by 11 equations and 14 variables. The independent variables are:

System	None
Local	h_1, s_1, $\dot{m}_1$

Table 3.3: System and local independent variables for pumps.

The equations are:

$$p[2] = f\left(\frac{\dot{m}[1]}{\dot{m}[1]_{des}}\right)$$

$$T[2] = f\left(\frac{\dot{m}[1]}{\dot{m}[1]_{des}}\right)$$

$$\eta_p[i] = f\left(\frac{\dot{m}[1]}{\dot{m}[1]_{des}}\right)$$

$$h[2] = Enthalpy(Steam; p = p[2]; T = T[2])$$

$$s[2] = Entropy(Steam; p = p[2]; T = T[2])$$

$$x[2] = Quality(Steam; p = p[2]; T = T[2])$$

$$h_{\mathrm{is}}[i] = Enthalpy(Steam; p = p[2]; s = s[1])$$

$$\eta_{\mathrm{is}}[i] = \frac{h_{\mathrm{is}}[i] - h[1]}{h[2] - h[1]}$$

$$\dot{m}[2] = \dot{m}[1]$$

$$P_{\mathrm{m}}[i] = \dot{m}[1] * (h[2] - h[1])$$

$$P_{\mathrm{el}}[i] = P_{\mathrm{m}}[i] * \eta_{\mathrm{p}}[i]$$

The functions for $p[2]$, $T[2]$ and the electric efficiency are taken from [67]. As the power consumed by the pumps is small compared to the overall production, the model for these components has been kept simple.

3.3.4 Feedwater preheater

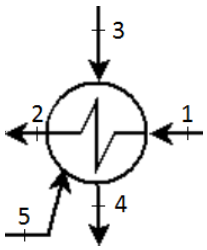

Figure 3.6: Feedwater preheater

In this system, a total of nine feedwater preheaters are present (see figure 3.1): three of them are fed by low pressure steam extractions, the remaining six are divided in two parallel lines which receive the input steam from the two high pressure turbine stages and the first intermediate pressure stage. To simplify the model, in the EES system the two parallel lines are modelled as a single line with doubled mass flow rates: the purpose of the double line is mainly to provide a backup in case of preheater malfunctioning.

A general preheater scheme includes five flows, three inputs and two outputs: the feedwater receives the heat from the steam extraction, which is then condensed,

cooled and expanded in a valve to be sent to the previous heater (or to another point in the cycle). The drainage from the previous preheater can be present. In the model validation step, the model comprises 30 equations and 39 variables (9 independent variables, table 3.4); in the second step it is made by 30 equations and 42 variables (12 independent variables, 3.5):

System	None
Local	p_1, T_1,$\dot{m}_1, p_3, T_3, \dot{m}_3, p_5, T_5, \dot{m}_5$

Table 3.4: System and local independent variables for a feedwater preheater (first step).

System	None
Local	p_1, T_1,$\dot{m}_1, p_3, T_3, \dot{m}_3, p_5, T_5, \dot{m}_5, \Delta T1, \Delta T2$

Table 3.5: System and local independent variables for a feedwater preheater (second step).

The equations (for the simulation step) are:

$$h[1] = Enthalpy(Steam; p = p[1]; T = T[1])$$

$$s[1] = Entropy(Steam; p = p[1]; T = T[1])$$

$$x[1] = Quality(Steam; p = p[1]; T = T[1])$$

$$h[3] = Enthalpy(Steam; p = p[3]; T = T[3])$$

$$s[3] = Entropy(Steam; p = p[3]; T = T[3])$$

$$x[3] = Quality(Steam; p = p[3]; T = T[3])$$

$$h[5] = Enthalpy(Steam; p = p[5]; T = T[5])$$

$$s[5] = Entropy(Steam; p = p[5]; T = T[5])$$

$$x[5] = Quality(Steam; p = p[5]; T = T[5])$$

$$p[4] = p[3]$$

$$h[4] = Enthalpy(Steam; p = p[4]; T = T[4])$$

$$s[4] = Entropy(Steam; p = p[4]; T = T[4])$$

$$x[4] = Quality(Steam; p = p[4]; T = T[4])$$

$$RP = f\left(\frac{\dot{m}[1]}{\dot{m}[1]_{des}}\right)$$

$$p[2] = p[1] * RP$$

$$h[2] = Enthalpy(Steam; p = p[2]; T = T[2])$$

$$s[2] = Entropy(Steam; p = p[2]; T = T[2])$$

$$x[2] = Quality(Steam; p = p[2]; T = T[2])$$

$$\dot{Q}_{\mathrm{c}}[i] = \dot{m}[1] * (h[2] - h[1])$$

$$\dot{Q}_{\mathrm{h}}[i] = \dot{m}[3] * (h[3] - h[4]) + \dot{m}[5] * (h[5] - h[4])$$

$$\dot{Q}[i] = \frac{\dot{Q}_{\mathrm{c}}[i] + \dot{Q}_{\mathrm{h}}[i]}{2}$$

$$\dot{Q}[i] = KS[i] * \Delta Tm, l[i]$$

$$\Delta Tm, l[i] = \frac{\Delta T1[i] - \Delta T2[i]}{ln(\frac{\Delta T1[i]}{\Delta T2[i]})}$$

$$\Delta T1[i] = T[3] - T[2]$$

$$\Delta T2[i] = T[4] - T[1]$$

$$\Delta T1[i] = f\left(\frac{\dot{m}[1]}{\dot{m}[1]_{des}}\right)$$

$$\Delta T2[i] = f\left(\frac{\dot{m}[1]}{\dot{m}[1]_{des}}\right)$$

$$\dot{m}[2] = \dot{m}[1]$$

$$\dot{m}[4] = \dot{m}[3] + \dot{m}[5]$$

The experimental data for the preheaters are taken from [67]. An interpolating equation has been found for both the pressure loss and the temperature differences defining the $\Delta Tm, l$ using the results from the reference model. The equations are function of the feedwater mass flow rate entering the heat exchanger.
The overall exchanged heat is calculated as the arithmetic mean between the heat received by the cold fluid and the heat ceded by the hot fluid: the difference

between these two values has been evaluated and then neglected, since it assumes very small values. The product of the global heat transmission coefficient and the heat exchanger surface can be evaluated as well.

3.3.5 Deaerator

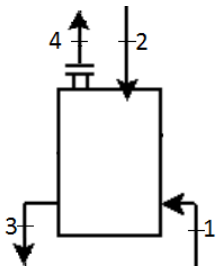

Figure 3.7: Deaerator

The deaerator is a heat exchanger with the purpose of removing air from the feedwater. It is fed by the steam extraction from the second intermediate pressure turbine; the outlet flow's pressure is equal to that of the steam extraction, its enthalpy is calculated from the energy balance of the component and the steam quality is 0 (saturated liquid). There are 10 equations and 16 variables. The 6 independent variables are:

System	x[3], x[4], $\dot{m}_{1,\text{des}}$
Local	$\dot{m}_1, p_2, \dot{m}_2$

Table 3.6: System and local independent variables for the deaerator.

The equations are:

$$p[3] = p[2]$$

$$T[3] = Temperature(Steam; p = p[3]; x = x[3])$$

$$h[3] = Enthalpy(Steam; p = p[3]; x = x[3])$$

$$s[3] = Entropy(Steam; p = p[3]; x = x[3])$$

$$p[4] = p[2]$$

$$T[4] = Temperature(Steam; p = p[4]; x = x[4])$$

$$h[4] = Enthalpy(Steam; p = p[4]; x = x[4])$$

$$s[4] = Entropy(Steam; p = p[4]; x = x[4])$$

$$\dot{m}[4] = f\left(\frac{\dot{m}[1]}{\dot{m}[1]_{des}}\right)$$

$$\dot{m}[3] + \dot{m}[4] = \dot{m}[1] + \dot{m}[2]$$

3.3.6 Combustion chamber

The combustion chamber's model adopted here is taken from [67]. The fuel components's mass fractions are intepolated as functions of the mass flow rate entering the deaerator. The lower heating value is not assumed as a constant because all the Lookup Tables are built from field measurements, and for each of them a sample of fuel is analyzed: different conditions such oxidation and moisture affects slightly the chemical composition, hence the varying heating value. The independent variables assumed in this model are the fuel, air and gas pressure (1 bar) and the inlet fuel temperature is set to 80 C).

3.3.7 Boiler heat exchanger

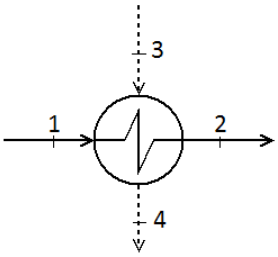

Figure 3.8: Boiler heat exchanger

The heat exchangers modelled here are: economizer (ECO), evaporator (EVAP), low temperature superheater (LTSH), high temperature superheater (HTSH) and reheater (RH). Between the LTSH and the HTSH there tempering water is mixed with the feedwater: its purpose is to control the temperature in this section. The

feedwater receives heat from the exhaust combustion gas. Exhaust gases properties are evaluated with the correspondent procedure. The independent variables change depending on the analysed heat exchanger; for example, the quality at the economizer outlet is 0, and that at the evaporator outlet is 1. The model for the economizer is showed here as an example. The model has 10 equations and 17 variables. The 7 independent variables are:

System	x_2, p_3
Local	p_1, h_1, $\dot{m}_1, h_3, \dot{m}_3$

Table 3.7: System and local independent variables for a boiler heat exchanger.

The equations are:

$$p[2] = p[1]$$

$$p[3] = p[4]$$

$$T[2] = Temperature(Steam; p = p[2]; x = x[2])$$

$$h[2] = Enthalpy(Steam; p = p[2]; x = x[2])$$

$$s[2] = Entropy(Steam; p = p[2]; x = x[2])$$

$$\dot{Q}[i] = \dot{m}[1] * (h[2] - h[1])$$

$$\dot{Q}[i] = \dot{m}[3] * (h[3] - h[4])$$

$$\dot{m}[2] = \dot{m}[1]$$

$$\dot{m}[3] = \dot{m}[4]$$

$$T[4] = f(h[4])$$

3.3.8 Pressure and/or enthalpy loss

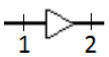

Figure 3.9: Pressure/enthalpy loss

In the reference model ([67]), there are some coefficients for pressure or enthalpy drops, which have been maintained in this case study. After applying the coefficient for pressure and/or enthalpy loss, the thermodynamic state is evaluated again. The following model shows the situation in which both pressure and enthalpy are reduced. The system is composed by 8 equations and 11 variables. The 3 independent variables are:

System	None
Local	p_1, h_1, $\dot{m}_1$

Table 3.8: System and local independent variables for pressure and enthalpy loss.

The equations are:

$$RP = f\left(\frac{\dot{m}[1]}{\dot{m}[1]_{des}}\right)$$

$$RH = f\left(\frac{\dot{m}[1]}{\dot{m}[1]_{des}}\right)$$

$$p[2] = p[1] * RP$$

$$T[2] = Temperature(Steam; p = p[2]; h = h[2])$$

$$h[2] = h[1] * RH$$

$$s[2] = Entropy(Steam; p = p[2]; h = h[2])$$

$$x[2] = Quality(Steam; p = p[2]; h = h[2])$$

$$\dot{m}[1] = \dot{m}[2]$$

3.3.9 Flow divider

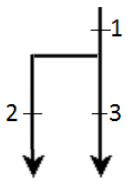

Figure 3.10: Flow divider

In some point the mass flow rate has to be divided, for example in the two parallel lines high temperature preheaters. No losses have been taken into account, so the outlet flows are in the same thermodynamic states. The system includes 11 equations and 18 variables. The 7 independent variables are:

System	None
Local	p_1, T_1, h_1, s_1, x_1, $\dot{m}_2, \dot{m}_3$

Table 3.9: System and local independent variables for flow dividers.

The equations are:

$$p[2] = p[1]$$
$$T[2] = T[1]$$
$$h[2] = h[1]$$
$$s[2] = s[1]$$
$$x[2] = x[1]$$
$$p[3] = p[1]$$
$$T[3] = T[1]$$
$$h[3] = h[1]$$
$$s[3] = s[1]$$
$$x[3] = x[1]$$
$$\dot{m}[1] = \dot{m}[2] + \dot{m}[3]$$

3.3.10 Mixer

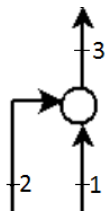

Figure 3.11: Mixer

In this component, two entering flows mix togherter and form one outlet flow. It is assumed, as in [67], that the final pressure equals the lower between the two inlet values. The ethalpy of the outlet flow is evaluated as the weighted average of the inlet enthalpies. The system consists of 6 equations and 12 variables. The 6 independent variables are:

System	None
Local	p_1, h_1,$\dot{m}_1, p_2, h_2, \dot{m}_2$

Table 3.10: System and local independent variables for mixers.

The equations are:

$$p[3] = min(p[1], p[2])$$

$$T[3] = Temperature(Steam; p = p[3]; h = h[3])$$

$$s[3] = Entropy(Steam; p = p[3]; h = h[3])$$

$$x[3] = Quality(Steam; p = p[3]; h = h[3])$$

$$\dot{m}[3] = \dot{m}[1] + \dot{m}[2]$$

$$\dot{m}[3] * h[3] = \dot{m}[1] * h[1] + \dot{m}[2] * h[2]$$

3.3.11 Lamination valve

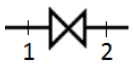

Figure 3.12: Lamination valve

These valves are used to reduce the pressure of the fluid; in this model the inlet and outlet flows have the same enthalpy. The system is composed by 6 equations and 8 variables. The 2 independent variables are:

System	None
Local	h_1, $\dot{m}_1$

Table 3.11: System and local independent variables for a lamination valve.

$$T[2] = Temperature(Steam; p = p[2]; h = h[2])$$

$$h[2] = h[1]$$

$$s[2] = Entropy(Steam; p = p[2]; h = h[2])$$

$$x[2] = QualitySteam; p = p[2]; h = h[2])$$

$$\dot{m}[2] = \dot{m}[1]$$

3.3.12 Solar heat exchanger

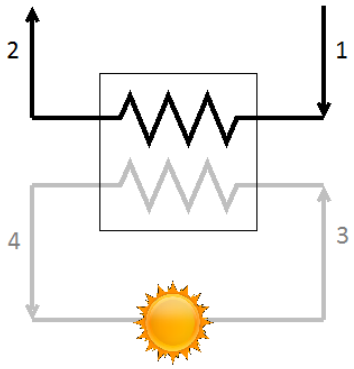

Figure 3.13: Solar heat exchanger

When the CSP integration requires an intermediate thermal fluid, such as thermal oil and molten salts, an additional heat exchanger is required. To establish the size of the heat exchanger, a heat trasfer coefficient is approximated with one of the values listed in [66], which depend on the fluids involved in the process. In this case, the fluids are water and an organic liquid: the heat transmission coefficient is chosen from the viscosity of the latter.

Once the area has been calculated, the purpose of the model is to evaluate the

solar field area needed to provide the desired energy to the working fluid. The data regarding each CSP technology are found in ([38]), and a value of 800 W/m^2 has been assumed for the design DNI. The values for the feedwater inlet and outlet are determined by the rest of the system. The system has 12 equations and 22 variables: the 10 independent variables are:

System	$\Delta T_{\min}, T[3], \eta_{\text{solar}}, KS, DNI$
Local	T_1, h_1, $\dot{m}_1, T_2, h_2$

Table 3.12: System and local independent variables for the solar heat exchanger.

The equations are:

$$T[4] = T[1] + \Delta T_{min}$$

$$\Delta T_{ml} = \frac{\Delta T_1 - \Delta T_2}{ln\left(\frac{\Delta T_1}{\Delta T_2}\right)}$$

$$\Delta T_1 = T[3] - T[2]$$

$$\Delta T_2 = T[4] - T[1]$$

$$\dot{Q}_{solar} = \dot{m}[1] * (h[1] - h[2])$$

$$\dot{Q}_{solar} = \dot{m}[3] * c_p * (T[3] - T[4])$$

$$c_p = f\left(\frac{T[3] + T[4]}{2}\right)$$

$$\dot{Q}_{solar} = K * S * \Delta T_{ml}$$

$$\dot{Q}_{solar} = \dot{Q}_{CSP} * \eta_{solar}$$

$$\dot{Q}_{CSP} = DNI * A_{solarfield}$$

$$\dot{m}[1] = \dot{m}[2]$$

$$\dot{m}[3] = \dot{m}[4]$$

3.3.13 Direct steam generation

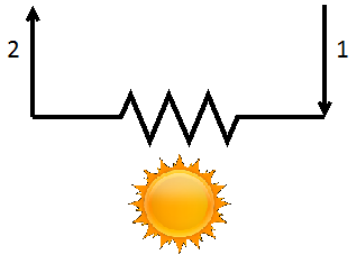

Figure 3.14: DSG heat exchange

When linear Fresnel collectors are applied, the solar section scheme is simplified as there is no need for an intermediate heat exchanger. There are 3 equations and 8 variables; the 5 independent variables are:

System	DNI, η_{solar}
Local	h_1, $\dot{m}_1, h_2$

Table 3.13: System and local independent variables for the solar heat exchanger.

The equations are:

$$\dot{Q}_{solar} = \dot{m}[1] * (h[1] - h[2])$$

$$\dot{Q}_{solar} = \dot{Q}_{CSP} * \eta_{solar}$$

$$\dot{Q}_{CSP} = DNI * A_{solarfield}$$

3.4 Model validation

To verify the accuracy of the model, its results have been compared to the references. In this case, some factors must be considered:

- The flow chart differs from the real power plant layout; as already mentioned, flows have been simplified in the high and intermediate turbine sections and some have been neglected.

- Experimental data have been taken from two different sources: the plant could be considered as divided in two sections, one (the expansion line) referring to its source and the other (feedwater line and boiler) referring to the other.

- To write the components's models, interpolating equations have been derived from the experimental data and included in the system.

These effects justify the high difference between the model results and the reference's in some points. The results are presented in Appendix A, where there are also the reference data and the percetange difference between the new model's results and the reference.

3.5 Integration options

The solar integration options suitable for a conventional power plant can be grouped into three main categories, depending on which section the renewable contribution is added:

- Integration on the feedwater line, which involves the feedwater preheaters.

- Integration on the turbine, in which steam is added before a stage to increase the expanding flow rate.

- Integration on the boiler, in which the boiler's heat exchangers are replaced by the solar heat.

The general method to achieve the hybridzation is to extract a certain amount of mass flow rate from a point in the system, heat this flow until the desired thermodynamic state is reached, and then adding it to another point in the cycle.
The starting point for simulating the hybrid configurations is the base plant's EES model described before. The integration is implemented with little modifications to the system of equations. A solar mass flow rate, named $\dot{m}_{CSP}$, is defined as an independent variable for each case, either as a fraction of another flow or as an absolute value, depending on the case. Different situations with varying solar

mass flow rate are evaluated with Parametric Tables. The modification to the cycle in terms of number of equations is minimal: the flow has to be subtracted to a point and added to another, or in some cases a temperature must be fixed and one equation removed. The system of equations for the solar section (reported in section 3.3.12) does not affect the base model, from which it receives the inlet and outlet thermodynamic conditions of the stream sent to the CSP plant.
As already explained in chapter 2, two strategies that can be applied in a hybrid coal-solar plant simulation: fuel saving, where the electrical power output is maintained constant (and equal to the base case scenario), and power boosting, where the fuel consumptions is fixed. For this case study, only the fuel saving mode is considered, since power boosting would not be easily applied in the reality of the power generation.
For this case study, the integration options analysed in literature are applied, and some more are proposed and implemented in the system of equations. The considered options are listes in the following sections.

3.5.1 Integration options on the feedwater preheating line

In the real power plant layout, two parallel high temperature feedwater lines are present, with three preheaters each. To simplify the system, only one line is modelled in EES, with doubled extensive properties. This assumption is justified by the reference model ([67]), which shows that the intensive properties are the same for the two series of preheaters, the feedwater is divided in half after the pump, and the steam extractions are divided almost in equal parts. When the feewater line is modified with a solar integration, the results are referred to the real situation by transposing the amount of flow sent to the solar section to six preheaters (with half mass flow rates). For example, the case where 50% of the water is extracted after the pump and sent to the solar field can be translated in one series of three preheaters working at design condition and the other cut off from operation.
Two strategies can be applied when feedwater preheaters are involved in the solar integration: extracting part of the feedwater and heating it in a section parallel to the preheater, or mixing additional steam into the steam extraction. In both

cases, it is assumed here that the steam extraction mass flow rate entering the preheater is controlled by the feedwater's outlet temperature. This temperature assumes the value correspondent to the off design condition with the same feedwater flow rate. Since the steam extractions were not controlled in the base model, the equation determining their entity must be removed; in the variable count, they are replaced by the imposed temperatures. The hypothesis of controlled steam extractions is adopted instead of maintaining the flow rates uncontrolled because of the chosen heat exchanger model. Here, the terminal temperature differences are set with an interpolating equation as functions of the feewater mass at the component's inlet, in order to simplify the simulation and to make better use the available experimental data. Moreover, this method is often applied in power plants to define the heat exchange. With an uncontrolled steam extraction, the temperature at the preheater's outlet increases: in the case of the highest temperature preheater integration, this lead to a higher temperature at the economizer inlet. On the other hand, this effect could present an issue for the economizer's thermal stability.

To control a steam extraction, a valve should be used. The valve is actually present in the power plant, with the only purpose of excluding the steam extraction in case of preheater mulfunctioning. They do not serve as means of load regulation, since they introduce thermal and mechanical fatigue; in the case of solar integration, their employment is justified by the slow variation in DNI condition and the damping effect of heat transfer fluid, when present, and the possible application of a thermal storage.

In order to reduce alteration in the components's working conditions after hybridization, in the cases where the solar section works in parallel with a preheater the temperature at the economizer's inlet is fixed at its off design value. This assures a more stable thermodynamic cycle.

Figure 3.15 serves as an example for this category: extraction and mixing points vary with the considered synergy.

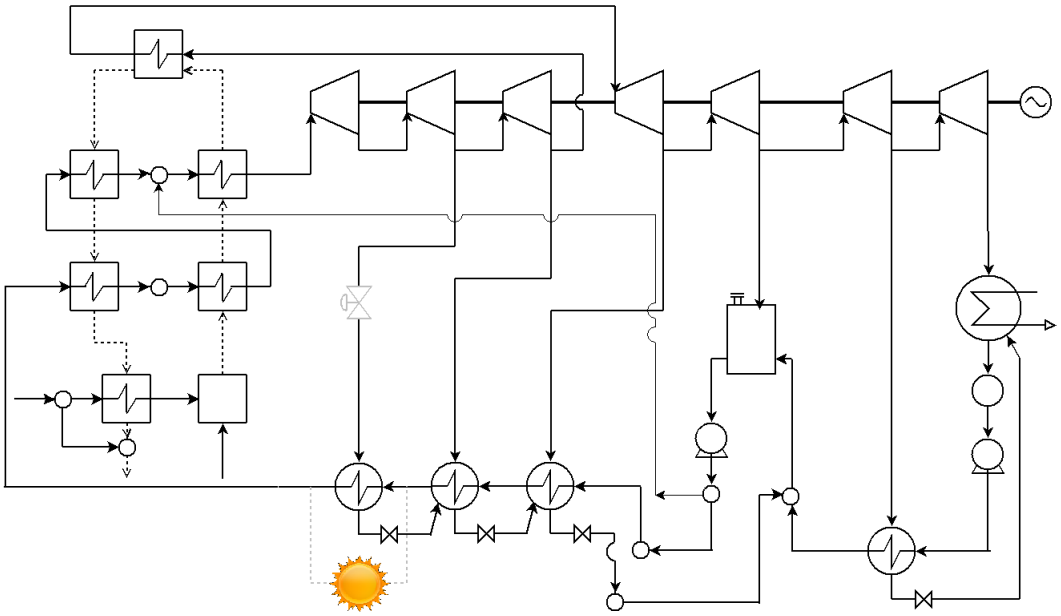

Figure 3.15: Simplified flowchart of a feedwater line integration

Integration 1: HPH3 replacement with a parallel stream, design economizer's inlet temperature

The feedwater is divided before entering the HPH3 preheater, and the flow evolving in the CSP section is heated up to the temperature needed to reach the design condition at the economizer's inlet (301,5 C). The feedwater fraction which proceeds in the traditional cycle reaches its off design temperature. The two streams mix before entering the boiler.

Integration 2: Mixer on the steam extraction feeding HPH3

A different approach involving the las high temperature preheater consists in adding the solar stream not on the feedwater line but on the corresponding steam extraction. This is done with a mixer, with water extracted from after the deaerator and evaporated in the CSP section.

Integration 3: All high temperature feedwater prehaters replacement with a parallel stream, design economizer's inlet temperature

In this solution, the stream directed to the CSP section is drawn after the feedwater pump and mixed back into the traditional section before the boiler. The output of the mixing process will have a fixed temperature set to the design value of that poit. All the three involved steam extractions are controlled, and the feedwater temperatures after each preheater are set with their off design value.

3.5.2 Integration options on the expansion line

To increase the mass flow rate expanding in the turbine, water is extracted either after the deaerator (as in figure 3.16) or from the drainage water of the same pressure. For the intermediate pressure, both points before and after the reheater are considered for integration. A pump is necessary when drawing the water from after the deaerator, since this point is at the same pressure as the second intermediate turbine stage (IP2). To simplify the model, this effect is not modelled.

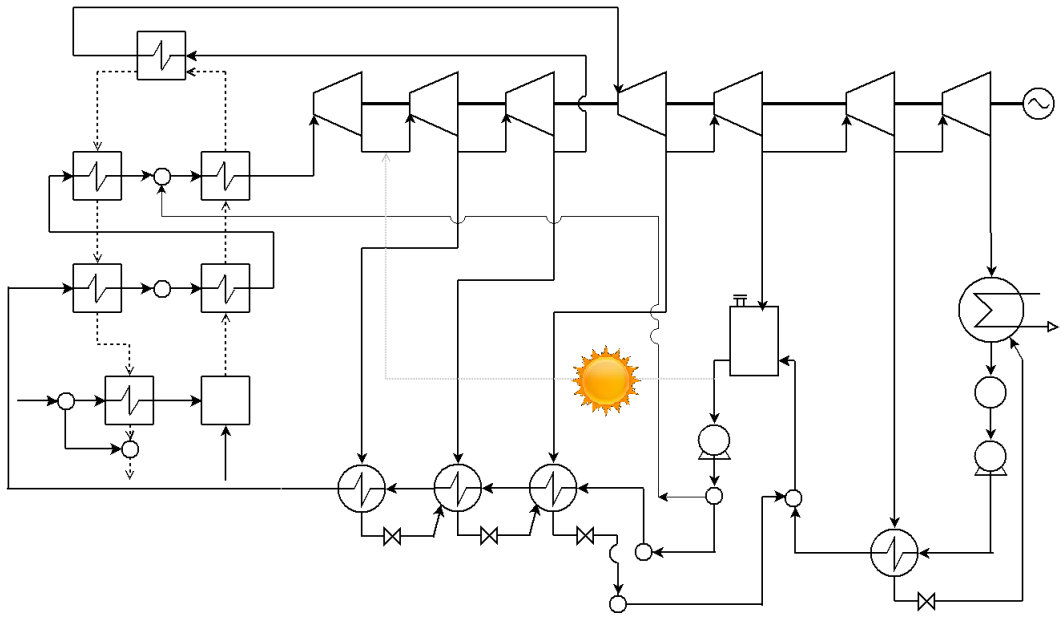

Figure 3.16: Simplified flowchart of an expansion line integration

The turbines are designed to work in a situation where on of the stream

extractions is cut off: therefore, the capacity limit for a given turbine stage is calculated as the sum of the design value of that stage's inlet mass flow rate and the mass flow rate of the bigger steam extraction, also in design condition.

Integration 4: Steam addition in the first high pressure turbine stage, extraction after deaerator

Water is taken from the deaerator outlet, and heated up to the same conditions as the flow at the first stage turbine inlet, where there a mixing process takes place. In this case the flow sent to the CSP section is not defined by a ratio but by its absolute value, which must not lead to an inlet turbine mass flow rate higher than the capacity limit.

Integration 5: Steam addition in the second high pressure turbine stage, extraction from drainage water

The drainage water of the highest temperature feedwater preheater is at the same pressure as the second stage turbine's inlet: this stream is sent to the solar section (partially or totally) and mixed with the flow at that point.

Integration 6: Steam addition before reheating, extraction after deaerator

The layout is the same as the one for Integration 4, only the mixing point of the solar generated steam is after the high pressure turbine stages, in the intermediate pressure section before the reheating process.

Integration 7: Steam addition before reheating, extraction from drainage water

The drained water from the second high temperature preheater (HPH2) is sent to the same point as Integration 6.

Integration 8: Steam addition after reheating, extraction after deaerator

The layout is the same as the one for Integration 6, with the steam addition after the reheater. Higher temperature conditions are required.

Integration 9: Steam addition after reheating, extraction from drainage water

The integration is the same as before, with steam generated from the drainage water at the same pressure (from the preheater HPH2).

Integration 10: Steam addition in the first high pressure turbine stage, generated from tempering water

An integration option involving the tempering water is also taken into consideration. Tempering water is required to control the heat exchange in the high temperature superheater and reheater in the boiler: this is achieved by mixing this flow with the steam from the low temperature superheater, in order to decrease its temperature. It is supposed here that this effect could instead be achieved by heating the tempering water at the expenses of the steam from the low temperature superheater, until the required temperature is met; afterwards, the tempering water is further heated by the solar field and sent to the turbine to expand. The selected temperature at the high temperature superheater is the design value.
Possible issues could come from the reduced steam flow in the boiler, and from a different balance of the combustion gases thermodynamic states.

3.5.3 Integration options on the boiler

Two synegies are proposed for this category, both found in the reviewed articles. The integration scheme is similar to the one in figure 3.15, involving a parallel CSP section.

Integration 11: Economizer replacement with a parallel stream

This option is realised by dividing the flow before the component and mixing back the solar stream before the evaporator. The case of full replacement is considered.

Integration 12: Highest temperature feedwater preheater and economizer replacement

This solution mixes the previous one with Integration 1: the flow is divided before the considered preheater (HPH3) and mixed before the evaporator. The steam extraction feeding the preheater is controlled.

The cases considered here are summarised in table 3.14:

Category	Integration
FW	HPH3 replacement with parallel streams
	Integration on HPH3, mixer on the steam extraction
	All high temperature preheaters replacement
T	Steam addition in HP1, extraction after deaerator
	Steam addition in HP1, extraction from drainage
	Steam addition before RH, extraction after deaerator
	Steam addition before RH, extraction from drainage
	Steam addition after RH, extraction after deaerator
	Steam addition after RH, extraction from drainage
	Steam addition in HP1, from tempering water
B	ECO replacement
	HPH3 and ECO replacement

Table 3.14: Integration options case studies

3.6 CSP technologies for hybridization

For a given integration option, the CSP technologies eligible for that option are determined by the desired feedwater temperature. Each technology, as reported

in chapter 1, can reach a certain temperature, depending on the collectors and absorber's structure and on the applied thermal fluid. A minimum temperature difference must be considered to allow the heat exchange: with these factors, it is possible to relate the CSP application to the proper integration point. Table 3.15 reports the different technologies features used here as well as the maximum temperature reached ([38]) and the global heat exchange coefficient K for the cases with an intermediate fluid ([66]).

Technology	**Thermal fluid**	**Max temperature [C]**	**K [kW/(m^{2}K)]**
PTC	Thermal oil	393	0,85
PTC	Molten salts	500	0,325
ST	Molten salts	565	0,325
LFR	-	500	-

Table 3.15: CSP technologies and parameters applied for integration

The global heat transmission coefficient (K) is approximated as suggested in *Trasmissione del calore* by Bonacina et al.. To choose a value from those proposed in the reference, the viscosity of the heat transfer fluid (HTF) is calculated in EES from the average between the inlet and outlet HTF's temperatures for each application. The fluids chosen for the simulations are Dowtherm A (thermal oil, used in the Andasol plants ([1])) and a mixture of NaNO3 and KNO3 for molten salts (used in the Archimede plant ([1])); both are included in the software's substances library. From the evaluation of the kinematic viscosity, it derives that the thermal oil is a light organic fluid and the molten salts are a heavy organic fluid, hence the value of K are selected. The minimum temperature difference ΔT_{min} depends on the substances evolving in the heat exchanger: a higher temperature difference implies that the heat exchange efficiency is lower, since the gap between the hot fluid's outlet temperature and the cold fluid's inlet. The values chosen in this work are:

Fluids	ΔT_{min} **[C]**
Liquid - liquid	5
Liquid - steam	10

Table 3.16: Minimum temperature difference for heat exchange

A concentrating solar technology is associated to a certain integration option depending on whether or not its maximum temperature is compatible with the required feewater outlet point.
A further selection criteria is applied, in order to obtain a better thermal matching between feedwater and heat transfer fluid, when this is present. This is achieved by choosing the lowest CSP temperature closer to the required feedwater temperature. For example, since solar towers with molten salts reach 565C, it would be possible to apply them for preheating the feedwater in parallel with HPH3, whose outlet temperature is 290C. A better thermal matching happens, however, when PTC with thermal oil is selected, since its maximum temperature (393C) is closer to the desired one. For each integration option, then, the following technologies can be implemented and evaluated (table 3.17):

Integration	PTC+oil	PTC+salts	ST+salts	LFR+DSG
1	•			•
2	•			•
3	•			•
4		•	•	
5		•	•	
6	•			•
7	•			•
8			•	
9			•	
10		•		•
11	•			•
12	•			•

Table 3.17: Combinations of CSP technology and synergy: a dot indicates a considered synergy-technology match.

Other features of a CSP technology are the receiver and collector effciency. The product between the two parameters is the solar field effciency. The values chosen here are derived from the literature and are reported in table 3.18:

CSP Technology	η_{rec}	η_{col}	η_{sol}
PTC	0,85	0,87	0,74
ST	0,94	0,64	0,60
LFR	0,96	0,64	0,61

Table 3.18: Reference efficiencies for CSP technologies

3.6.1 Performance parameters for hybrid plants

To evaluate the performance of a hybrid plant and to compare different integration strategies, specific parameters have been defined.

- $\dot{m}_{f,des}$ is the fuel consumption in [kg/s] evaluated in the design model. $\dot{m}_f$

represents the fuel consumption in the hybrid system.

- LHV_{des} is the lower heating value [kJ/kg] in the design condition.
- $\dot{Q}_{f,des}$ and $\dot{Q}_f$ are, respectively, the products of fuel mass flow rate and lower heating value for the design and hybrid systems [kW]:

$$\dot{Q}_{f,des} = \dot{m}_{f,des} \cdot LHV_{des} \tag{3.6}$$

$$\dot{Q}_f = \dot{m}_f \cdot LHV_{des} \tag{3.7}$$

  $\dot{Q}_f$ is evaluated with the design lower heating value to provide a more uniform comparison.

- $\dot{Q}_{b,des}$ and $\dot{Q}_b$ are, respectively, the products of $\dot{Q}_{f,des}$ and $\dot{Q}_f$ and the boiler efficiency η_b:

$$\dot{Q}_{b,des} = \dot{Q}_{f,des} \cdot \eta_b \tag{3.8}$$

$$\dot{Q}_b = \dot{Q}_f \cdot \eta_b \tag{3.9}$$

  η_b is assumed equal to 0,92 ([67]).

- The fuel consumption reduction is evaluated both in absolute and relative value as:

$$\Delta\dot{m}_f = \dot{m}_{f,des} - \dot{m}_f \tag{3.10}$$

$$\Delta\dot{m}_{f\%} = \frac{\Delta\dot{m}_f}{\dot{m}_{f,des}} \tag{3.11}$$

- The base cycle efficiency is defined as:

$$\eta_{th,base} = \frac{P_{net}}{\dot{Q}_{f,des}} \tag{3.12}$$

- To define the entity of the electric power generated by the solar integration, a hypothetical definition is given, since it is not possible to discern the traditional and solar streams. Once the desired flow is generated from the renewable source, it is mixed with the mass evolving in the traditional cycle. The solar power is then conventionally calculated as the power that would be generated by the amount of saved fuel mass, if this evolved in the base cycle:

$$P_{sol} = |\Delta\dot{m}_f| \cdot LHV_{des} \cdot \eta_{th,base} \tag{3.13}$$

- The solar radiation energy and the energy given to the heating fluid are:

$$\dot{Q}_{rad} = DNI \cdot A_{sol} \tag{3.14}$$

$$Q_{CSP} = \dot{Q}_{rad} \cdot \eta_{sol} \tag{3.15}$$

where A_{sol} is the solar field surface and η_{sol} is the solar field efficiency. This is the product of the collector and receiver efficiencies:

$$\eta_{sol} = \eta_{col} \cdot \eta_{rec} \tag{3.16}$$

It is important to notice that $\dot{Q}_{CSP}$ is determined once the integration points (solar mass flow rate and thermodynamic conditions) have been defined, and does not vary when different technologies are compared for that integration. $\dot{Q}_{rad}$ depends on the concentrating solar technology by means of $\eta_{solarfield}$, and thus will be different for different CSP applications. By using both energies to assess the hybrid plant's performance, it is possible to compare both different synergies (using $\dot{Q}_{CSP}$) and, for a given synergy, to estimate the occupied land required by each feasible technology (using $\dot{Q}_{rad}$).

- The solar share is defined as:

$$F_{sol} = \frac{P_{net} - \dot{Q}_f \cdot \eta_{th,base}}{P_{net}} \tag{3.17}$$

and it represents the fraction of the power output generated by the additional solar input.

- The conversion efficiency from primary energy sources is:

$$\eta_p = \frac{P_{net}}{\dot{Q}_f + \dot{Q}_{rad}} \tag{3.18}$$

By applying the boiler efficiency and the solar field effciency, the thermal efficiency is obtained:

$$\eta_{th} = \frac{P_{net}}{\dot{Q}_b + \dot{Q}_{CSP}} \tag{3.19}$$

- Solar radiation-to-electric and solar heat-to-electricity effciencies are calculated as:

$$\eta_{r-el} = \frac{P_{sol}}{\dot{Q}_{rad}} \tag{3.20}$$

$$\eta_{h-el} = \frac{P_{sol}}{\dot{Q}_{CSP}} \tag{3.21}$$

3.7 Results

The parameters listed above have been evaluated for all the considered integration options. The following diagrams show the trends for η_p, η_{r-el} and η_{h-el}: this initial comparison allows to understand how well the new hybrid cycle performs in terms of conversion efficiency. Figure 3.17 shows the resulting η_p plotted against the solar share for all the integration options; for reasons of clarity, diagrams 3.18, 3.19 and 3.20 report the same parameter for each integration category. A black dotted line representing the base cycle efficiency $\eta_{th,base}$ is included. When the direct steam generation is applicable, its results are plotted with a dashed line.

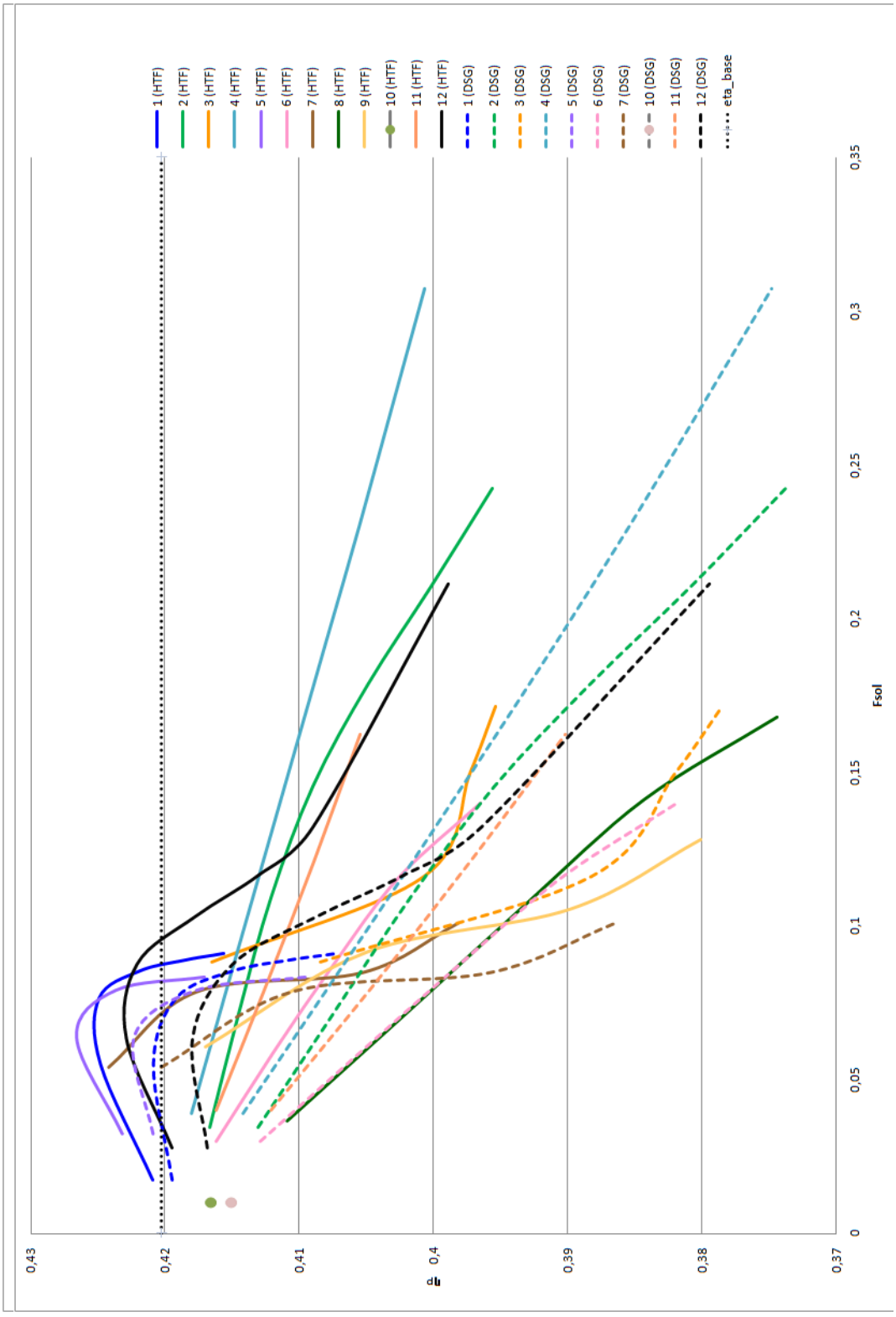

Figure 3.17: Conversion efficiency from primary sources plotted for all integration options.

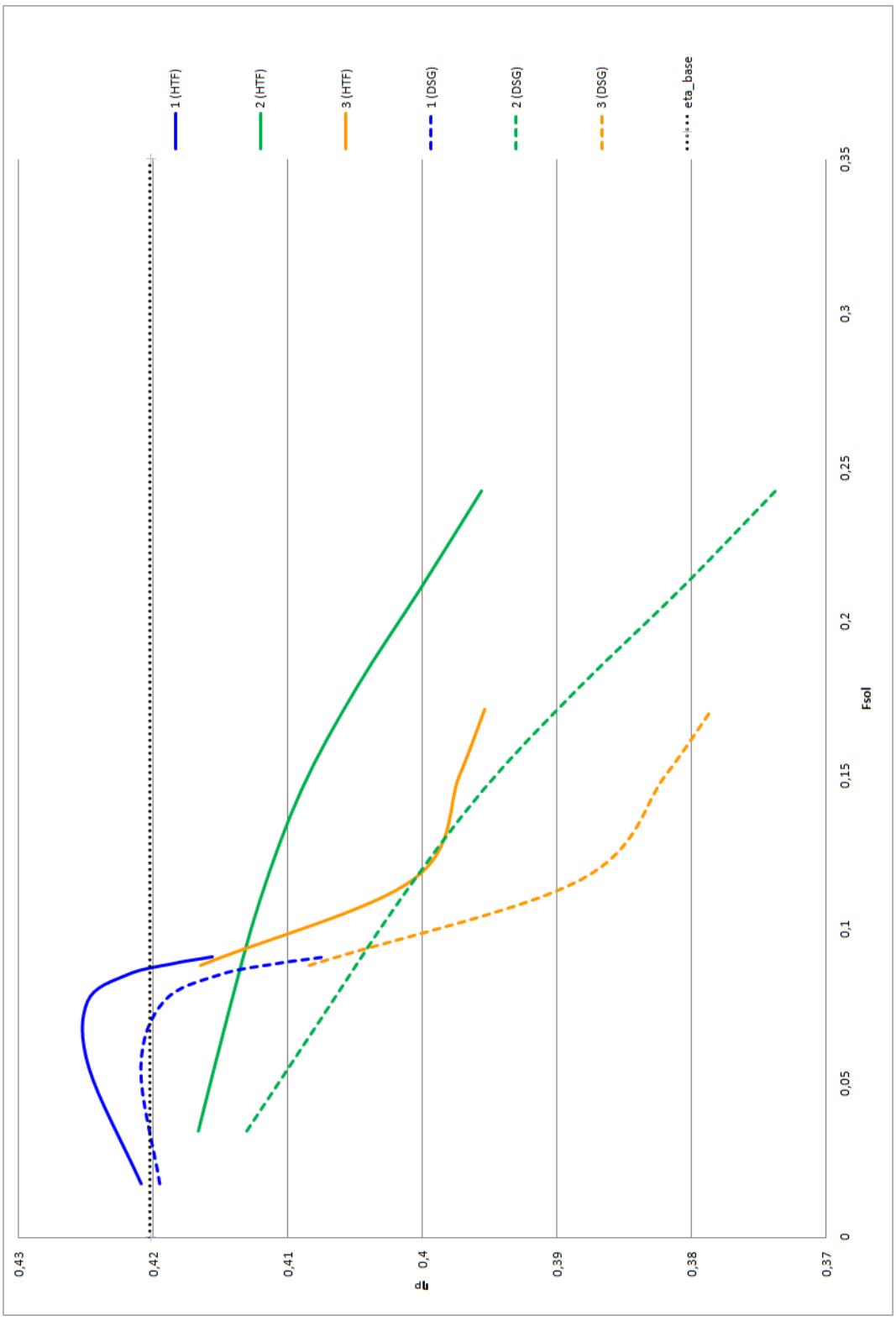

Figure 3.18: Conversion efficiency from primary sources plotted for the feedwater line integration options.

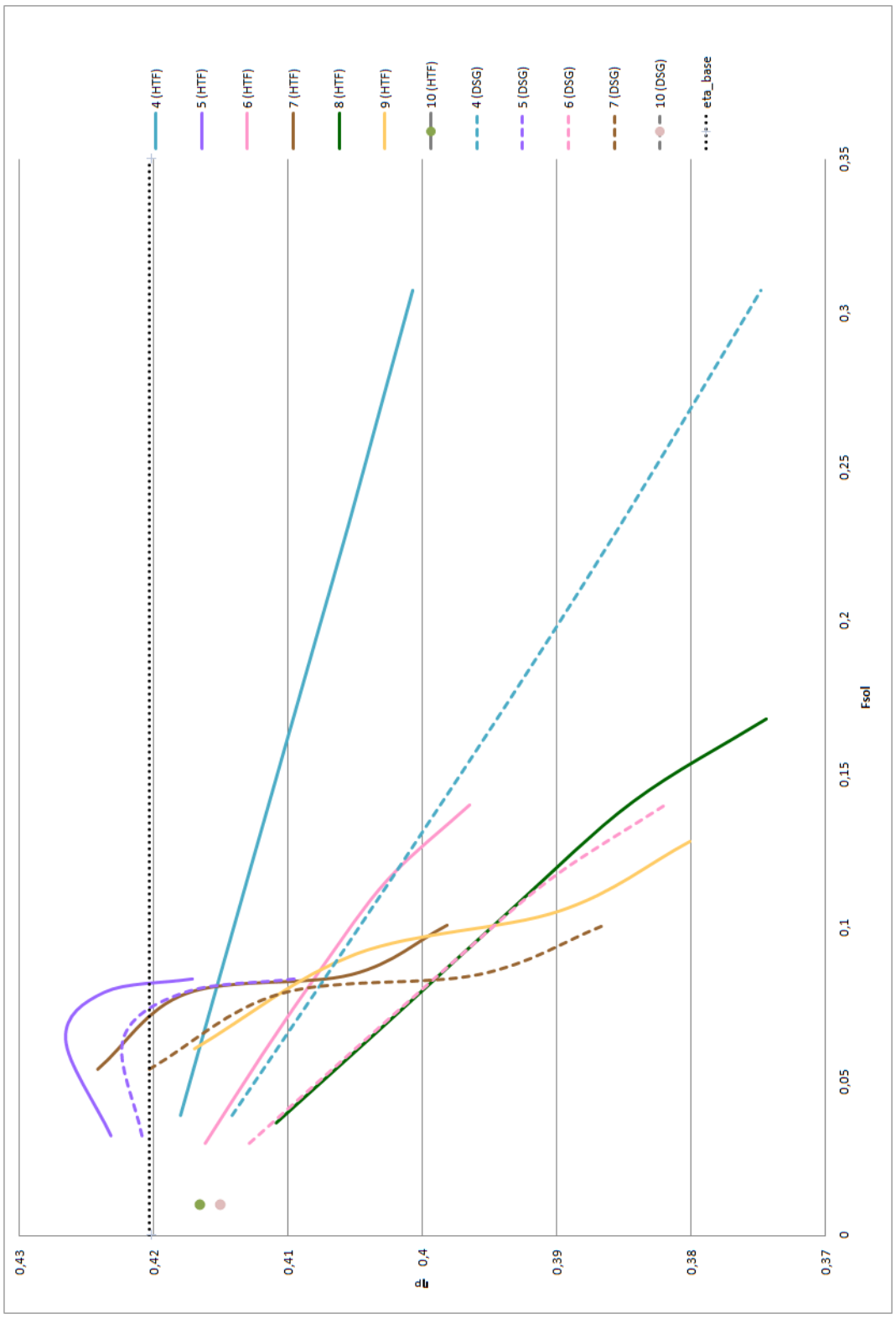

Figure 3.19: Conversion efficiency from primary sources plotted for the expansion line integration options.

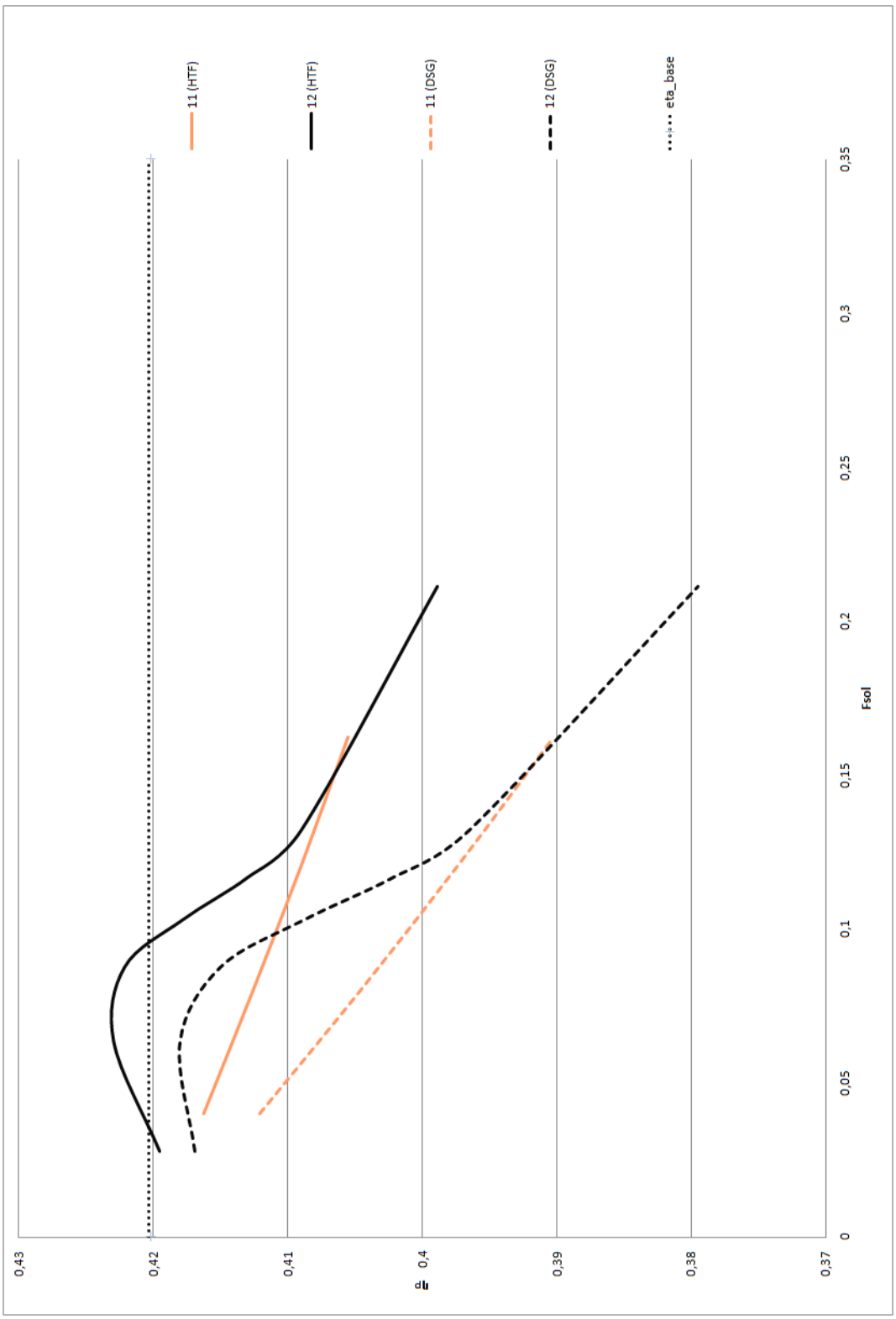

Figure 3.20: Conversion efficiency from primary sources plotted for the boiler integration options.

From the previous diagrams, it can be seen that not all the synergies present a conversion efficiency higher than the base cycle's. The two efficiencies η_p and $\eta_{th,base}$ are defined by a ratio with the same numerator, the net electric power output, which is a constant in fuel saving mode; the denominator for η_p is the sum of the fuel and radiation powers ($\dot{Q}_f$ and $\dot{Q}_{rad}$). When this sum is lower than the base cycle's fuel power $\dot{Q}_{f,des}$, the hybrid conversion efficiency is higher than the base thermal efficiency, and vice versa when the sum is higher.
In most synergies, η_p decreases linearly with increasing solar share F_{sol}: this trend is caused by the amount of solar radiation required for that option, whose growth rate is higher than the reduction in the fuel power obtained with that solar input. The synergies with a conversion efficiency higher than the base cycle efficiency are:

- Integration 1: last feedwater preheater replacement with a parallel heat exchanger, controlled steam extraction and design temperature at the economizer's inlet.
- Integration 5: steam generation from drainage water after preheater HPH3, addition to the second high pressure stage turbine HP2.
- Integration 7: steam generation from drainage water after preheater HPH2, addition before the reheater.
- Integration 12: last feedwater preheater and economizer replacement with a parallel heat exchanger, controlled steam extraction.

Regarding the feedwater line and boiler integration options, from the previous considerations it could be deduced that it is preferable to intervene on the feedwater preheaters than on the economizer alone, whose conversion efficiency is lower than the base cycle efficiency in its whole range of solar share. The solution with a parallel solar stream performs better than the one involving a mixing process on the steam extraction for the last preheater HPH3: in this second situation, water streams are divided before the high temperature feedwater line, thus affecting the working condition of all three preheaters HPH1, HPH2, HPH3 instead of just the last one. The steam additions before a turbine stage perform

better when steam is generated from the drainage water at the same pressure than when it comes from after the deaerator: using the drained water implies less modifications to the cycle working condition, particularly for the feedwater mass flow rate. When steam is added in the intermediate pressure section, the best point is before the reheater, where lower temperature conditions are required.
The next group of diagrams show the solar radiation-to-electric efficiency η_{r-el} and the solar heat-to-electric efficiency η_{h-el}. The former parameter indicates how well the input radiation energy is converted into net electric power, and it assumed different values with different CSP technologies; on the other hand, η_{h-el} only depends on the integration point and it is the same for all possible technologies.

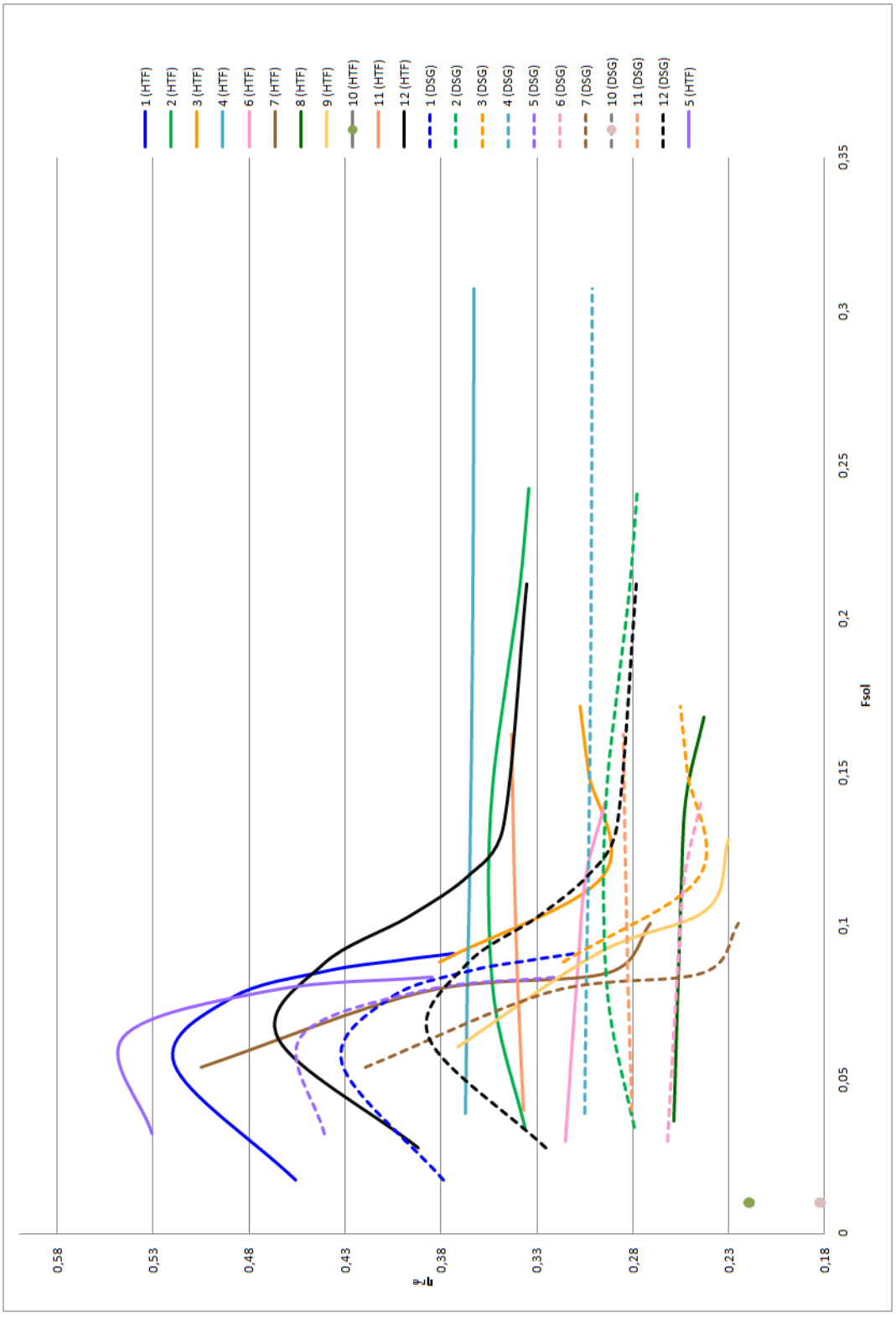

Figure 3.21: Solar radiation-to-electricity efficiency plotted for all integration options.

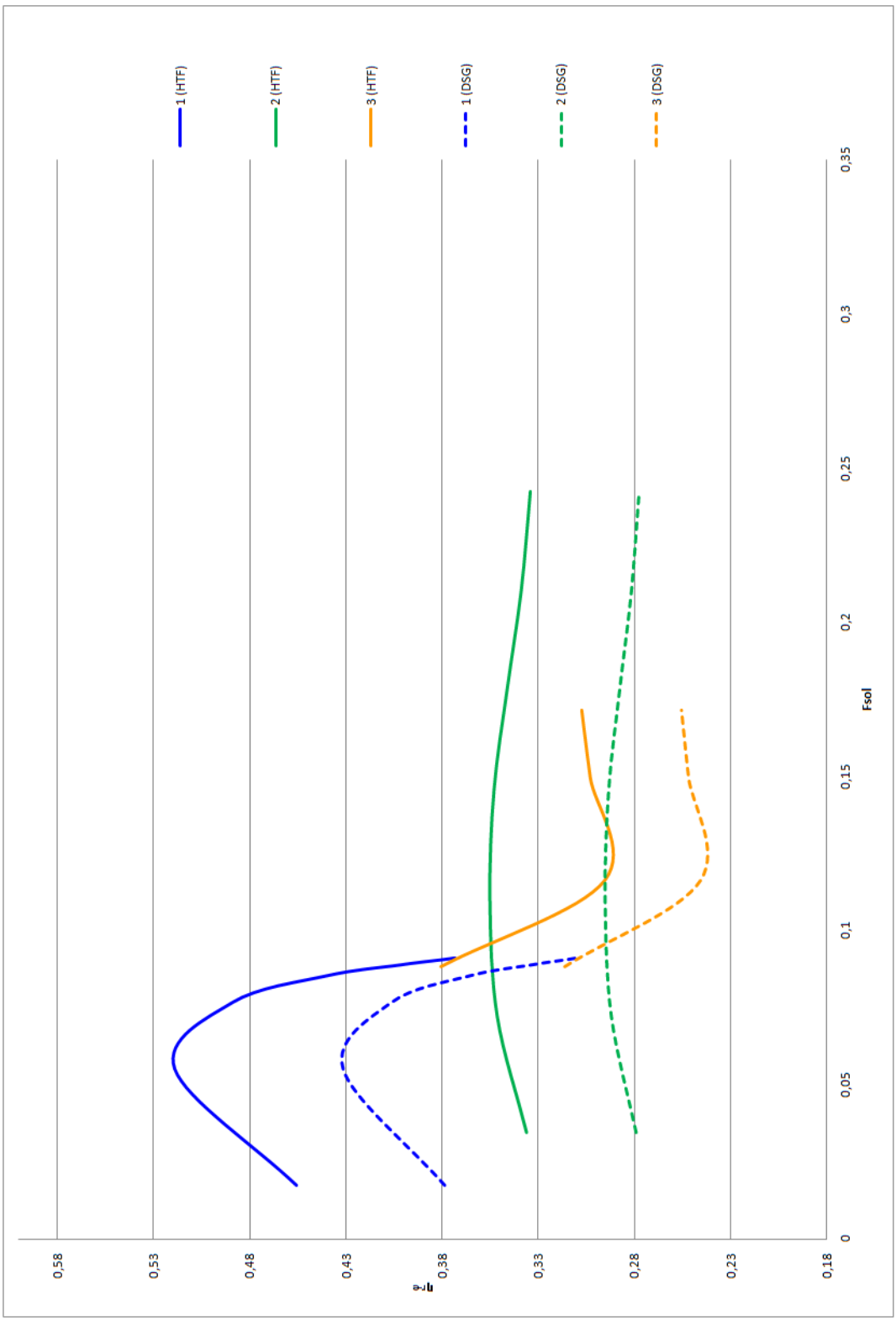

Figure 3.22: Solar radiation-to-electricity efficiency plotted for the feedwater line integration options.

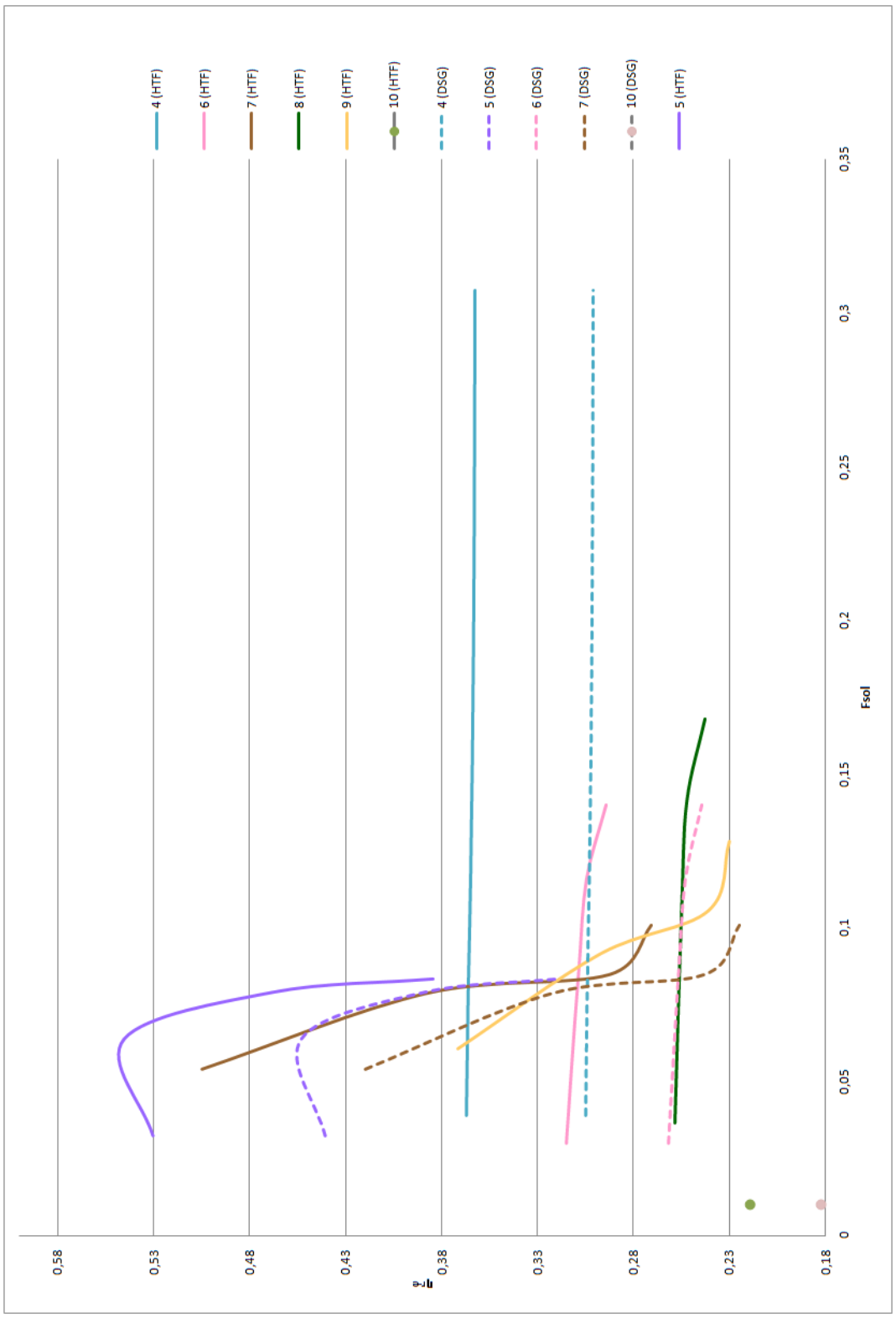

Figure 3.23: Solar radiation-to-electricity efficiency plotted for the expansion line integration options.

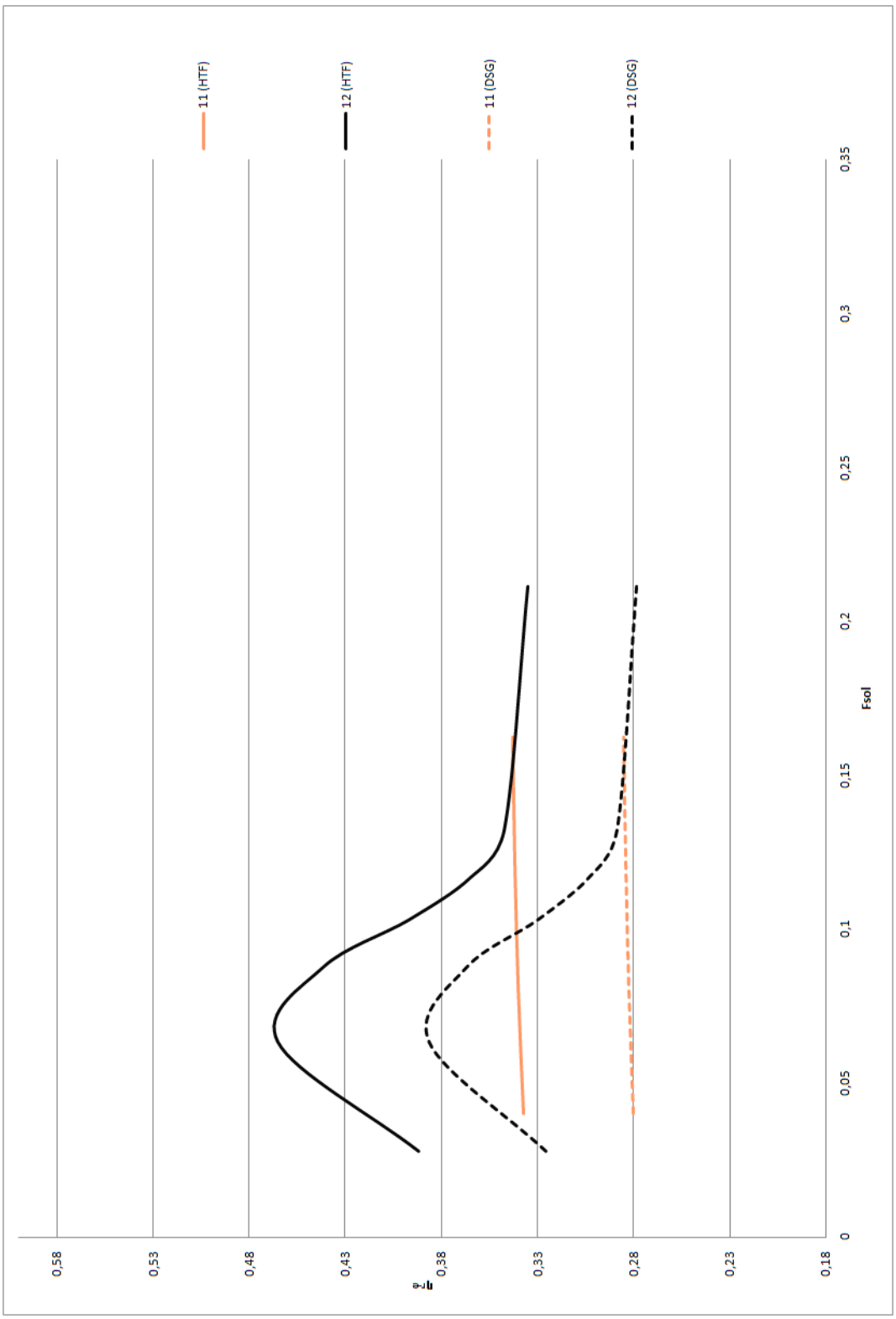

Figure 3.24: Solar radiation-to-electricity efficiency plotted for the boiler integration options.

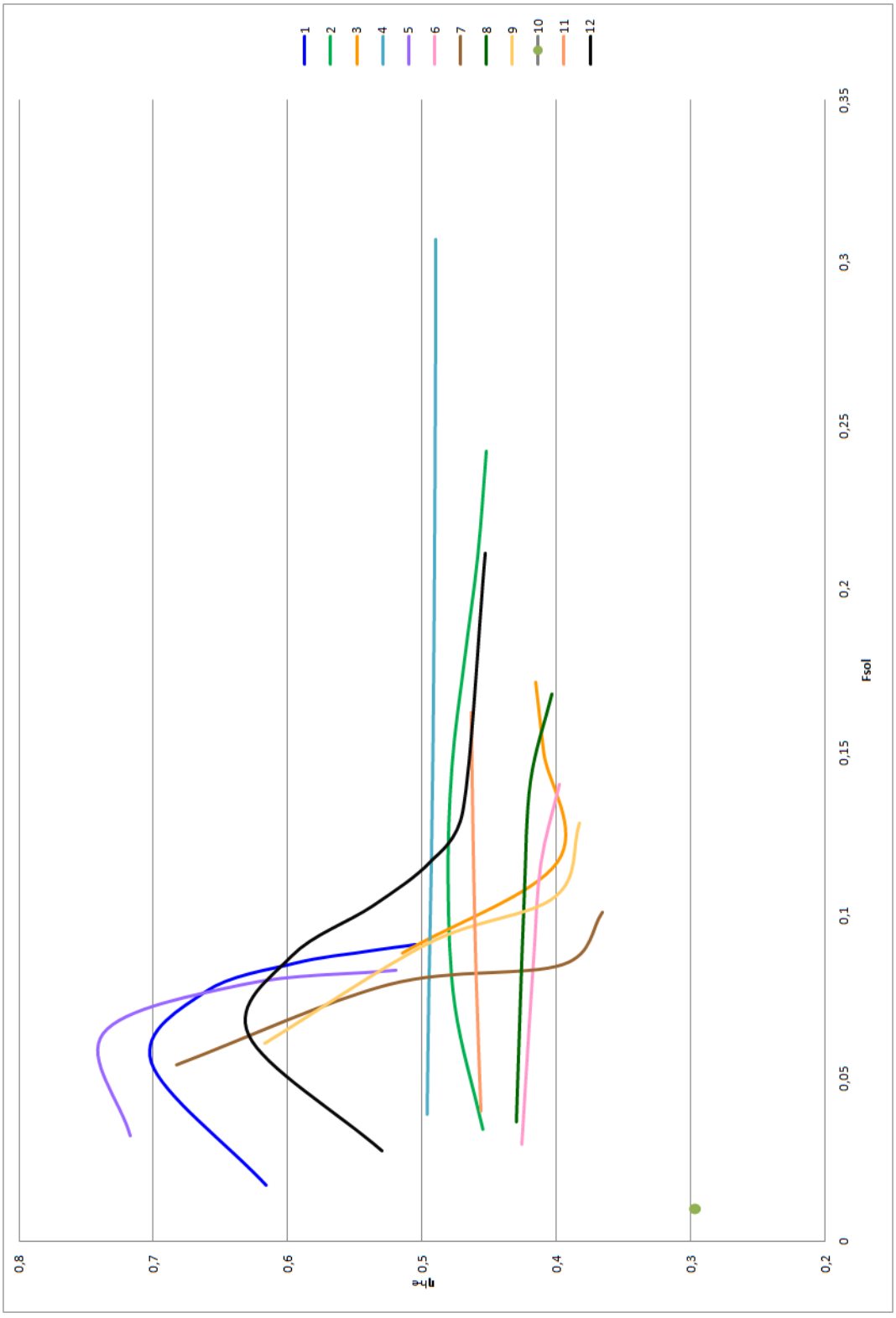

Figure 3.25: Solar heat-to-electricity efficiency plotted for all integration options.

Figure 3.26: Solar heat-to-electricity efficiency plotted for the feedwater line integration options.

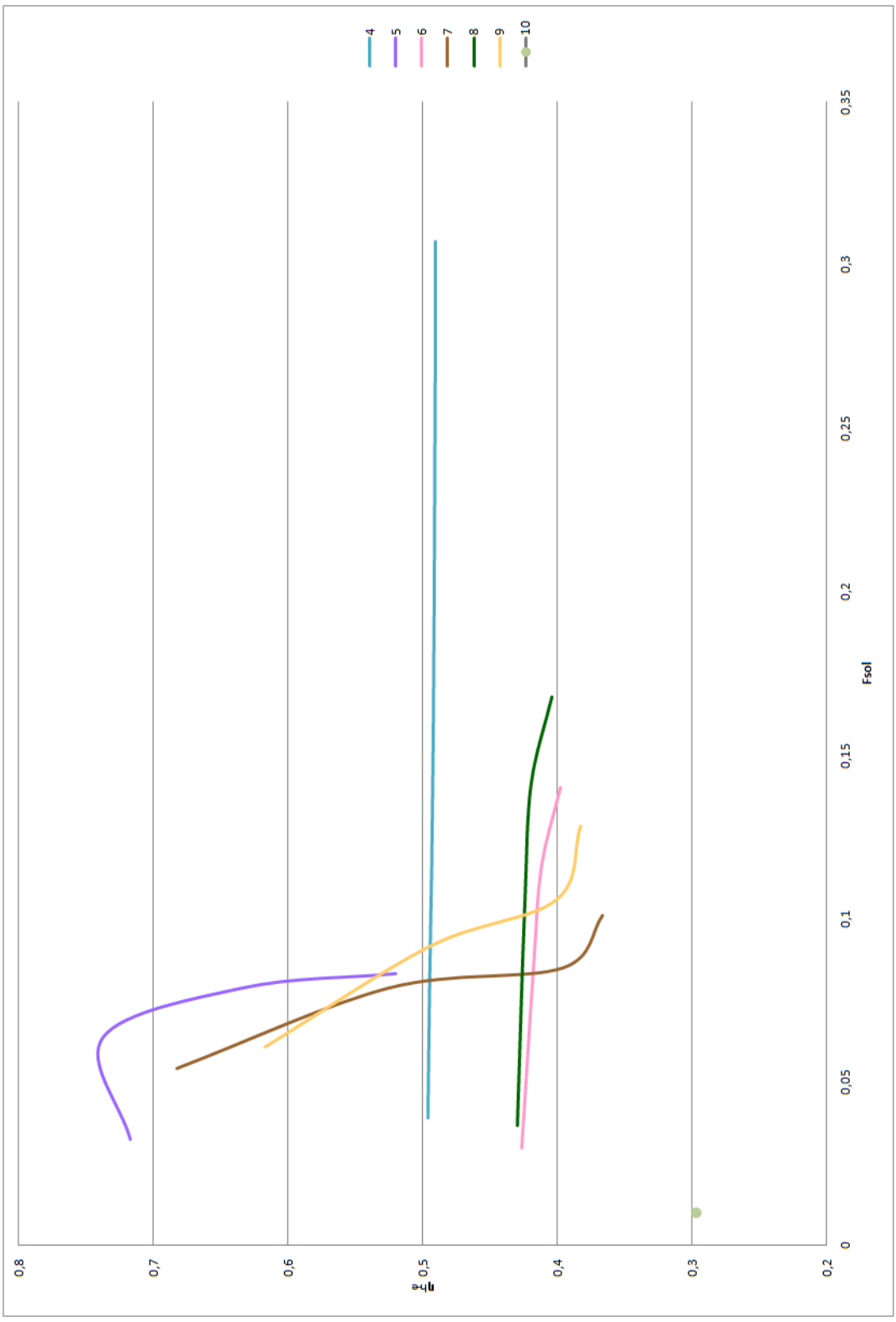

Figure 3.27: Solar heat-to-electricity efficiency plotted for the expansion line integration options.

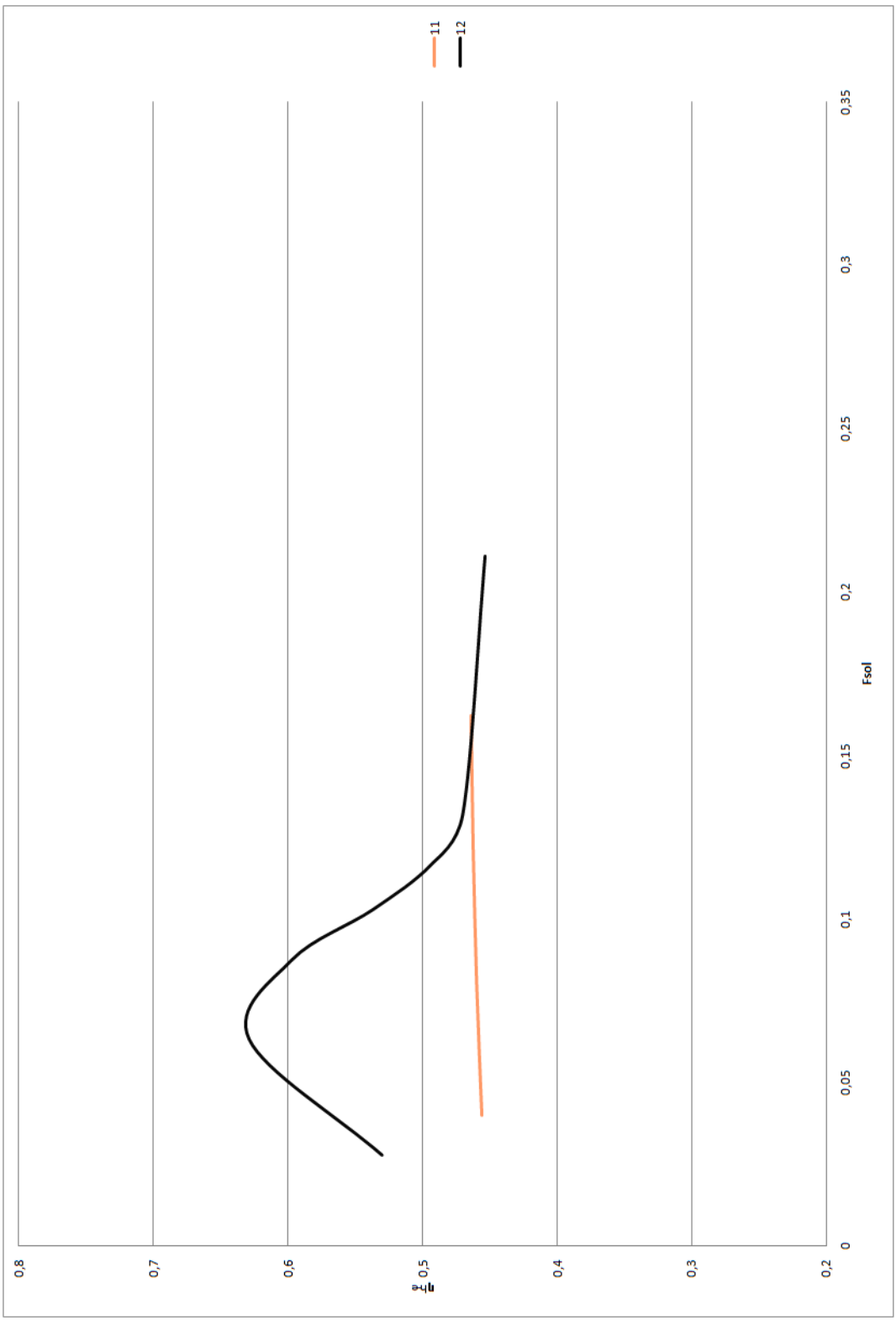

Figure 3.28: Solar heat-to-electricity efficiency plotted for the boiler integration options.

The synergies that present a decreasing η_p in 3.17 have an almost constant solar radiation-to-electric and solar heat-to-electric with increasing solar share. A constant value for η_{r-e} and η_{h-e} implies that the fuel saving grows proportionally with increasing solar input. Some options (Integrations 1,5 and 12) have a maximum efficiency value for a given solar share, while for others (Integrations 3, 7 and 9) the efficiency decreases with increasing solar share.
For all options, the absolute value of the fuel reduction is linear with the solar share:

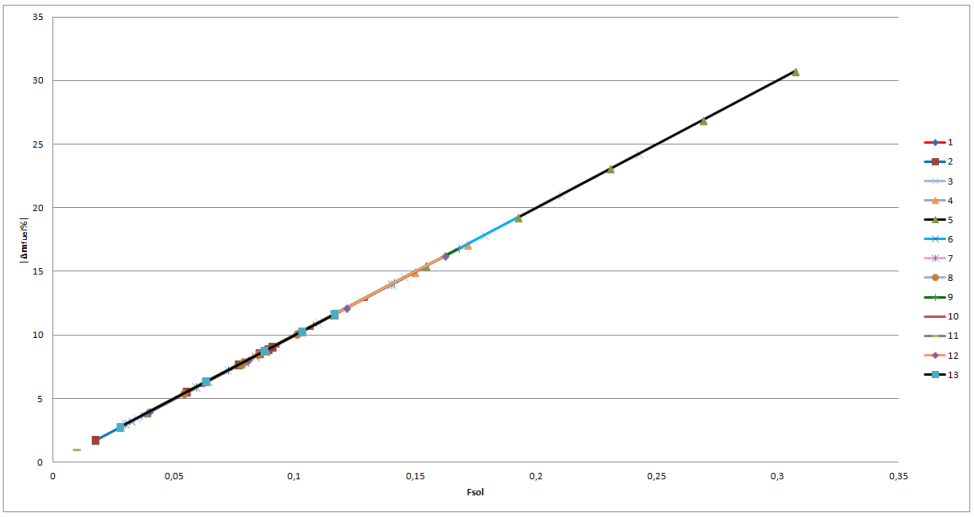

Figure 3.29: Absolute value of the fuel reduction (%).

Of the synergies proposed and simulated above, only a few will be further discussed and examined: the selection criteria adopted here, for the purposes of an energetic analysis, consists of choosing those synergies with a primary conversion efficiency η_p, higher than the base cycle efficiency $\eta_{th,base}$.
From figure 3.17, the integration options which fulfill the requirement (for at least one point in the considered solar share range) are:

- Integration 1: HPH3 preheater replacement, carried out with PTC and thermal oil or LFR with direct steam generation
- Integration 5: steam addition to stage HP2 from drainage water, carried out with PTC and molten salts or LFR with direct steam generation

- Integration 7: steam addition before RH from drainage water, carried out with PTC and thermal oil
- Integration 12: HPH3 preheater and economizer replacement, carried out with PTC and thermal oil

For each of these cases, more parameters are reported and the entity of the variation to the thermodynamic cycle is investigated. Finally, a comparison between all the options is provided.

3.7.1 Case 1: Preheater replacement with a parallel stream

The extraction of part of the water before preheater HPH3 causes a reduction of the outlet feedwater temperature, because this variable is a function of the mass flow rate through the component. The inlet feedwater temperature (HPH2 otlet temperature) is determined as in the base model, and it is consequently only slightly affected by the integration: it happens then that for some values of the solar share, the temperature at HPH3 outlet temperature becomes lower that the one at its inlet. In particular, this happens when the extracted solar stream is equal or higher than the 70% of the feedwater. This range is not considered here. The case of complete substitution is considered: in this situation the steam extraction is cut off and the solar section performs entirely the last preheating process. The following diagram shows how the temperatures at the feedwater preheater's and solar section's outlets vary with the solar share:

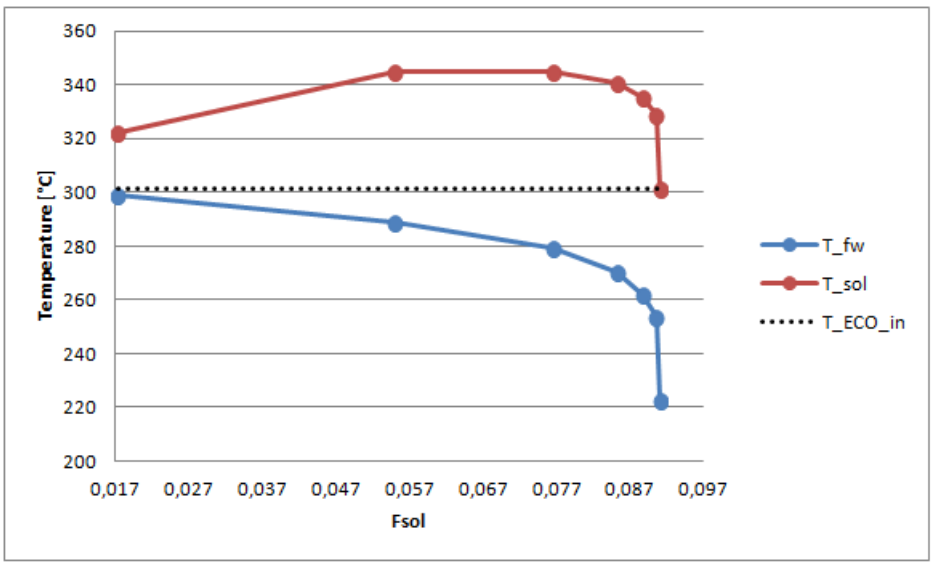

Figure 3.30: Variation of the outlet preheater and solar section temperatures.

The feedwater tempearture is reported even for the complete substitution case because of the way the synergy is modelled: the HPH3 preheater's equations are left in the model, so the intensive variable are evaluated normally.
The next figure includes the variation of the involved mass flow rates: the sum of the solar stream and the feedwater remaining in the cycle, or in other words the economizer's inlet mass flow rate, decreases slightly with increasing solar share. This implies that the boiler load is not heavily affected by this integration. The reduction of the steam extraction has the same trend because, in this model, it is directly proportional to the turbine inlet mass flow (which, apart from the tempering water mixing, is equal to the economizer's load).

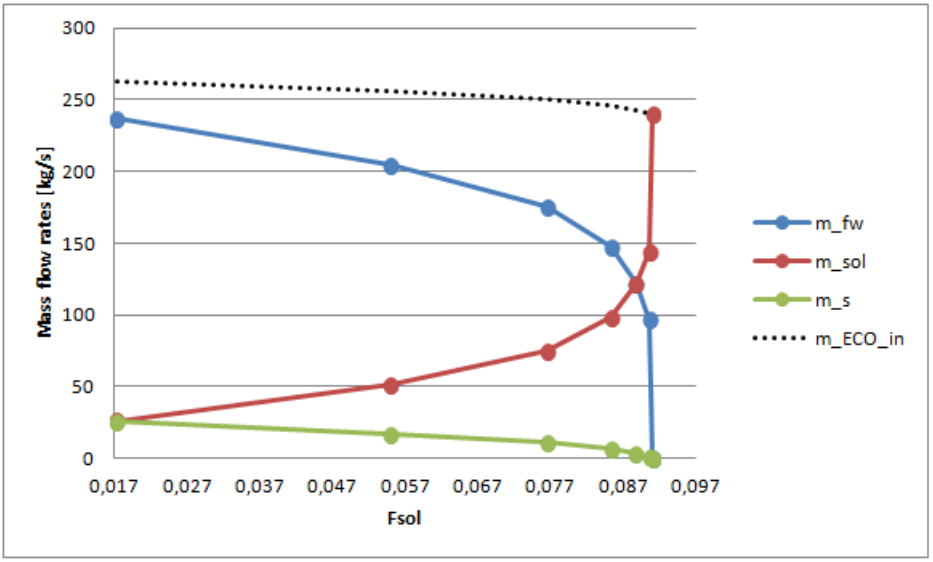

Figure 3.31: Variation of the mass flow rates in the preheater and solar section.

Since in this option a steam extraction is progressively reduced, and eventually cut off, it is useful to evaluate the modification to the whole expansion line. The next graph include, with varying solar share, the trends for each inlet stage's pressure and mass flow rate. Steam extractions are also showed in figure.

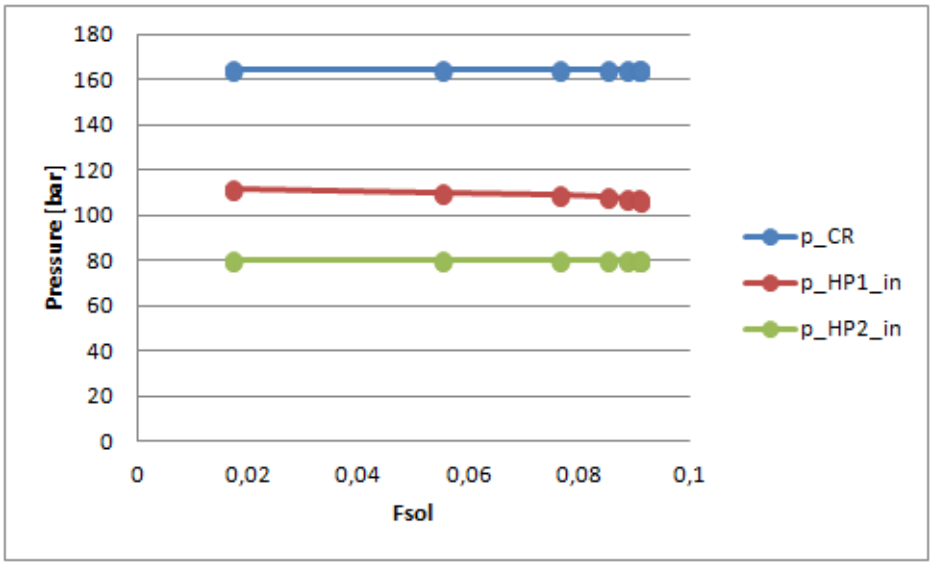

Figure 3.32: Variations of high pressure inlet stages pressures.

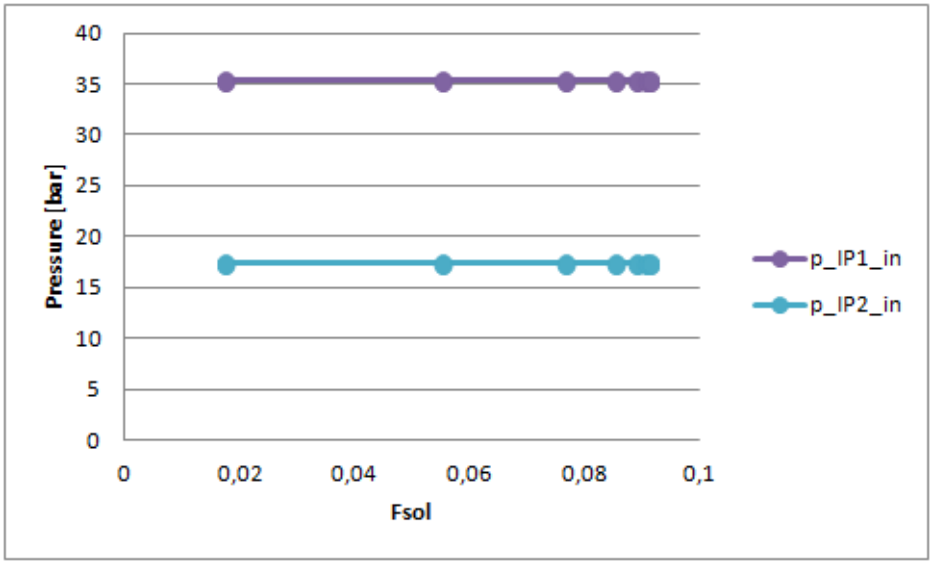

Figure 3.33: Variations of intermediate pressure inlet stages pressures.

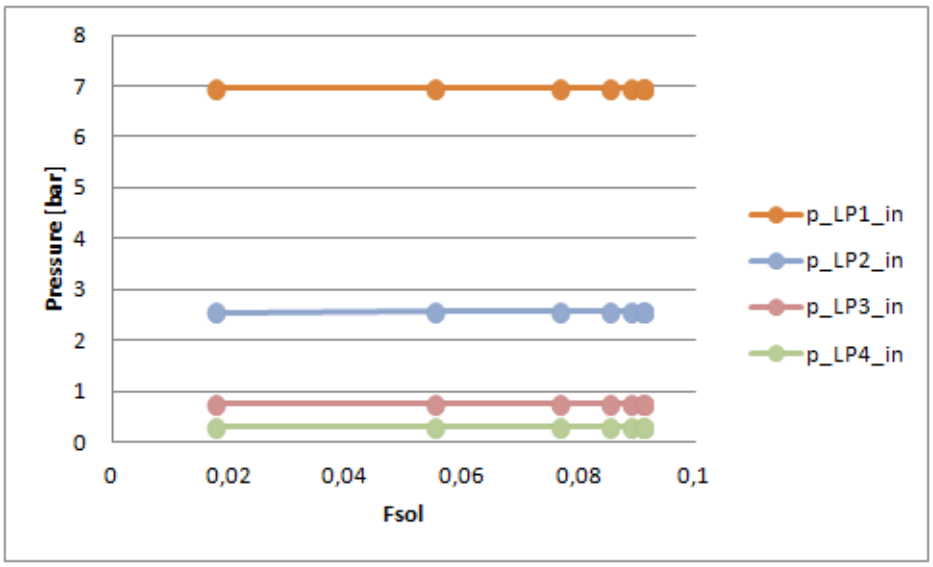

Figure 3.34: Variations of low pressure inlet stages pressures.

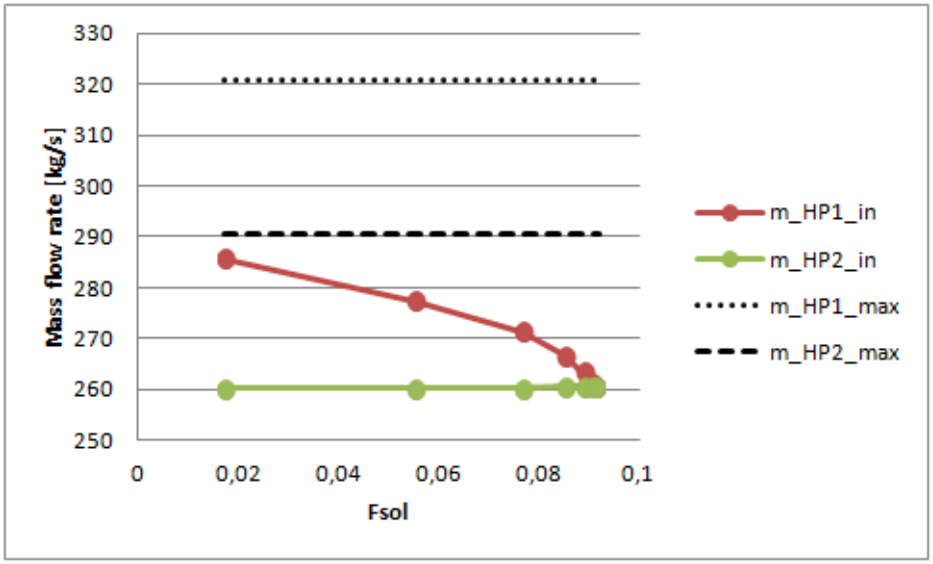

Figure 3.35: Variations of high pressure inlet stages mass flow rates.

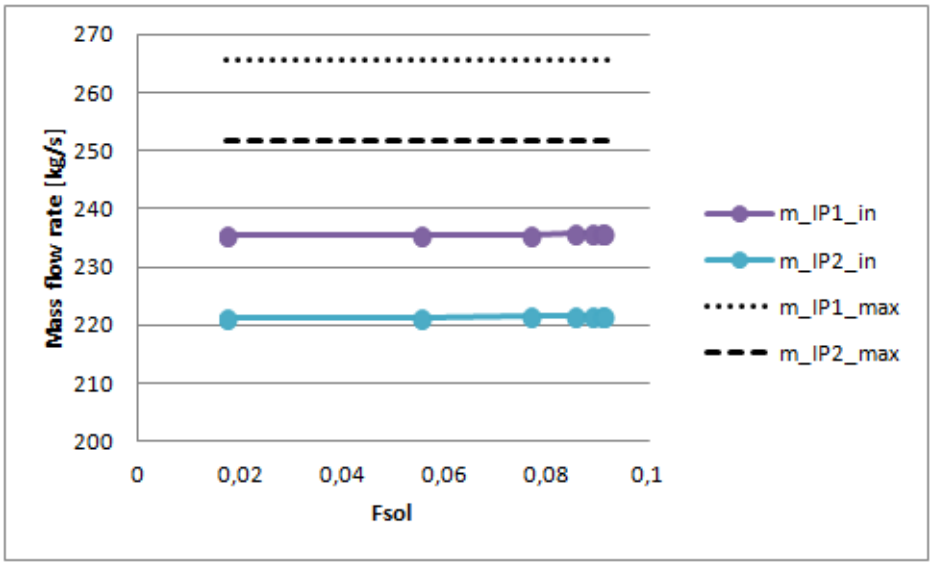

Figure 3.36: Variations of intermediate pressure inlet stages mass flow rates.

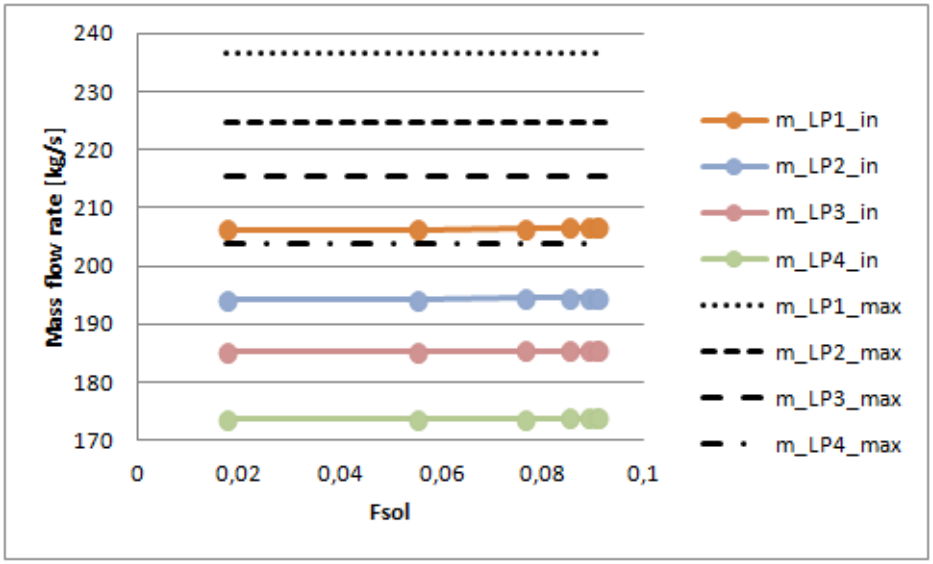

Figure 3.37: Variations of low pressure inlet stages mass flow rates.

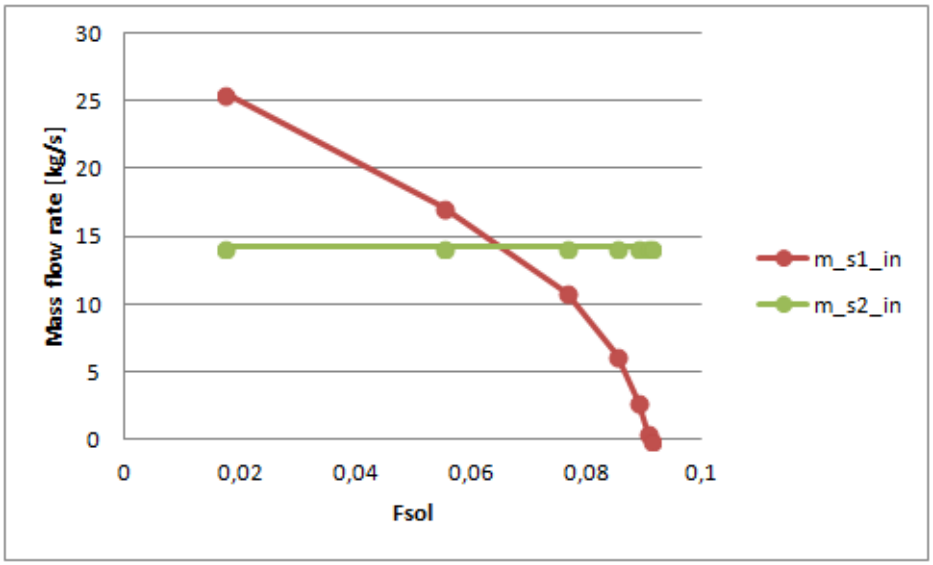

Figure 3.38: Variations of high pressure steam extractions flow rates.

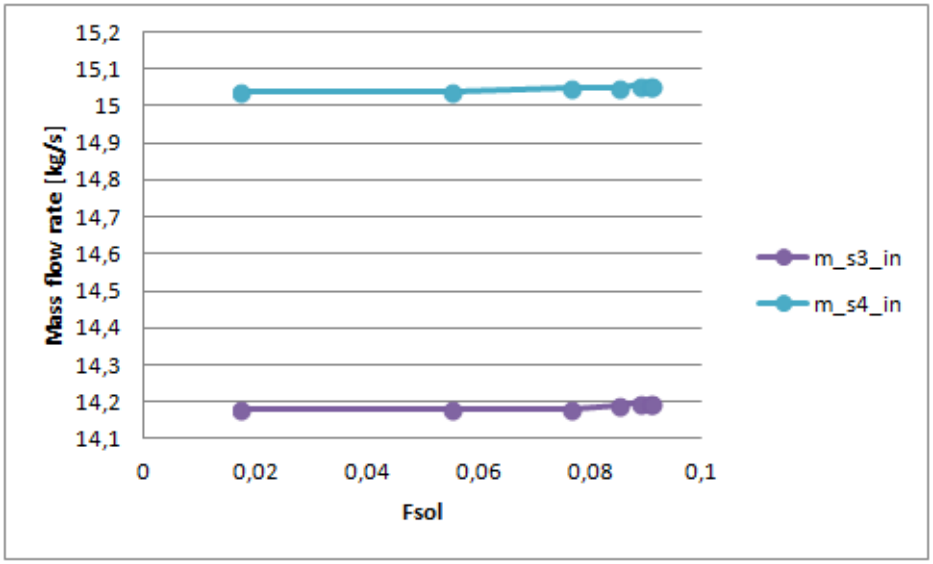

Figure 3.39: Variations of intermediate pressure steam extractions flow rates.

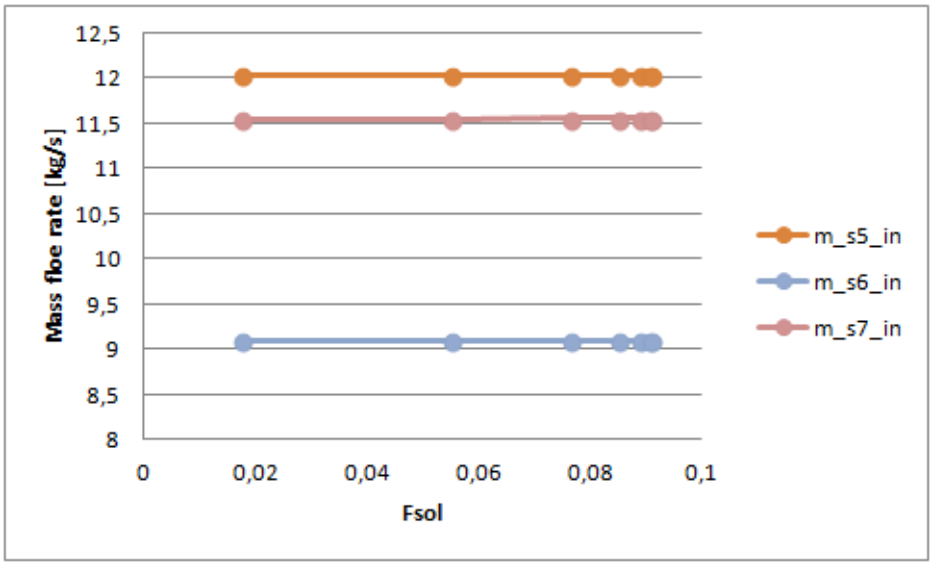

Figure 3.40: Variations of low pressure steam extractions flow rates.

Excluding the first high pressure turbine stage and its relative steam extraction, no substantial modification happens with this integration option. Turbine capacity limits are not exceeded.

When the preheater substitution is complete, the heat exchange in preheater HPH2 is reduced by 7.54% from its design value. This preheater is affected because the drainage from HPH3 is reduced (or null); the feedwater flow rate also

changes, but in the overall model the working conditions remain similar.
The next goup of diagrams reports the different integration parameters evaluated for this case.

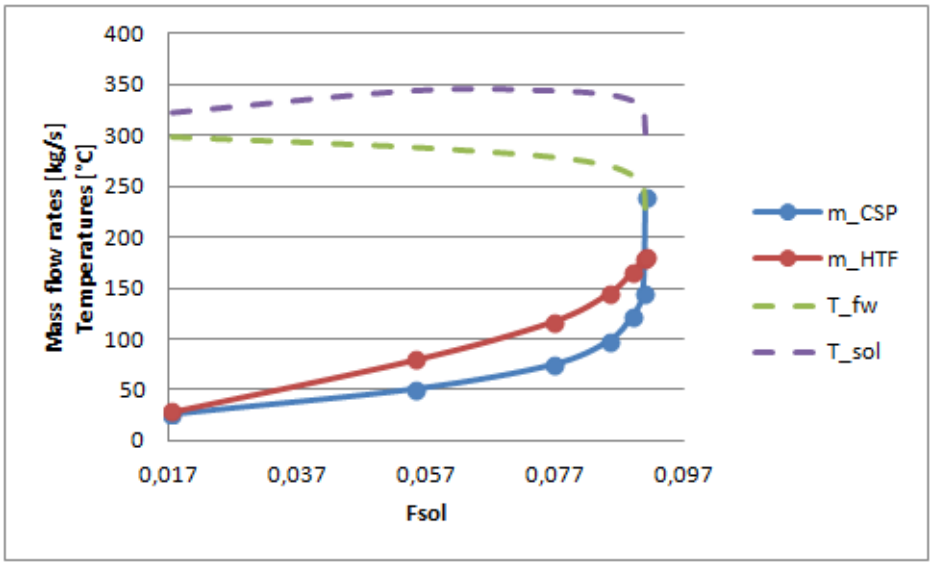

Figure 3.41: Solar and heat transfer fluid mass flow rates for Case 1.

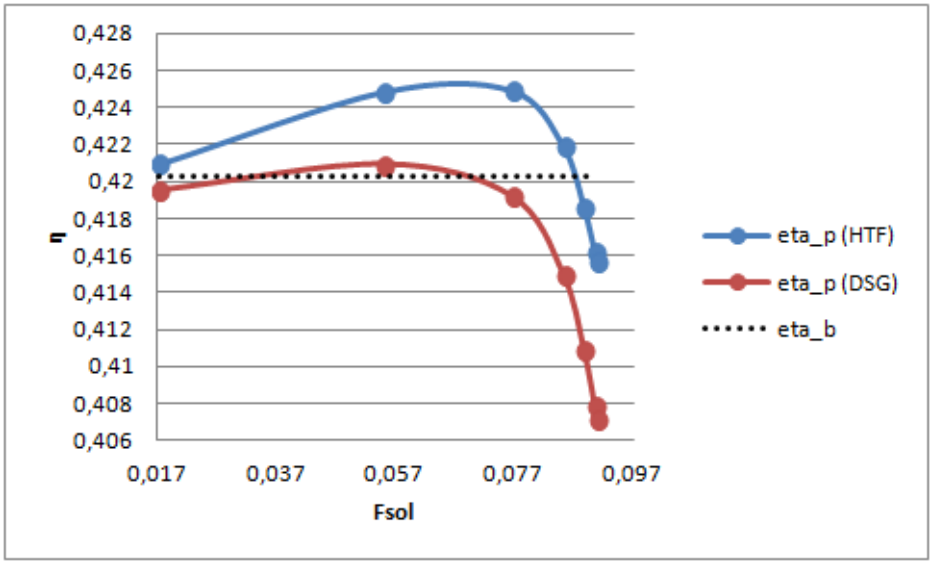

Figure 3.42: Conversion efficiency from primary sources for Case 1.

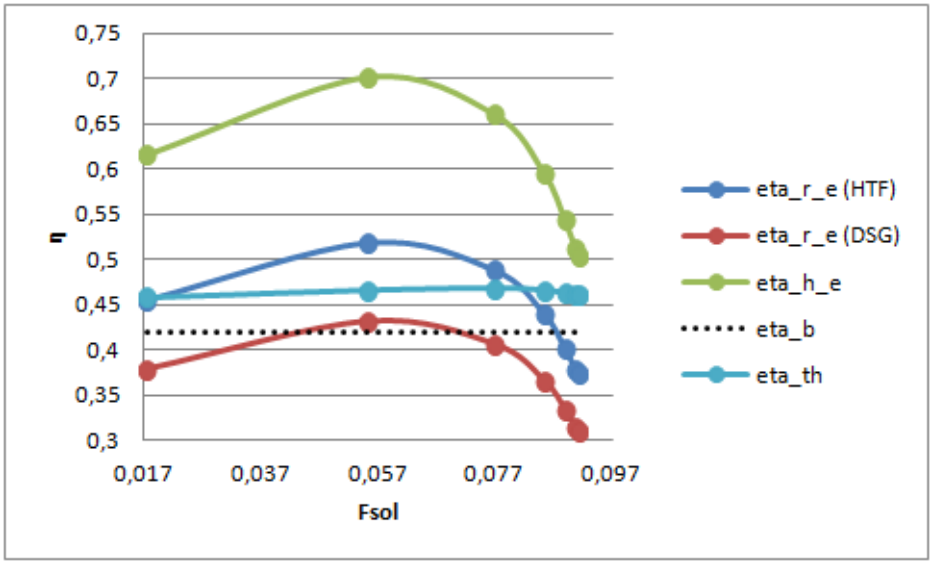

Figure 3.43: Solar radiation and heat-to-electric efficiencies for Case 1.

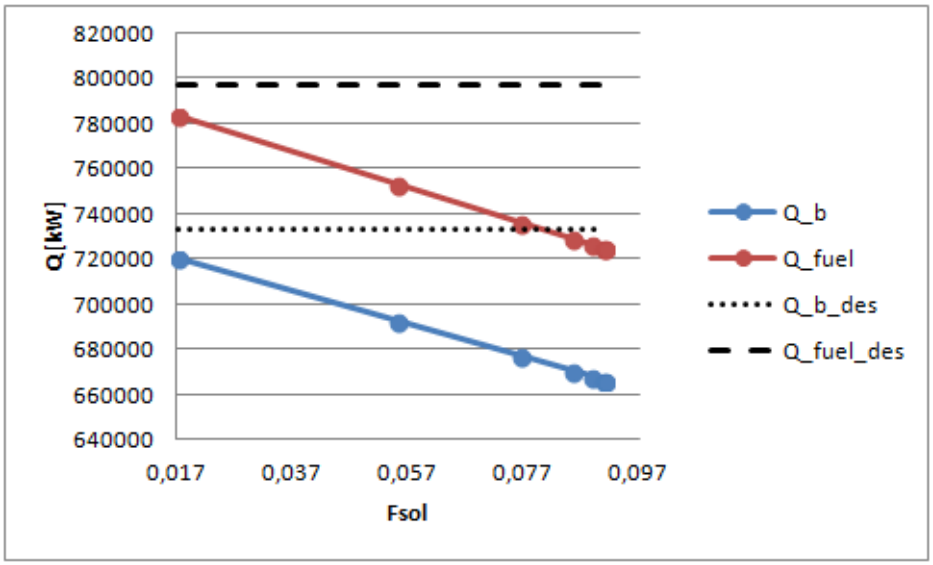

Figure 3.44: Boiler and fuel powers for Case 1.

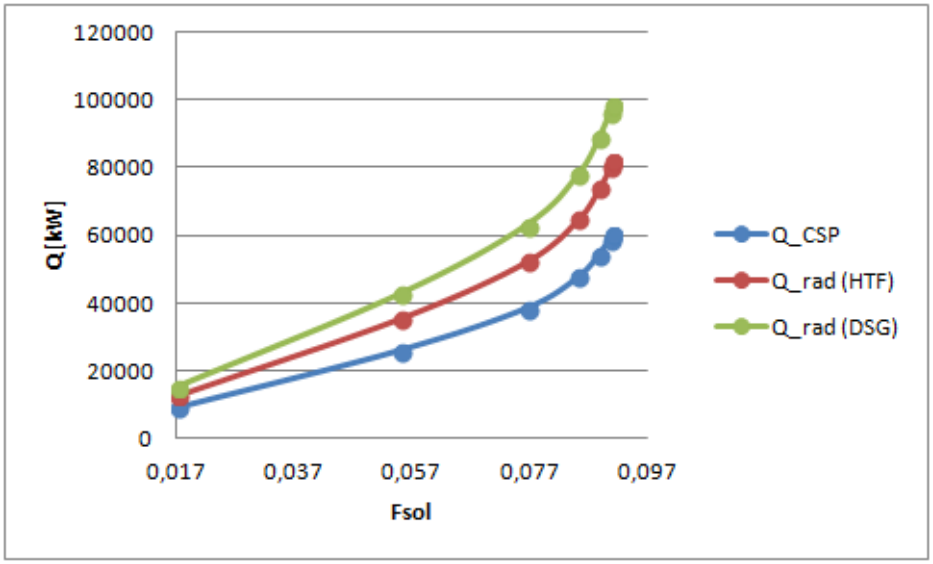

Figure 3.45: Radiation and solar heat powers for Case 1.

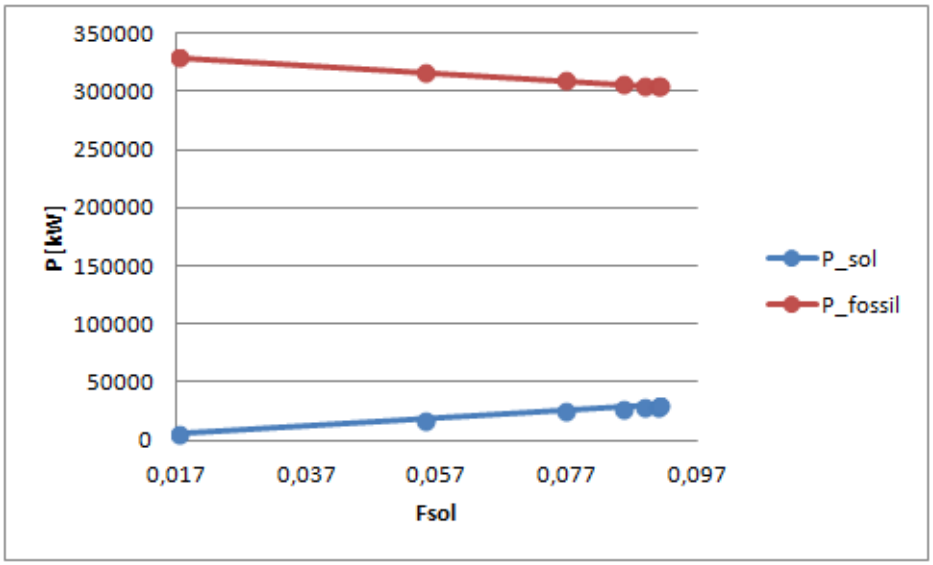

Figure 3.46: Solar and fossil powers for Case 1.

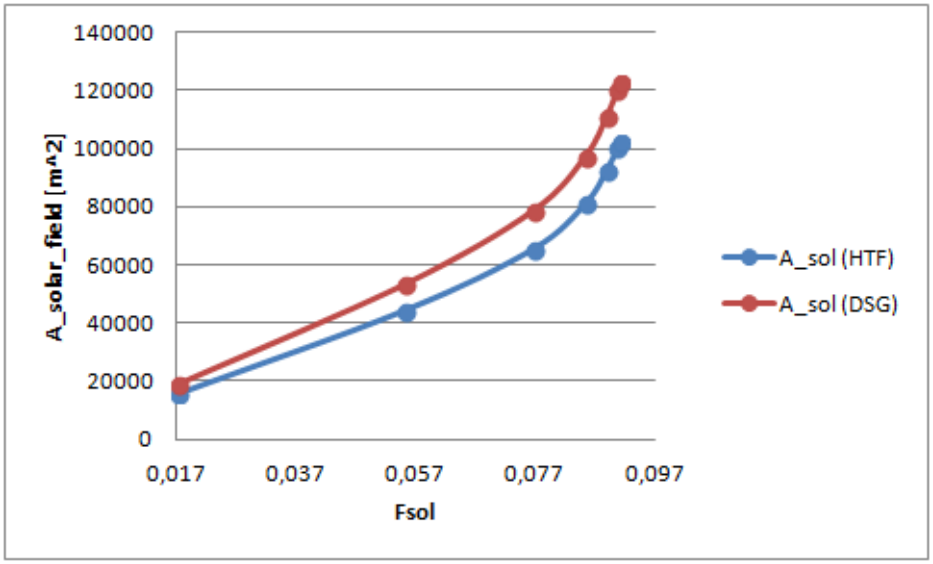

Figure 3.47: Solar field area for Case 1.

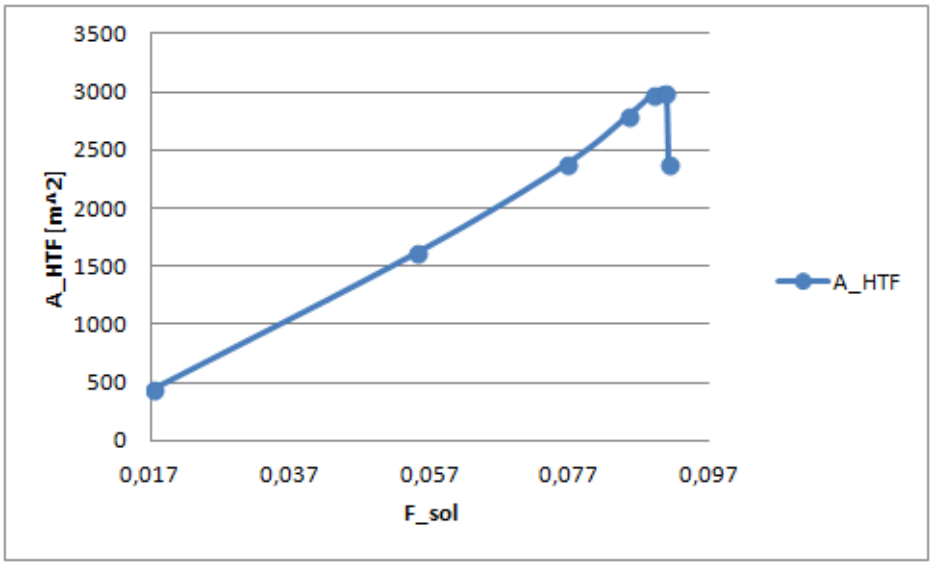

Figure 3.48: Intermediate heat exchanger area for Case 1.

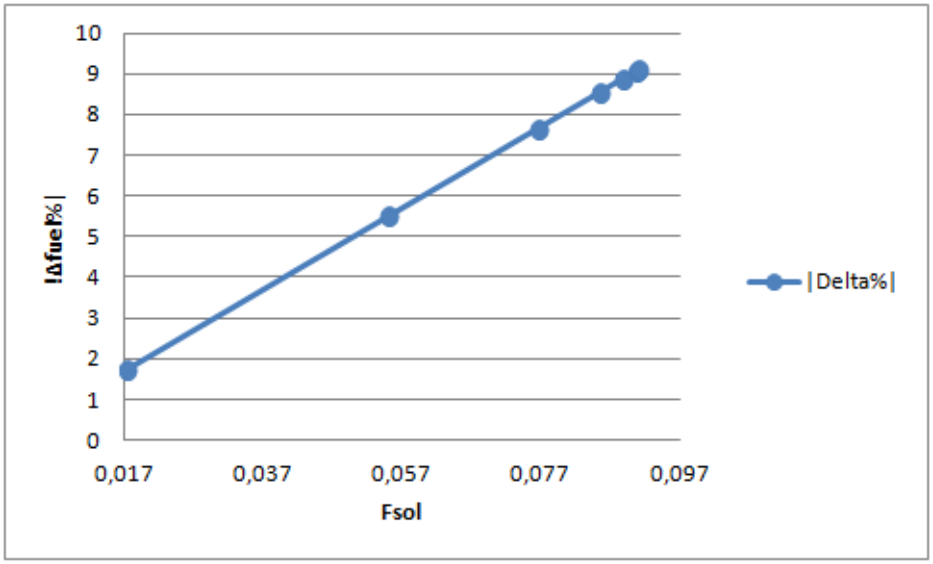

Figure 3.49: Absolute value of the percentage fuel saving for Case 1.

3.7.2 Case 2: Steam generation from drainage water, immission in the second high pressure turbine stage

The drainage from the highest temperature preheater is sent, all or in part, to the CSP section to be evaporated to the same conditions found at the first high pressure turbine stage's outlet. There, the solar stream is mixed with the main flow rate. No particular modifications have to be added to the base cycle to implement this situation. Preheaters models are kept as in the base system.
The temperature at the solar field outlet slightly increases with the solar share (3.50): this is caused by the way the intensive variables in the first stages react to the integration.

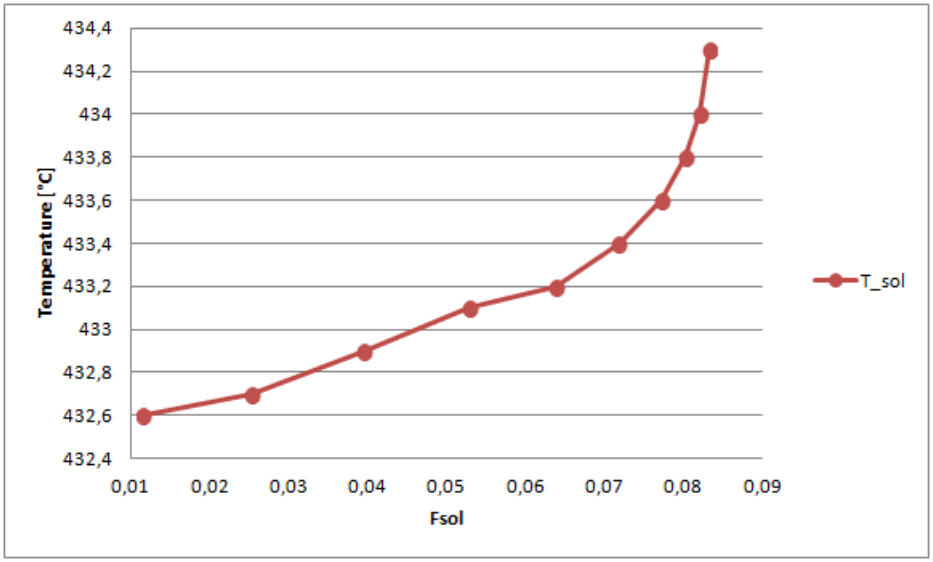

Figure 3.50: Solar field outlet temperature with varying solar share for Case 2.

From figures 3.51 and following, it can be seen that the pressure at the first stage outlet decreases. The other pressures remain nearly unchanged.

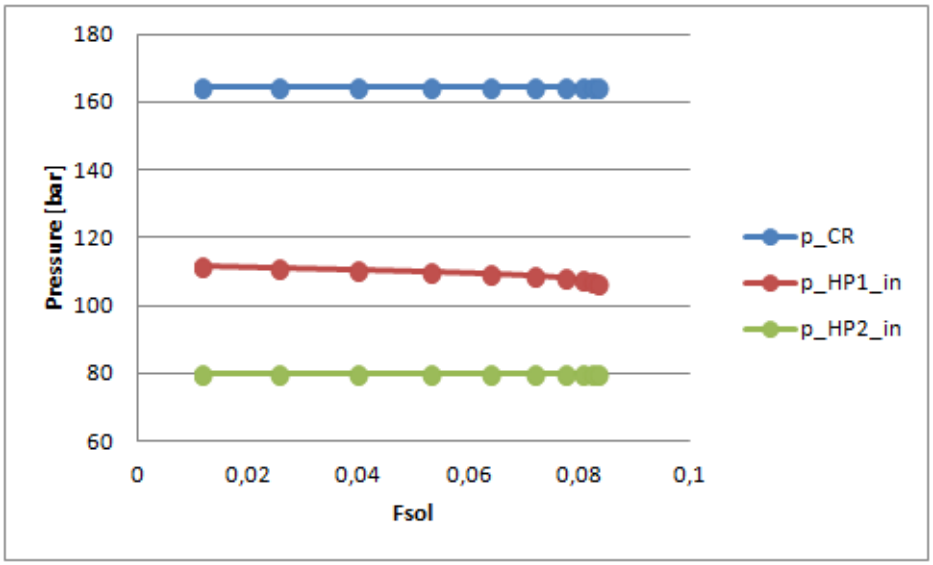

Figure 3.51: Variations of high pressure inlet stages pressures.

Figures 3.54 ond on, includes the expansion line's mass flow rates trends: when the additional stream is added, the mass flow rate at the outlet of the first stage varies in such a way to keep the mass flow rate after the mixing at a constant value.

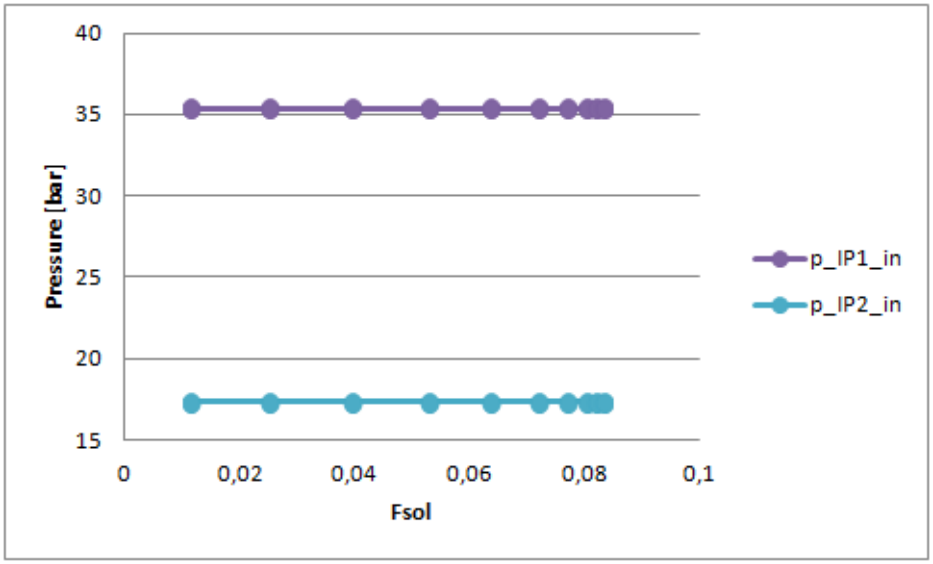

Figure 3.52: Variations of intermediate pressure inlet stages pressures.

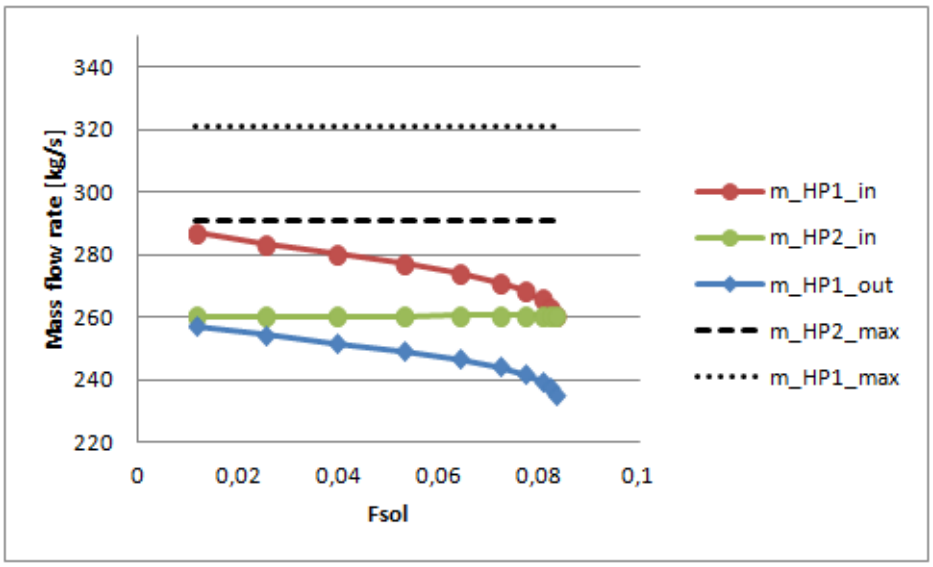

Figure 3.54: Variations of high pressure inlet stages mass flow rates.

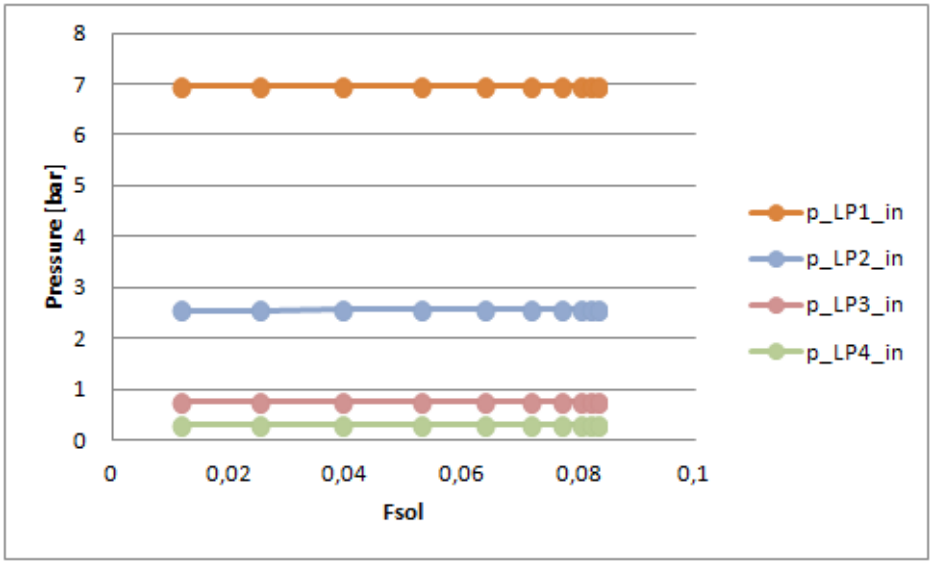

Figure 3.53: Variations of low pressure inlet stages pressures.

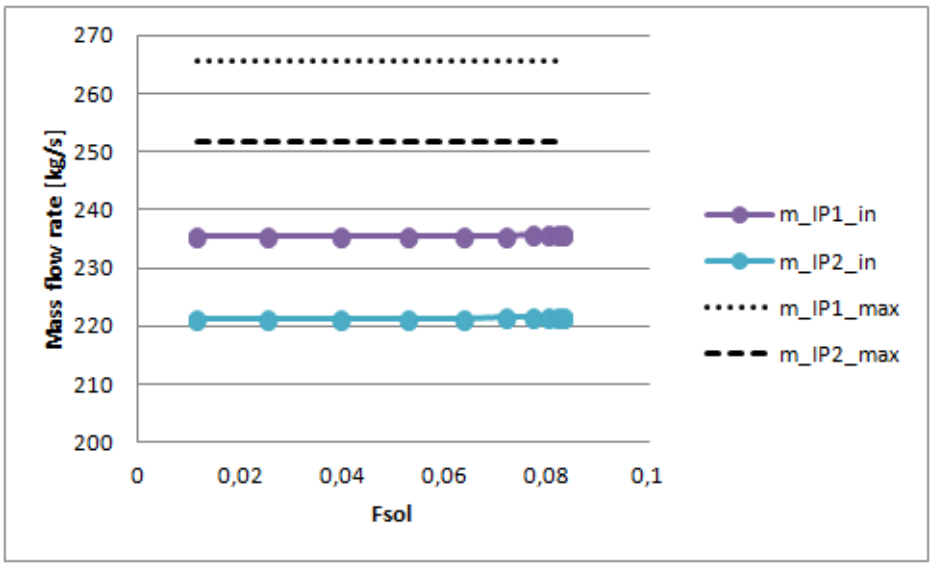

Figure 3.55: Variations of intermediate pressure inlet stages mass flow rates.

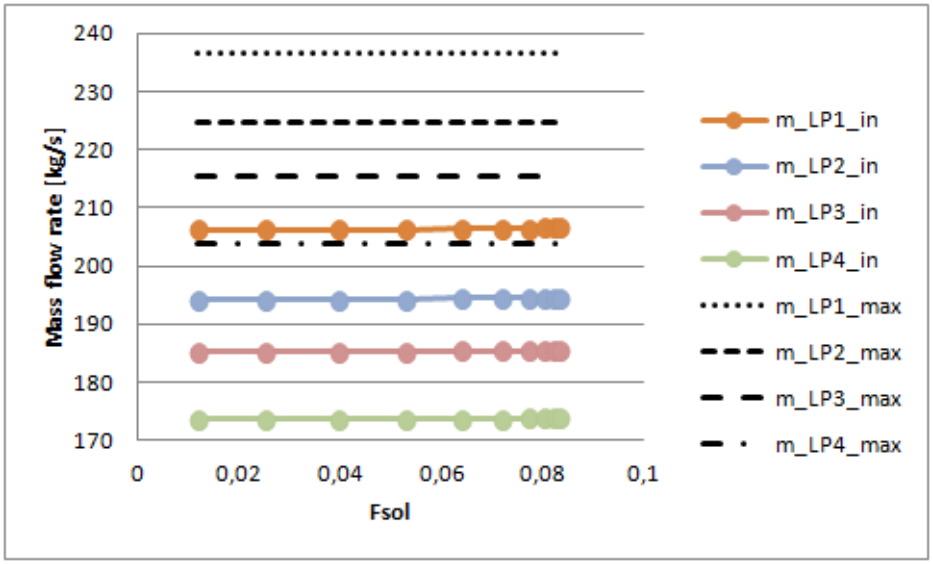

Figure 3.56: Variations of low pressure inlet stages mass flow rates.

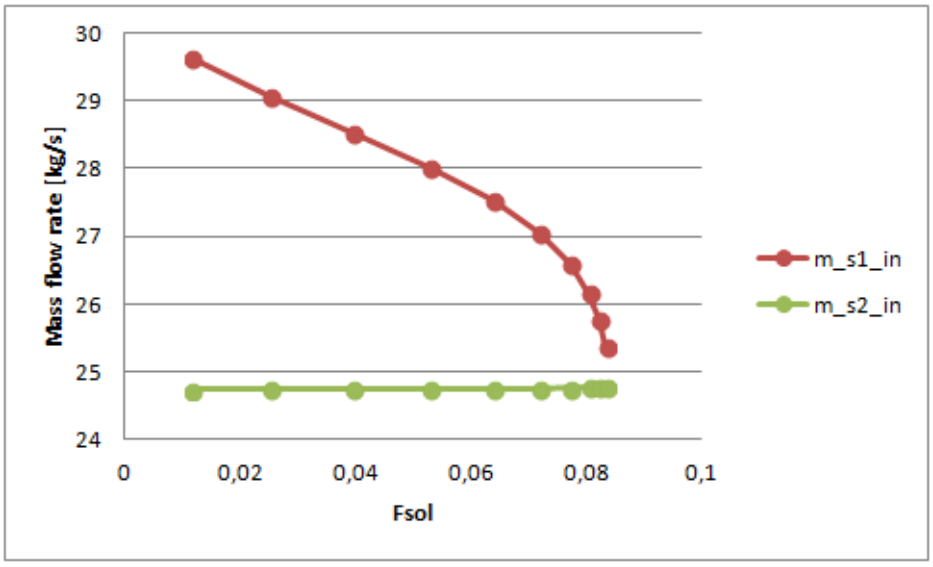

Figure 3.57: Variations of high pressure steam extractions flow rates.

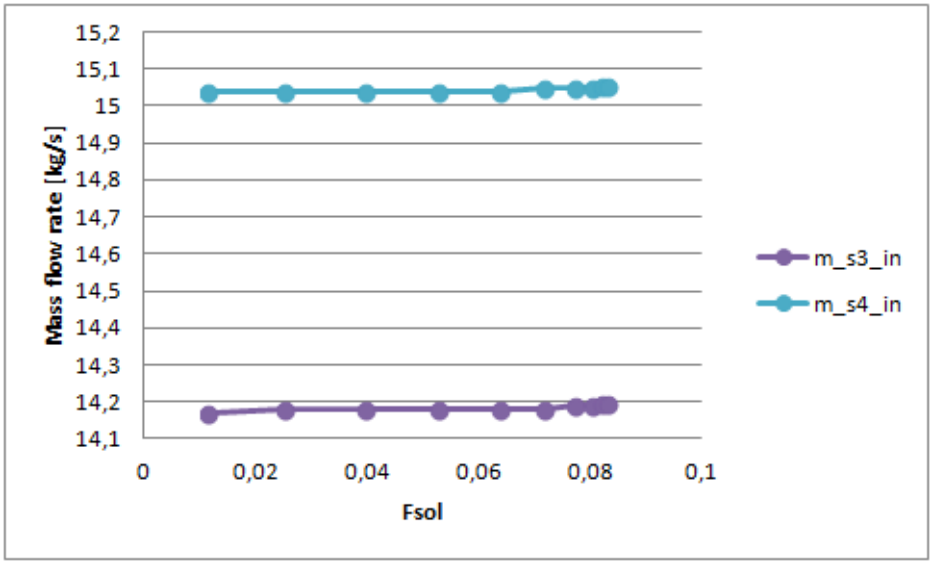

Figure 3.58: Variations of intermediate pressure steam extractions flow rates.

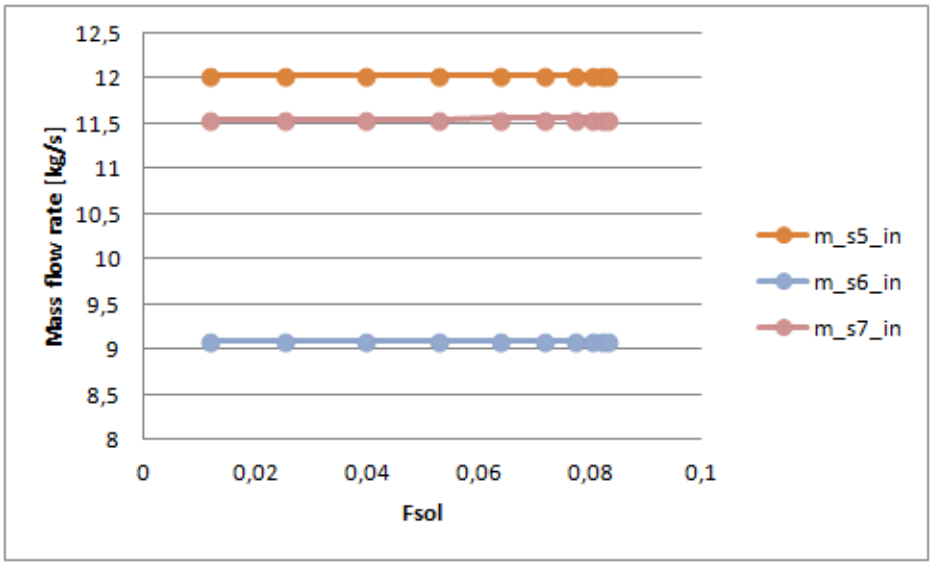

Figure 3.59: Variations of low pressure steam extractions flow rates.

When the entire drainage mass is sent to the turbine, the heat exchanged in the last preheater is reduced by 15% from its design value. For the previous preheater, HPH2, the heat variation is the same as Case 1, since it is affected in the same way. The next figures plot the integration parameters results.

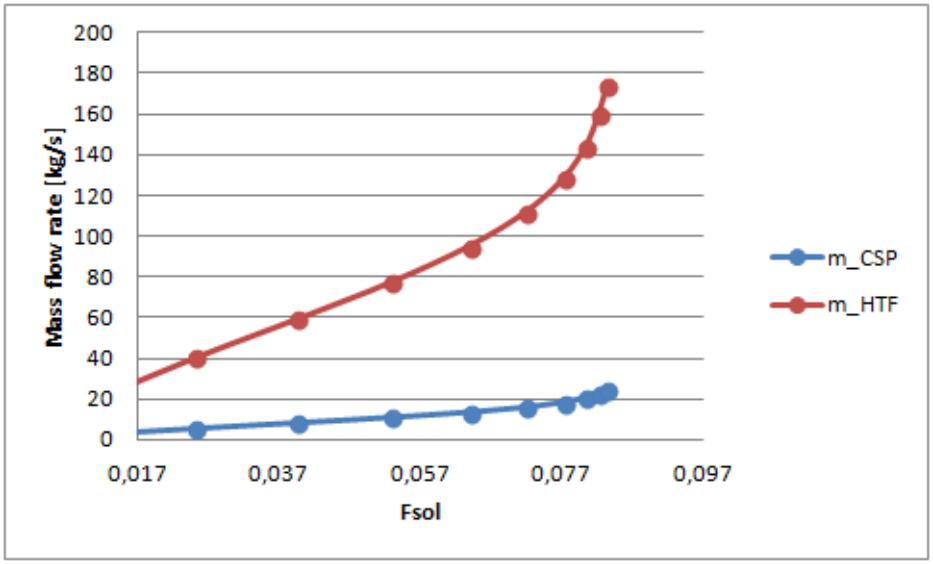

Figure 3.60: Solar and heat transfer fluid mass flow rates for Case 2.

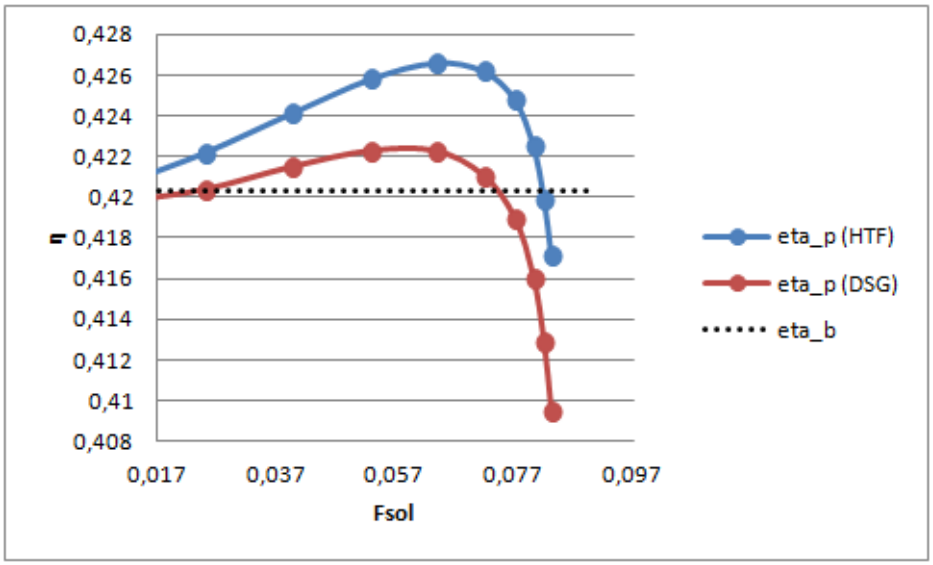

Figure 3.61: Conversion efficiency from primary sources for Case 2.

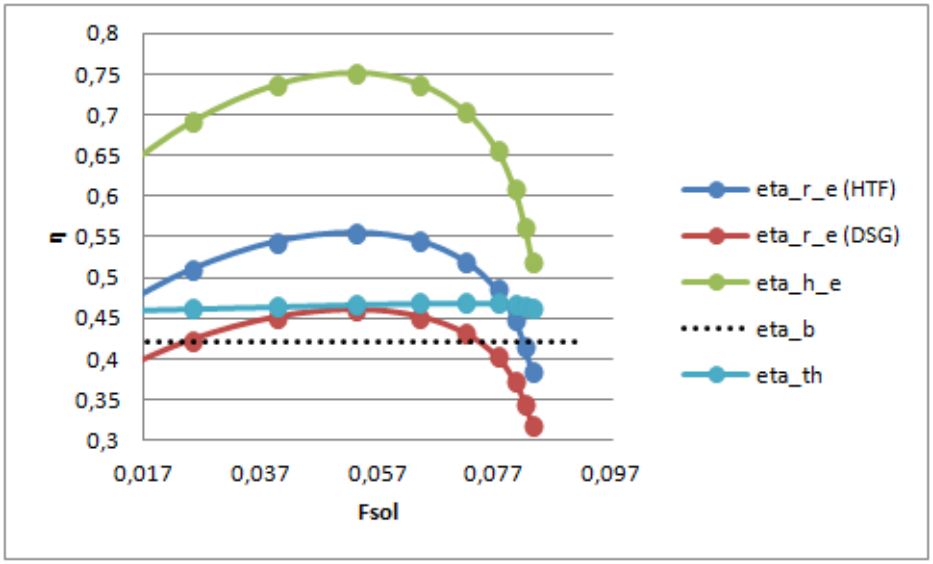

Figure 3.62: Solar radiation and heat-to-electric efficiencies for Case 2.

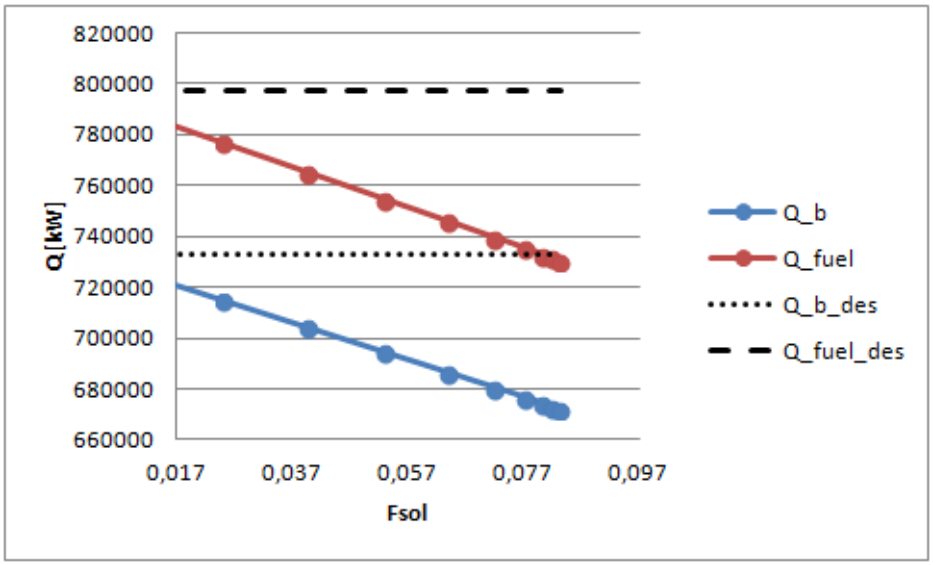

Figure 3.63: Boiler and fuel powers for Case 2.

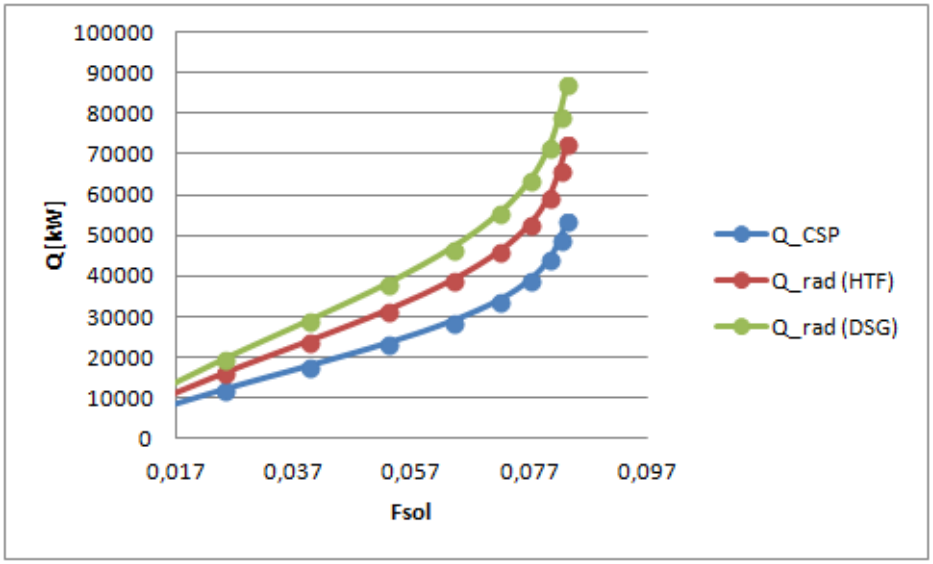

Figure 3.64: Radiation and solar heat powers for Case 2.

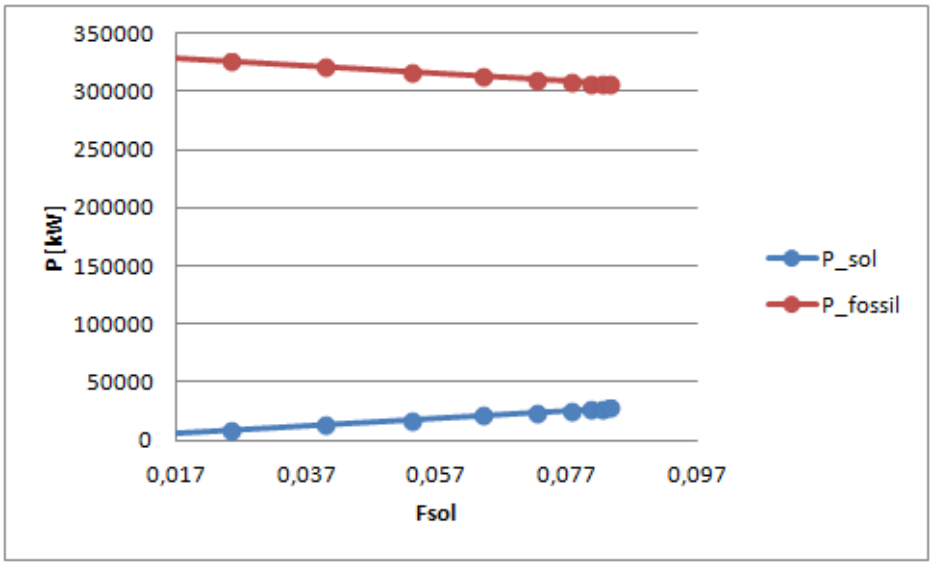

Figure 3.65: Solar and fossil powers for Case 2.

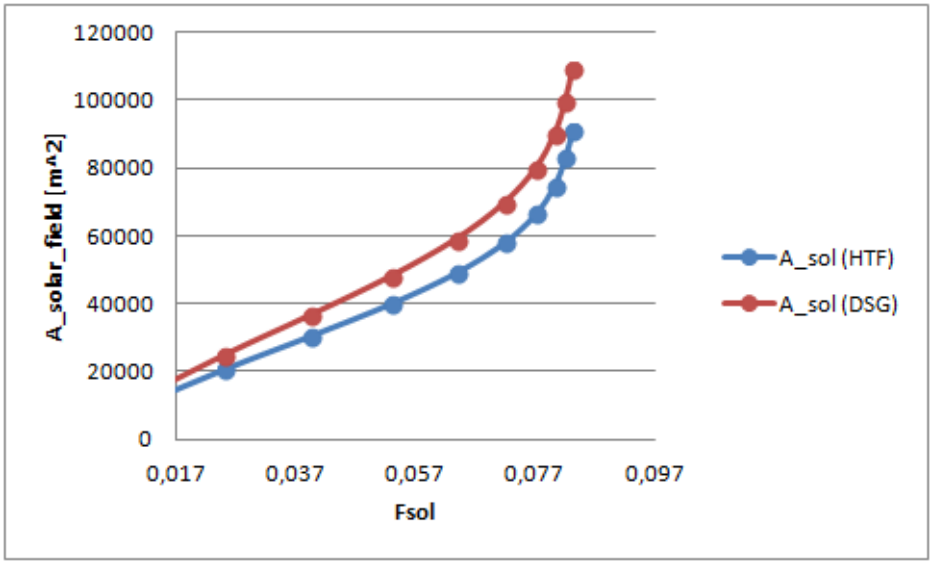

Figure 3.66: Solar field area for Case 2.

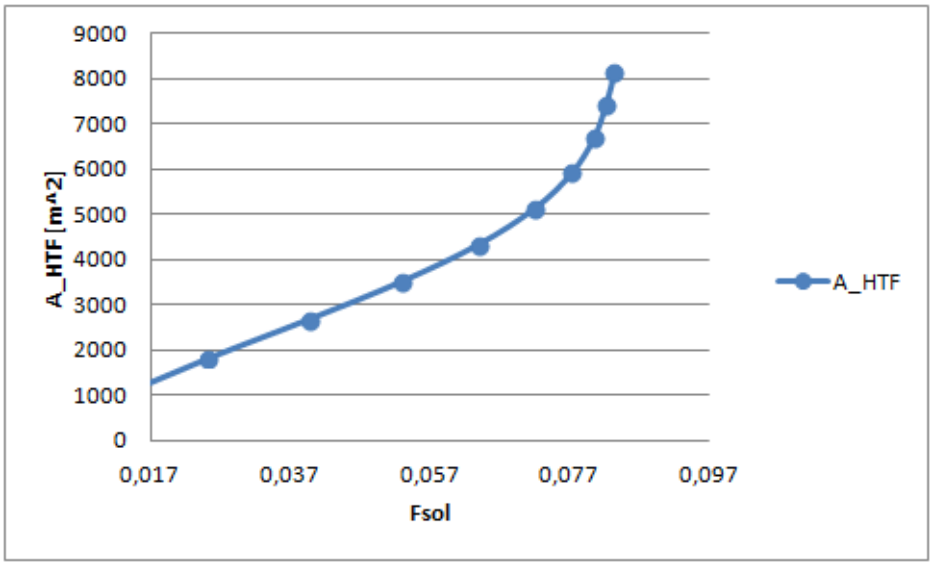

Figure 3.67: Intermediate heat exchanger area for Case 2.

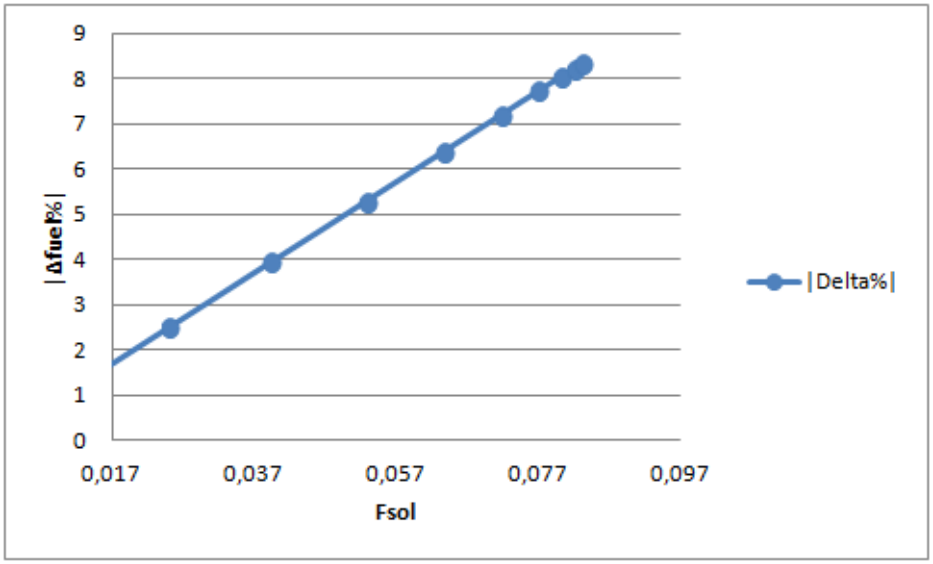

Figure 3.68: Absolute value of the percentage fuel saving for Case 2.

3.7.3 Case 3: Steam generation from drainage water, immission before the reheater

This case is similar to the previous one: only the drainage and the addition point change: now the drainage from the second high temperature preheater is heated to reach the same conditions found before the reheater. The pressures in the steam extraction's line are more sensitive to the system modification than in the previous synergy. The variations is more evident in the first two stages; overall, their entities are limited.

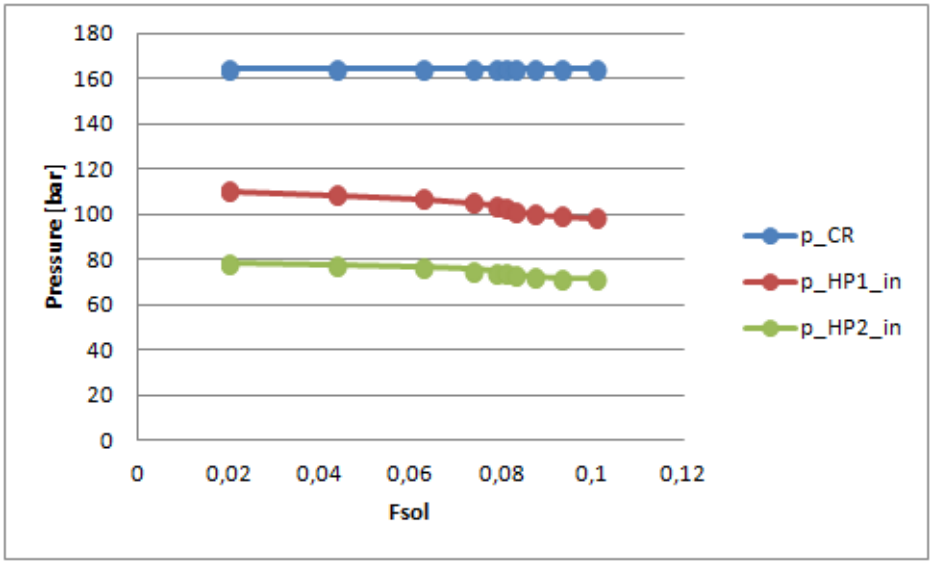

Figure 3.69: Variations of high pressure inlet stages pressures.

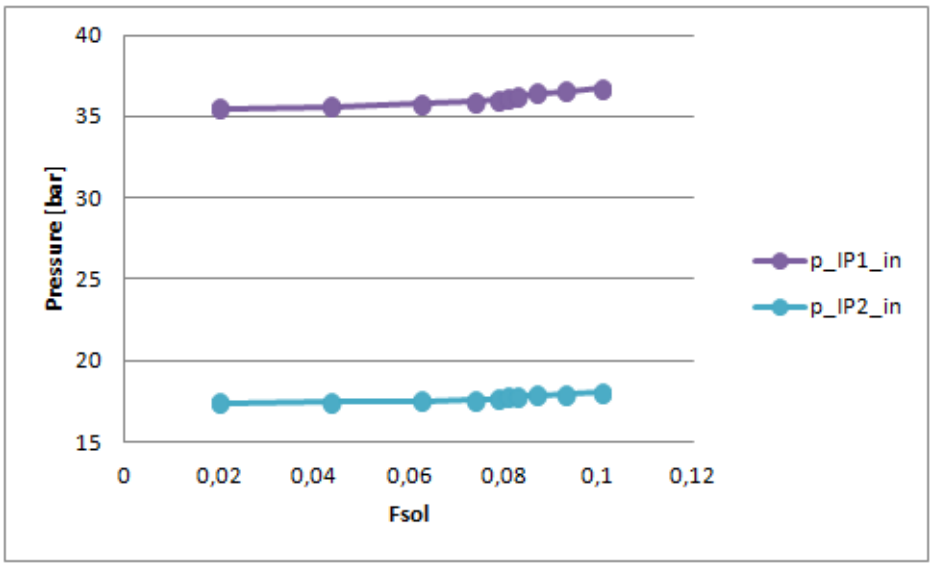

Figure 3.70: Variations of intermediate pressure inlet stages pressures.

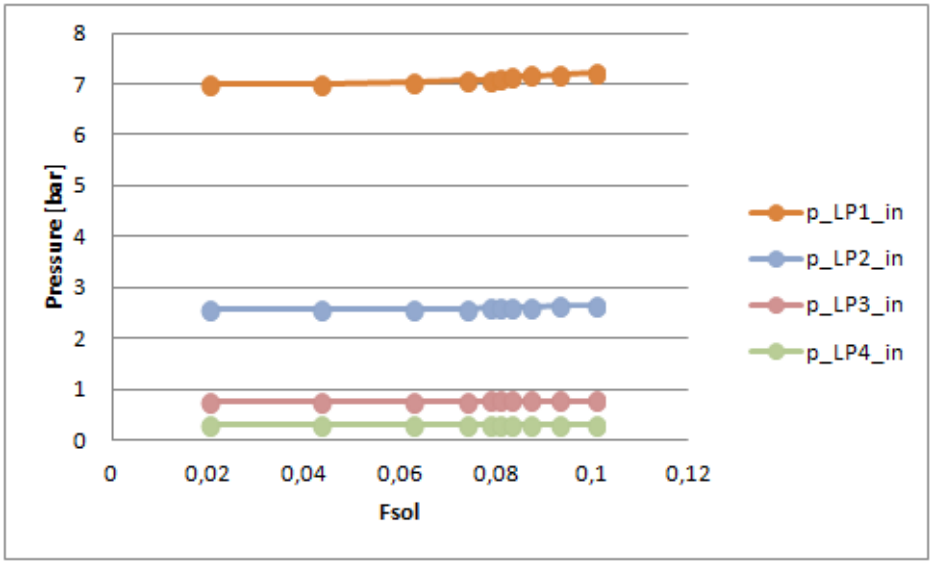

Figure 3.71: Variations of low pressure inlet stages pressures.

The mass flow rates changes more drastically, even if always inside the allowed capacity range. This could be caused by the way the expansion line's model is built: the steam is added in an intermediate stage, while in Case 1 it was added in the first section. The drainage water is also more consistent. The high pressure steam extractions decrease when the solar share increases, while all the other exctractions increase.

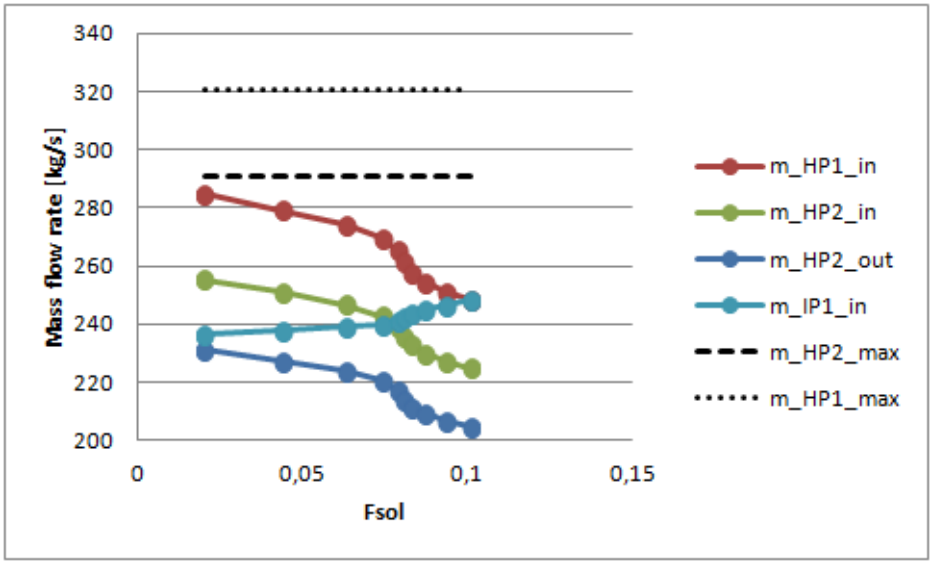

Figure 3.72: Variations of high pressure inlet stages mass flow rates.

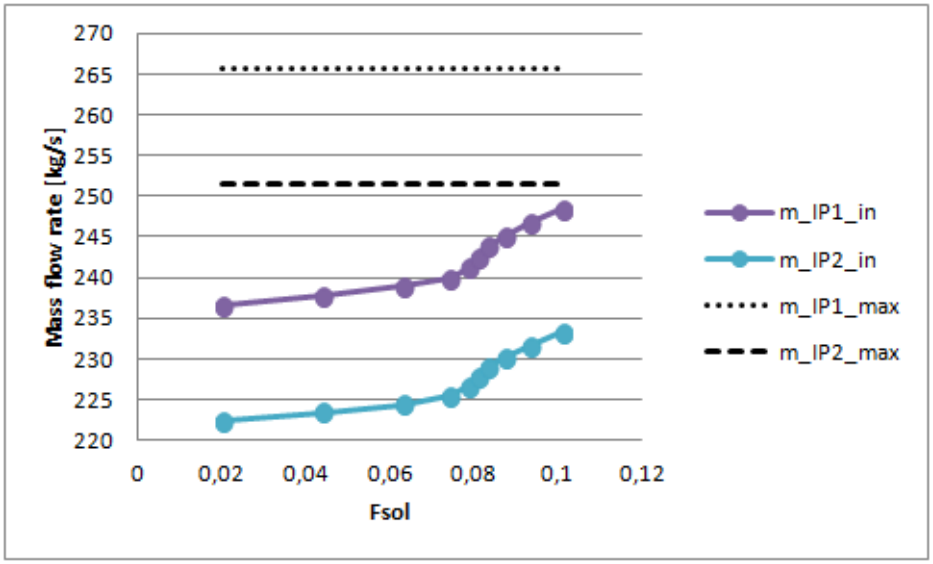

Figure 3.73: Variations of intermediate pressure inlet stages mass flow rates.

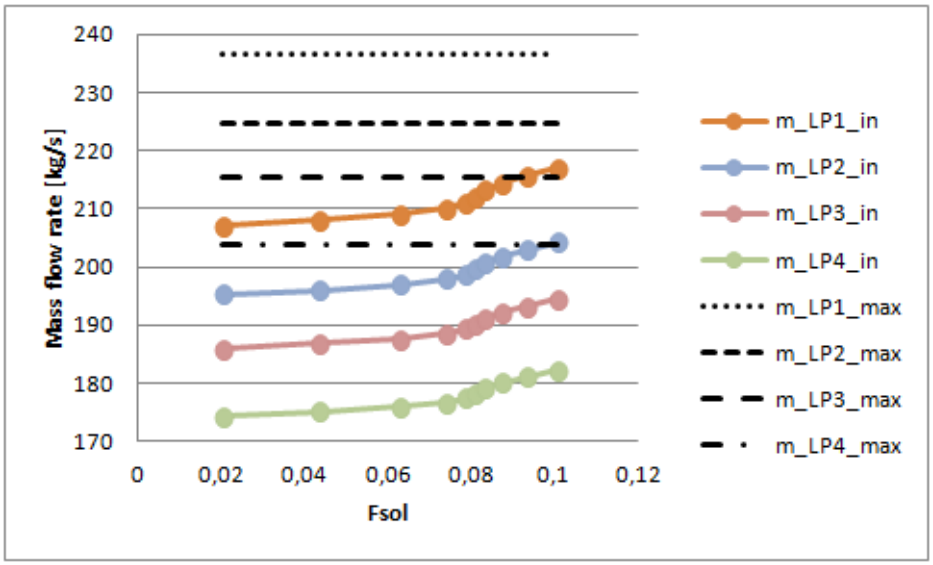

Figure 3.74: Variations of low pressure inlet stages mass flow rates.

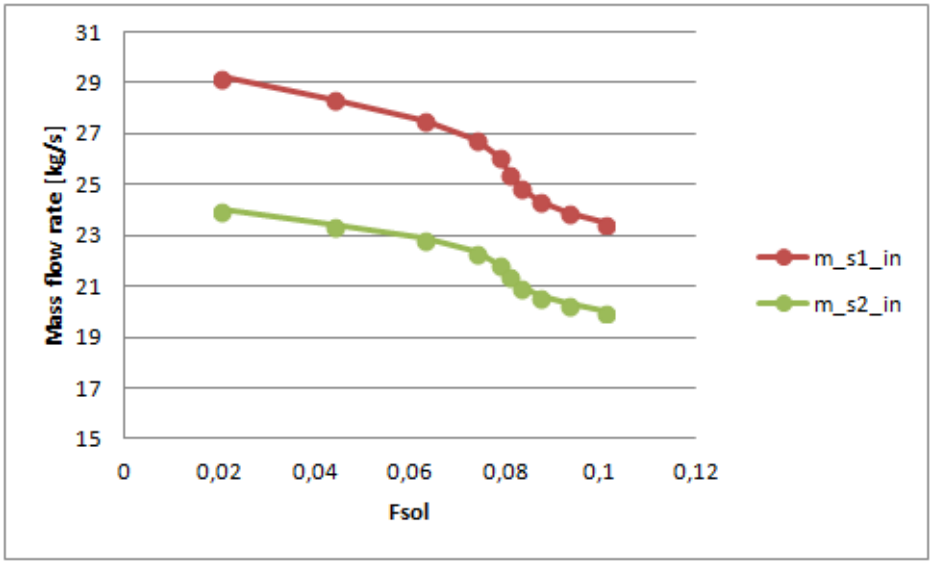

Figure 3.75: Variations of high pressure steam extractions flow rates.

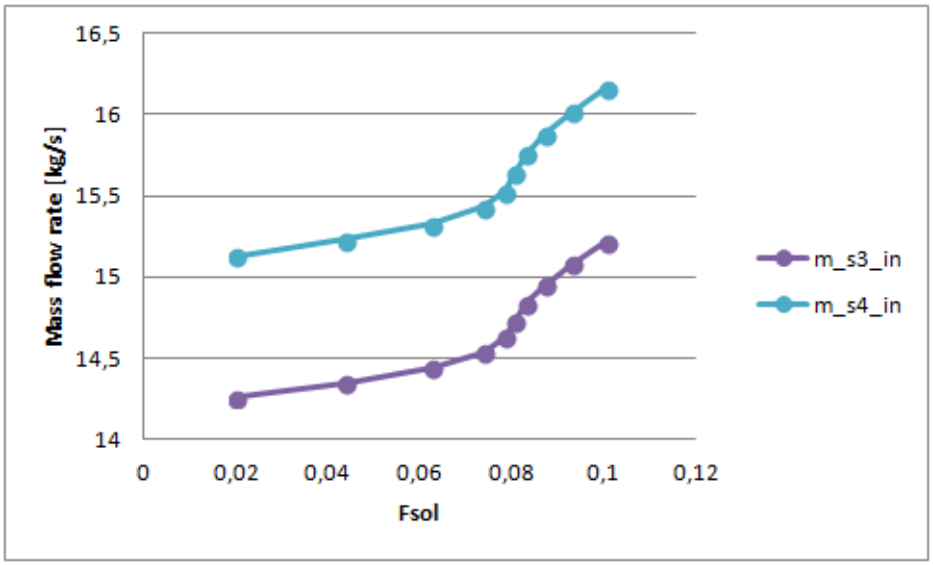

Figure 3.76: Variations of intermediate pressure steam extractions flow rates.

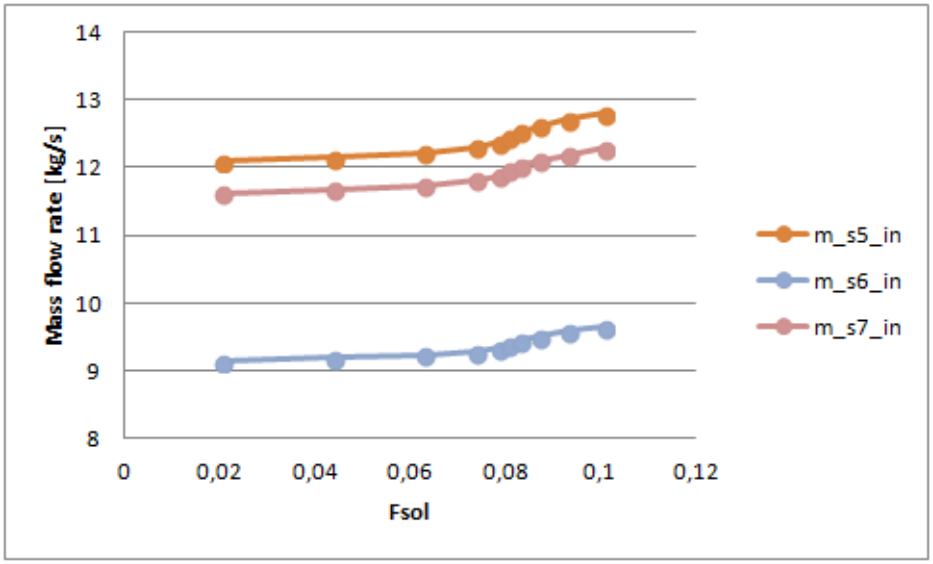

Figure 3.77: Variations of low pressure steam extractions flow rates.

Only the solution with parabolic trough and intermediate thermal fluid is considered, because if direct steam generation is applied the conversion efficiency is lower than the base cycle efficiency. The results for the integration parameters are:

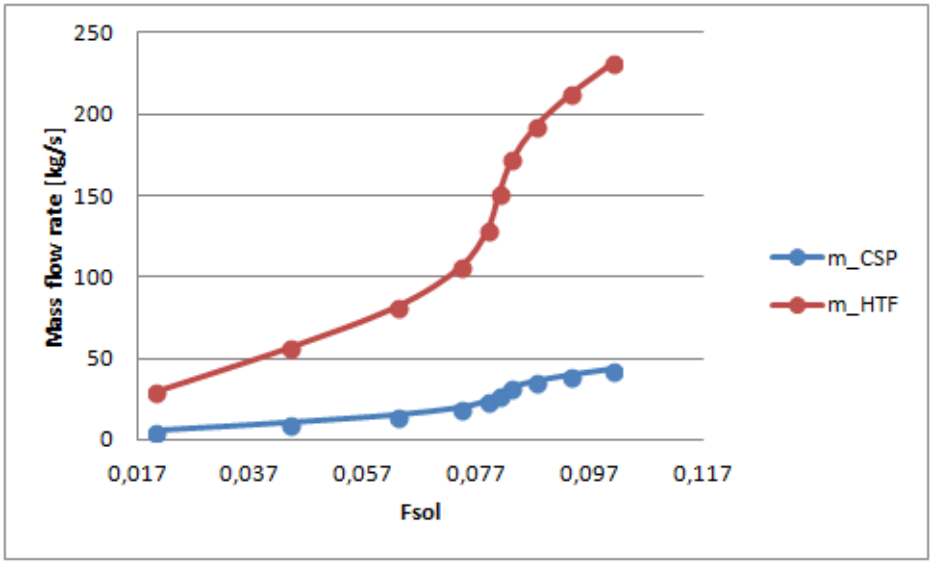

Figure 3.78: Solar and heat transfer fluid mass flow rates for Case 3.

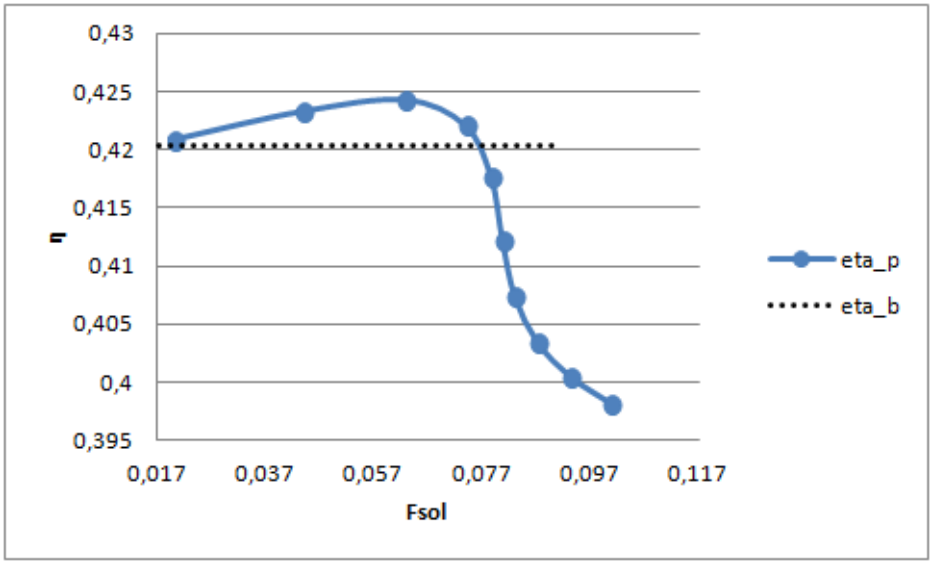

Figure 3.79: Conversion efficiency from primary sources for Case 3.

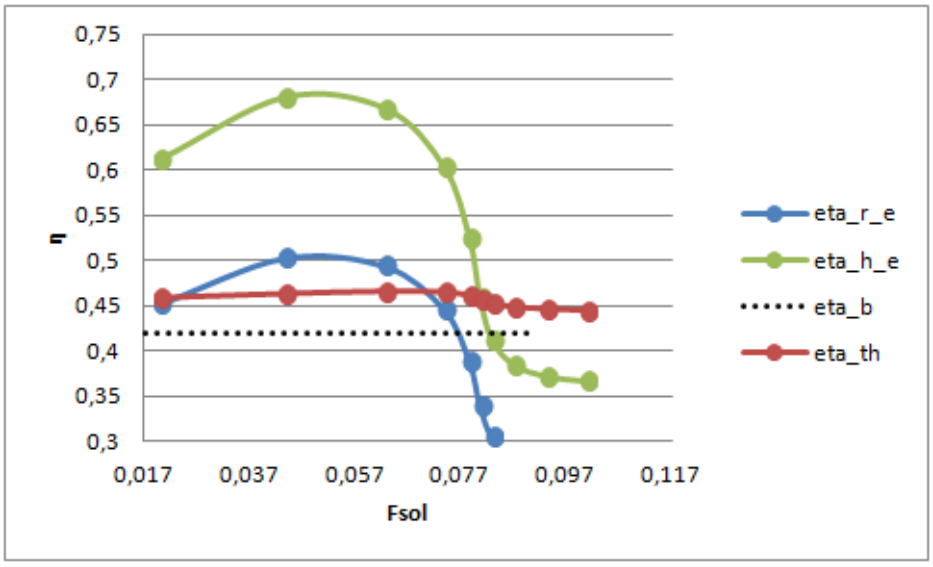

Figure 3.80: Solar radiation and heat-to-electric efficiencies for Case 3.

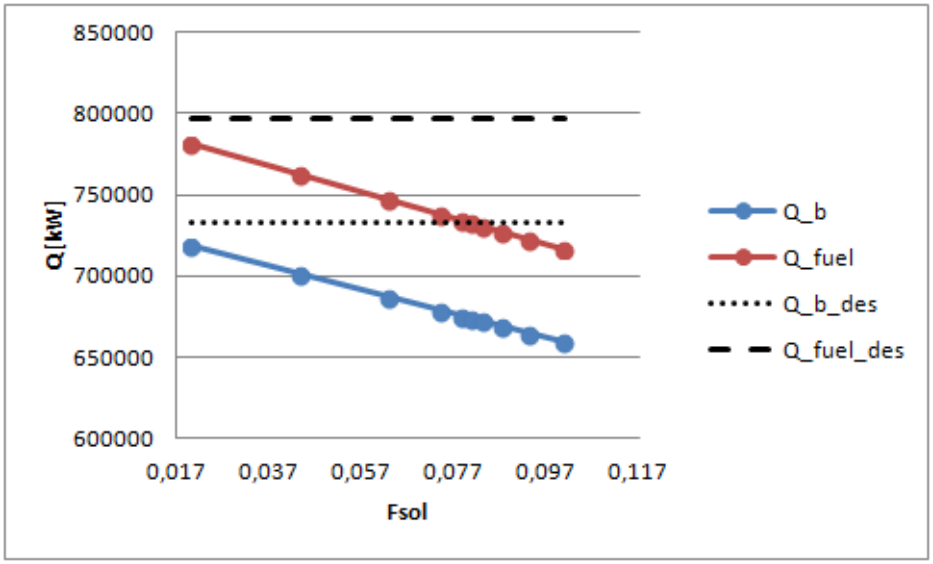

Figure 3.81: Boiler and fuel powers for Case 3.

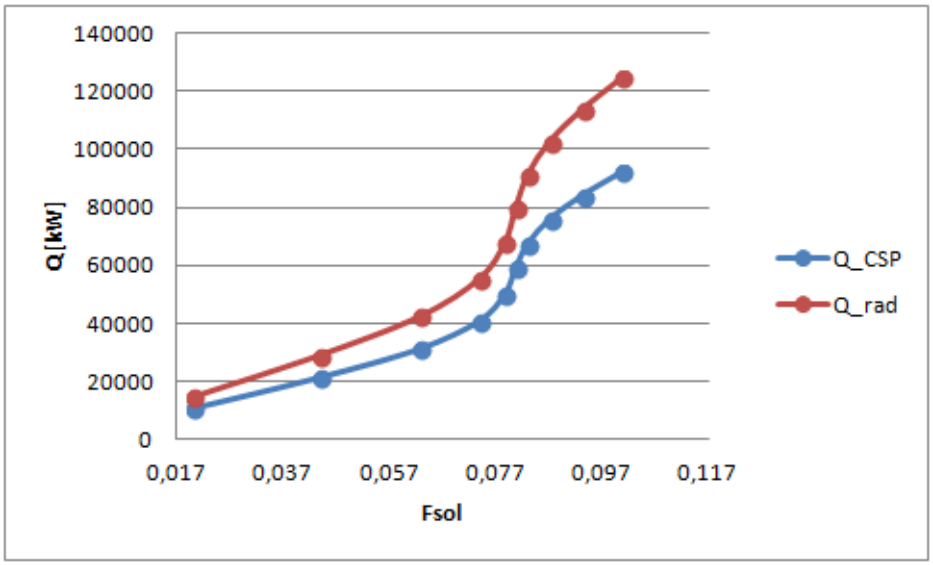

Figure 3.82: Radiation and solar heat powers for Case 3.

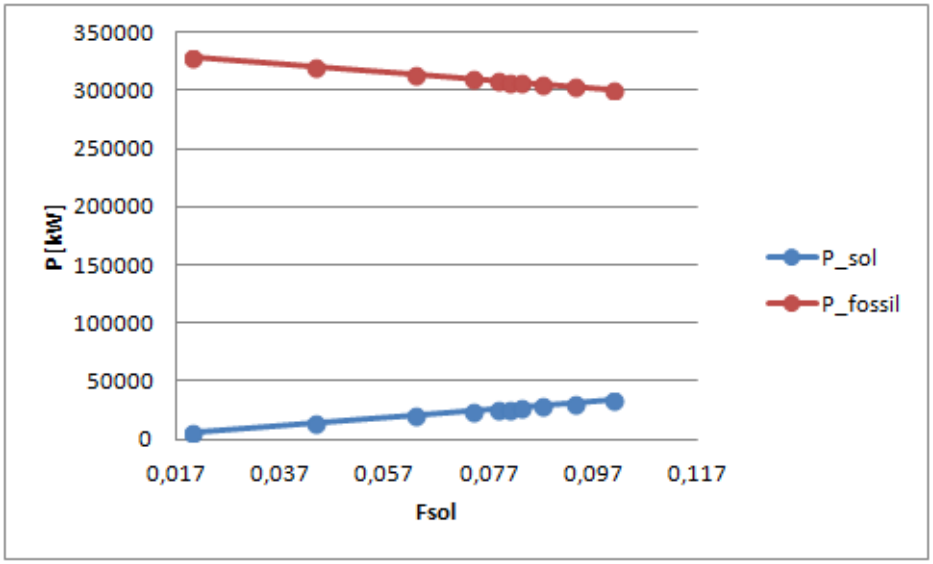

Figure 3.83: Solar and fossil powers for Case 3.

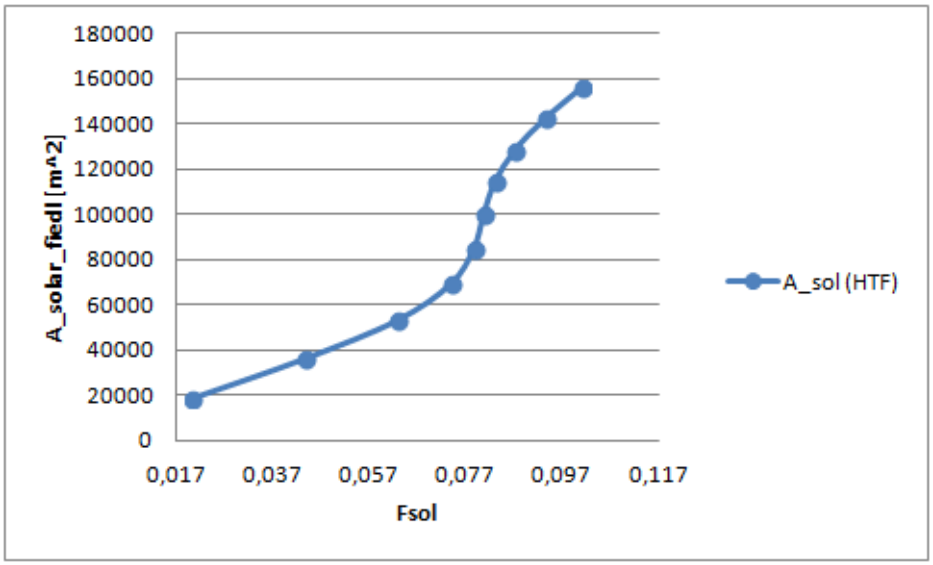

Figure 3.84: Solar field area for Case 3.

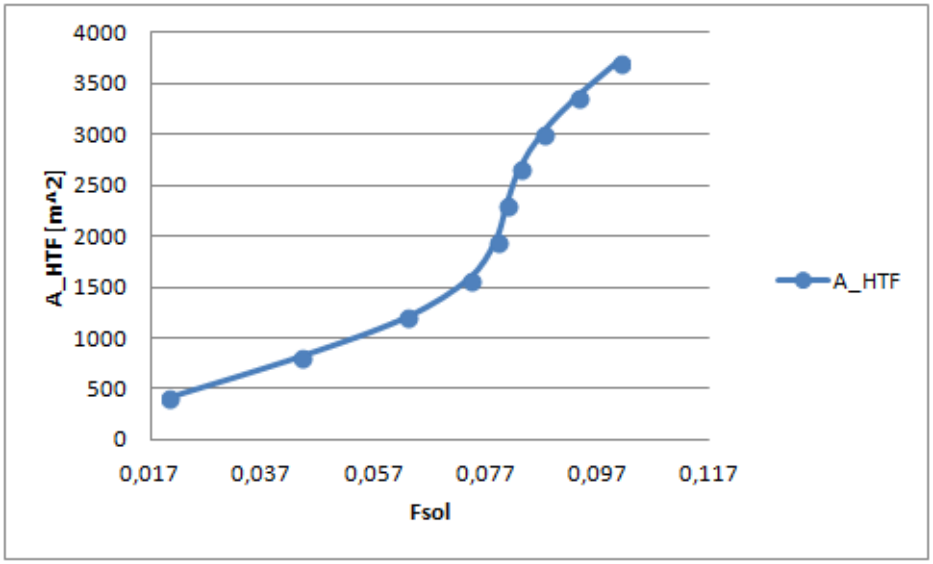

Figure 3.85: Intermediate heat exchanger area for Case 3.

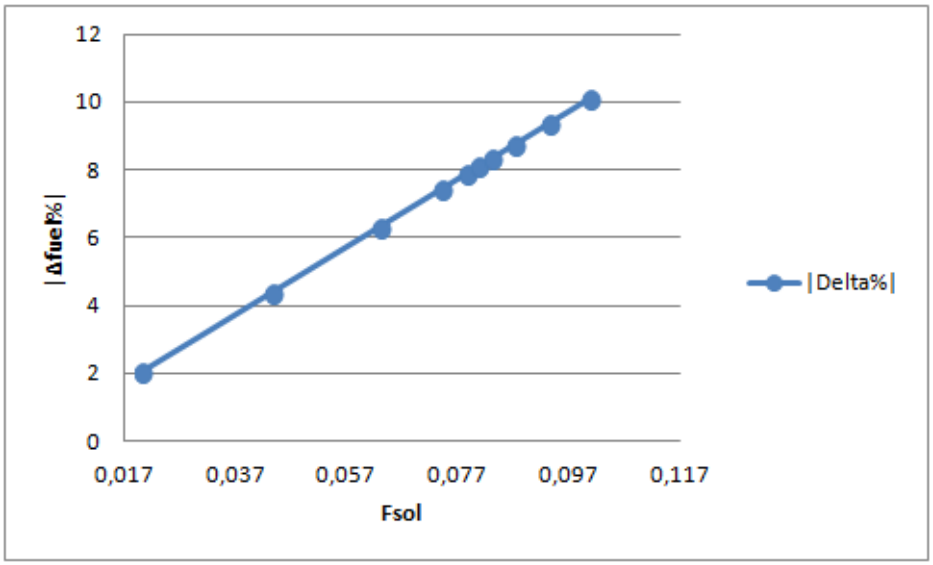

Figure 3.86: Absolute value of the percentage fuel saving for Case 3.

3.7.4 Case 4: Preheater and economizer replacement with a parallel stream

The integration is carried out with the same concept applied in Case 1. Another similarity with the first solution is the limited range of solar share that can be evaluated: the last high temperature preheater is, in fact, modelled in the

same way, which leads to an outlet temperature lower then the inlet's. The full replacement is analysed. The solar section outlet temperature is constant in this case, because of the imposed steam quality conditions at the economizer's outlet. No relevant modifications are found in the expansion line's pressures. Among the mass flow rates, only the one at the turbine inlet is modified.

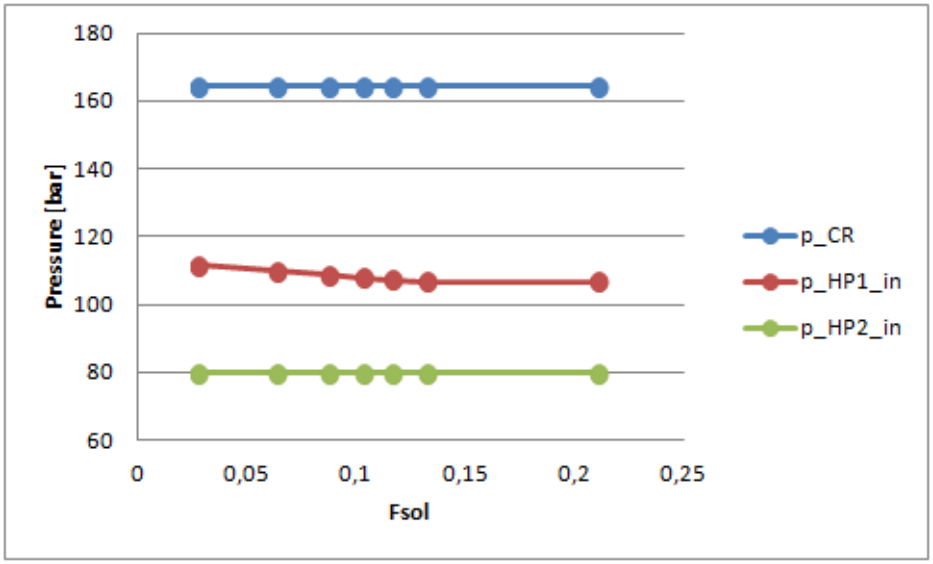

Figure 3.87: Variations of high pressure inlet stages pressures.

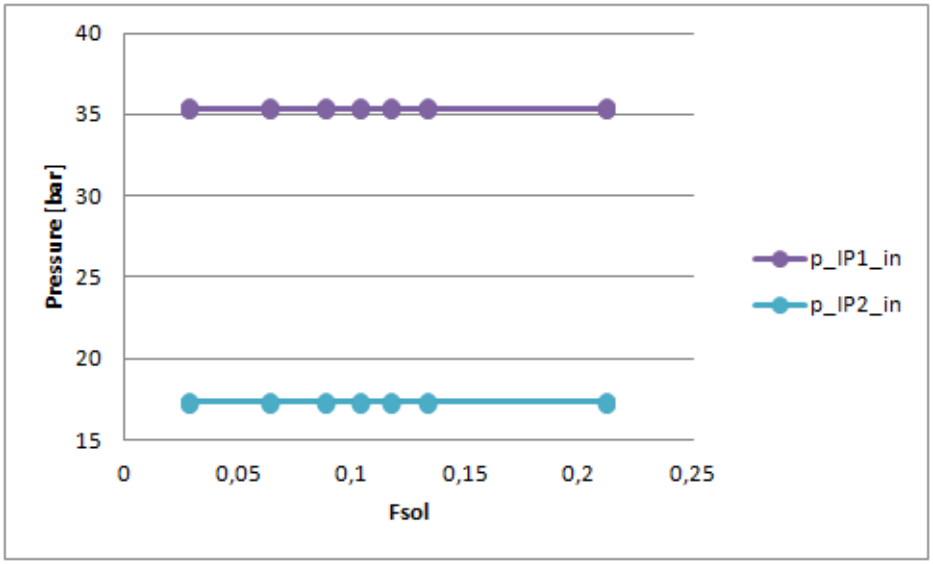

Figure 3.88: Variations of intermediate pressure inlet stages pressures.

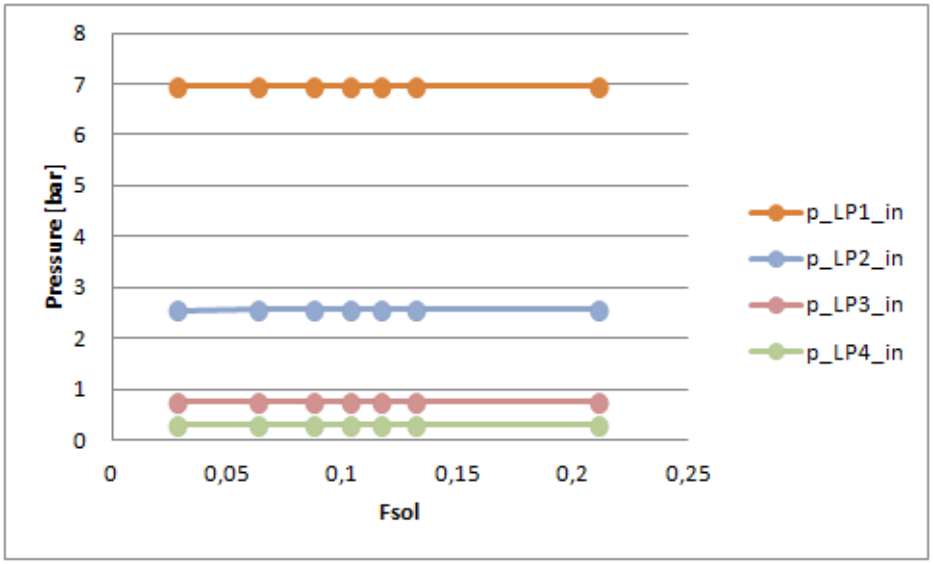

Figure 3.89: Variations of low pressure inlet stages pressures.

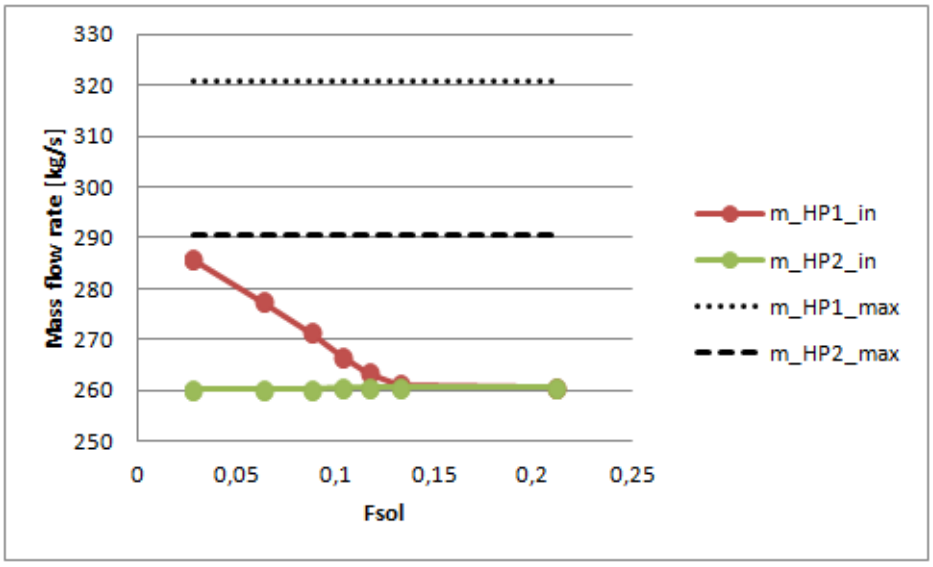

Figure 3.90: Variations of high pressure inlet stages mass flow rates.

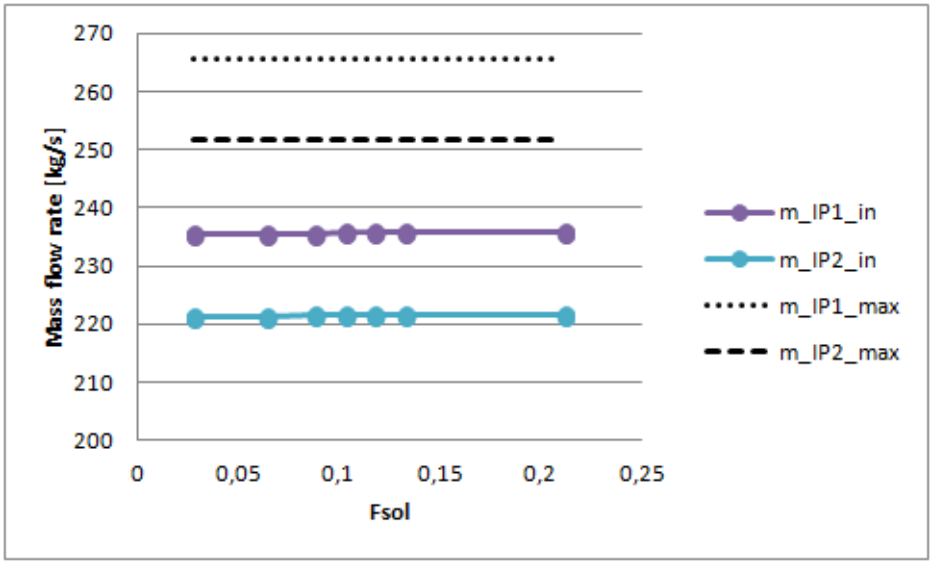

Figure 3.91: Variations of intermediate pressure inlet stages mass flow rates.

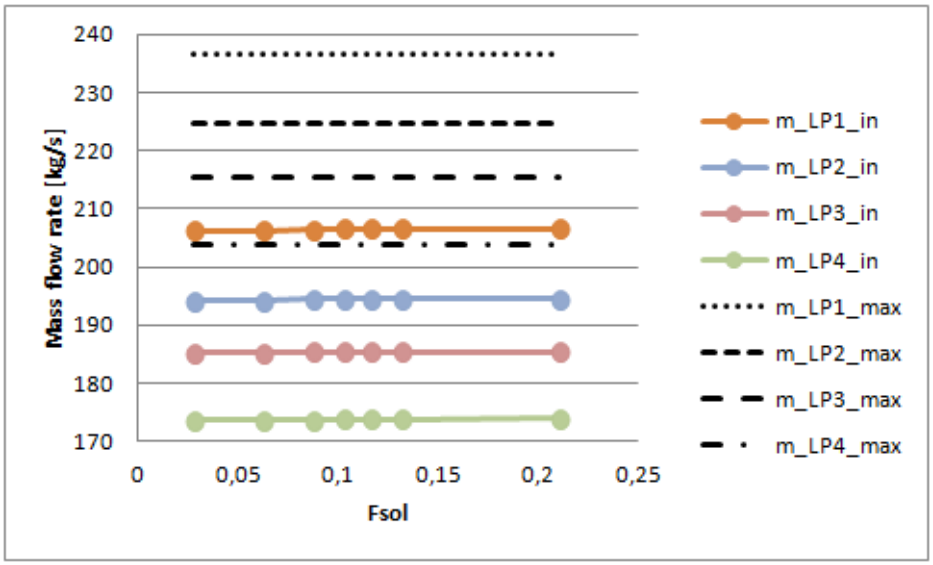

Figure 3.92: Variations of low pressure inlet stages mass flow rates.

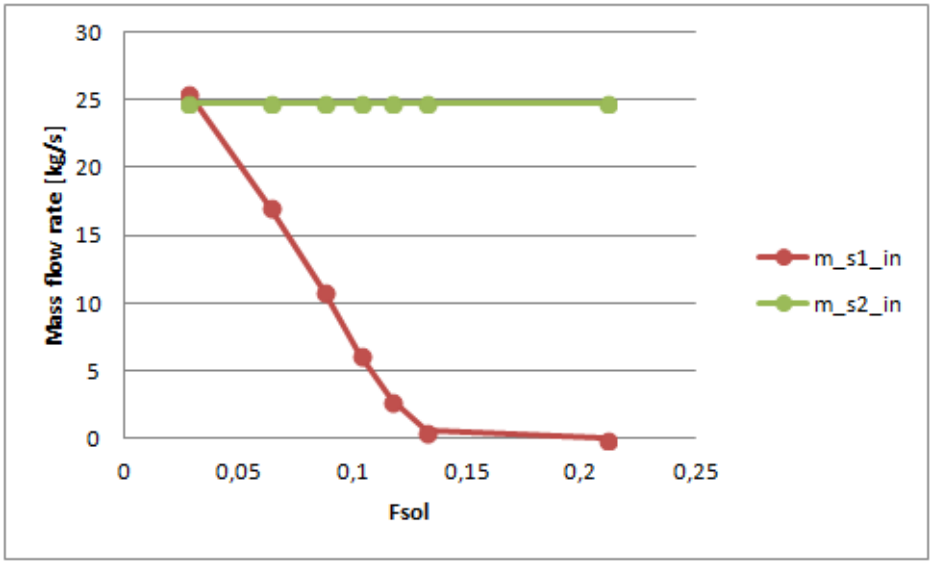

Figure 3.93: Variations of high pressure steam extractions flow rates.

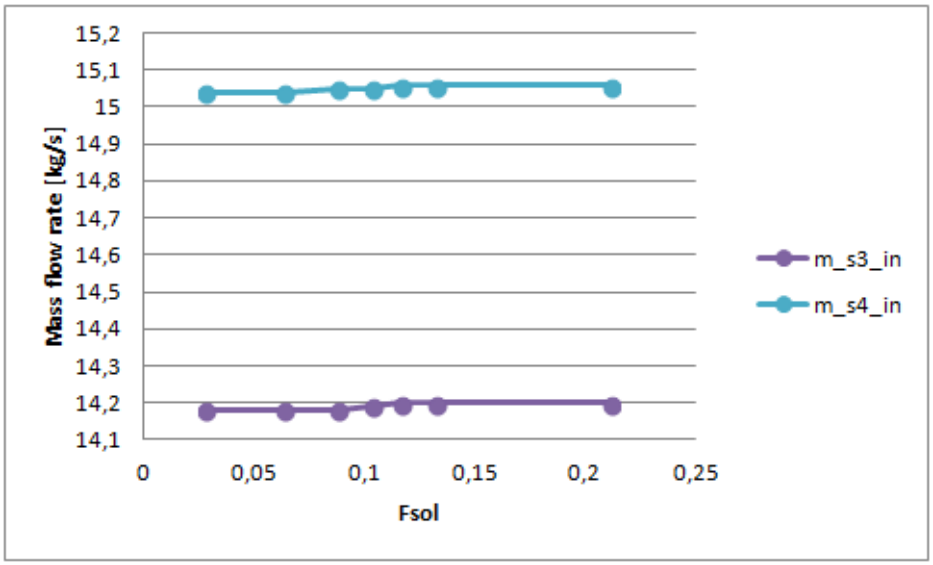

Figure 3.94: Variations of intermediate pressure steam extractions flow rates.

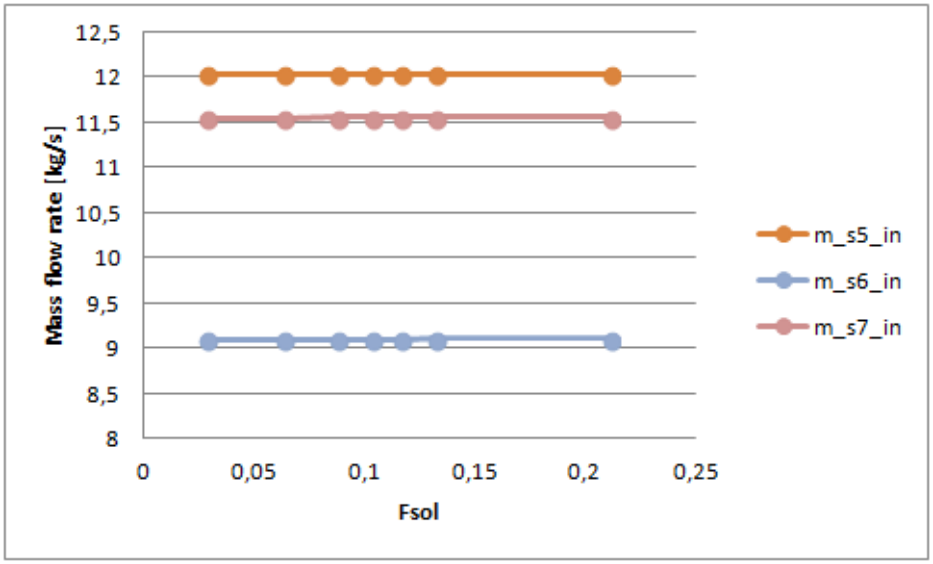

Figure 3.95: Variations of low pressure steam extractions flow rates.

In this case, the boiler is directly affected by the integration, as part of its load is covered by an external heat source. From the feedwater side, there are no differences because the conditions at the boiler outlet are kept constant. The exhaust gases, however, are involved in an altered heat exchange process: for this reason, the heat power, temperature and enthalpy conditions for each point are plotted.

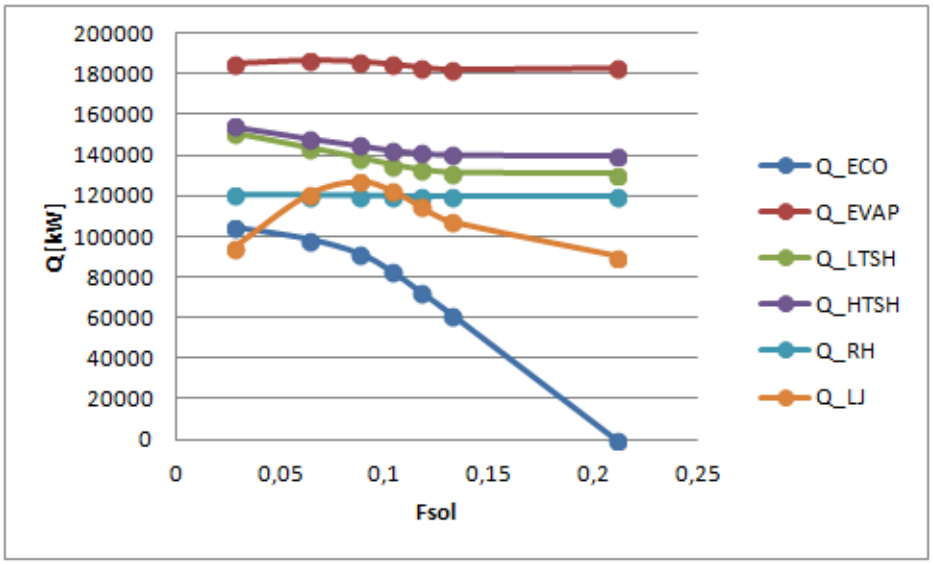

Figure 3.96: Power variations for each boiler's heat exchanger.

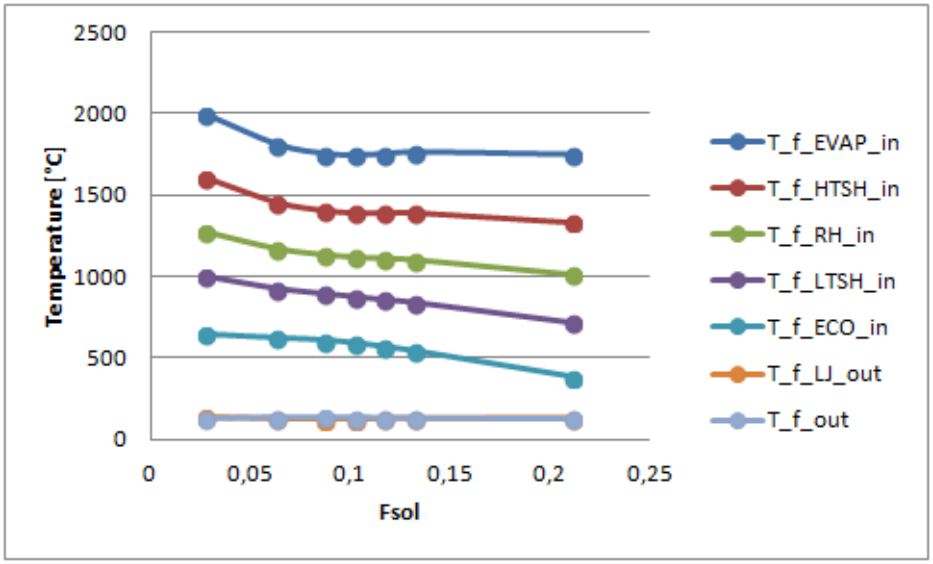

Figure 3.97: Fume temperature variations in the boiler.

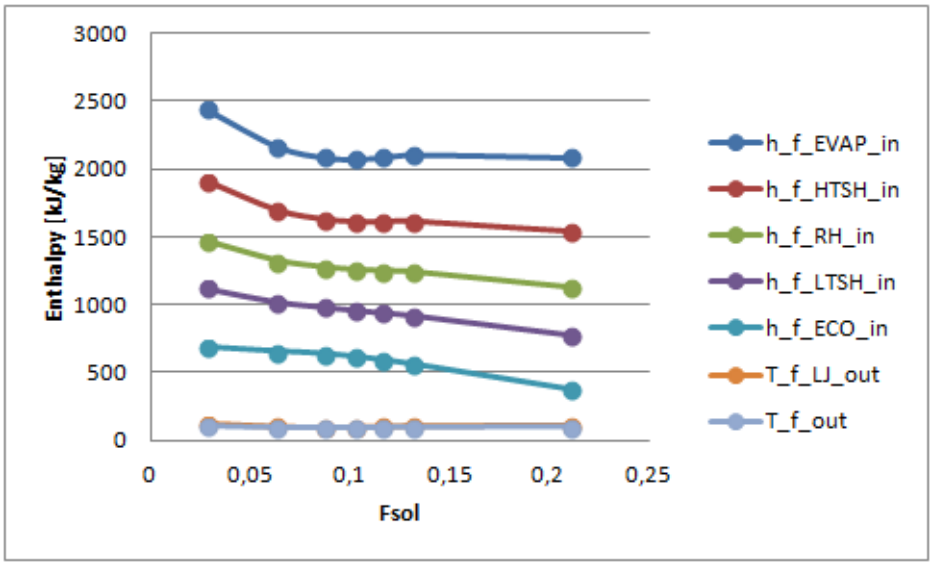

Figure 3.98: Fume enthalpy variations in the boiler.

When the economizer is fully replaced, the percentage variations from design of the heat exchanged for each component are: 0.68% for the evaporator, -15.85% for the low temperature superheater, -11% for the high temperature superheater, -0.65% for the reheater and 11.6% for the air preheater (Ljungstroem). Temperature and enthalpy conditions vary, but with nearly the same trend for all the preheaters. The following figures contains the integration parameter for this

solution.

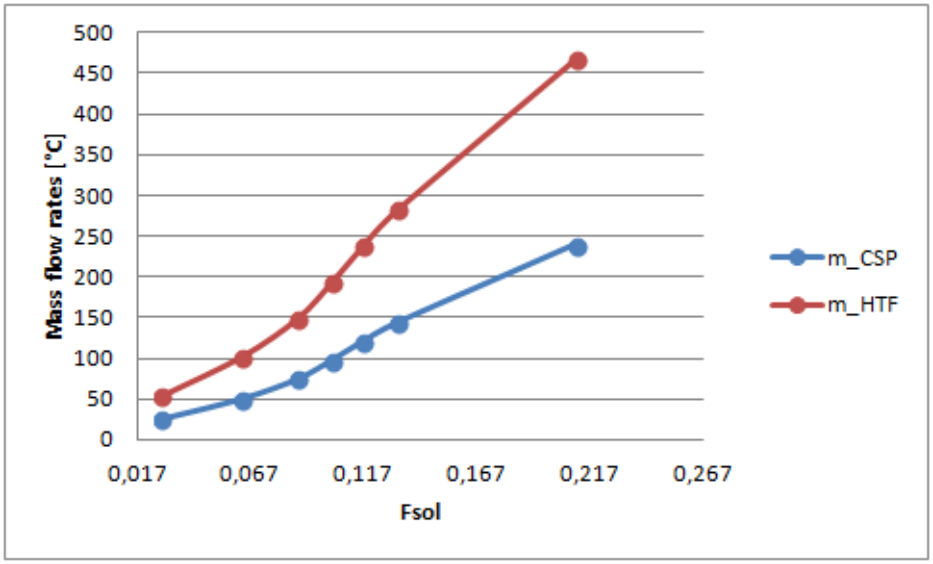

Figure 3.99: Solar and heat transfer fluid mass flow rates for Case 4.

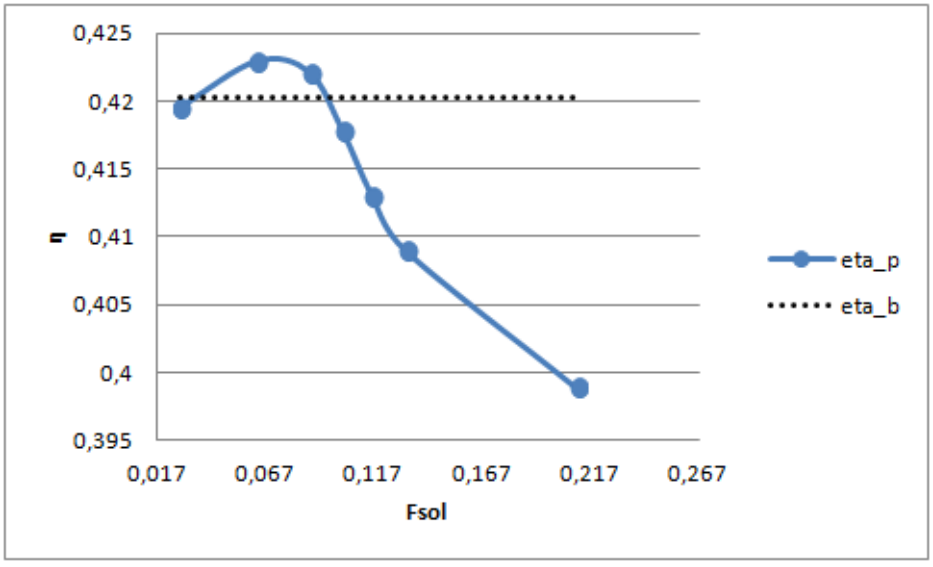

Figure 3.100: Conversion efficiency from primary sources for Case 4.

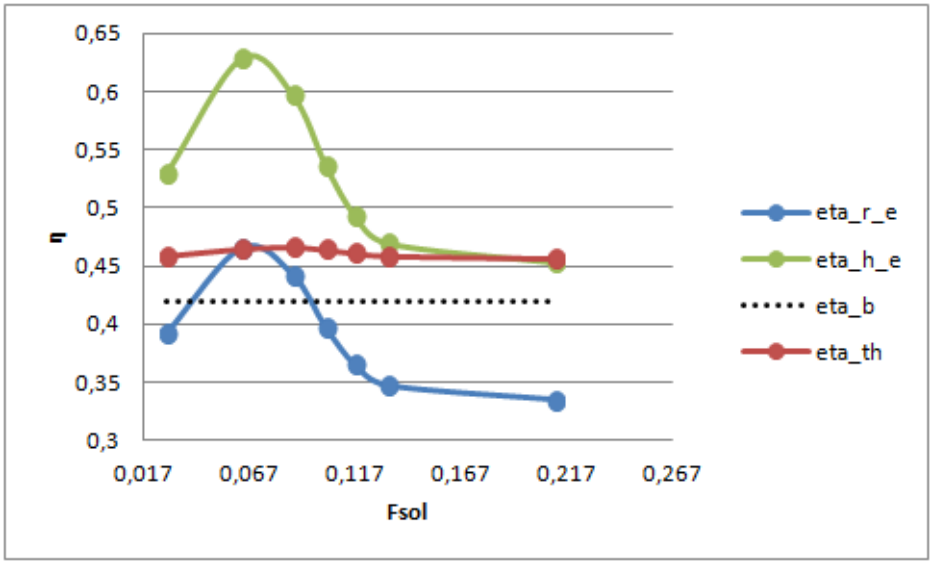

Figure 3.101: Solar radiation and heat-to-electric efficiencies for Case 4.

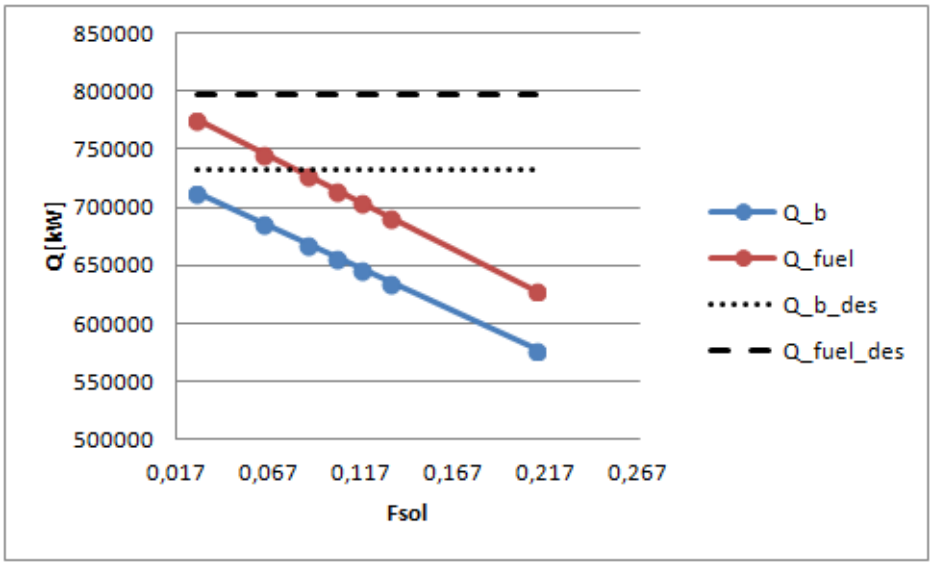

Figure 3.102: Boiler and fuel powers for Case 4.

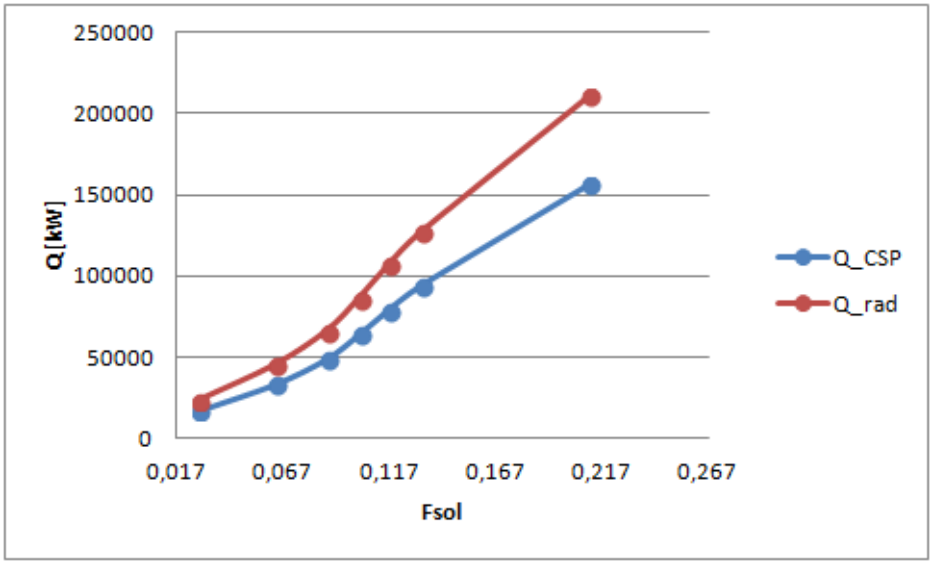

Figure 3.103: Radiation and solar heat powers for Case 4.

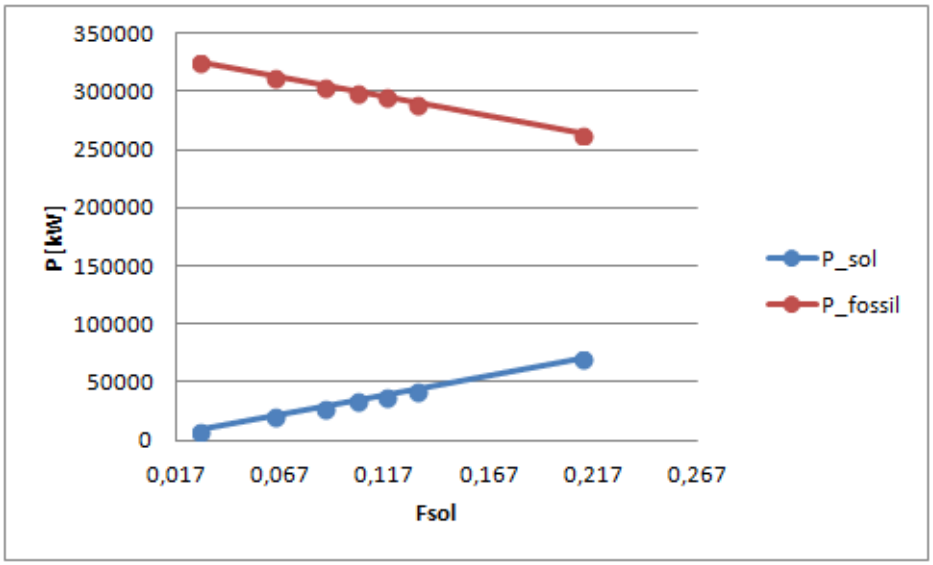

Figure 3.104: Solar and fossil powers for Case 4.

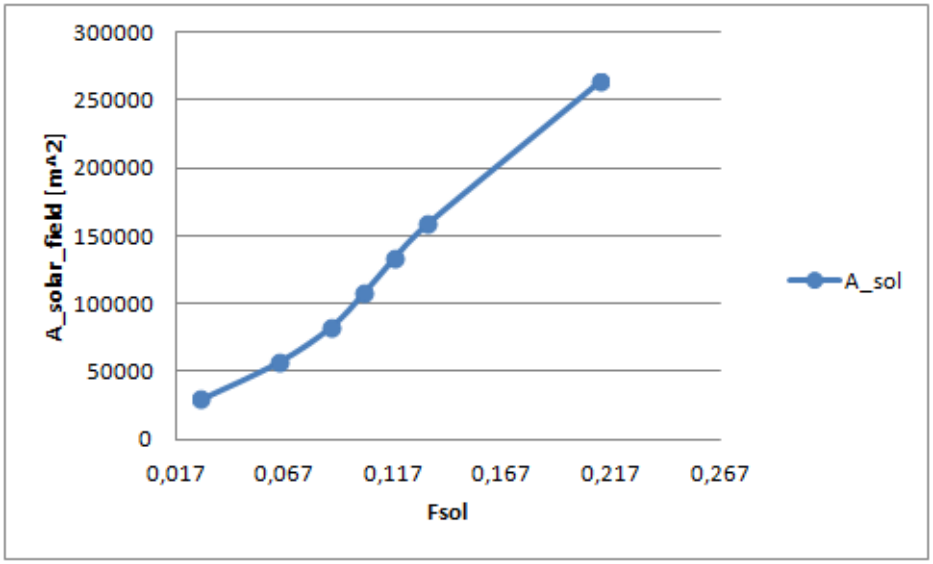

Figure 3.105: Solar field area for Case 4.

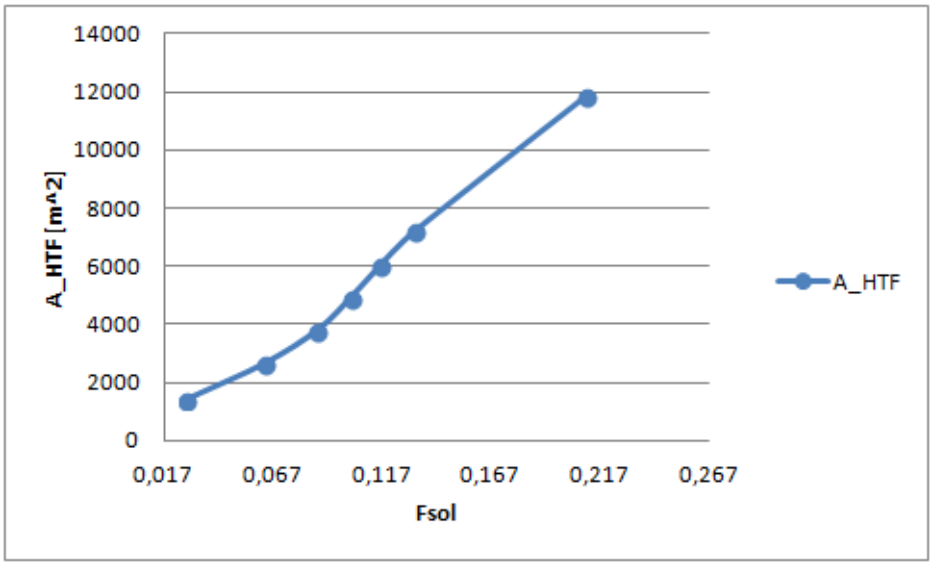

Figure 3.106: Intermediate heat exchanger area for Case 4.

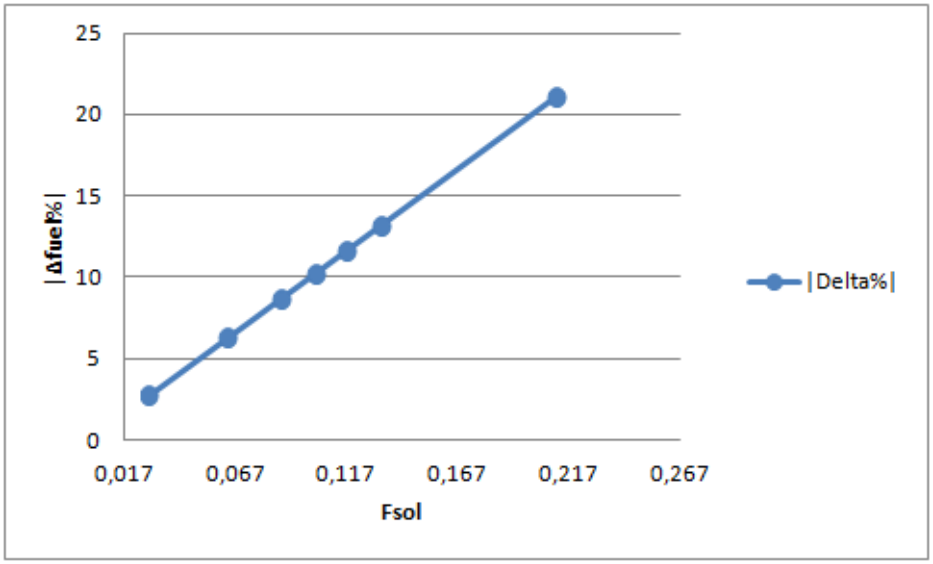

Figure 3.107: Absolute value of the percentage fuel saving for Case 4.

3.8 Integration options comparisons

In the previous sections, the conversion efficiency from primary sources and solar to electric efficiencies have been plotted against the solar share for all the proposed solutions. After selecting four synergies, results and considerations have been presented for each of them. A comparison will be made in this paragraph to evaluate how the selected integrations perform compared to each other.

3.8.1 Performance at varying solar share

The efficiencies trends with varying solar share have already been presented in section 3.7. Efficiencies η_p, η_{th}, η_{r-e} and η_{h_e} are once again plotted for varying solar share, for the selected options.

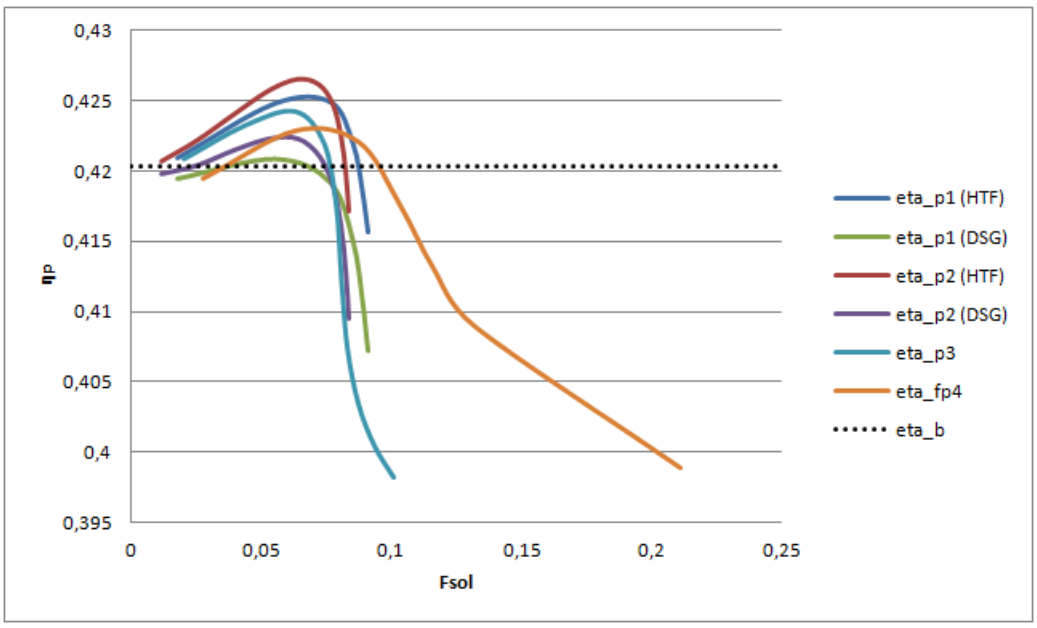

Figure 3.108: Conversion efficiency from primary energy sources with varying solar share.

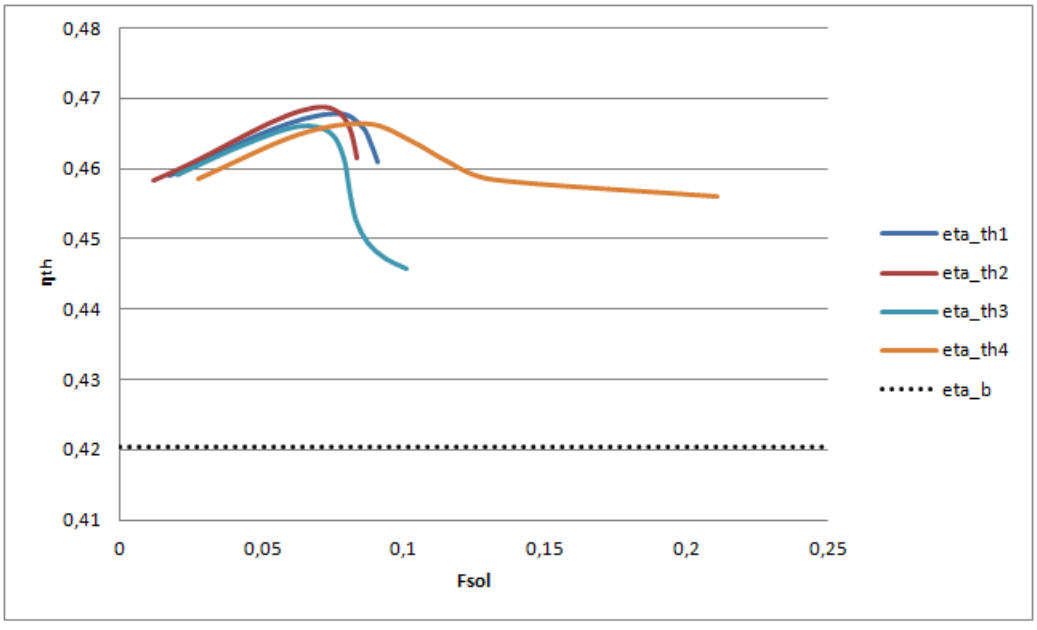

Figure 3.109: Thermal efficiency of the hybrid cycle with varying solar share.

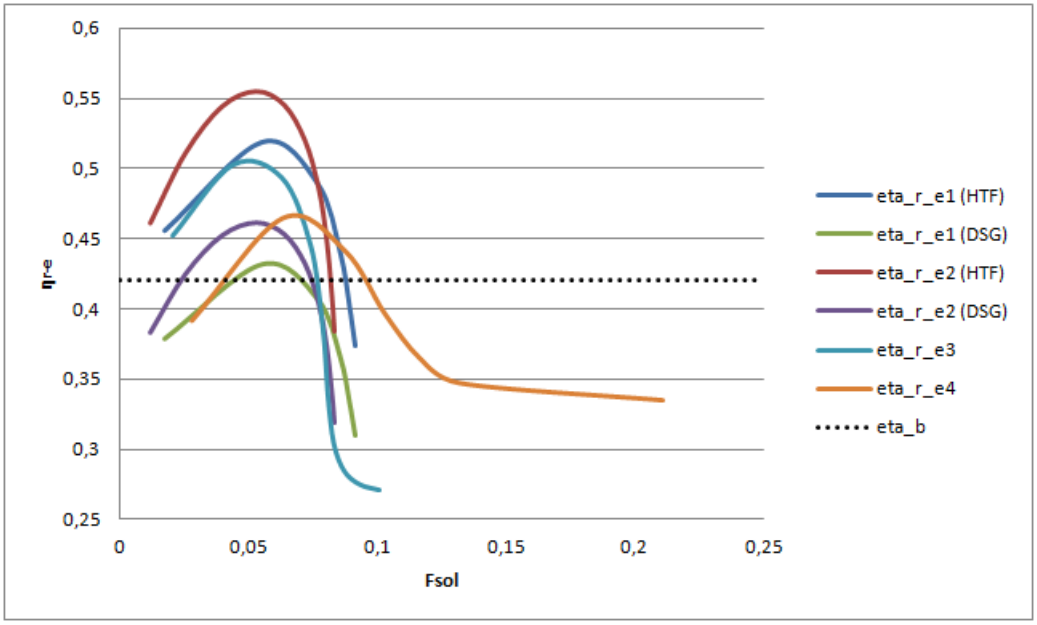

Figure 3.110: Solar radiation-to-electric efficiency with varying solar share.

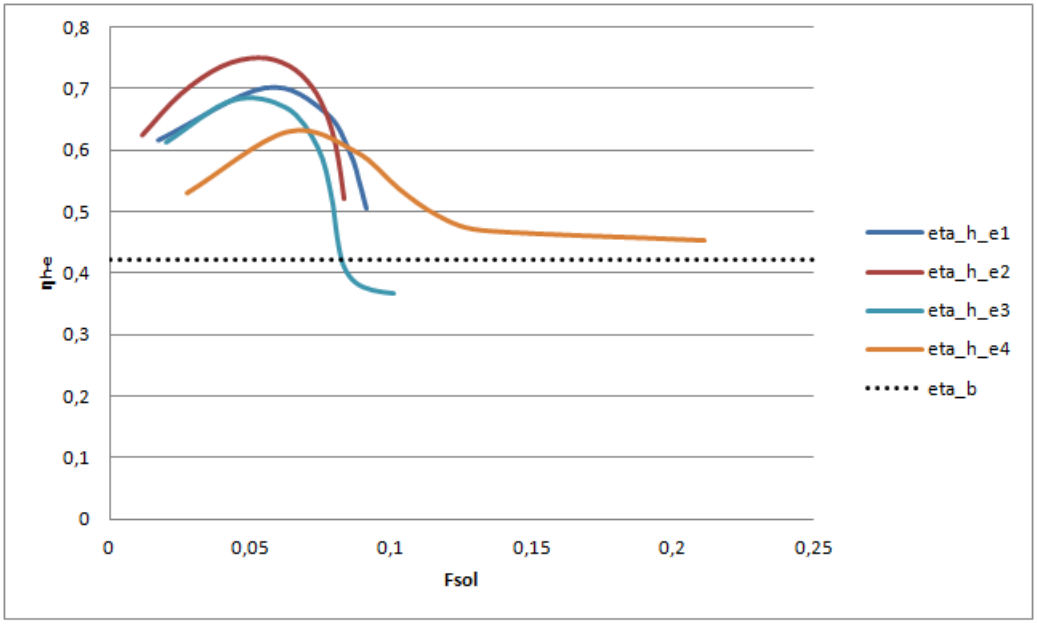

Figure 3.111: Solar heat-to-electric efficiency with varying solar share.

The solar input, both in terms of radiation and heat, is showed in the next figures:

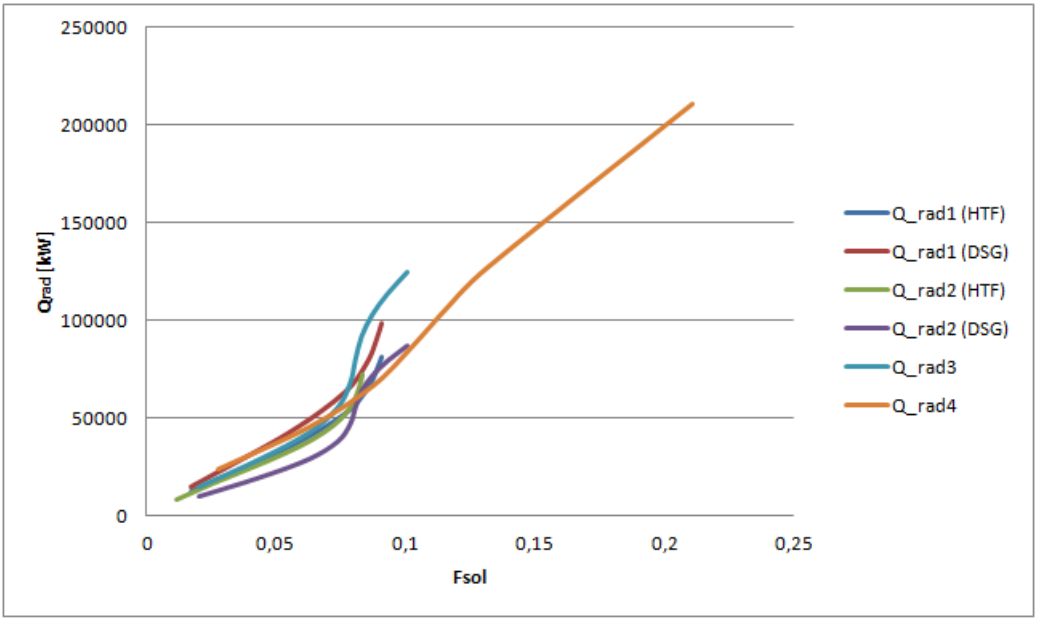

Figure 3.112: Solar radiation with varying solar share.

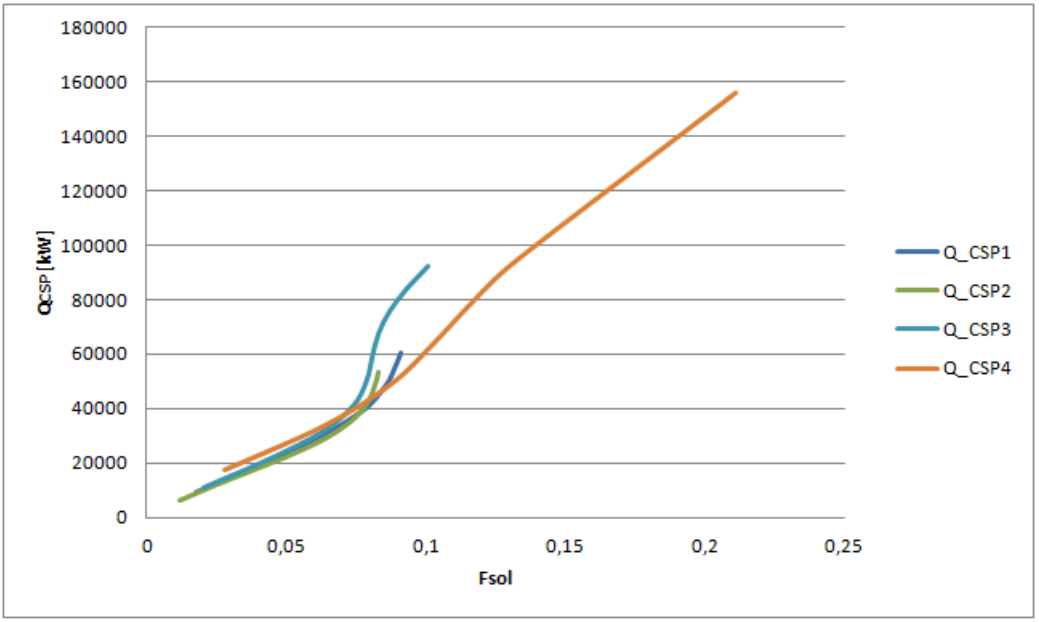

Figure 3.113: Solar heat with varying solar share.

The highest solar share, 21.1%, is reached with the full replacement of the highest temperature feedwater preheater and the economizer. This solution also require the highest solar field area to be realised (3.114). Apart from Case 4, the solar field area has almost the same trend with increasing solar share.

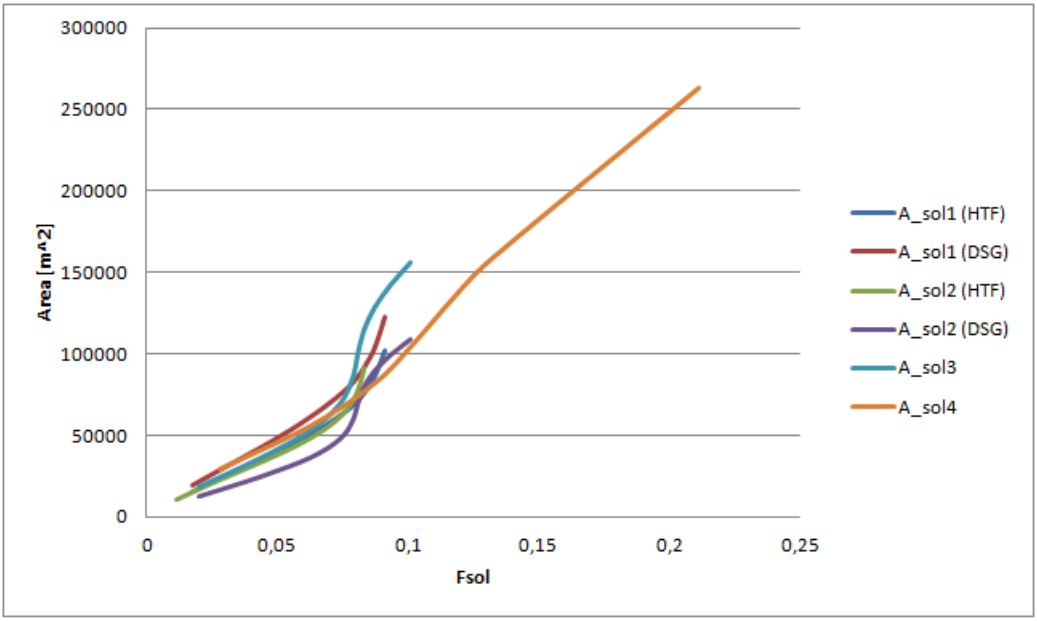

Figure 3.114: Solar field area with varying solar share.

Lastly, the additional heat exchanger area is reported, in the cases where an intermediate fluid is contemplated.

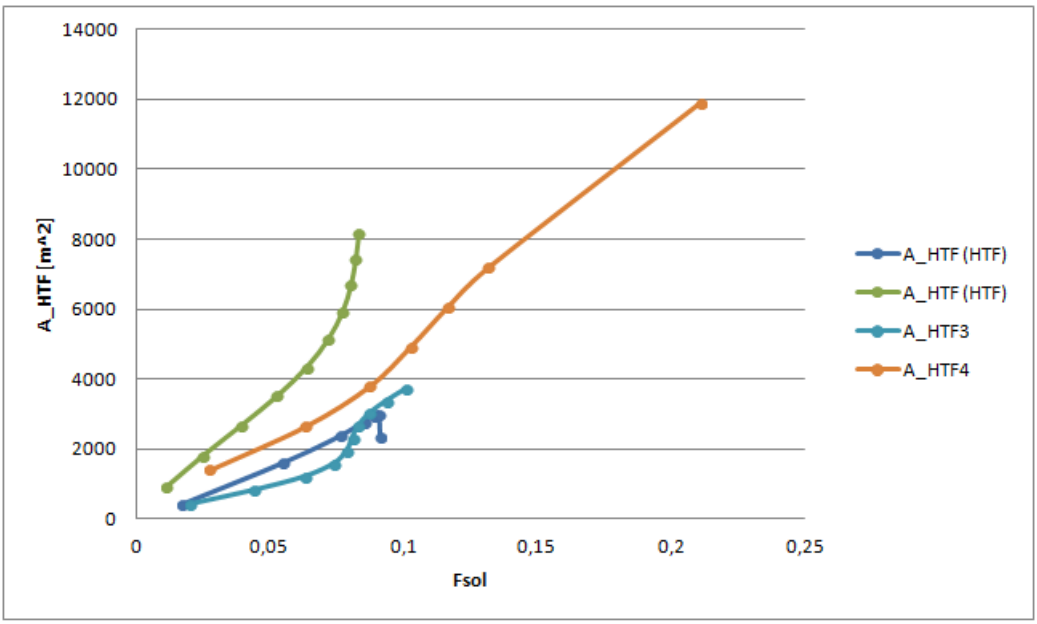

Figure 3.115: Intermediate heat exchanger area with varying solar share.

3.8.2 Performance at varying solar mass flow rate

Efficiencies and other parameters have been compared with reference to the solar ratio R betweer the solar mass flow rate and the feedwater from which it is extracted.

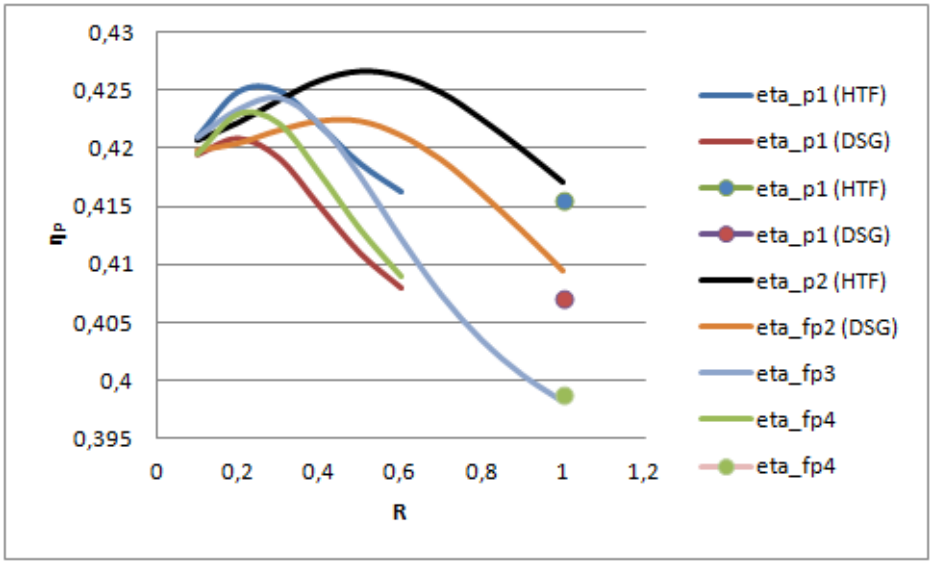

Figure 3.116: Conversion efficiency from primary sources with varying solar ratio.

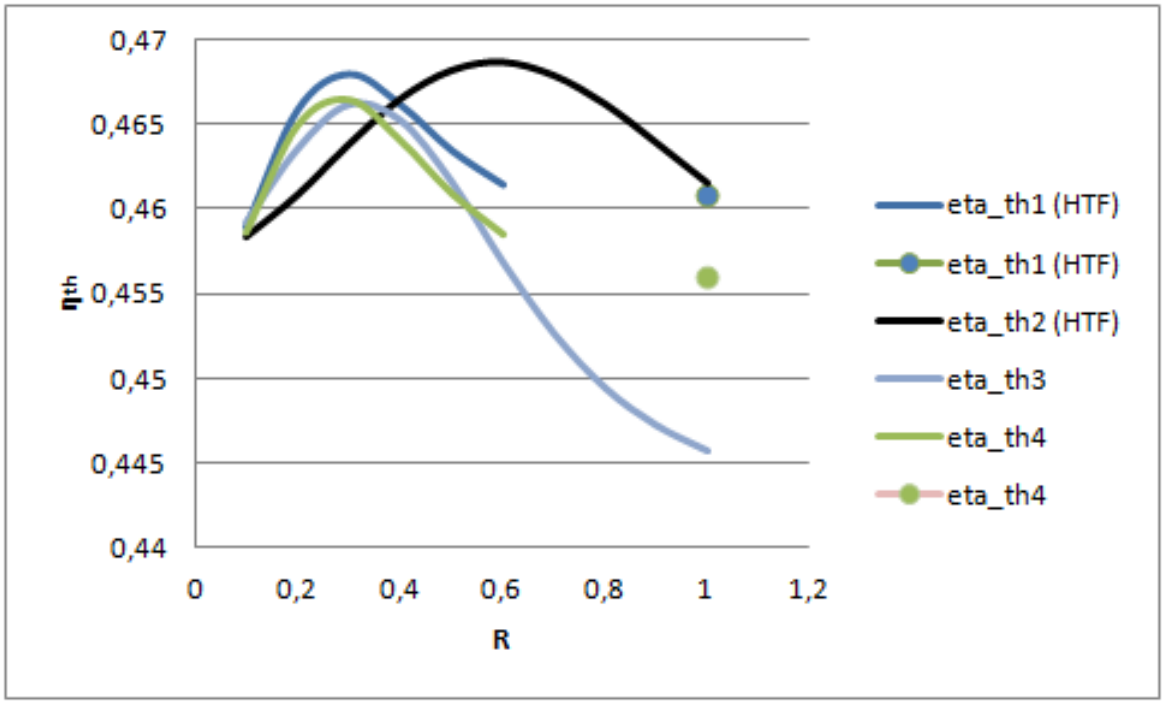

Figure 3.117: Hybrid cycle thermal efficiency with varying solar ratio.

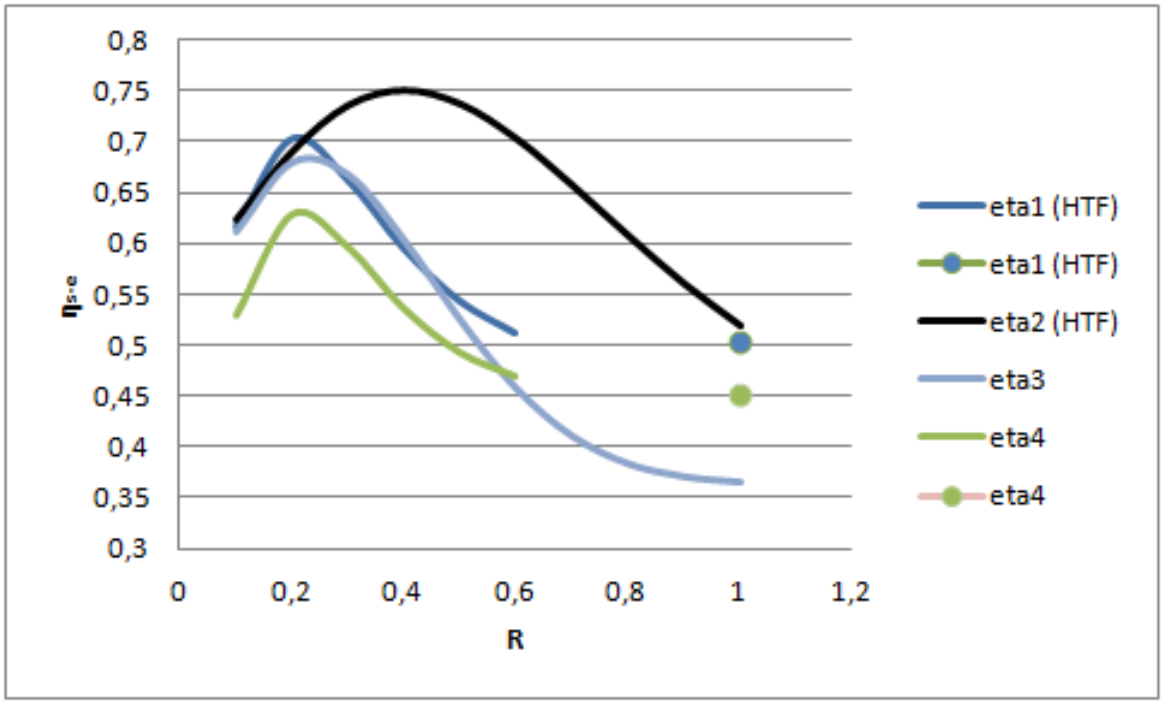

Figure 3.118: Solar radiation-to-electric efficiency with varying solar ratio.

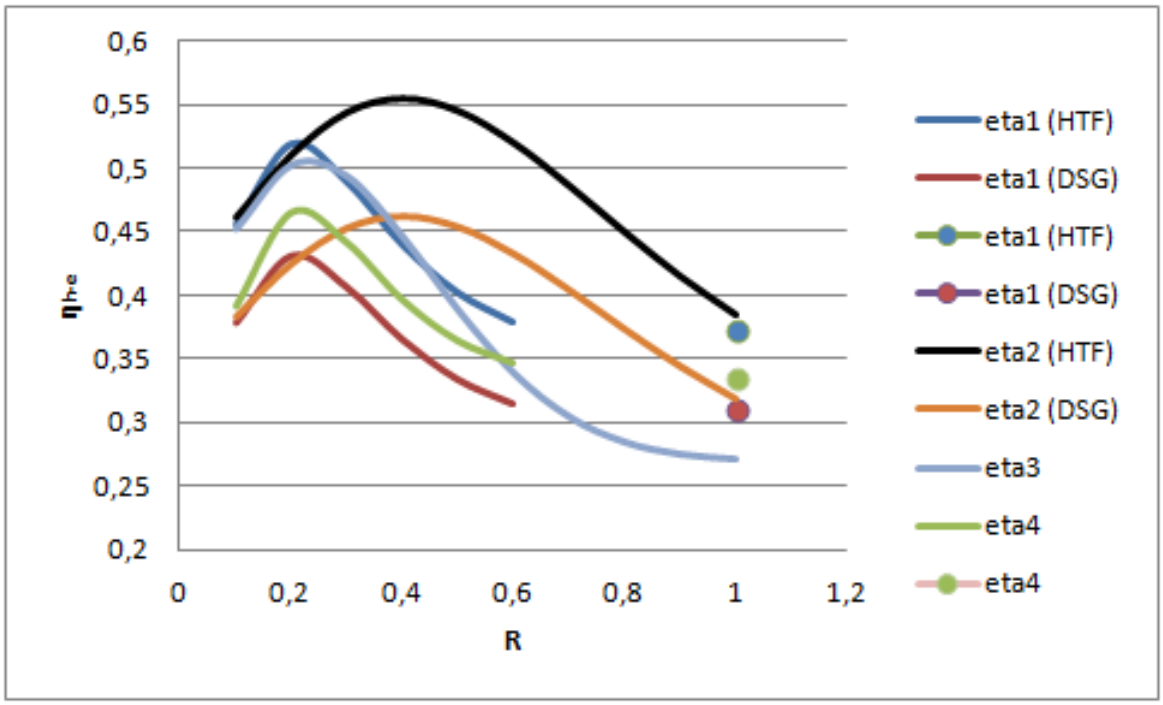

Figure 3.119: Solar heat-to-electric efficiency with varying solar ratio.

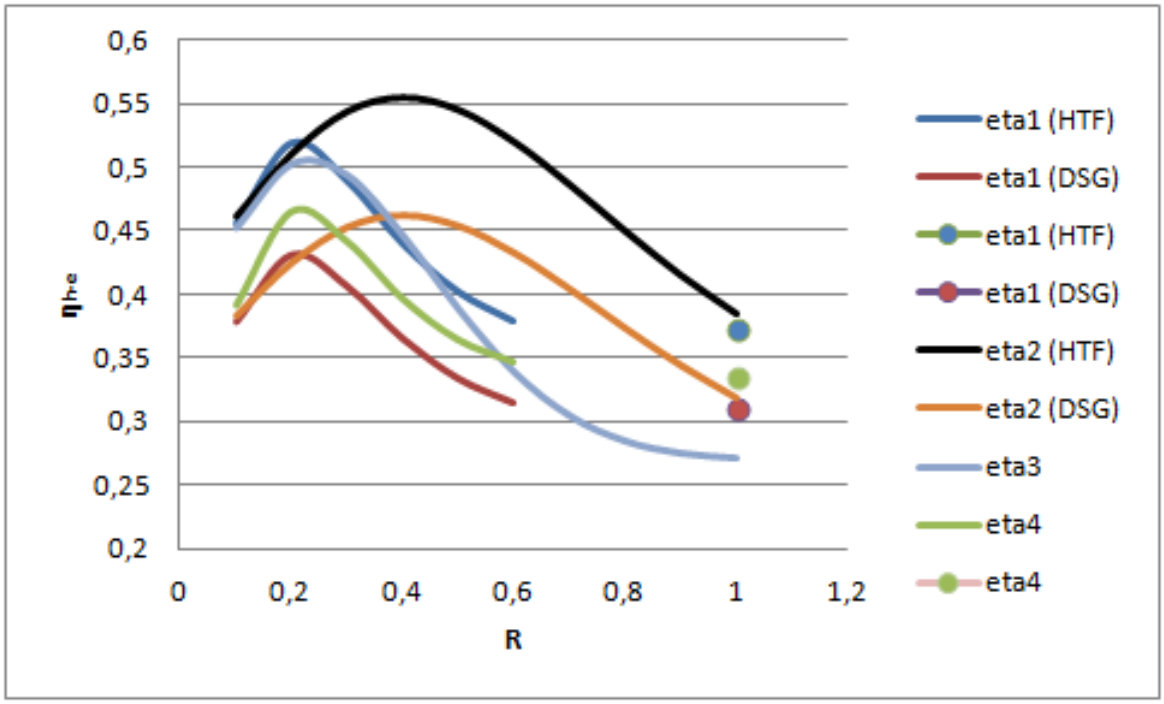

Figure 3.120: Solar share with varying solar ratio.

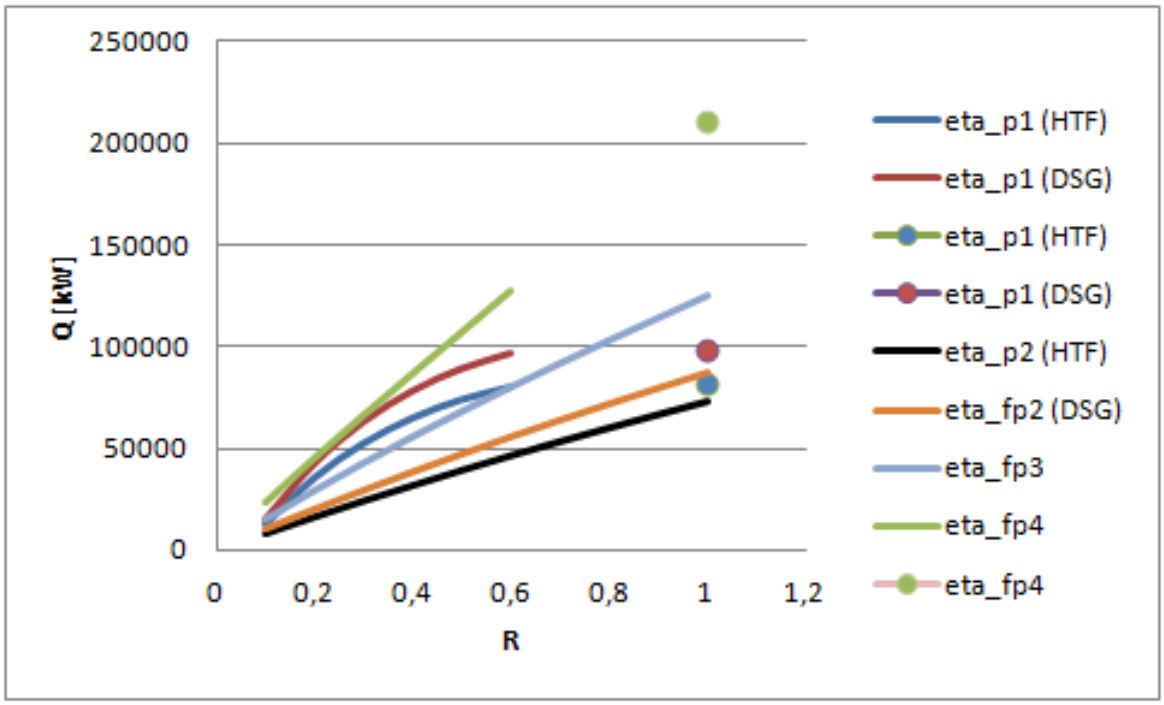

Figure 3.121: Solar radiation with varying solar ratio.

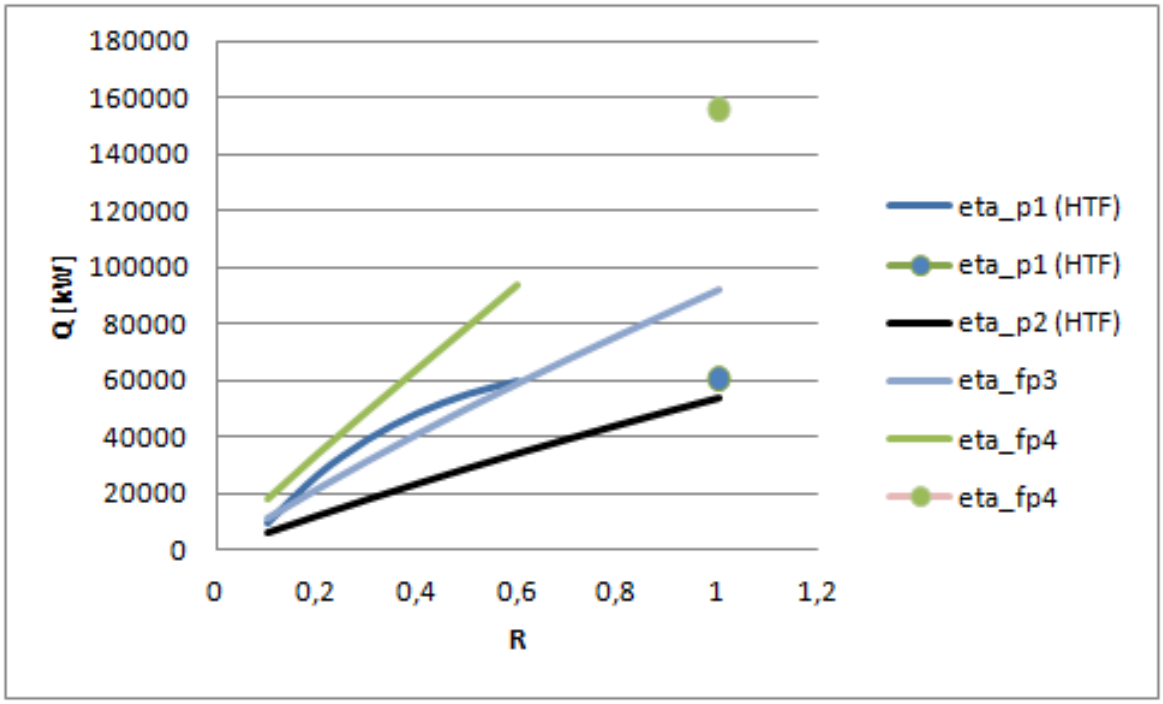

Figure 3.122: Solar heat with varying solar ratio.

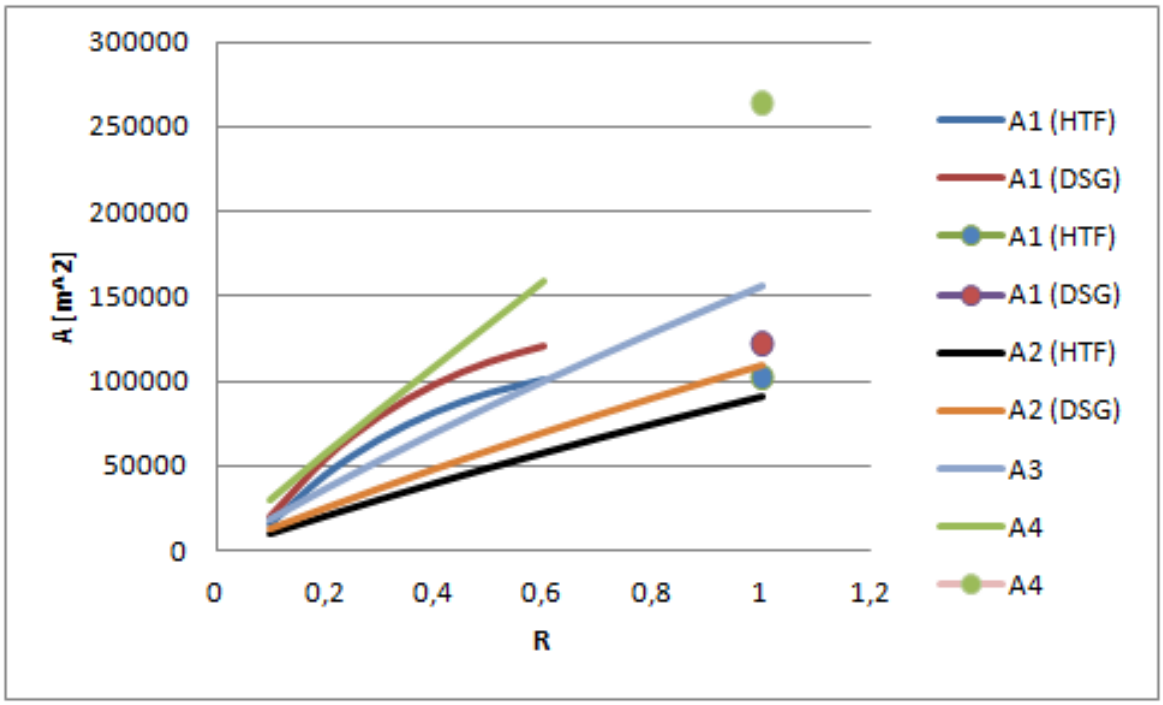

Figure 3.123: Solar field area with varying solar ratio.

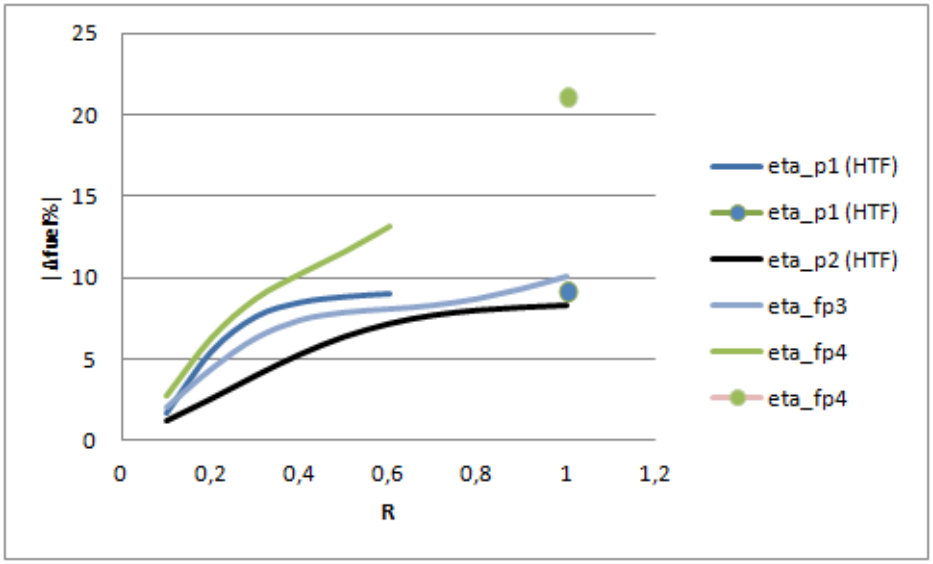

Figure 3.124: Percentage fuel saving with varying solar ratio.

3.8.3 Design point comparison

After analysing the different parameters with varying solar share, a design point is chosen for each integration option: this corresponds to the situation of highest conversion efficiency η_p. The various parameters found at the design point are then compared in histograms, to give the idea of how the four solutions compare when working at a fixed point. The following table 3.19 reports all the parameters (R is the ration of the solar mass flow rate $\dot{m}_{CSP}$ and the feedwater mass flow rate from which it is extracted):

Case	1(a)	1(b)	2(a)	2(b)	3	4
Technology	PTC	LFR	PTC	LFR	PTC	PTC
Thermal fluid	oil	water	salts	water	oil	oil
Max HTF temp. [C]	393	500	470	500	393	393
R [-]	0,3	0,2	0,5	0,5	0,3	0,2
$\dot{m}_{CSP}$ **[kg/s]**	75,04	51,14	13,76	13,76	15,12	51,14
$\dot{m}_{HTF}$ **[kg/s]**	117	-	94,85	-	81,56	102
$\mathbf{A_{HTF}}$ **[m²]**	2388	-	4336	-	1206	2646
$\mathbf{A_{solar\ field}}$ **[m²]**	65495	53420	48962	58932	53235	56908
$\Delta\dot{m}_{fuel}$ **[%]**	-7,654	-2,898	-6,379	-6,379	-6,277	-6,322
$\dot{Q}_{CSP}$ **[kW]**	38747	26257	28966	28966	31494	33667
$\dot{Q}_{rad}$ **[kW]**	52396	42736	39170	47145	42588	45527
η_p **[-]**	0,4249	0,4209	0,4266	0,4223	0,4243	0,4229
η_{th} **[-]**	0,4679	0,4658	0,4682	0,4682	0,4661	0,4649
η_{r-e} **[-]**	0,4893	0,4314	0,5455	0,4532	0,4936	0,4651
η_{h-e} **[-]**	0,6616	0,702	0,7376	0,7376	0,6675	0,629
$\mathbf{F_{sol}}$ **[%]**	7,65	5,5	6,38	6,38	6,3	6,32

Table 3.19: Integration parameters at design point for the selected integration options.

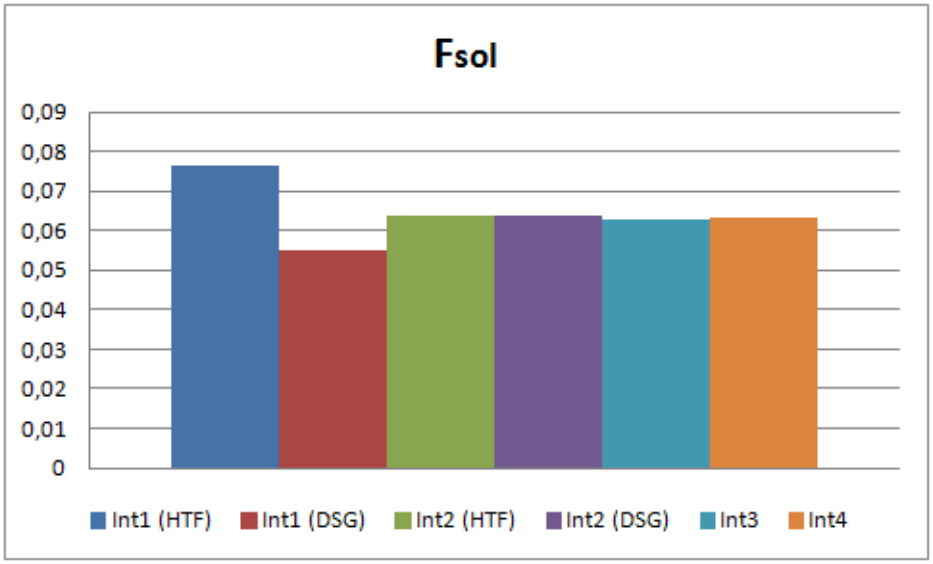

Figure 3.125: Solar share at design point for each integration solution.

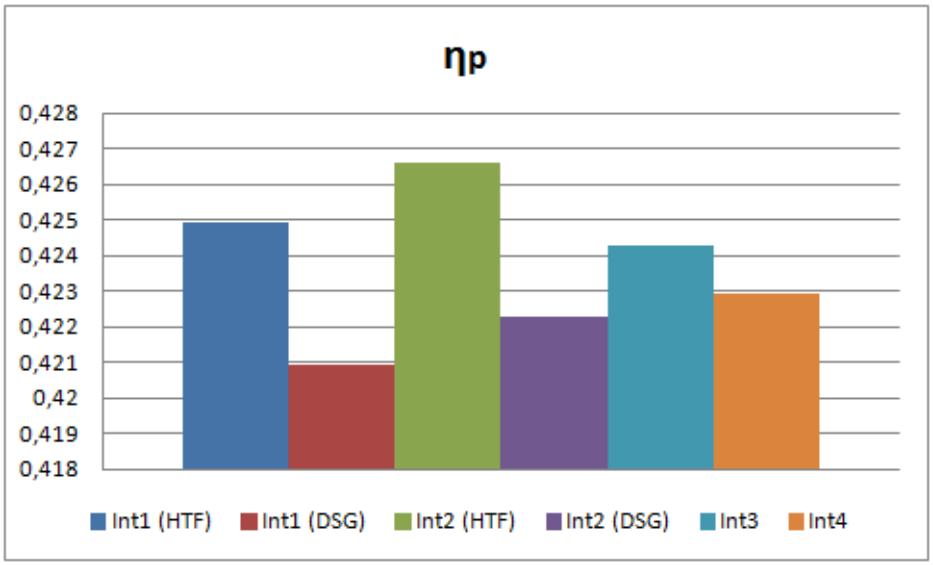

Figure 3.126: Conversion efficiency from primary sources for each integration solution.

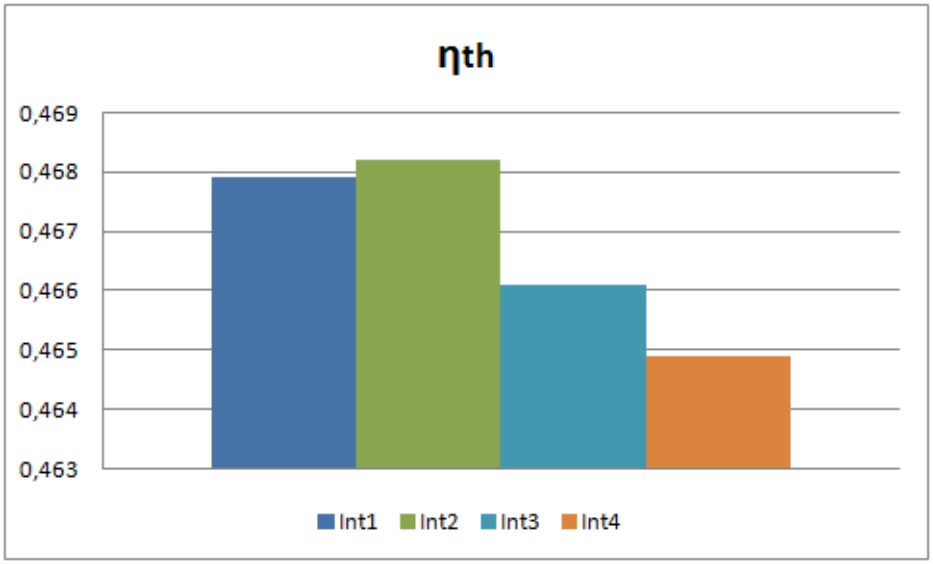

Figure 3.127: Hybrid cycle thermal efficiency for each integration solution.

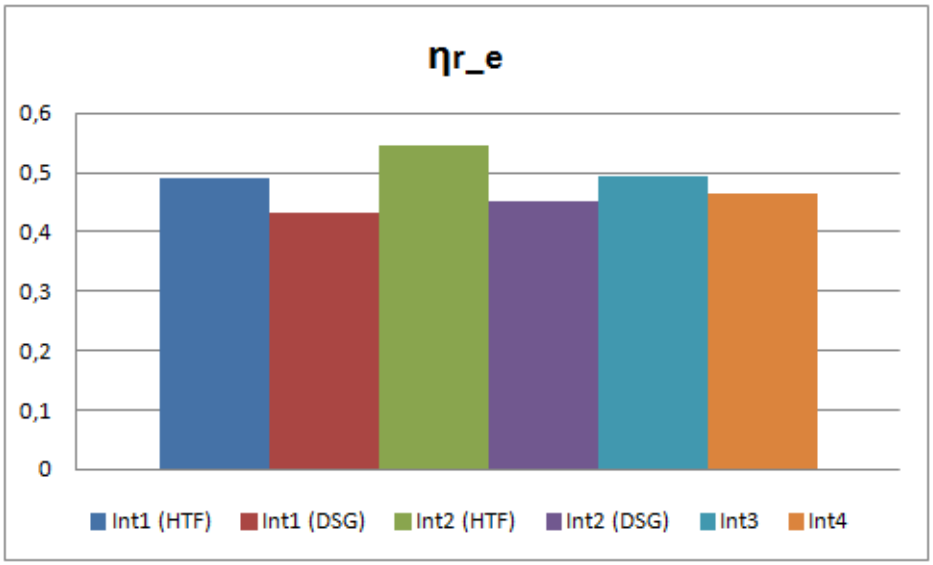

Figure 3.128: Solar radiation-to-electric efficiency at design point for each integration solution.

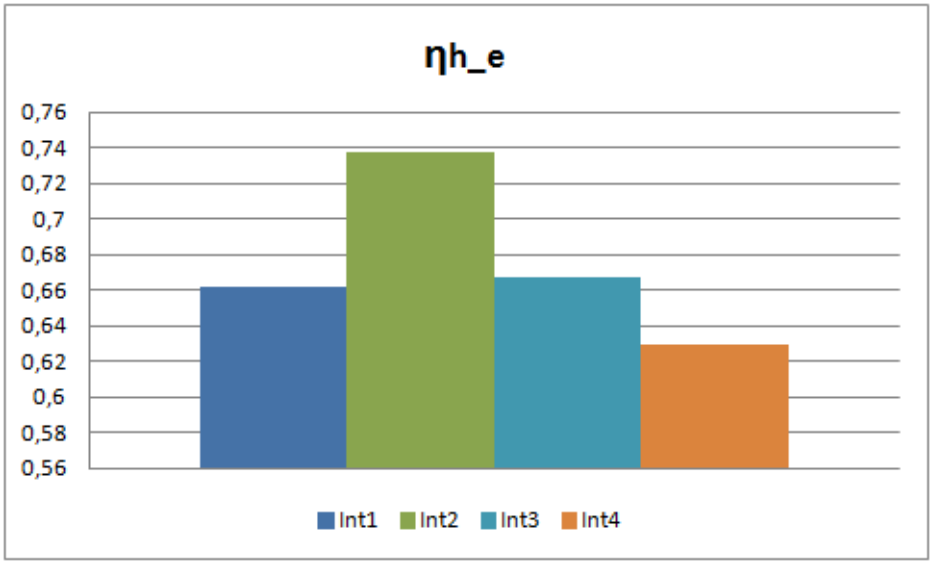

Figure 3.129: Solar heat-to-electric efficiency at design point for each integration solution.

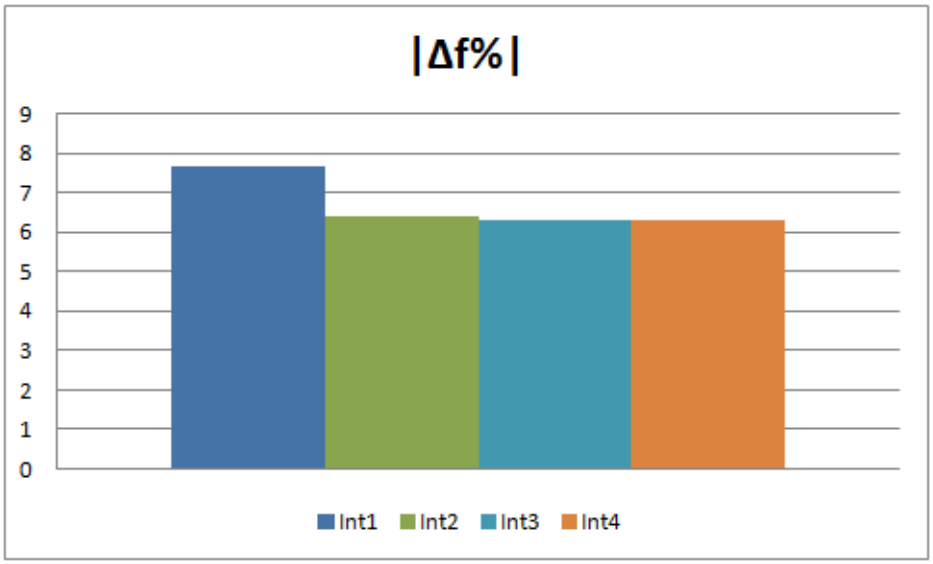

Figure 3.130: Fuel saving at design point for each integration solution.

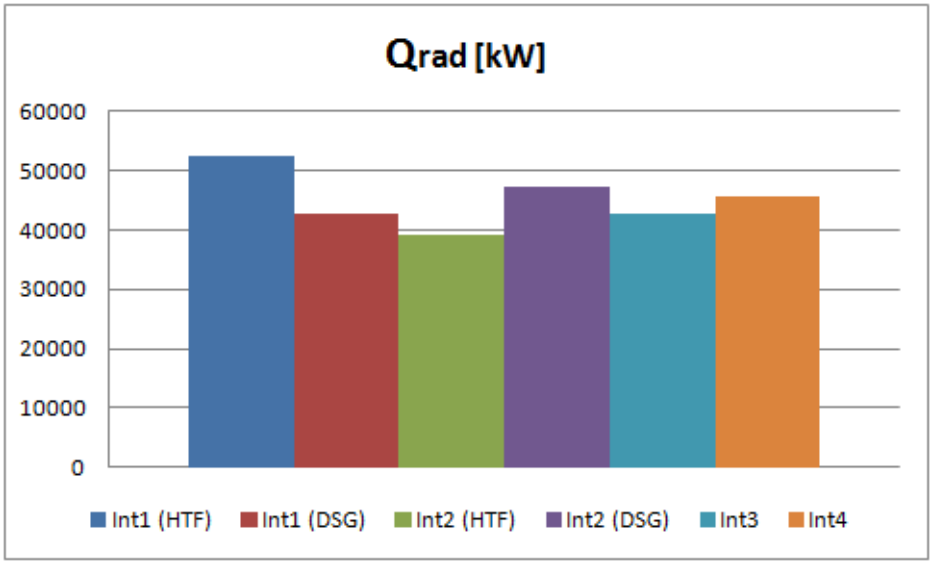

Figure 3.131: Solar radiation area at design point for each integration solution.

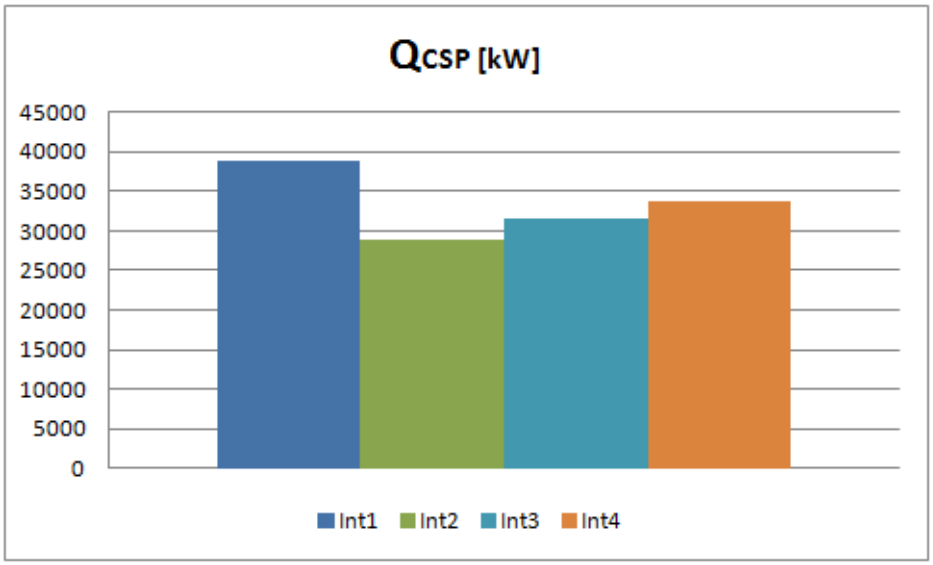

Figure 3.132: Solar heat area at design point for each integration solution.

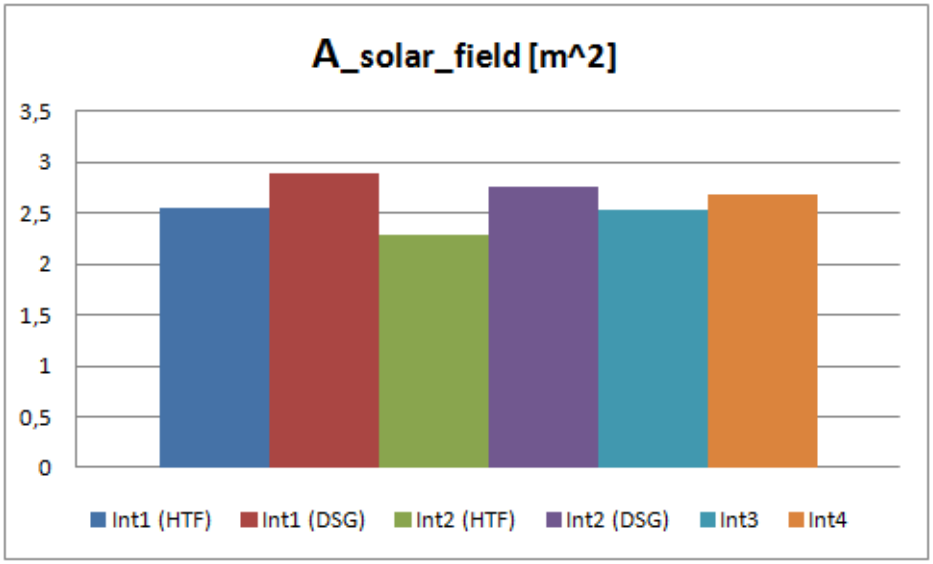

Figure 3.133: Solar field area at design point for each integration solution.

From the analysis it comes that the highest value of η_p is reached when drainage water is sent to the turbine (with parabolic trough and molten salts): 42.66%. This solution also presents the highest solar to electric efficiencies (η_{r-e} and η_{h_e}) and thermal efficiency of the hybrid cycle η_{th}. Another positive aspect is the required land area, which is the lowest. The highest solar share and fuel saving are associated with the highest temperature feedwater preheater (Case 1).

3.9 Simplified annual analysis

A method for evaluating the useful solar thermal output of a CSP plant over a period of time has been proposed by Morin et al. ([69]). The procedure is applied here for the first integration option (high temperature preheater HPH3 replacement with a parallel heat exchanger, with parabolic trough technology), to have an example of how the solar field will perform over a year. This case has been selected because it is the most frequent analysed in the literature.
Some simplifying hypothesis are introduced here:

- A full load operation is considered for the power plant during 8760 hours (unitary load factor).

- For each month, a representative day is chosen: results will be multiplied by the number of days in the corresponding month.
- It is assumed that the collectors do not shadow each other.
- Piping loss are neglected.

The input data needed to carry out the simulation are the hourly direct normal irradiance, the solar elevation and azimuth angles, and the average monthly temperature for the chosen location (Fusina). The solar heat exchange model has to be modified to carry out the off-design simulation.
The first variable is calculate with the *PVGIS* tool ([70]), while the two angles describing the solar position are provided by the software *SOLPOS* ([71]). The average monthly temperature is take from [72]. The input variables are written in a parametric table, each for every month, for the number of hours when solar radiation is present.
The outputs for each hour are:

- Useful solar thermal energy E_{CSP}.
- Boiler energy during the hybrid operation E_{boiler}.
- Fuel energy during the hybrid operation E_{fuel}.
- Fuel mass flow rate reduction in [kg/hr].

The daily solar heat energy is obtained by adding the hourly results. To calculate the boiler and fuel daily energies, the hourly values are summed to the non-hybrid cycle energies for the number of hours without solar radiation. The daily hours are the multiplied by the month's number of days and, lastly, the monthly results are summed to obtain the yearly energies and fuel saving.
With the results, the efficiency that describe the performance of the hybrid cycle are once again evaluated starting from the energies. The results of the analysis are listed in table 3.20:

Primary conversion efficiency η_p	41,5%
Hybrid cycle thermal efficiencyη_{th}	45,8%
Radiation-to-electric efficiency η_{r-e}	10,8%
Heat-to-electric efficiency η_{h-e}	27,9%
Solar share F_{sol}	0,3 %
Fuel saving $\Delta\dot{m}_{f\%}$	-0,93 %

Table 3.20: Annual analysis efficiency results.

Even with a simplified analysis, the obtained results are compatible with the ones proposed by other studies, in particular for the solar heat-to-electric efficiency.

3.10 Conclusions

In this chapter, the base model has been described by reporting the models used for each subsystem, and the methods used to evaluate its performance are explained. The model validation allows to verify the correctness of the equations with a view to integrating the solar input. In terms of equations, the solar integration does not modify excessively the base system.
The different integration options are found in the literature (chapter 2), except the one involving the tempering water. This solution has been proposed because the use of this mass flow rate causes energetic losses when it is mixed with the other flow (at the low temperature superheater outlet) but it is necessary for the normal boiler funcioning condition; it has been assumed that the same task of lowering the temperature could be carried out by heating the tempering flow rate instead of mixing it. After this process, this stream is further heated by the solar section and sent to expand in the turbine.
Some assumption are introduced for the simulations: when the integration involves a preheater, its outlet temperature is determined by the flow rate which continues in the traditional cycle, and the steam extraction is controlled by that temperature. The economizer's inlet temperature is maintained at its de-

sign value, in order to keep the thermodynamic cycle as close as possible to the base case. For the steam generation srategy it is assumed that, at the solar section outlet, the stream is at the same thermodynamic conditions as the immission point.
Twelve synergy option are proposed, and the four which resulted in a conversion efficiency higher than the base efficiency are:

- HPH3 preheater replacement, carried out with PTC and thermal oil or LFR with direct steam generation
- steam addition to stage HP2 from drainage water, carried out with PTC and molten salts or LFR with direct steam generation
- steam addition before RH from drainage water, carried out with PTC and thermal oil
- HPH3 preheater and economizer replacement, carried out with PTC and thermal oil

The final comparison between these options shows that the steam addition in the second high pressure turbine stage has the highest efficiencies and the lowes required solar field area. The highest fuel reduction is obtained with the feedwater preheater replacement.
By way of example, a simplified annual analysis has been carried out to evaluated the efficiency parameter over a year: the selected synergy is the feedwater heater replacement.

Conclusions

This thesis work provides a bibliographic review for the researches on integrated solar power plants. This summary is useful to have a general view on the feasibility and performance of the hybrid plants, and for the specific case study carried out it also produces a solid reference to compare the analysis results.
From the review, it is deduced that Integrated Solar Combined Cycles are the most mature and implemented solution when it comes to hybrid solar-conventional plants. The solar input can be used both in the heat recovery steam generator, to perform heat exchange in different points, and to preheat the exhaust gases at the turbine outlet.
For the specific case of coal-solar hybrid plants, the most frequently studied integration consists in substituting the highest temperature feedwater preheater: the solar stream is heated in parallel to the feedwater and mixed back before the economizer. This reduces the mass flow rate of the steam extraction. Another common solution is steam generation: water is drawn from some point in the cycle, evaporated in the solar section and sent to expand in the turbine.
The case study is based on the model of a real power plant, validated with reference experimental data. The EES model has been written in order to work in off design conditions, and the different simulations have been added to this starting point. Twelve solutions have been proposed; to make an initial selection, the integrations which resulted in a conversion efficiency higher than the base cycle efficiency ($\eta_{th,base} = 0{,}4203$) have been chosen for further investigation. These integration options are:

- HPH3 preheater replacement, carried out with PTC and thermal oil or LFR with direct steam generation (with maximum conversion efficiency

from primary sources, η_p, equal to 0,4249).

- Steam addition to stage HP2 from drainage water, carried out with PTC and molten salts or LFR with direct steam generation (maximum η_p = 0,4266).
- Steam addition before RH from drainage water, carried out with PTC and thermal oil (maximum η_p = 0,4243).
- HPH3 preheater and economizer replacement, carried out with PTC and thermal oil (maximum η_p = 0,4229).

This selection is consistent with the bibliographic review. At the point of maximum conversion efficiency, the second integration has the highest solar radiation-to-electric efficiency (η_{r-e} = 0,5455), solar heat-to-electricity (η_{h-e} = 0,7376) and thermal efficiency of the hybrid cycle (η_{th} = 0,4682). It is also the solution with the lower specific solar field area, equal to 2,29 m^2/kW_{solar}. The highest fuel saving, 7,65%, is found for the first integration.
From the annual analysis of the last preheater replacement integration option, it comes that the primary conversion efficiency η_p is 41,5%, with a radiation-to-electric efficiency and solar to electric efficiency of, respectively, 10,8 % and 27,9%. The solar fraction over the year is 0,3%, and the overall fuel reduction is 0,93%. These results are in line with the references.

Bibliography

[1] NREL. http://www.nrel.gov/csp/solarpaces.

[2] Oil embargo, 1973-1974. https://history.state.gov/milestones/1969-1976/oil-embargo.

[3] M. L. Ross. How the 1973 oil embargo saved the planet. https://www.foreignaffairs.com/articles/north-america/2013-10-15/how-1973-oil-embargo-saved-planet.

[4] Vincenzo Balzani and Nicola Armaroli. *Energy for a sustainable world: from the oil age to a sun-powered future*. John Wiley & Sons, 2010.

[5] Keith Lovegrove and Wes Stein. *Concentrating solar power technology: principles, developments and applications*. Elsevier, 2012.

[6] International Renewable Energy Agency. Concentrating solar power. In *Renewable Energy Technologies: Cost Analysis Series*, 2012.

[7] F Orioli and V Orioli. Parabolic or fresnel?

[8] Matthias Gunther, Michael Joemann, Simon Csambor, Amenallah Guizani, Dirk Kruger, and Tobisas Hirsch. Parabolic trough technology. In *Advanced CST teaching materials, enerMENA*. 2011.

[9] Franz Trieb. Global potential of concentrating solar power. In *Conference Proceedings*, 2009.

[10] Dhyia Aidroos Baharoon, Hasimah Abdul Rahman, Wan Zaidi Wan Omar, and Saeed Obaid Fadhl. Historical development of concentrating solar power

technologies to generate clean electricity efficiently–a review. *Renewable and Sustainable Energy Reviews*, 41:996–1027, 2015.

[11] Hank Price, Eckhard Lupfert, David Kearney, Eduardo Zarza, Gilbert Cohen, Randy Gee, and Rod Mahoney. Advances in parabolic trough solar power technology. *Journal of solar energy engineering*, 124(2):109–125, 2002.

[12] VK Jebasingh and GM Joselin Herbert. A review of solar parabolic trough collector. *Renewable and Sustainable Energy Reviews*, 54:1085–1091, 2016.

[13] Guangdong Zhu, Tim Wendelin, Michael J Wagner, and Chuck Kutscher. History, current state, and future of linear fresnel concentrating solar collectors. *Solar Energy*, 103:639–652, 2014.

[14] WT Xie, YJ Dai, RZ Wang, and K Sumathy. Concentrated solar energy applications using fresnel lenses: A review. *Renewable and Sustainable Energy Reviews*, 15(6):2588–2606, 2011.

[15] Arthur Davis and Frank Kühnlenz. Optical design using fresnel lenses. *Optik & Photonik*, 2(4):52–55, 2007.

[16] Vinod Kumar, RL Shrivastava, and SP Untawale. Fresnel lens: a promising alternative of reflectors in concentrated solar power. *Renewable and Sustainable Energy Reviews*, 44:376–390, 2015.

[17] Matthias Gunther, Michael Joemann, Simon Csambor, Amenallah Guizani, Dirk Kruger, and Tobisas Hirsch. Linear fresnel technology. In *Advanced CST teaching materials, enerMENA*. 2011.

[18] David R Mills and Graham L Morrison. Compact linear fresnel reflector solar thermal powerplants. *Solar energy*, 68(3):263–283, 2000.

[19] Najla El Gharbi, Halima Derbal, Sofiane Bouaichaoui, and Noureddine Said. A comparative study between parabolic trough collector and linear fresnel reflector technologies. *Energy Procedia*, 6:565–572, 2011.

[20] Technology CSTEP-Center for Study of Science and Policy. Global review of solar tower technology, August 2014.

[21] Omar Behar, Abdallah Khellaf, and Kamal Mohammedi. A review of studies on central receiver solar thermal power plants. *Renewable and sustainable energy reviews*, 23:12–39, 2013.

[22] Clifford K Ho and Brian D Iverson. Review of high-temperature central receiver designs for concentrating solar power. *Renewable and Sustainable Energy Reviews*, 29:835–846, 2014.

[23] Gregory J Kolb, Clifford K Ho, Thomas R Mancini, and Jesse A Gary. Power tower technology roadmap and cost reduction plan. *SAND2011-2419, Sandia National Laboratories, Albuquerque, NM*, 7, 2011.

[24] Germain Augsburger. *Thermo-economic optimisation of large solar tower power plants*. PhD thesis, École Polytechnique Fédérale de Lausanne, 2013.

[25] DOE. https://energy.gov/eere/energybasics/articles/dishengine-system-concentrating-solar-power-basics.

[26] AZ Hafez, Ahmed Soliman, KA El-Metwally, and IM Ismail. Design analysis factors and specifications of solar dish technologies for different systems and applications. *Renewable and Sustainable Energy Reviews*, 67:1019–1036, 2017.

[27] William B Stine and Richard B Diver. A compendium of solar dish/stirling technology. Technical report, DTIC Document, 1994.

[28] Robert Pitz-Paal. Concentrating solar power: Its potential contribution to a sustainable energy future. 2012.

[29] DOW. http://www.dow.com/heattrans/products/synthetic/dowtherm.htm.

[30] RADCO. http://www.radcoind.com/industrial-energy/xceltherm-sst/.

[31] EASTMAN. https://www.therminol.com.

[32] ARCHIMEDE SOLAR ENERGY. https://www.archimedesolarenergy.it.

[33] HL Zhang, Jan Baeyens, J Degrève, and G Cacères. Concentrated solar power plants: Review and design methodology. *Renewable and Sustainable Energy Reviews*, 22:466–481, 2013.

[34] Juergen H Peterseim, Stuart White, Amir Tadros, and Udo Hellwig. Concentrating solar power hybrid plants–enabling cost effective synergies. *Renewable Energy*, 67:178–185, 2014.

[35] Juergen H Peterseim, Stuart White, Amir Tadros, and Udo Hellwig. Concentrated solar power hybrid plants, which technologies are best suited for hybridisation? *Renewable Energy*, 57:520–532, 2013.

[36] C Libby, J Golden, R Bedilion, and C Turchi. Assessment of direct steam generation technologies for solar thermal augmented steam cycle applications. *Energy Procedia*, 49:1420–1428, 2014.

[37] Stefano Giuliano, Reiner Buck, and Santiago Eguiguren. Analysis of solar-thermal power plants with thermal energy storage and solar-hybrid operation strategy. *Journal of Solar Energy Engineering*, 133(3):031007, 2011.

[38] Giovanni Manente, Sergio Rech, and Andrea Lazzaretto. Optimum choice and placement of concentrating solar power technologies in integrated solar combined cycle systems. *Renewable Energy*, 96:172–189, 2016.

[39] Guangdong Zhu, Ty Neises, Craig Turchi, and Robin Bedilion. Thermodynamic evaluation of solar integration into a natural gas combined cycle power plant. *Renewable Energy*, 74:815–824, 2015.

[40] Jürgen Dersch, Michael Geyer, Ulf Herrmann, Scott A Jones, Bruce Kelly, Rainer Kistner, Winfried Ortmanns, Robert Pitz-Paal, and Henry Price. Trough integration into power plants—a study on the performance and economy of integrated solar combined cycle systems. *Energy*, 29(5):947–959, 2004.

[41] MA Ancona, M Bianchi, L Branchini, A De Pascale, F Melino, and A Peretto. Thermodynamic evaluation of repowering options for a small-size combined cycle with concentrating solar power technology. *Energy Procedia*, 82:584–590, 2015.

[42] A Baghernejad and M Yaghoubi. Exergoeconomic analysis and optimization of an integrated solar combined cycle system (isccs) using genetic algorithm. *Energy conversion and Management*, 52(5):2193–2203, 2011.

[43] Bruce Kelly, U Hermann, and M Hale. Optimization studies for integrated solar combined cycle systems. *Solar Engineering*, pages 393–398, 2001.

[44] Mechthild Horn, Heiner Führing, and Jürgen Rheinländer. Economic analysis of integrated solar combined cycle power plants: A sample case: The economic feasibility of an isccs power plant in egypt. *Energy*, 29(5):935–945, 2004.

[45] Antonio Rovira, María José Montes, Fernando Varela, and Mónica Gil. Comparison of heat transfer fluid and direct steam generation technologies for integrated solar combined cycles. *Applied Thermal Engineering*, 52(2):264–274, 2013.

[46] Tobias Vogel, Gerd Oeljeklaus, Klaus Görner, Jürgen Dersch, and Thomas Polklas. Hybridization of parabolic trough power plants with natural gas. *Energy Procedia*, 49:1238–1247, 2014.

[47] Peter Schwarzbözl, Reiner Buck, Chemi Sugarmen, Arik Ring, Ma Jesús Marcos Crespo, Peter Altwegg, and Juan Enrile. Solar gas turbine systems: Design, cost and perspectives. *Solar Energy*, 80(10):1231–1240, 2006.

[48] Craig S Turchi, Zhiwen Ma, and Michael Erbes. Gas turbine/solar parabolic trough hybrid designs. In *ASME 2011 Turbo Expo: Turbine Technical Conference and Exposition*, pages 989–996. American Society of Mechanical Engineers, 2011.

[49] Fahad A Al-Sulaiman. Exergy analysis of parabolic trough solar collectors integrated with combined steam and organic rankine cycles. *Energy Conversion and Management*, 77:441–449, 2014.

[50] D Olivenza-León, A Medina, and A Calvo Hernández. Thermodynamic modeling of a hybrid solar gas-turbine power plant. *Energy Conversion and Management*, 93:435–447, 2015.

[51] Hadi Ghasemi, Elysia Sheu, Alessio Tizzanini, Marco Paci, and Alexander Mitsos. Hybrid solar–geothermal power generation: Optimal retrofitting. *Applied energy*, 131:158–170, 2014.

[52] Dimityr Popov. Innovative solar augmentation of gas turbine combined cycle plants. *Applied Thermal Engineering*, 64(1):40–50, 2014.

[53] Shuo Peng, Zhaoguo Wang, Hui Hong, Da Xu, and Hongguang Jin. Exergy evaluation of a typical 330mw solar-hybrid coal-fired power plant in china. *Energy Conversion and Management*, 85:848–855, 2014.

[54] M ZekiYılmazoğlu, Ali Durmaz, and Derek Baker. Solar repowering of soma-a thermal power plant. *Energy Conversion and Management*, 64:232–237, 2012.

[55] Qin Yan, Yongping Yang, Akira Nishimura, Abbas Kouzani, and Eric Hu. Multi-point and multi-level solar integration into a conventional coal-fired power plant. *Energy & fuels*, 24(7):3733–3738, 2010.

[56] Rongrong Zhai, Yong Zhu, Yongping Yang, Kaiyu Tan, and Eric Hu. Exergetic and parametric study of a solar aided coal-fired power plant. *Entropy*, 15(3):1014–1034, 2013.

[57] Suvi Suojanen, Elina Hakkarainen, Matti Tähtinen, and Teemu Sihvonen. Modeling and analysis of process configurations for hybrid concentrated solar power and conventional steam power plants. *Energy Conversion and Management*, 134:327–339, 2017.

[58] Warrick Pierce, Paul Gauché, Theodor von Backström, Alan C Brent, and Amir Tadros. A comparison of solar aided power generation (sapg) and stand-alone concentrating solar power (csp): A south african case study. *Applied Thermal Engineering*, 61(2):657–662, 2013.

[59] Dimityr Popov. An option for solar thermal repowering of fossil fuel fired power plants. *Solar Energy*, 85(2):344–349, 2011.

[60] YongPing Yang, YingHong Cui, HongJuan Hou, XiYan Guo, ZhiPing Yang, and NinLing Wang. Research on solar aided coal-fired power generation system and performance analysis. *Science in China Series E: Technological Sciences*, 51(8):1211–1221, 2008.

[61] Rongrong Zhai, Pan Peng, Yongping Yang, and Miaomiao Zhao. Optimization study of integration strategies in solar aided coal-fired power generation system. *Renewable Energy*, 68:80–86, 2014.

[62] Tobias Prosin, Trevor Pryor, Christine Creagh, Lars Amsbeck, and Reiner Buck. Hybrid solar and coal-fired steam power plant with air preheating using a solid particle receiver. 2014.

[63] Yawen Zhao, Hui Hong, and Hongguang Jin. Evaluation criteria for enhanced solar–coal hybrid power plant performance. *Applied Thermal Engineering*, 73(1):577–587, 2014.

[64] Yongping Yang, Qin Yan, Rongrong Zhai, Abbas Kouzani, and Eric Hu. An efficient way to use medium-or-low temperature solar heat for power generation–integration into conventional power plant. *Applied thermal engineering*, 31(2):157–162, 2011.

[65] Marco Bettiol. *Integration of a concentrated solar plant into an ultra-supercritical steam power plant of 1000 MW: thermodynamic, economic and exergoeconomic analysis.* Tesi di laurea, Università degli Studi di Padova, 2011/2012.

[66] Cesare Bonacina, Alberto Cavallini, and Lino Mattarolo. *Trasmissione del calore*. Cleup, 1992.

[67] Denis Sasso. *Modello di simulazione di un impianto termoelettrico da 320 MW*. Tesi di laurea, Università degli Studi di Padova, 1999/2000.

[68] David H Cooke. On prediction of off-design multistage turbine pressures by stodola's ellipse. In *1984 Joint Power Generation Conference: GT Papers*, pages V001T04A004–V001T04A004. American Society of Mechanical Engineers, 1984.

[69] Gabriel Morin, Jürgen Dersch, Werner Platzer, Markus Eck, and Andreas Häberle. Comparison of linear fresnel and parabolic trough collector power plants. *Solar Energy*, 86(1):1–12, 2012.

[70] Jrc. http://re.jrc.ec.europa.eu/pvgis/apps4/pvest.php?

[71] Nrel. https://midcdmz.nrel.gov/solpos/solpos.html.

[72] http://www.temperatureweather.com/mediterr/meteo/it-meteo-in-italia-venezia.htm.

Appendix A

Model validation

The base model results are reported in figures A.1 and A.2 and compared to the reference data ([67]). Some points have been omitted to simplify the model.

	Reference results			Model results			Deviation from reference		
i	m_dot[i]	p[i]	T[i]	m_dot[i]	p[i]	T[i]	Δm	Δp	ΔT
	[kg/s]	[bar]	[°C]	[kg/s]	[bar]	[°C]	[%]	[%]	[%]
1	293,22	170,831	538,84	290,5	164,2	538	-0,926	-3,882	-0,156
4	289,62	165,438	536,65	290,5	164,2	538	0,303	-0,748	0,252
5	289,62	108,854	480,8	290,5	112,3	484,8	0,303	3,166	0,832
6	255,32	78,914	430,3	260,3	79,63	432,5	1,950	0,907	0,511
7	28,83	78,914	430,3	30,25	79,63	432,5	4,943	0,907	0,511
8	28,83	77,845	429,63	30,25	79,63	432,5	4,943	2,293	0,668
11	232,86	37,697	326,55	235,5	35,35	321,4	1,133	-6,226	-1,577
12	22,46	37,697	326,55	24,74	35,35	321,4	10,155	-6,226	-1,577
13	22,46	36,814	325,7	24,74	34,34	320,3	10,155	-6,720	-1,658
16	227,84	37,353	326,19	235,5	35,35	321,4	3,364	-5,362	-1,468
17	227,84	34,785	541,46	235,5	35,35	540,5	3,364	1,624	-0,177
18	231,90	34,529	541,35	235,5	35,15	540,5	1,554	1,798	-0,157
19	218,47	17,309	442,8	221,3	17,33	434,2	1,297	0,121	-1,942
20	13,43	17,309	442,8	14,17	17,33	434,2	5,519	0,121	-1,942
21	13,43	17,113	440,55	14,17	17,15	431,8	5,519	0,216	-1,986
24	204,03	7,328	319,7	206,3	6,952	313,3	1,112	-5,131	-2,002
25	14,43	7,328	319,7	15,04	6,952	313,3	4,195	-5,131	-2,002
26	12,71	7,21	317,31	15,04	6,745	310,9	18,301	-6,449	-2,020
28	213,01	7,328	319,7	206,3	6,952	313,3	-3,151	-5,131	-2,002
29	200,82	3,2	229,2	194,3	2,553	205	-3,248	-20,219	-10,558
30	12,19	3,2	229,2	12,02	2,553	205	-1,395	-20,219	-10,558
31	190,85	0,786	96,76	185,2	0,7417	92,92	-2,958	-5,636	-3,969
32	9,98	0,786	96,76	9,093	0,7417	92,92	-8,860	-5,636	-3,969
33	178,65	0,27	66,69	173,6	0,2854	67,97	-2,827	5,704	1,919
34	12,20	0,27	66,69	11,55	0,2854	67,97	-5,296	5,704	1,919
35	178,65	0,054	34,11	173,6	0,049	32,52	-2,827	-9,259	-4,661
36	213,01	0,054	34,11	206,3	0,049	32,52	-3,151	-9,259	-4,661
38	216,79	0,054	34,11	206,3	0,049	32,52	-4,837	-9,259	-4,661
39	216,79	13,44	34,39	206,3	12,64	32,97	-4,837	-5,952	-4,129
41	216,51	13,44	34,39	206,3	12,64	32,97	-4,714	-5,952	-4,129
42	12,20	0,27	54,27	11,55	0,2854	52,84	-5,296	5,704	-2,635
43	12,20	0,054	34,11	11,55	0,05	32,88	-5,296	-7,407	-3,606
44	216,51	13,061	65,28	206,3	12,31	66,64	-4,714	-5,750	2,083
45	22,17	0,786	65,89	21,11	0,7417	67,46	-4,769	-5,636	2,383
46	22,17	0,054	34,11	21,11	0,05	32,88	-4,769	-7,407	-3,606
47	216,51	12,683	93,35	206,3	11,99	86,1	-4,714	-5,464	-7,766
48	12,19	3,2	96,37	12,02	2,553	86,92	-1,395	-20,219	-9,806
49	12,19	0,786	93,02	12,02	0,7417	86,95	-1,395	-5,636	-6,525
50	216,51	12,094	126,9	206,3	11,44	102,4	-4,714	-5,408	-19,307

Figure A.1: Model validation (1)

	Reference results			Model results			Deviation from reference		
i	m_dot[i]	p[i]	T[i]	m_dot[i]	p[i]	T[i]	Δm	Δp	ΔT
	[kg/s]	[bar]	[°C]	[kg/s]	[bar]	[°C]	[%]	[%]	[%]
52	216,46	12,094	126,9	206,3	11,44	102,4	-4,695	-5,408	-19,307
53	281,13	12,094	141,15	275,7	11,44	123,9	-1,932	-5,408	-12,221
54	281,13	9,709	141,18	275,7	9,223	124,2	-1,932	-5,006	-12,027
55	0,20	7,21	166,16	0,1967	6,745	163,5	-0,962	-6,449	-1,601
56	293,79	7,21	166,6	290,5	6,745	163,5	-1,120	-6,449	-1,861
58	293,74	7,21	166,6	290,5	6,745	163,5	-1,104	-6,449	-1,861
59	293,74	197,901	169,4	290,5	195,2	168,8	-1,104	-1,365	-0,354
60	271,04	197,901	169,4	266,9	195,2	168,8	-1,528	-1,365	-0,354
61	135,52	197,901	169,4	266,9	195,2	168,8	96,943	-1,365	-0,354
62	135,52	196,985	205,4	266,9	193,8	196,9	96,943	-1,617	-4,138
63	32,07	17,113	187,3	69,16	17,15	187	115,631	0,216	-0,160
64	32,07	12,094	187,35	69,16	11,44	185,9	115,631	-5,408	-0,774
65	135,52	196,069	246,9	266,9	192,3	240,8	96,943	-1,922	-2,471
66	25,32	36,814	222,6	54,99	34,34	214	117,149	-6,720	-3,863
67	25,32	17,113	204,65	54,99	17,15	204,8	117,149	0,216	0,073
68	135,52	195,153	292,1	266,9	190,9	294	96,943	-2,179	0,650
69	14,09	77,845	253,1	30,25	79,63	246,9	114,751	2,293	-2,450
70	14,09	36,814	245,51	30,25	34,34	241,5	114,751	-6,720	-1,633
83	270,85	195,153	292,95	266,9	190,9	294	-1,457	-2,179	0,358
84	270,85	191,23	292,91	266,9	190,9	294	-1,457	-0,173	0,372
85	270,85	191,23	362,05	266,9	190,9	361,9	-1,457	-0,173	-0,041
88	270,52	188,19	360,72	266,9	190,9	361,9	-1,337	1,440	0,327
89	270,52	185,64	437,44	266,9	190,9	441,2	-1,337	2,833	0,860
90	293,22	170,831	399	290,5	190,9	401,1	-0,926	11,748	0,526
99	22,70	197,901	169,4	23,63	195,2	168,8	4,096	-1,365	-0,354
100	32,69	1	80	32,18	1	80	-1,571	0,000	0,000
101	317,59	1	294	297,5	1	287,9	-6,324	0,000	-2,075
102	345,57	1	2118,47	324,7	1	2203	-6,040	0,000	3,990
103	345,57	1	2054,41	324,7	1	2142	-6,040	0,000	4,264
104	345,57	1	1657,69	324,7	1	1736	-6,040	0,000	4,724
105	345,57	1	1319,11	324,7	1	1376	-6,040	0,000	4,313
106	345,57	1	1062,37	324,7	1	1094	-6,040	0,000	2,977
107	345,57	1	708,5	324,7	1	713,3	-6,040	0,000	0,677
108	345,57	1	384,84	324,7	1	377,3	-6,040	0,000	-1,959
109	345,57	1	141,89	324,7	1	143,8	-6,040	0,000	1,346
110	393,89	1	126,89	367,3	1	126,8	-6,751	0,000	-0,071
111	365,91	1	14,29	340,2	1	17,15	-7,025	0,000	20,014
112	317,59	1	14,29	297,5	1	17,15	-6,324	0,000	20,014
113	48,32	1	14,29	42,66	1	17,15	-11,713	0,000	20,014

Figure A.2: Model validation (1)

The expansion line results are compared to the available experimental data

in figure A.3:

	Experimental data			Model results			Deviation from reference		
i	m_dot[i]	p[i]	T[i]	m_dot[i]	p[i]	T[i]	Δm	Δp	ΔT
	[kg/s]	[bar]	[°C]	[kg/s]	[bar]	[°C]	[%]	[%]	[%]
1	290,51	166,7131	538	290,5	164,2	538	-0,003	-1,507	0,000
2	290,51								
4	290,51			290,5	164,2	538	-0,003		
5	285,16	110,8151		290,5	112,3	484,8	1,871	1,340	
6	254,02	79,23773	429,1	260,3	79,63	432,5	2,472	0,495	0,792
7	31,14	79,23773	430,1	30,25	79,63	432,5	-2,865	0,495	0,558
8				30,25	79,63	432,5			
11	225,65	38,14787	328	235,5	35,35	321,4	4,367	-7,334	-2,012
12	28,38	38,14787	329	24,74	35,35	321,4	-12,816	-7,334	-2,310
13				24,74	34,34	320,3			
16				235,5	35,35	321,4			
17				235,5	35,35	540,5			
18	229,66	34,32328	538	235,5	35,15	540,5	2,543	2,409	0,465
19	215,54	17,06357	433,1	221,3	17,33	434,2	2,672	1,561	0,254
20	14,12	17,06357	434,1	14,17	17,33	434,2	0,364	1,561	0,023
21				14,17	17,15	431,8			
24	201,63	7,256921	319,1	206,3	6,952	313,3	2,317	-4,202	-1,818
25	13,91	7,256921	320,1	15,04	6,952	313,3	8,111	-4,202	-2,124
26				15,04	6,745	310,9			
28	210,71	7,149048	321,5	206,3	6,952	313,3	-2,093	-2,756	-2,551
29	197,71	2,618376	211,6	194,3	2,553	205	-1,726	-2,497	-3,119
30	13,00	2,618376	212,6	12,02	2,553	205	-7,519	-2,497	-3,575
31	189,42	0,764919	98,9	185,2	0,7417	92,92	-2,225	-3,035	-6,047
32	8,30	0,764919	99,9	9,093	0,7417	92,92	9,595	-3,035	-6,987
33	178,43	0,2942	68,6	173,6	0,2854	67,97	-2,705	-2,991	-0,918
34	10,99	0,27	66,69	11,55	0,2854	67,97	5,114	5,704	1,919
35	167,44	0,049033		173,6	0,049	32,52	3,680	-0,068	

Figure A.3: Model validation (3)